Sujet de thèse :

Co-immobilisation du complexe (2,2'-bipyridyl) (pentaméthylcyclopentadiényl)-rhodium et de déshydrogénases NAD-dépendantes pour l'électrosynthèse enzymatique énantiosélective

Par

Lin ZHANG

Pour l'obtention de titre de **Docteur**

Ecole Doctorale : Synthèse, Simulations, Applications: de la Molécule aux Edifices Supramoléculaires (SESAMES), ED 412

Soutenance publique prévue le 15 December 2016 devant le jury composé de :

Rapporteurs:	Prof. Philip N Bartlett, University of Southampton, United Kingdom
	Dr. Elisabeth Lojou, BIP, CNRS, Marseille
Invités:	Dr. Alain Walcarius, LCPME, CNRS, Nancy
	Prof. François Lapicque, LRGP, CNRS, Nancy
Directeur :	Dr. Mathieu Etienne, LCPME, CNRS, Nancy
Examinateur :	Dr. Neus Vila, Université de Lorraine, Nancy

Laboratoire de Chimie Physique et Microbiologie pour l'Environnement (LCPME)
Unité mixte de recherche – UMR 756

405 Rue de Vandoeuvre, 54600, Villers-lès-Nancy, France

Acknowlegements

First of all, I would like to give my greatest thanks to my supervisors Mathieu ETIENNE and Neus VILA for their guiding and supporting me during these past three years. Without their constant advice and efforts, this thesis would not have been completed. I feel very lucky to be a student of them. I could still remember at the beginning of my Ph.D when I just enter the field of electrochemistry how they encourage me to go out of frustration when I meet difficulties. Mathieu teach me how to carry out research independently and systematically, giving me the confidence to continue my career in science. Neus not only help me in work, showing me the proper ways to carry out different experiments, but also help me in life when I meet difficulties. There are so many things they have teach me and help me that I‟m not able to list all here, but all the details are kept in my mind, which will become part of my great memories in my life.

I would like to acknowledge Alain WALCARIUS who is the director of the lab and our ELAN group for his scientific supports and useful discussions. I would also like to acknowledge Prof. Gert-Wieland KOHRING from Saarland University for his support in biological part of this thesis. I am also very grateful to my friend Ievgen MAZURENKO, who is the former post-doc in ELAN group, he give me detailed guidance at the beginning of my Ph.D, leading me to the field of bioelectrochemistry.

I would also like to thank all the members in ELAN Group, present and past, for their selfless support and friendships. They made my life more colorful during the three years. Special thanks to: Cheryl KARMAN, for her generous help when I was sick; Maciej MIERZWA, for being a good partner to have nice lunch time during two years; Mohana AFSHARIAN, for her help when I was looking for an apartment; Martha COLLINS, for her help in some documents preparation; Lukasz POLOTORAK, for his warm-hearted assistance.

There are also many people in LCPME who have help me from time to time, I‟m not able to thank them one by one here, I will always remember their kindness to me.

Here I also want to thank my Master supervisor Eric GRELET in Bordeaux, he teach me the right attitude toward science, which has influenced me on way of research.

I would like to thank my family, especially my parents for their constant support since I go abroad, I could always get sense of security from them no matter how difficult situation I was in. I would also like to thank my father in law for his advices for my scientific career.

At last, I would like to express my thanks to my husband Zhanming for his love, it‟s very important that we hold each other‟s hand, sharing the happiness and facing the difficulties together.

Table of content

Abstract

In this work we developed methods for co-immobilization of NAD-dependent dehydrogenase and the (2,2'-bipyridyl)(pentamethylcyclopentadienyl)-rhodium complex ([Cp*Rh(bpy)Cl]$^+$) on porous carbon electrodes for applications on electroenzymatic synthesis of chiral alcohols and sugars. The goal was to avoid degradation of the enzymatic activity originated from the interaction between enzyme surface functional groups (eg.-SH, -NH_2) and [Cp*Rh(bpy)Cl]$^+$ and to allow the recyclability for catalysts. Diazonium electrografting was used to introduce either alkene or azide groups on a carbon surface (flat glassy carbon, porous carbon felt or carbon nanotubes layers). Thiol-ene click chemistry was applied to bind D-sorbitol dehydrogenases with cysteine tag (either 1 or 2 cysteine moieties at the N terminus of the polypeptide chain) onto carbon electrodes. Azide-alkyne Huisgen cycloaddition reaction was used to bind an alkyne modified [Cp*Rh(bpy)Cl]$^+$. Then co-immobilization of the redox enzymes (D-sorbitol and Galactitol dehydrogenase) with [Cp*Rh(bpy)Cl]$^+$ was tested by encapsulation of the proteins in a silica gel layer, inside a rhodium-functionalized porous carbon felt. The immobilized [Cp*Rh(bpy)Cl]$^+$ was stable over weeks for NADH regeneration, but this electrode architecture led to the inhibition of the enzymatic activity, possibly because of local microenvironment (increase of pH and product concentration). The combination of „thiol–ene" and Huisgen cycloaddition was then investigated for sequential immobilization of [Cp*Rh(bpy)Cl]$^+$ and cysteine-tagged D-sorbitol dehydrogenase on an azide-alkene bifunctionalized electrodes. Finally, considering the different lifetime of enzymes and [Cp*Rh(bpy)Cl]$^+$ catalyst, and the need for better separation of this element from the bioelectrochemical system, the best configuration was achieved by overlaying a porous silica layer with the immobilized enzyme on the top of [Cp*Rh(bpy)Cl]$^+$ functionalized bucky paper. The reusability of this rhodium complex functionalized bucky paper electrode was proved and the designed bioelectrode was successfully applied to bioelectrochemical conversion of D-fructose to D-sorbitol.

Résumé

Dans ce travail, nous avons développé différentes méthodes pour la co-immobilisation sur des électrodes poreuses de carbone de déshydrogénases NAD-dépendantes avec le complexe (2,2'-bipyridyle)(pentaméthylcyclopentadiényl)-rhodium ($[Cp^*Rh(bpy)Cl]^+$) pour des applications de synthèse électroenzymatique d'alcools et de sucres chiraux. L'objectif était d'éviter la dégradation de l'activité enzymatique provenant de l'interaction entre les groupes fonctionnels de surface de l'enzyme (-SH, -NH2) et le complexe $[Cp^*Rh(bpy)Cl]^+$, et également de permettre le recyclage des catalyseurs. L'électrogreffage de diazonium a été utilisé pour introduire des fonctions alcène et/ou azoture sur une surface de carbone (carbone vitreux plan, feutre de carbone poreux ou couches de nanotubes de carbone). La chimie click « thiol-ène » a été utilisée pour lier de manière covalente une D-sorbitol déshydrogénases modifiée par un tag cystéine (soit 1 ou 2 fragments cystéine à l'extrémité N-terminale de la chaîne polypeptidique) à des électrodes de carbone. Ensuite, la réaction de cycloaddition de Huisgen alcyne-azoture a été utilisé pour lier le complexe $[Cp^*Rh(bpy)Cl]^+$ à l'électrode. Ensuite la co-immobilisation des enzymes redox (D-sorbitol et galactitol déshydrogénases) avec le complexe $[Cp^*Rh(bpy)Cl]^+$ a été testée par l'encapsulation des protéines dans une couche de gel de silice, à l'intérieur d'un feutre de carbone poreux préalablement fonctionnalisé par le complexe de rhodium. Le catalyseur est alors stable pendant plusieurs semaines pour la réaction de régénération de NADH, mais cette architecture d'électrode conduit à l'inhibition de l'activité enzymatique, probablement causé par un microenvironnement local (augmentation du pH et de la concentration du produit). La combinaison des chimies clicks « thiol-ène » et cyclo-addition de Huisgen a ensuite été étudié pour l'immobilisation séquentielle de $[Cp^*Rh(bpy)Cl]^+$ et d'une D-sorbitol déshydrogénase porteuse d'un tag cystéine, sur une électrode poreuse bi-fonctionnalisée par les groupes azoture et alcène. Enfin, compte tenu de la différence de durée de vie des enzymes et du complexe $[Cp^*Rh(bpy)Cl]^+$ et de la nécessité d'améliorer la séparation de ces éléments du système bioélectrochimique, l'assemblage optimal a été obtenu en associant une couche poreuse de silice dans laquelle est immobilisée l'enzyme avec un papier de nanotubes de carbone fonctionnalisé par le complexe de rhodium. Le catalyseur $[Cp^*Rh(bpy)Cl]^+$ pour la régénération de NADH peut être réutilisé successivement avec plusieurs couches de protéines. Ce système optimal a finalement été appliqué à la conversion bioélectrochimique du D-fructose en D-sorbitol.

General introduction

Enzymatic synthesis is an alternative and a very promising field of research for addressing some challenges in organic synthesis since it offers facile routes to selectively prepare some valuable products without suffering from side-reactions as in conventional organic synthesis methods [1]. Among the different enzymatic catalytic systems, dehydrogenase is an important class of oxidoreductase that catalyze redox reactions to produce valuable products from broad substrates taking advantage of their enantioselectivity, showing great potential in industrial applications [2]. For nicotinamide adenine dinucleotide (phosphate) (NAD(P))-dependent enzymes whose cofactor is freely diffusing in the solution, the expensive cofactor needs to be regenerated in long-term biosynthesis. Electrochemical cofactor regeneration is a continuous process based on electron transfer reactions which would largely simplify the purification step, showing thus great potential in enzymatic synthesis [3,4].

Because the direct electrochemical regeneration of NAD(P)H results in inactivation of the cofactor, indirect electrochemical regeneration methods have been developed from the last decades [5]. Up to now, the (2,2'-bipyridyl)(pentamethylcyclopentadienyl)-rhodium complex ($[Cp^*Rh(bpy)Cl]^+$) family was found to be the most efficient non-enzymatic NAD(P)H regeneration catalyst, however, it suffers from degradation in the presence of proteins due to the interaction between rhodium center and surface functional groups of proteins. This interaction can also inactivate the proteins in some conditions [6,7]. So it is important to separate the rhodium complex from enzymes if we want to achieve a long-term stability of bioenzymatic catalysis and electrocatalysis. Moreover, immobilization of enzymes and rhodium complex separately can not only avoid the unfavorable interaction, but also simplify the product purification process and increase the reusability of catalyst or enzymes.

There are several methods for immobilization of the enzymes on the electrodes. Among these approaches, covalent bonding and encapsulation provide stable immobilization which ensured the long-term stability. Usually, covalent reaction occurred between the functional groups on the electrode surface and amino acid residues of the enzyme, but the disadvantage is that the orientation of the enzyme was not ensured upon grafting and essential amino acid residues close to the enzyme active site could be involved in the chemical reaction, leading to a reduction of enzyme activity [8]. To overcome the disadvantages of conventional

covalent reactions, „tag" residues can be introduced onto the specific positions of the enzymes. This has been reported in the past with histidine tags [9,10]. With this method, the orientation of enzymes can be controlled and the activity of the enzymes was kept. However, the attachment of proteins with this tag does not allow long term stability of the immobilization. This stability can only be achieved with chemical bonding or encapsulation. There are already several surface functionalization processes that been developed by means of covalent bonds. Among them the „click chemistry" approaches are attracting increasing attention being an easy and powerful mean for joining molecular species to each other in rather mild conditions [11–13]. In this thesis we have explored the immobilization of a cysteine-tagged dehydrogenase via „thiol-ene" click reaction. Silica gel encapsulation developed in previous studies was also applied in this thesis to electroenzymatic reduction reactions.

Covalent immobilization of $[Cp^*Rh(bpy)Cl]^+$ was carried out in two steps to avoid unfavorable interaction. A bipyridine ligand was first bound on an electrode surface followed by a metal complexation step. This bipyridine was immobilized by either a two step process involving surface functionalization and azide-alkyne Huisgen cycloaddition click chemistry, or a direct bipyridyl diazonium electrografting process. The efficiency of NADH regeneration with these rhodium functionalized electrodes was evaluated as well as the stability of the catalytic reactions.

Based on the methodology developed above, electrodes with co-immobilized dehydrogenases and rhodium complex have been fabricated. One strategy was to encapsulate enzymes inside silica gel deposited inside a porous rhodium complex functionalized electrode. Another approach was a covalent functionalization of these two components through two different kinds of „click" reactions on a bi-functionalized surface. Taking into account some difficulties met in the electrosynthesis process and the different lifetime scale of enzymes and rhodium complex, we have finally considered this reversible co-immobilization. Bioelectrode with co-immobilized rhodium complex and NAD-dependent dehydrogenase were systematically tested in bioconversion experiment.

Introduction générale

L'utilisation de la catalyse enzymatique est une alternative prometteuse à certaines voies de synthèse organique car cela offre la possibilité de préparer sélectivement des produits à haute valeur sans être limité par les réactions secondaires rencontrées avec les méthodes usuelles de synthèse organique [1]. Parmi les différents systèmes enzymatiques, les déshydrogénases sont une classe importante des protéines redox permettant la production énantiosélective de molécules d'intérêt industriel [2]. La plus grande partie des déshydrogénases dépendent du cofacteur NAD(P), nicotinamide adénine di-nucléotide (phosphate). Celui-ci a la particularité de diffuser librement au sein de la solution. En raison du coût de ce cofacteur il est nécessaire de considérer sa régénération dans un procédé biotechnologique impliquant des déshydrogénases. La régénération électrochimique de ce cofacteur est un processus continu basé des réactions de transfert d'électron, permettant une simplification des étapes de purification des molécules synthétisées, présentant donc un grand intérêt pour les processus de synthèse enzymatiques [3,4].

La régénération électrochimique directe du cofacteur NAD(P)H conduit cependant à son inactivation. Des approches permettant cette régénération indirecte ont donc été développées au cours des dernières décennies [5]. Aujourd'hui, le complexe 2,2'-bipyridyl)(pentamethylcyclopentadienyl)-rhodium ($[Cp^*Rh(bpy)Cl]^+$) est un des plus efficaces pour cette régénération non-enzymatique du cofacteur NAD(P)H. Malheureusement, certains auteurs ont observé une dégradation de ce complexe en présence de protéines causée par l'interaction entre le centre rhodium et les groupes fonctionnels de surface de la protéine. De plus, cette interaction peut aussi inactiver l'enzyme dans certaines conditions [6,7]. Pour ces raisons, il est important de séparer le complexe de rhodium de l'enzyme si l'on souhaite atteindre une grande stabilité du système bioélectrochimique. Enfin, Cette séparation peut aussi simplifier la purification des produits synthétisés et augmenter la réutilisation du catalyseur et de l'enzyme.

Il existe plusieurs méthodes pour immobiliser des enzymes à la surface d'une électrode. Parmi ces méthodes, la création de liaisons covalentes et l'encapsulation dans une matrice permettent d'immobiliser durablement l'enzyme. Les liaisons covalentes impliquent généralement des groupes fonctionnels à la surface de l'électrode et des acides aminés de l'enzyme. Un désavantage est que l'orientation de la protéine n'est pas nécessairement contrôlée. Par ailleurs, des acides aminés impliqués dans le site actif de l'enzyme peuvent être

impliqués et conduire à une modification de l'activité enzymatique [8]. Pour résoudre ces problèmes, des acides aminés « tag » peuvent être introduits à des positions spécifiques de l'enzyme. Ainsi, des tags histidines ont été produits [9,10] qui permettent l'orientation de l'enzyme lors de son immobilisation. Cependant, cet accrochage est irréversible (c'est en fait son principal intérêt pour la séparation de protéines) et ne peut pas permettre cette stabilité à long-terme que nous recherchons, cette stabilité pouvant seulement être obtenue par une liaison covalent irréversible dans les conditions d'utilisation du bioréacteur. Il y a déjà de nombreux procédés de fonctionnalisation de surface par le moyen d'une liaison covalente. Parmi celles-ci, la chimie click est particulièrement attrayante car elle permet de faire des jonctions moléculaires dans des conditions relativement douces [11–13].

Dans cette thèse, nous avons exploré l'immobilisation de déshydrogénases porteuses d'un ou deux tags cystéines via la chimie click « thiol-ene ». L'encapsulation sol-gel optimisée dans des études précédentes a également été appliquée dans cette thèse à l'immobilisation des déshydrogénases pour l'électrosynthèse enzymatique cathodique.

L'immobilisation covalente du complexe $[Cp^*Rh(bpy)Cl]^+$ a ensuite été menée en deux étapes pour éviter les interactions défavorables observées dans de précédents travaux. Tout d'abord, le ligand bipyridine a été lié à la surface de l'électrode afin de faire la complexation. Ce ligand bipyridine a ainsi été fixé en suivant deux voies de synthèse, en deux étapes impliquant la fonctionnalisation de surface par un sel de diazonium et une cyclo-addition de Huisgen azoture-alcène, ou l'électrogreffage direct d'une aminopyridine. L'efficacité de la régénération de NADH par ces électrodes fonctionnalisées par le complexe de rhodium a alors été étudiée ainsi que la stabilité de cette réaction électrocatalytique.

Sur la base des méthodes développées dans ce travail, nous avons ensuite fabriqué des électrodes sur lesquelles étaient co-immobilisées une déshydrogénase et le complexe de rhodium. Une première stratégie fut d'encapsuler l'enzyme dans une matrice sol-gel déposée au sein d'une électrode poreuse fonctionnalisée par le complexe de rhodium. Une autre stratégie impliquait la combinaison de deux voies de chimies de manière séquentielle à la surface d'une électrode bi-fonctionnalisée. Enfin, prenant en compte certains écueils rencontrés lors des expériences d'électrosynthèse enzymatique nous avons finalement considéré une co-immobilisation réversible. Toutes les bioélectrodes qui ont été élaborées dans cette étude ont été évaluées dans des expériences de bioconversion.

Chapter 1. Literature survey

The general principle of enzymatic electrosynthesis (also named electroenzymatic synthesis) is described in this chapter for different classes of proteins, i.e. NAD-dependent dehydrogenases, flavoenzymes and metalloproteins. Typical target reactions are given. Electrode materials used for cofactor regeneration and for the immobilization of enzymes and/or mediators are described. Immobilization of proteins has been achieved by membrane confinement, encapsulation in various materials (gel, polymers, surfactant molecules) or chemical bonding to the electrode surface. An important requirement for electroenzymatic synthesis is the stability of the bioelectrochemical reaction over a long period of time to allow quantitative conversion of the enzymatic substrates to the targeted products and recycling of the bioelectrode for successive bioconversion experiments.

1.1 Introduction

Enzymatic synthesis is an alternative and a very promising field of research for addressing some challenges in organic synthesis since it offers facile routes to selectively prepare some valuable products without suffering from side-reactions as in conventional organic synthesis methods [1]. Different classes of enzymes such as acylases, amidases, hydrolases or cellulases are already used in the industrial production of antibiotics, herbicides, fuel alcohols and pharmaceutical intermediates. In industrial processes, some enzymes like lipases or nitrilases have been produced in large scale or have been used for production of valuable products like enantiopure alcohols or R-mandelic acid [14,15].

Proteins can be broadly categorized as either soluble or membrane-associated. Soluble proteins, which include enzymes, antibodies, regulatory proteins and many others, reside in an aqueous environment, and thus are generally amenable to aqueous processing methods for immobilization. The solubility of these proteins arises owing to the presence of polar or charged amino acid residues on the exterior surface. Therefore, immobilization techniques for soluble proteins must provide a hydrated environment at a pH that does not alter the membrane of proteins and does not have significant polarity differences relative to water. On the other hand, membrane-associated proteins, contain either fully (intrinsic membrane proteins) or partially (extrinsic membrane proteins) embedded within cellular lipid membranes [16]. Therefore, successful immobilization of membrane proteins must address two important issues. Firstly, the method must allow retention of the tertiary folded structure of the protein as is the case for soluble proteins. Secondly, it must accommodate the phospholipid membrane structure, which is held together mainly through hydrophobic interactions [16] or replace these lipids by surfactant molecules. These issues are necessary to accommodate both the hydrophilic and hydrophobic parts of the protein.

Among the different enzymatic catalytic systems, redox enzymes are an important class of proteins that catalyze redox reactions. Enzymatic cofactors which are involved in redox reactions are used for transferring both electrons and protons. The structures of some of these cofactors are illustrated in **Figure 1.1** including their different redox states. Flavin adenine dinucleotide (FAD), flavin mononucleotide (FMN), heme or transition metals are associated with the enzymes. Nicotinamide adenine dinucleotide ($NAD(P)^+$/NAD(P)H are dissociated from the enzymes [4,17].

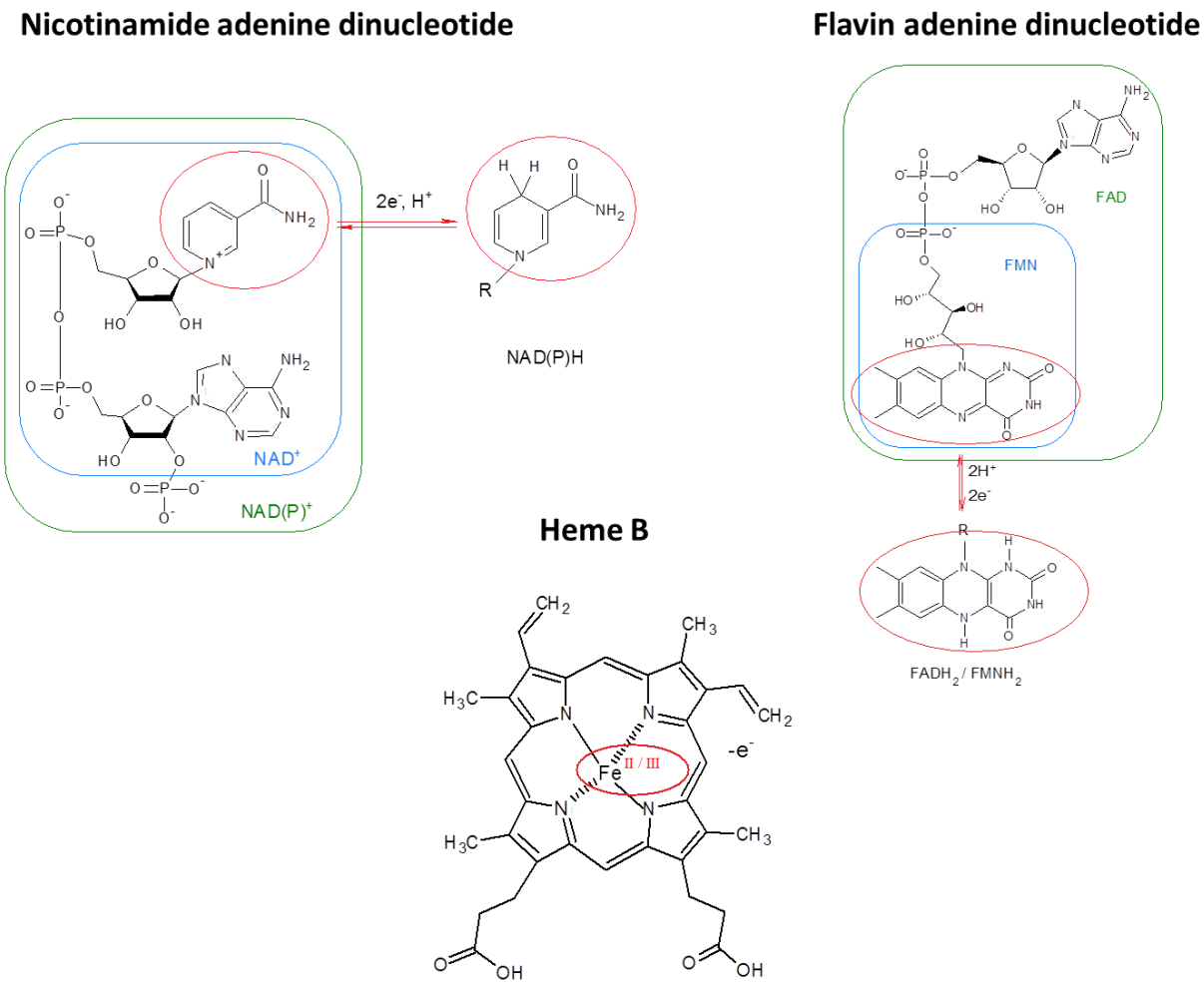

Figure 1.1. *Structures of some cofactors with their different redox states: (A) Nicotinamide adenine dinucleotide (phosphate); (B)Flavin adenine dinucleotide (mononucleotide); (C) Heme B.*

Efficient regeneration and re-use of the cofactors are required for large-scale synthetic applications [18–20]. Any method for regenerating cofactors has to be practical and should enable an enzymatic process to be inexpensive and convenient. The reaction used for regeneration has to proceed in high yield and the total turnover numbers (TTN) for the cofactor must be high. Cofactor regeneration will facilitate the thermodynamically and kinetically favorable product formation. Any reagents or by-products of the regenerative system must not interfere with isolation of the desired product. Methods including chemical, electrochemical, photochemical, microbial and enzymatic reactions have all been developed

for cofactor regeneration [18–20]. Chemical regeneration of cofactor can be realized by introducing reducing agents (e.g. sodium dithionite, sodium borohydride, H_2, etc.) or chemical oxidants (e.g. O_2) into the system. However, this method suffers from low TTN and low selectivity, along with the purification difficulties [21]. Enzymatic approaches are favored for industrial processes due to their high selectivity and efficiency. There are two different ways to achieve enzymatic regeneration. One is through the use of substrate-coupled reaction systems, in which only one enzyme is used and both the reduced and oxidized forms of a cofactor are applied to catalyze both the desired product and another molecule. The other way to catalyze the cofactor regeneration reaction is through the use of a second enzyme (enzyme-coupled reaction systems), which has been adapted for the majority of cofactor regeneration processes. This usually affords broader options of substrates for the cofactor regeneration reaction, and thus makes it much easier to achieve large thermodynamic driving forces for both reactions. Enzymatic methods usually lead to high turnover number. The reaction takes place under mild conditions. A disadvantage is the high cost of protein as well as the possible inhibition effect and purification difficulties coming from the second substrate [20].

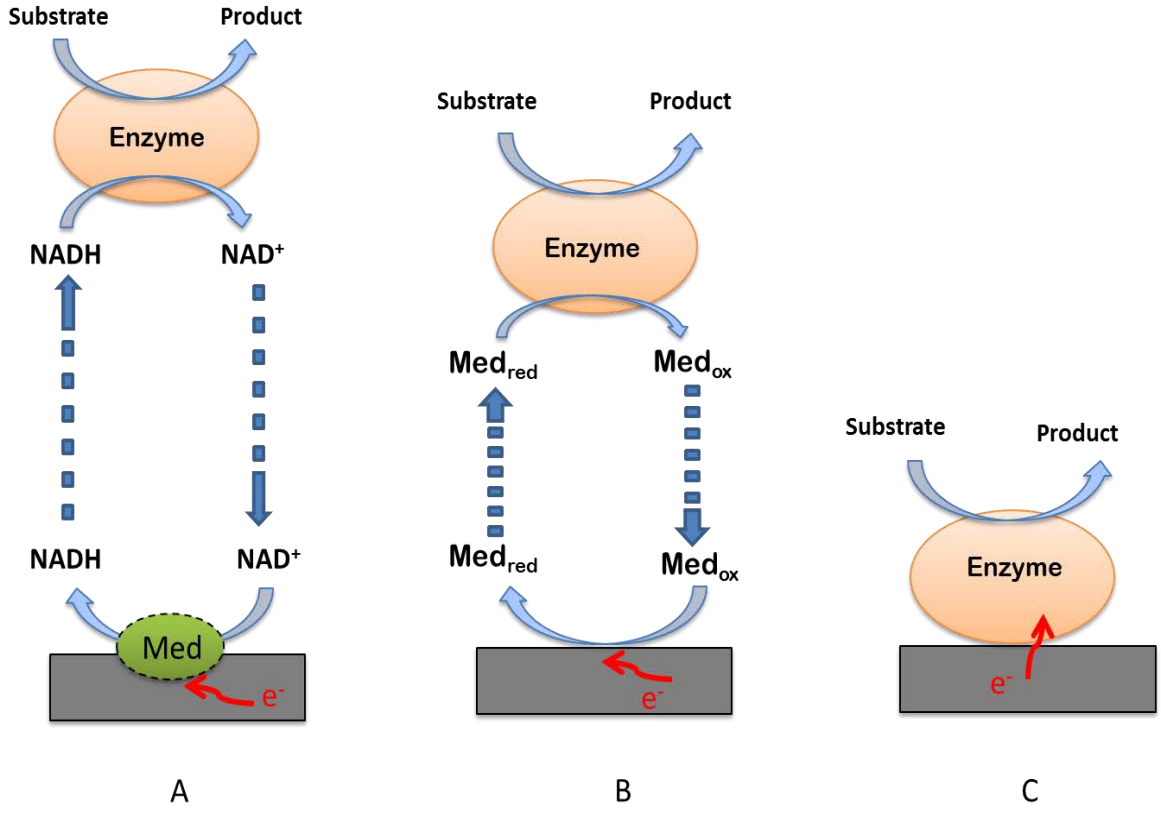

Figure 1.2. *Schematic representation of three bioelectrochemical routes for redox enzymes: (A) Electrochemical regeneration of diffusing cofactors for NAD(P)-dependent proteins using proper molecular catalyst or a second redox protein; (B) Electrochemical regeneration of enzyme bounded redox cofactors through a mobile mediator; (C) Direct electron transfer with the protein redox center at the electrode surface.*

Compared to the two aforementioned methods, electrochemical regeneration is a continuous electron-transfer process, the regeneration equivalents are only provided by the electrode. As the purification step could be largely simplified, electrochemical regeneration method has great potential in enzymatic synthesis. **Figure 1.2** reports three different electronic pathways that can be encountered in bioelectrochemistry of redox proteins. With NAD(P)-dependent proteins such as dehydrogenase, the cofactor is freely diffusing in the solution and can thus be regenerated at the electrode surface when using the proper catalyst (Figure 1.2A), either molecular or enzymatic (see section 2.1). Other redox proteins (oxidase, cytochrome…) possess a bound redox cofactor and its regeneration implies either a mediated electron transfer with a mobile mediator, shuttling the electrons between the cofactor and the electrode (**Figure 1.2B**), or in some cases a direct electron transfer with the protein redox center at the electrode surface (**Figure 1.2C**).

In general, "enzymes are versatile catalysts in the laboratory and on an industrial scale. To broaden their applicability in the laboratory and to ensure their (re)use in manufacturing the stability of enzymes can often require improvement. Immobilization can address the issue of enzymatic instability. Immobilization can also help to enable the employment of enzymes in different solvents, at extreme pH and temperature values and exceptionally high substrate concentrations" [22]. Furthermore, in electroenzymatic synthesis, the local concentration of enzymes on the electrode can be significantly increased, which can facilitate electron transfer reactions [23]. Therefore, immobilization of enzymes on electrodes offers a possibility to improve the efficiency of the bioelectrochemical system. In addition, the immobilization of electron mediator can be advantageous in order to limit the quantity of molecule needed (increasing the total turnover), to promote their reusability and limit the need for further purification steps. **Table 1** is a summary of some investigations carried out in the field of electroenzymatic synthesis with immobilized redox enzymes or mediators on electrodes, providing the enzymes involved and their cofactor, the target reactions, the mediators used, the electrode materials, the strategies for protein or cofactor immobilization as well as some information available about the bioconversion process. In the first section of this chapter, we

will discuss the most typical target reactions that have been used in electroenzymatic synthesis for different classes of redox enzymes according to their redox cofactor: NAD(P)-dependent-redox enzymes, flavoenzymes and metal complex-based cofactors from cytochromes or tyrosinase (heme, copper, …). The purpose is not to provide an exhaustive view of the bioelectrochemistry of these redox proteins that have been covered by specific reviews in others fields such as enzymatic biosensor [24] and enzymatic biofuel cell [25], but to provide a detailed description of their application in electroenzymatic synthesis, focusing on the strategies used to immobilize the enzyme and/or the mediator.

1.2 Enzymatic systems, cofactor recycling and target reactions

1.2.1 NAD(P)-dependent-redox enzymes

Both nicotinamide adenine dinucleotide phosphate ($NADP^+$/NADPH) and nicotinamide adenine dinucleotide (NAD^+/NADH) have been used in electroenzymatic synthesis. These different forms of the nicotinamide adenine dinucleotide cofactor display similar electrochemical properties. For this reason, the discussion will be focused on the regeneration of NAD^+ or NADH and all considerations and conclusions could be, in principle, applied to $NADP^+$ and NADPH.

The electrochemistry of NAD^+/NADH is highly irreversible, and the oxidation of NADH or the reduction of NAD^+ at a bare electrode only occurs at high overpotential. Several efficient methods have been developed for cofactor regeneration. Synthesis where the cofactor NAD^+/NADH has to be regenerated to its oxidized/reduced state can be carried out with direct, indirect and enzyme-coupled electrochemical cofactor regeneration [4]. Direct regeneration means that the species to be regenerated itself reacts at the electrode, however, it can result in inactivation of the cofactor [5]. Indirect regeneration means that a mediator catalyst acts as an electron shuttle between the electrode and the cofactor and decreases the overpotential of the electrochemical reaction. Different molecules are involved to catalyze either the oxidation of NADH or the reduction of NAD^+. If a second enzyme is used, eg. diaphorase, the process is called enzyme-coupled electrochemical cofactor regeneration. With few exceptions that will be discussed in the section related to electrode materials (section 3), direct regeneration is not used in practice, so the discussion will be mainly focused on indirect

regeneration and enzyme-coupled electrochemical cofactor regeneration. Both NADH and NAD^+ regeneration will be discussed in the following sections for electrosynthesis applications.

1.2.1.1 NADH regeneration by NAD^+ electrochemical reduction

In NADH regeneration process, NAD^+ reduction occurs through two discrete $1e^-$ steps with a radical protonation process concerted with the second electron transfer [5]. The first electron transfer to NAD^+ is a reversible process. However, the dimerization of the NAD radical is more favorable than the second electron transfer in a direct electrochemical reduction [26] and the enzymatically inactive NAD^+-dimers can be formed, resulting in the degradation of the electro-regeneration system [3,4,27]. In consequence, it is critical to avoid the formation of electrochemically inactive NAD-dimers, and indirect NADH regeneration methods have been developed.

The non-enzymatic indirect regeneration of NADH consists of using a mediator catalyst who could transfer two electrons in one step [3]. As the formal potential of the NAD^+/NADH redox couple is −0.56 V (vs. SCE), which means catalytic reduction of NAD^+ into NADH is thermodynamically favorable when the potential is more negative than -0.56V [5], to avoid direct electrochemical regeneration, the operating window of the mediator should be in the potential window between −0.56 V and -0.9 V. Many efforts have been made to find the appropriate mediator.

$Rh(bpy)_3$ was the first kind of rhodium-based mediator used for indirect electrochemical regeneration of NADH. The synthesis of cyclohexanol from cyclohexanone catalyzed by alcohol dehydrogenase in the presence of this mediator was carried out [28] and its electropolymerized form on the electrode was also tested [29]. Later on, the mediator selectivity has been highly improved up to 99% when the pentamethyl cyclopentadienyl (Cp*) ligand was incorporated. After the first electroenzymatic synthesis from pyruvate to lactate in the presence of $[Cp^*Rh(bpy)Cl]^+$ catalyzed by D-Lactate dehydrogenase, it was later combined with alcohol dehydrogenase to synthesize different products (e.g. cyclohexanol [30,31], (S)-4-phenyl-2-butanol [32], (R)-phenylethanol [33], L-malate [34]). Besides, $[Cp^*Rh(phen)Cl]^+$ with a 1,4-phenanthroline ligand instead of 2,2'-bipyridine ligand was also proved to be efficient in electroenzymatic synthesis of L-glutamate [35]. Moreover,

polymerized neutral red (NR) film (at a potential of -0.6V vs. SCE) was also successfully applied to NADH regeneration [36].

The enzymatic electrochemical regeneration of NADH consists on the combination of a NAD-dependent dehydrogenase with a second enzyme (usually a flavoenzyme) in the presence of a mediator to prevent the dimer formation. If one refers to **Figure 1.2**, the electron transfer pathway of the dehydrogenase is described by **Figure 1.2A**, while the electron transfer pathway of the second enzyme is described by **Figure 1.2B**. The most commonly used regeneration enzymes include diaphorase [37–39], lipoamide dehydrogenase [31,39,40], ferredoxin $NAD(P)^+$ reductase [40,41], and AMAPORS (artificial mediator accepting oxidoreductases) [42]. Then the electron mediators like viologen derivatives [31,37–42] and flavin [43,44] or quinone [45] have been used to mediate the electron transfer reaction from the electrode to the flavin adenine cofactor of the enzymatic catalyst. Electrons were then transferred to the NAD^+ cofactor in the enzyme catalytic site. Some redox enzymes can also directly communicate with electrode supports (as schematically drawn in **Figure 1.2C**) and thus stimulate the regeneration of the NADH cofactor. Hydrogenases (from *Rhodococcus opacus* and *Atcaligenes eutrophus* H16) have been successfully applied for the bioelectrocatalytic regeneration of NADH without the use of a redox-mediator [46–49] and have been applied to the bioconversion of alpha-ketoglutarate into L-glutamate catalyzed by an L-glutamate dehydrogenase [50]. However, the absence of protein confinement at the electrode surface was pointed out at that time as a limit of the experiment. More recently, isolated diaphorase fragment has been described as a catalyst for regeneration of NADH in the presence of H_2 and hydrogenase on pyrolytic graphite [51,52] and direct electron transfer reaction starts to be explored for NAD^+ - NADH interconversion by Escherichia coli flavohemoglobin [53].

D-lactate is by far the most studied target. It is an important product in industrial manufacture (e.g. cosmetic, food), that can be synthesized from pyruvate in the presence of D-lactate dehydrogenase [54–64]. The conversion of cyclohexanone to cyclohexanol [30,31,65], acetophenone to (R)-phenylethanol [7,33], and 2-methyl-cyclohexanone to (1S,2S)-(+)-2- methylcyclohexanol [37] have also been reported. The synthesis of (L)/(S)-glutamate which is a compound used as flavor enhancer and applied in pharmacology have been carried out with the redox enzyme glutamate dehydrogenase [35,40,42,50,66].

1.2.1.2 NAD^+ Regeneration by NADH electrochemical oxidation

The potential of direct NADH oxidation is close to 0.9 V (vs. SCE) [4]. The electroenzymatic synthesis using direct NAD^+ oxidation has been applied in the conversion of alcohol to aldehyde in the very early stages of electroenzymatic synthesis [67]. The production of gluconic acid from glucose catalyzed by glucose dehydrogenase using this direct electrochemical oxidation of NADH was also reported [68]. But, the overpotential for this reaction can be dramatically decreased in the presence of a mediator electrocatalyst, as commonly used in biosensors [24]. It prevents the risk of side reaction that could occur when the electrode surface is poised at a high potential. If a mediator is introduced in NAD^+ regeneration, the mechanism of the mediated electrochemical regeneration of NAD^+ can be described in the following steps: first, the mediator is oxidized by applying a suitable potential; then the reduced NADH is oxidized by the oxidized mediator [69], the mediator itself will go back to its reduced form; finally, the reduced mediator will be oxidized again on the electrode, in the meantime, the oxidized NAD^+ will participate in the enzymatic reaction. An additional possibility to regenerate cofactors is through photoelectrochemical methods [70,71], but this approach has not been applied in the field of electroenzymatic synthesis yet.

Different mediators have been used for indirect electrochemical regeneration of NAD^+ in electroenzymatic synthesis [5,21,72]. Two-electron mediators are the most commonly found, like bipyridine and phenanthroline metal complexes [73,74], azine dyes like methylene green [75] or phenazine methosulfate [76], 4-carboxy-2,5,7-trinitro fluorenyliden-malonnitrile [77], 3,4- dihydroxybenzaldehyde [78]. Another kind of mediators for NAD^+ regeneration are based on single-electron transfer processes like 2,2‟-azinobis(3-ethylbenzothiazoline-6-sulfonate) (ABTS). Compared to two-electron based mediators, one-electron mediator was reported to be more stable under basic conditions, which could be suitable for some large scale synthesis [79]. It is also possible to combine indirect regeneration of NAD^+ with an enzymatic regeneration step. For example, diaphorase has been applied to oxidize NADH using a variety of quinone compounds [45], ferrocene derivatives [80,81], or osmium redox polymers [82].

By using different mediators as electron carriers, a variety of substrates catalyzed by different NAD-dependent enzymes are obtained. The production of gluconic acid catalyzed by glucose dehydrogenase [78] or glucose-6-phosphate dehydrogenase [76] were reported. Alcohol dehydrogenase has been applied on different substrates to regio-selectively oxidize

alcohols to corresponding carbonyl group products (e.g. cyclohexanone [73,80,83], 2-butanon [84]). Glycerol dehydrogenase was applied to synthesize (S)-Phenylethane-1,2-diol [85]. D-sorbotol dehydrogenase was used for D-fructose production from D-sorbitol [75]. Moreover, there are examples suggesting the electrosynthesis of D-sorbose catalyzed by ribitol dehydrogenase [86] and hydroxyacetone with galactitol dehydrogenase [77].

1.2.2 Flavoenzymes

Flavoenzymes contain a flavin nucleotide (FMN or FAD) as a prosthetic group. Glucose oxidase is a typical flavoenzyme which has been used for gluconic acid production in the presence of oxygen, however, hydrogen peroxide which is consequently formed could deactivate the redox enzymes. In some system, the conversion rate of glucose was significantly improved (from 4% to 30% [87]) by eliminating the H_2O_2 through electrochemical method, by which the H_2O_2 was oxidized back to O_2 [31,88,89]. However, for the majority of flavoenzymes applied in electrosynthesis, the bioprocess was accomplished by electrochemical regeneration of cofactor FAD or FMN using an electron mediator (see **Figure 1.2B**). For example, instead of using oxygen, when benzoquinone was introduced into the system, the formed hydroquinone was electrochemically regenerated back to benzoquinone. The operational stability for gluconic acid production was increased in this case by a factor 50 [90]. p-Cresol methylenehydroxylase and 4-ethylphenol methylenehydroxylase have been applied for synthesis of 4-hydroxybenzaldehyde or 1-(4-hydroxy phenyl)ethanol in the presence of ferrocene as electron mediator, a high TTN up to 400000 and a high conversion rate up to 100 % were achieved in the electrochemical bioreactor [91]. Ferrocenedimethanol was used for wiring membrane-bounded (S)-mandelate dehydrogenase (S-MDH) which is a FMN associated enzyme and applied to the catalytic conversion of (S)-mandelic acid to phenylglyoxylic acid in order to separate (S)-mandelic and (R)-mandelic [92]. In electroenzymatic reduction, l-aminopropyl-1 methyl-4,4'-dipyridine (ADPy) amino acid oxidase (AOx) was used in the production of D-alanine from pyruvic acid. The conversion was almost total and a TTN more than 36000 was achieved for immobilized ADPy [93].

1.2.3 Metalloproteins

Most of the metalloproteins used in electroenzymatic synthesis contain a heme prosthetic group with a central iron atom (see an illustration in **Figure 1.1C**). Cytochrome P450 (CYP) is a representative class of heme-containing monooxygenase enzymes responsible for oxidative metabolism of most drugs and xenobiotics [94]. For most applications, CYP needs to be immobilized on the electrode to benefit from direct electron transfer in electrochemical regeneration as shown in **Figure 1.2C.** The immobilization is not only necessary for stabilizing or recycling the enzyme (as for dehydrogenases and flavoenzymes), it is also a requirement for electrochemical recycling of the electroactive redox cofactor. CYP catalysis route is a two electrons transfer process, a catalytic cycle using electrochemistry as driving force is illustrated in **Figure 1.3** [95]. The first electron is used for heme reduction, then the reduced iron group is associated with the co-substrate O_2. The second electron is further used for reducing the oxygenated heme, forming the target product in the presence of protons.

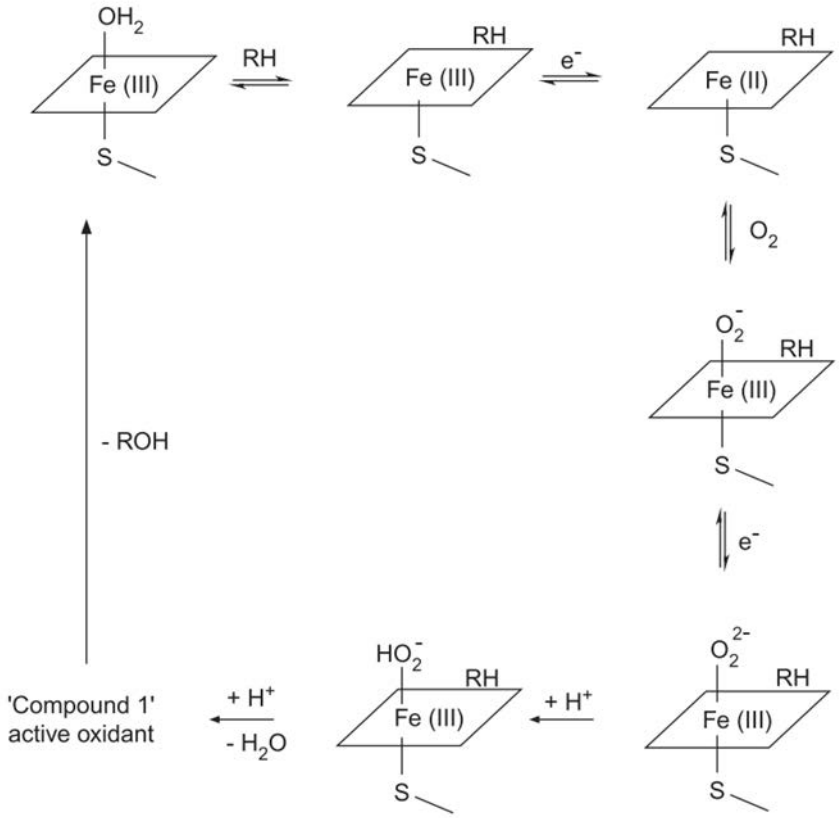

Figure 1.3. *Illustration of two-electron transfer steps in electrochemical catalytic cycle of P450 enzymes [95].*

CYP 119 was used for electrocatalytic reduction of nitrite to ammonia. This is a two steps electrocatalytic process with two redox peaks corresponding to the reduction of nitric oxide and production of ammonia [96]. Human CYP 2E1 enzyme was immobilized on gold electrode surface for synthesizing p-nitrocatechol by applying a potential of -500 mV (vs. Ag/AgCl) for 30 min [97]. Hydroxylation of 3-phenoxytoluene was catalyzed by immobilized CYP BM-3 by applying a potential of -0.7V (vs. SCE), showing the possibility of using electrochemical method as electron donor [98]. The same protein was also used for synthesis of p-nitrophenolate by hydroxylation of p-nitrophenoxycarboxylic acid [99]. Not only single enzymes have been considered in electrosynthesis but also bi-enzymatic systems have been studied. Recently, a work combining two species of cytochrome P450, CYP1A2 and CYP3A4, on an electrode was described. Two redox peaks of the bi-enzyme complex were observed at -0.531V and -0.474V respectively. Clopidogrel carboxylic acid was then obtained as metabolite [100]. Instead of using the direct electrochemical reduction of the P450 redox center, Rusling et al. reported the combination of a human cytochrome P450 / cytochrome P450 reductase (CYP/CPR) in a bioelectronic film on pyrolytic graphite electrode. They developed the idea that electrons could be delivered from cytochrome P450 through CPR [101].

Chloro-peroxidase is another family of enzymes containing heme cofactor that catalyzes the chlorination of organic chemicals. In a CPO-containing composite film functionalized electrode, H_2O_2 which was used for catalytic oxidation cinnamyl alcohol to produce aldehydes was constantly generated by the electrochemical reduction of O_2, giving a high yield of 52 % and TTN of 80500 [102]. H_2O_2 can also be provided for this enzyme by a gas diffusion electrode (GDE) [103,104]. The role of electrochemistry was not to provide electrons to the redox center of the enzyme, but to regenerate a co-substrate of the enzymatic reaction, production that could be carefully tuned by electrochemistry. GDE with chloroperoxidase (CPO) catalyzed system has also been employed for monochlorodimedone chlorination [105], halogenation of the phenolic monoterpenes thymol and carvacrol [106].

A final example of redox enzyme is tyrosinase which contains a coupled binuclear copper active site that has been used as catalyst for hydroxylation of L-tyrosine to L-3,4-dihydroxyphenylalanine (L-DOPA). Tyrosinase catalyzed the ortho-hydroxylation of l-tyrosine to l-DOPA by its cresolase activity, and subsequently also catalyzed the oxidoreduction of l-DOPA to DOPAquinone by its catecholase activity. The by-product DOPAquinone was then electrochemically reduced to L- DOPA [107,108]. According to the

authors, this electroenzymatic system, showed the highest conversion rate and a highly enhanced productivity if compared to other approaches for l-DOPA synthesis reported previously.

1.2.4 Electrode materials

Several factors could limit the efficiency of a biosystem to be applied for a bioreactor [109], among them the electrode materials is an important factor. Metal, metal oxides and carboceous materials were used, as a flat or as a porous electrode.

1.2.4.1 Metals

The use of platinum electrodes is mostly encountered in membrane electroenzymatic reactors in which the enzymes stay in solution [31,54,65,87]. It has been reported that the adsorption of some hydrogenases on a platinum electrode would yield efficient catalysis for NAD^+ reduction [47,48]. The usage of platinum is expected to decrease the regeneration potential in the presence of *Alcaligenes eutrophus* H16 hydrogenase. However, the working potential window of platinum is quite limited since hydrogen evolution often occurs in the range of NAD^+ reduction. Another kind of applicable metal electrode is gold, even though it suffers from the similar hydrogen evolution problem in reduction reactions, it offers a possibility to modify the electrode surface by means of the formation of a self-assembled monolayer with thiol containing molecules [9,77,97]. The use of macroporous gold electrodes was also suggested in order to take advantage of the high porosity which would facilitate the mass transport through the electrode macrostructure to favor electrochemical bioconversion processes [110–112]. Finally, platinum and nickel nanoparticles deposited on a glassy carbon electrode were recently evaluated for NAD^+ reduction. The role of Pt and Ni was to provide 'active' adsorbed hydrogen (Pt-H_{ads} or Ni-H_{ads}) for the fast protonation of electrochemically formed NAD-radical. The authors could demonstrate that up to a 100% recovery of 1,4-NADH from NAD^+ was possible on the produced electrodes at relatively low potentials, making them excellent candidates for regeneration of 1,4-NADH in industrial bioreactors [113]. The same research group also tested other electrode materials (Ti, Ni, Co and Cd) [114].

1.2.4.2 Metal oxides

Tin (IV) oxide electrode was prepared using an anodization and annealing method and was used for mediator free electrochemical cofactor regeneration. Both oxidation of NADH and reduction of NAD^+ were studied. The electrochemical oxidation of NADH and NAD(P)H were performed at -0.5 V versus a Ag/AgCl reference electrode. The NAD^+ reduction was performed at -0.95 V. Only the NAD^+ regeneration was however applied to electroenzymatic reaction. The authors suggested that the method can be applied to various cofactor-dependent enzyme reactions for chemical production, biosensor or enzyme fuel cell construction [115]. A thermally prepared iridium/ruthenium-oxide coating (Ir0.8Ru0.2-oxide) formed on a titanium substrate was also proposed as a possible electrode for direct electrochemical regeneration of enzymatically-active 1,4-NADH from its oxidized form, NAD^+. The coating surface was characterized by „cracked mud" morphology, yielding a high surface roughness. The percentage of enzymatically-active 1,4-NADH present in the product mixture was strongly dependent on the electrode potential, reaching a maximum (88%) at -1.70 V versus a mercury/mercurous sulfate reference electrode [116]. The use of conductive vanadia-silica gels with encapsulated GDH was also reported for NADH regeneration, allowing complete conversion of alpha-ketoglutarate to l-glutamate [66].

1.2.4.3 Carbon materials

Carbon materials are widely used due to their low cost, large potential window, relatively inert surface, and active electrochemical properties for redox reactions [117]. Compared to metal electrodes, different carbon materials exhibit different microstructure as well as surface functional groups, leading to different electrochemical behaviors. There are already reviews exhaustively explaining the interfacial as well as the electroanalytical properties of carbon materials [117,118]. Here, we only focus the discussions on the application of carbon materials as electrodes in the electroenzymatic synthesis with immobilized proteins.

Carbon paste electrodes (CPE) have also been used after its introduction in 1958. Basically, it is made from a mixture of carbon powder with a liquid non-electroactive binder. The carbon paste could be „modified" by adding one or more components (e.g. enzymes or mediators) [119]. The CPEs are popular because they are easily obtained at minimal costs and

certain electrode properties can be pre-determined by adding additional admixtures [120]. It can be applied for encapsulation of enzymes on electrode [121]. However, its properties differ from one preparation to another and limit their applications.

The most conventional carbon electrode is glassy carbon (GC), its use is convenient since its surface is renewable by polishing. As it is a flat electrode with uniform functional groups on the surface, it is a good candidate to be covalently modified for bounding enzymes or molecules [63,93], or deposited with uniform membranes [57], nanoparticles [113] or films [86,98,99]. If the GC is produced as a foam, it is then called reticulated vitreous carbon (RVC), which also been used in electrochemical bioreactors [55,58].

Porous carbon felt (CF) electrodes have been largely used electrode in the field of electroenzymatic synthesis, taking benefit from their low-cost and large surface area, which lead to high current density and high conversion efficiency. CF electrodes have been used as working electrodes in electroenzymatic synthesis reactors with dialysis [30,31,65] or ultrafiltration membranes [91]. From another point of view, the functional groups on the surface make it an appropriate substrate for surface modification, which could be further used for different covalent reactions. CF was used for example as electrode support for immobilization of enzymes with carbodiimide or glutaraldehyde as linking agent [33,64,90].

Furthermore, to increase the surface area as well as the biocatalytic property of the electrodes, carbon nanoparticles [107,108], carbon nanotubes [75], graphene nanosheets [122] and graphene oxide nanocomposite [100], allowed to improve significantly the efficiency of the electroenzymatic synthesis system by increasing the enzyme loading and/or by tuning some electrochemical properties.

1.3 Immobilization of enzymes on electrodes

In the past years, different strategies have been developed to build enzyme-immobilized electrodes [23,123]. There are several conditions that need to be fulfilled in enzymes immobilization. First, the activity of enzymes needs to be kept upon immobilization. Second, the stability of enzymes towards microenvironments on the electrode needs to be ensured. Usually, adsorption is the easiest method for enzyme immobilization, but it is inappropriate for bioconversion, because the electrosynthesis process requires long-term stability especially when the solution is under continuous stirring, the adsorbed enzymes would be rapidly leached out into the solution. In the field of electro-enzymatic synthesis, the

immobilization methods that have been typically used are membrane confinement in a small volume at close distance from the electrode (**Figure 1.4A**), surface immobilization with chemical bonding (**Figure 1.4B&C**) and encapsulation (**Figure 1.4D-F**). The next sections will provide a discussion of these different strategies.

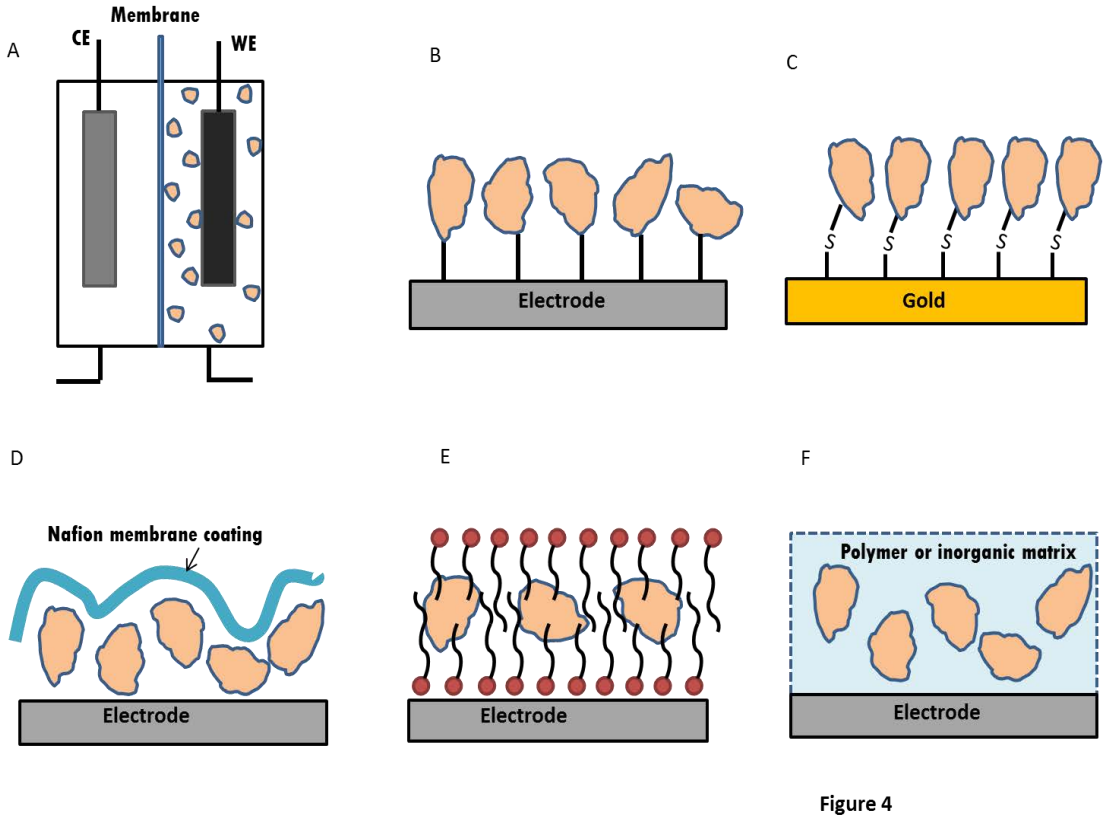

Figure 1.4. *Typical enzyme immobilization methods on electrodes (A - F): (A) Membrane confinement; (B) Covalent bonding; (C) 'Thiol-gold' self-assembly monolayer; (D) Nafion membrane coating; (E) Surfactant film embedding; (F) Encapsulation in solid matrix.*

1.3.1 Membrane confinement with membranes

Membrane confinement is a simple way to immobilize enzymes in an electrosynthesis bioreactor. The enzymes are confined in solution near the electrode without any physical or chemical modification, but only soluble redox enzymes can be immobilized by this method. Generally, two kinds of membrane configuration are used for immobilization: dialysis or

ultra-filtration membrane. The formation of a Nafion coating on an electrode surface can be considered as a surface confinement comparable to encapsulation and will be discussed in another section.

Commercial dialysis or ultra-filtration membranes have been used inside a bioreactor [30,31,54,56,59–61,65,67,68,87,91]. These membranes are made of different kinds of materials, e.g. cellulose [30,31,54,65,87], hollow fiber [67], Nafion 117 [55,56,60,61,68]. Generally speaking, the ability to immobilize the enzyme is dependant on the pore size of the membrane. Enzymes larger than the membrane cutoff value are confined in the membrane near electrode and small molecules can freely pass through the membrane.

In a dialysis membrane reactor (D-MER), the transport of compounds through the membrane was mainly due to the gradient of concentration, while in ultra-filtration membrane UF-MER, solution passing through the membrane in a direction perpendicular to the electrode was driven by a pressure gradient. The influence of flowing mode on the transformation rate in a bioreactor has been studied. An ultrafiltration-membrane electrochemical reactor (UF-MER) (**Figure 1.5A**) was compared with D-MER (**Figure 1.5B**) in synthesis of cyclohexanol by alcohol dehydrogenase with $[Cp(Me)_5Rh(bpy)Cl]$ as mediator. The transformations rate in these two configurations are compared in **Figure 1.5C**, leading to 92% in 45 days for D-MER and 100% in 3 days for UF-MER. UF-MER was the more efficient reactor configuration, and a limiting step in D-MER was observed: the inhibition of the enzyme by increasing concentration of the products at the end of the electrolysis [30].

In an early stage, membrane confinement of redox enzymes has been used in the bioreactor with direct electrochemical regeneration of NAD^+. Coughlin et al. use a continuous-flow reactor with ultra-filtration membrane to confine NAD-dependent alcohol dehydrogenase for direct electrochemical regeneration of NAD^+ in electro-synthesis of aldehyde from alcohol. Compared with dialysis, the ultra-filtration membrane was able to keep the cofactors and enzymes persistently in the continuous-flow process, while the products left the system through the membrane [67]. Later on, the confinement of glucose dehydrogenase in a dialysis Nafion membrane reactor for synthesis of gluconic acid with direct regeneration of NAD^+ was also achieved [68]. To avoid the large overpotential which may cause inactivation of the cofactor, diffusing mediators were added in the system afterwards to facilitate the electron transfer between electrodes and cofactors [68].

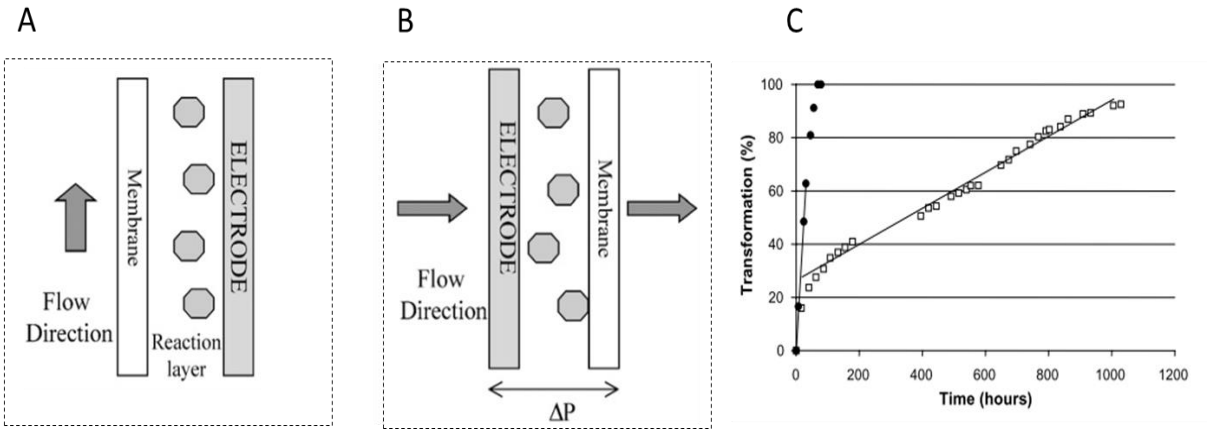

Figure 1.5. *(A, B) Schematic discription of (A) Dialysis-membrane electrochemical reactor (D-MER) and (B) Ultra-filtration-membrane electrochemical reactor (UF-MER). (C) Comparison of the transformation of cyclohexanol obtained with the D-MER (square) and the UF-MER(circle) with recycling [30].*

When mediators were added into the system, the membrane could be used to confine only the redox enzymes [30,31,60,65], or enzymes together with mediators [54,56,61,91]. The confinements of the mediators were achieved by coupling it with large size polymers in order to achieve a size larger than the cut-off of the membrane. In an electro-enzymatic membrane flow cell, ferrocene was for example modified with polymers and immobilized together with p-cresol methylenehydroxylase or 4-ethylphenol methylenehydroxylase for electrosynthesis of 4-hydroxybenzaldehyde or 1-(4-hydroxy phenyl)ethanol. Turnover numbers up to 400,000 were achieved in a continuous synthesis [91].

In addition, in an enzymatic NADH electroregeneration system, two kinds of redox enzymes could be co-immobilized. The regeneration coenzyme LipDH and the NAD-dependent lactate dehydrogenase used for lactate synthesis were confined together inside the cellulose membrane (12 -14 kDa cutoff). In this case, the substrate, cofactor, as well as the low molecular weight mediator methyl viologen could be freely transferred in the system. The substrate alpha-keto acid (2.5 mmol) was converted at 95% after 8 days with constant addition of new lipoamide dehydrogenase every 2 days, and the product was obtained with

98% enantiomeric excess which was comparable to that obtained in a non-membrane system [54].

1.3.2 Chemical bonding

Compared to adsorption, the leaching of enzymes from electrode was minimized with covalent bonding and long-term stability was ensured. Generally, the chemical reaction occurred between the functional groups on the electrode surface and active amino acid residues of the enzyme. But an obvious disadvantage of covalent binding is that enzyme itself is chemically modified when immobilized, if essential amino acid residues close to the enzyme active site are involved in the chemical reaction, enzyme activity might be reduced. So when covalently immobilizing the enzymes on electrodes, physical and chemical nature of the electrode, the nature of the linkage or binding chemistry, and even enzyme orientation need to be considered [8].

Different kinds of carbon materials (carbon felt [33,64,90], graphene felt [78], graphene oxide nanocomposite (RGO) [100], carbon nanopodwer [107,108], rotating disc graphite [76], glassy carbon [63,93]) can be used for covalent immobilization of enzymes in the field of electroenzymatic synthesis. These carbon materials have advantages such as chemical and physical stability, large surface area, and rich surface functional groups. It is already reported that several chemical methods could be applied for covalent immobilization of enzymes [124,125], but the chemical reactions that have been used in the electroenzymatic synthesis are quite limited. The generally used methods include carbodiimide [64,90,107,108], and glutardialdehyde crosslinking [33,63,93]. Sometimes the carbodiimide and glutardialdehyde are used together in two successive steps [76,78,100]. On gold electrode, self-assemble monolayers could be also involved [77,97].

1.3.2.1 Carbodiimide activation

There are three steps to immobilize the enzymes on electrode surface by means of carbodiimide activation. As shown in **Figure 1.6A**: first, the carbon surface is oxidized to create carboxylic groups, then the carboxylic groups are activated by carbodiimide, meanwhile the active amino group from the enzyme is reacting.

For the production of gluconic acid from glucose oxidase in the presense of benzoquinone in the solution as mediator, the enzyme was covalently immobilized on the carbon felt electrode by carbodiimide [90]. Tyrosinase was immobilized to functionalized carbon nanoparticles via (1-ethyl-3-(3-dimethylaminopropyl) carbodiimide, before being integrated in a 3-D bioelectrode [107,108]. In some systems, both mediator and enzymes could be covalently co-immobilized on the electrode by using carbodiimide. For the electrosynthesis of lactate, the coenzyme viologen-accepting pyridine nucleotide oxidoreductases (VAPORS) combined with viologen directives (DAPV) was co-immobilized on an electrode for NADH regeneration. Different immobilization order of both components were tested, either first covalent binding DAPV to VAPORS then followed by attachment of the DAPV-VAPORS to a functionalized carbon electrode, or covalent binding of the enzyme to viologen functionalized carbon electrode. These different covalent bonding strategies allowed optimization of the enzyme orientation. A relationship was drawn between electron transfer reactions and bioconversion efficiencies [64].

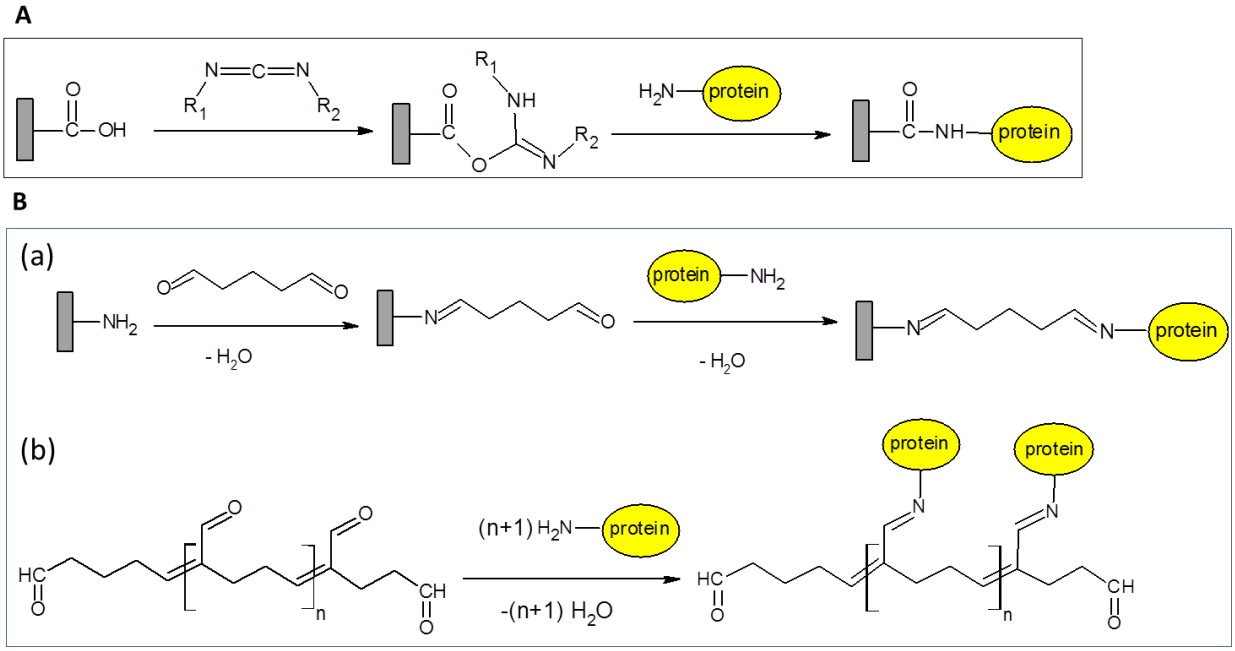

Figure 1.6. *Chemical reactions applied on covalent immobilization of enzymes on electrodes: (A) Carbodiimide; (B) Glutardialdehyde.*

1.3.2.2 Glutaraldehyde crosslinking

Another popular linking agent for covalent immobilization of enzymes is glutaraldehyde. There are two types of possible reactions as shown in **Figure 1.6B.** The first possible process carried out on the amino functionalized electrodes, they can be activated by glutaraldehyde, before the enzymes are covalently attached on the glutaraldehyde functionalized electrode by reacting with surface amino groups. The second possible process is to use glutaraldehyde as cross-linking agent in a polymerization process by reacting with enzyme surface amino groups. Cross-linking provides a facile route to achieve co-immobilization. Amino acid oxidase (AOx) as well as the mediator ADPy were co-immobilized on electrode through glutaraldehyde crosslinking [93]. Co-immobilization of a polymerized viologen and LipDH on electrode by glutaraldehyde crosslinking was also applied in lactate production [63]. In an aqueous–organic two-phase system, alcohol dehydrogenase was covalently bound to porous amino-epoxy sepabeads support (reaction of amine groups from the protein with epoxy groups) and a subsequent cross-linking with glutaraldehyde was used. The enzyme-support preparation was applied to the production of (R)-phenylethanol from acetophenone in the presence of Cp*Rh(bpy) as mediator for NADH regeneration [33]. The stability of the enzyme in a bioreactor was strongly increased after glutaraldehyde treatment, resulting in a half-life time of over 1200 h when stored at 30 °C. This was a 60-fold increase in stability compared to the soluble enzyme [126].

1.3.2.3 Self-assembled monolayer (SAM)

In some applications, enzymes can be bound to a gold electrode surface with a self-assembled monolayer (SAM) due to the interaction between thiol groups and gold. Mak et al. reported the immobilization of CYP2E1 and its mutants on gold electrodes that were first modified with dithio-bismaleimidoethane (DTME) forming a SAM. Then the functionalized DTME electrode was allowed to react with the exposed cysteine group on the enzyme surface. The orientation of the protein was well controlled and better catalytic activity was kept in the presence of the molecular spacer provided by the SAM [97].

A successful immobilization by direct reaction between the thiol group of a cysteine tag on the protein and a gold electrode was also reported. The schematic representation of this electrochemical system is shown in **Figure 1.7A**. Galactitol dehydrogenase modified with a

cysteine tag at the N-terminal of protein surface is immobilized on the surface of an gold electrode by SAM without losing the active configuration of the enzymes, the electroenzymatic oxidation from 1,2-hexanediol to hexane was achieved. This immobilized electrode had a good stability, similar Michaelis-Menten plots were observed after 10 days immobilization at the gold surface (**Figure 1.7B**) [77].

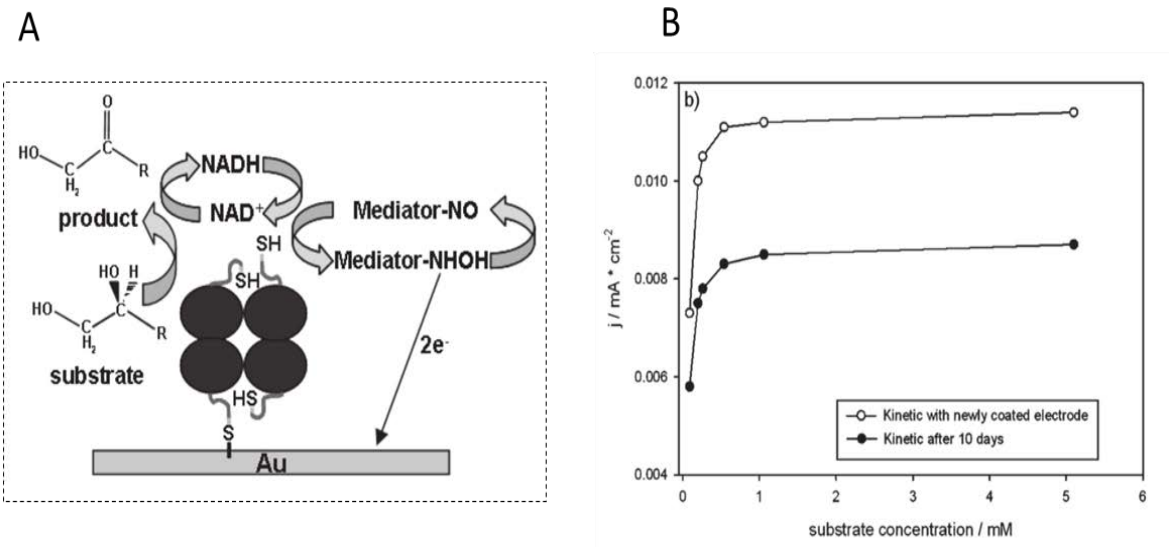

Figure 1.7. *(A) Schematic principle of the immobilization of the cysteine-modified GatDH with electrochemical NAD^+ regeneration for enzymatic synthesis of hydroxyacetone; (B) Michaelis-Menten plots of the current at +500 mV vs the substrate concentrations for GatDH-immobilized electrode before and after 10 days [77].*

Another kind of self-assembled immobilization is based on histidine group of protein. Histidine-tag not only has been widely used in protein purification due to its prominent affinity, but also employed in enzyme immobilization by the interaction between histidine tag and transition metal ion (e.g. Cu^{2+} , Ni^{2+} , Co^{2+} and Zn^{2+}) [10]. This self-assembled immobilization is a reversible process with controlled enzyme orientation. In a bioelectrochemical system for $NADP^+$ production, ferredoxin: $NADP^+$ reductase were immobilized on a modified gold electrode using combination of nitrilotriacetic -Cu^{2+} reaction and SAM. The gold electrode was first covered with a self-assembled monolayer of thiols appended with nitrilotriacetic acid groups complexed with copper complex, then enzymes contains histidine are immobilized through its histidine residues [9].

1.3.3 Encapsulation

The immobilization of proteins by encapsulation can be done either with conductive electrode materials (conducting polymers) or more often with insulating materials such as Nafion, alginate, silica gel or hybrid materials.

1.3.3.1 Nafion coating

Nafion layer from a Nafion solution can be deposited on the top of enzyme modified electrodes [55,57–59,62] as shown in **Figure 1.4C**. This method was generally applied for co-immobilization of enzymes and mediators in electrosynthesis of lactate. The Nafion coating electrode was prepared by first dipping an electrode into the solution containing the enzymes and mediators. After drying, the modified electrode was dipped into a polymer Nafion solution to get a Nafion membrane coating electrode.

In an electroenzymatic synthesis of lactate, MV and LipDH have been confined together on the cathode by a Nafion coating membrane, allowing the extension of LipDH lifetime [58]. Compared to dialysis or ultrafiltration membrane reactors, this kind of coating membrane was easier to prepare, but it had the disadvantage of slow leakage of MV into the solution. As MV species are very toxic which may bring undesirable contamination, a viologen derivative was first chemically attached to LipDH before immobilization on the electrode with a Nafion coating [55,62].

Alternatively, the toxic viologen species could be replaced by a natural redox cofactor such as flavin adenine dinucleotide (FAD). Both electropolymerized FAD or monomeric FAD were immobilized together with LipDH on the electrode by a Nafion coating, a relatively slower conversion rate of lactate was observed when using FAD in place of viologen, but the long-term stability of the enzyme was improved with electropolymerized FAD immobilized electrode, LipDH kept 80% of the initial activity after 30 days with constant performance [57].

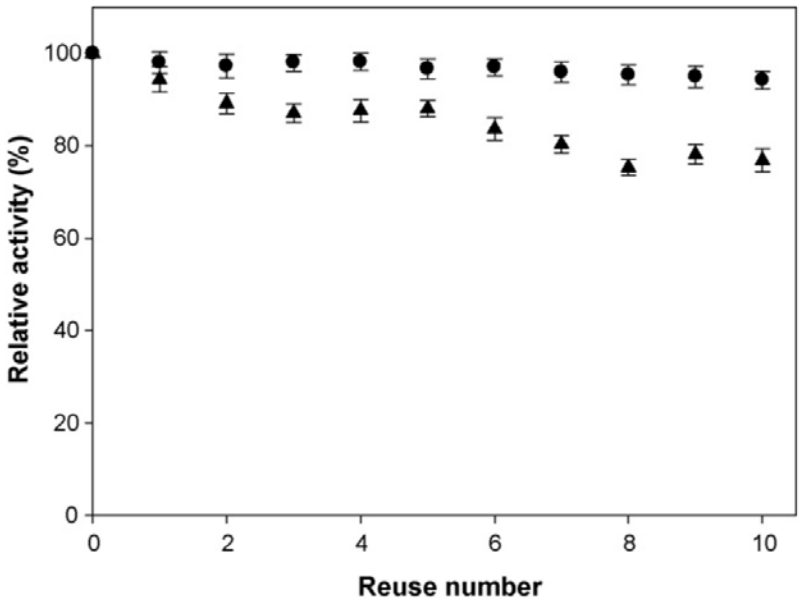

Figure 1.8. *Stability of tyrosinase-immobilized electrode as function of reusenumber (●, tyrosinase–carbon nanoparticle –polypyrrole composite electrode; ▲, tyrosinase-modified carbon felt electrode). Relative activity was measured by synthesized l- DOPA concentration for 4h.*

A comparison of immobilization with a Nafion coating and chemical bonding was recently reported by Min et al. [107] for the bioelectrochemical synthesis of L-DOPA (**Figure 1.8**). The recyclability of the electrode prepare with a Nafion coating (triangles) was much lower, decreasing by 20 % after 10 cycles, than the one observed after glutaraldehyde grafting of tyrosinase on carbon nanoparticles and construction of the 3D bioelectrode with polypyrrole electropolymerization (circles).

1.3.3.2 Surfactant and lipidic layers

The embedding of membrane proteins into a surfactant film is another attempt for immobilization of enzymes for electroenzymatic synthesis (**Figure 1.4E**). The surfactant films are usually consisting of water insoluble alkyl long-chain molecule like didodecyldimethylammonium bromide (DDAB). One approach is to mix the enzyme solution with surfactant vesicles dispersion, then the mixture solution is cast on the electrode, a multilayer film is formed after drying [127]. A CYP119-DDBA film was prepared on an electrode by this approach, its electrocatalytic response toward nitrite reduction to ammonia

was studied [96]. Chloro-peroxidase (CPO)-DDAB film functionalized electrode was also reported for electrooxidation of cinnamyl alcohol to produce cinnamic aldehyde. The lifetime of CPO was extended and a high production yield of 52% and a total turnover number of 80500 for CPO were obtained [102]. Of related interest is the immobilization of lipid vesicles with embedded membrane proteins. A recent study was reported by Mazurenko et al. for the application of mandelate dehydrogenase to electrosynthesis. The lipid vesicles could be simply deposited on glassy carbon electrode, but the stability of the modified bioelectrode was greatly improved by combining this approach with encapsulation in a sol-gel silica matrix [92]. CYP/DDAB liquid crystal system could also be encapsulated in a hydrophobic sol-gel layer before further crosslinking with glutaraldehyde [128].

1.3.3.3 Alginate-based gel and sol-gel silica

An early attempt on enzyme encapsulation is through calcium alginate gels [129]. A carbon felt electrode was soaked in the solution containing enoate reductase and alginate, then it was gelated by calcium ions. This ionotropic gel encapsulation approach not only increased the concentration of enzymes close to the electrode surface, but also significantly increased the half-life of the enzyme up to 350 h in electrochemistry cell under continuous operation.

Silica „sol-gel" process has been used for immobilization of enzymes. The sol-gel process involves hydrolysis and condensation of silica precursors during which the enzymes are incorporated into the gel matrix [125]. This is a mild process for enzymes to retain their structures and activities, and the mechanical properties of silica matrix also facilitate its application in a flow-through reactor [130]. Another advantage of silica sol–gel encapsulation is the successful application of membrane-bound enzymes in electroenzymatic synthesis as discussed in the previous section [92]. When membrane-bounded (S)-mandelate dehydrogenase (S-MDH) was immobilized on electrode by silica gel, a conversion rate of 96% after 9 hour and a high current efficiency of 91% was obtained in the presence of ferrocenedimethanol as mediator. Vanadia-silica gels were also involved to immobilize glucose dehydrogenase [66].

Recently, a proof-of-concept of an enzymatic electrosynthesis reactor containing an immobilized bioanode with D-sorbitol dehydrogenase encapsulated in silica matrix, and an oxygen gas-flow cathode was reported (**Figure 1.9A**) [75] the enzymes immobilized in the

silica film show very good operational stability for two weeks, which was much better than that in solution (half- life period of 48h at 28 ℃). In simultaneous energy production mode, as shown in **Figure 1.9B,** 60% D-sorbitol was converted to D-fructose. Gluconic acid production from glucose was also achieved in a membraneless, flow-through electroenzymatic reactor operating in the mode of co-generating chemicals and electrical energy [131].

Hybrid gel can be used for immobilization of redox proteins. Recently, a bioelectrode was prepared with alcohol dehydrogenases embedded in an alginate–silicate hybrid gel. This study is very intriguing as the authors argue for a direct electron transfer reaction into the biocatalysts for reduction of butyraldehyde to butanol [132], however the reaction should occur in the presence of a NAD^+ cofactor that is not mentioned in the bioelectrochemical reaction.

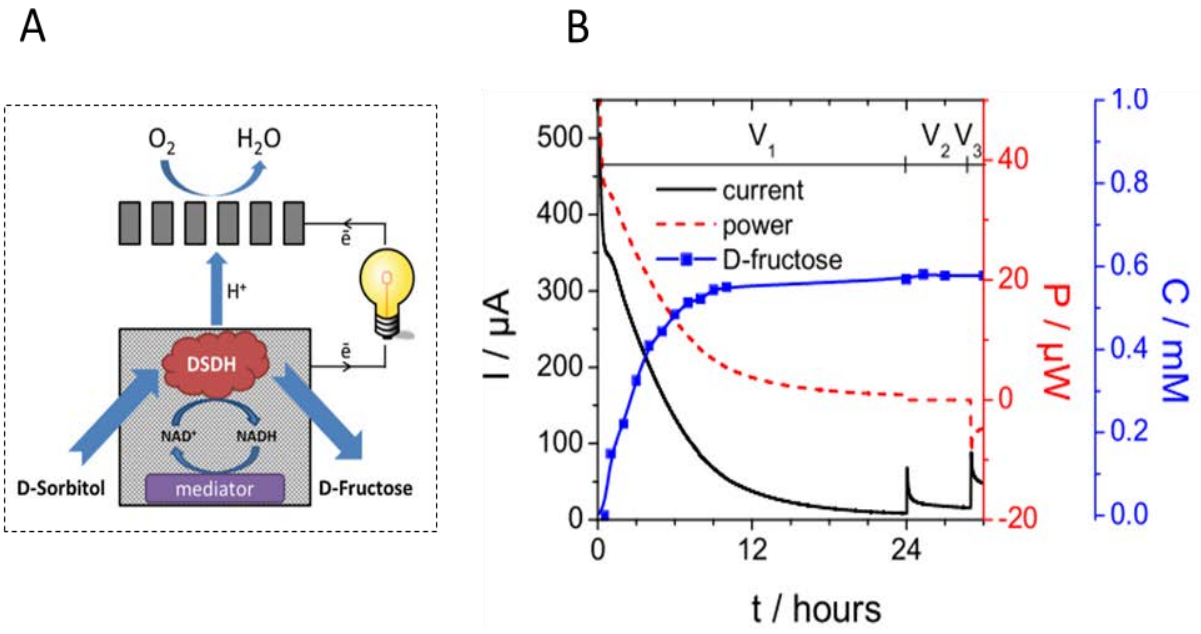

Figure 1.9. *(A) Scheme of the flow bioreactor using D-sorbitol dehydrogenase (DSDH) immobilized bioelectrode as anode while a gas diffusion electrode (GDE) as cathode. (B) Conversion of 1 mM D-sorbitol to D-Fructose in the GDE bioreactor with simultaneous energy production [131].*

1.3.3.4 Conducting polymers

As electrochemistry is involved in enzymatic electrosynthesis, conducting polymers could provide unique advantages allowing both the protein immobilization and cofactor regeneration and wiring. Conducting biocompatible polymer materials (e.g. polypyrrole, poly(3,4-ethylenedioxythiophene)) have indeed been applied to this field. In a work with enzymes encapsulated in polypyrrole matrix, the film was electrografted on a platinum electrode from pyrrole solution in the presence of glucose oxidase, resulting in a uniform polymer structure and enzyme distribution. The modified electrode was adaptable to a bioelectrochemical process for gluconic acid production [88]. The electrochemical process benefited from the oxygen regeneration at the electrode and from the enzyme protection effect from the polymer matrix, leading to an increase in the transformation ratios by a factor of two [89].

The P450 enzymes were immobilized in conducting polymers like polypyrrole films [99] and poly(3,4-ethylenedioxythiophene) doped with polystyrene sulfonic acid (PEDOT/PSS) [98] on electrode in an active form, the conductive polymer was electrochemically wiring the enzymes for direct electron transfer reaction (see scheme 2C). **Figure 1.10** reports a comparison of enzymatic production in the presence of the natural cofactor NADPH (black symbols) with the electrochemically-driven biocatalysis (white symbols). Both experiments have been performed with the cytochrome P450 CYP102A1 immobilized in a polypyrrole matrix. Two different kinds of electrode material were used, either Pt (squares) or glassy carbon (circles). This immobilization did not hinder the enzymatic activity of the proteins on glassy carbon electrode. The electrochemically-driven biocatalysis was as efficient as the one fed by NADPH on this latter electrode material. The enzymatic activity determined on Pt electrodes show at the contrary a more complex behavior, largely unfavorable to electrochemically-driven reactions [99].

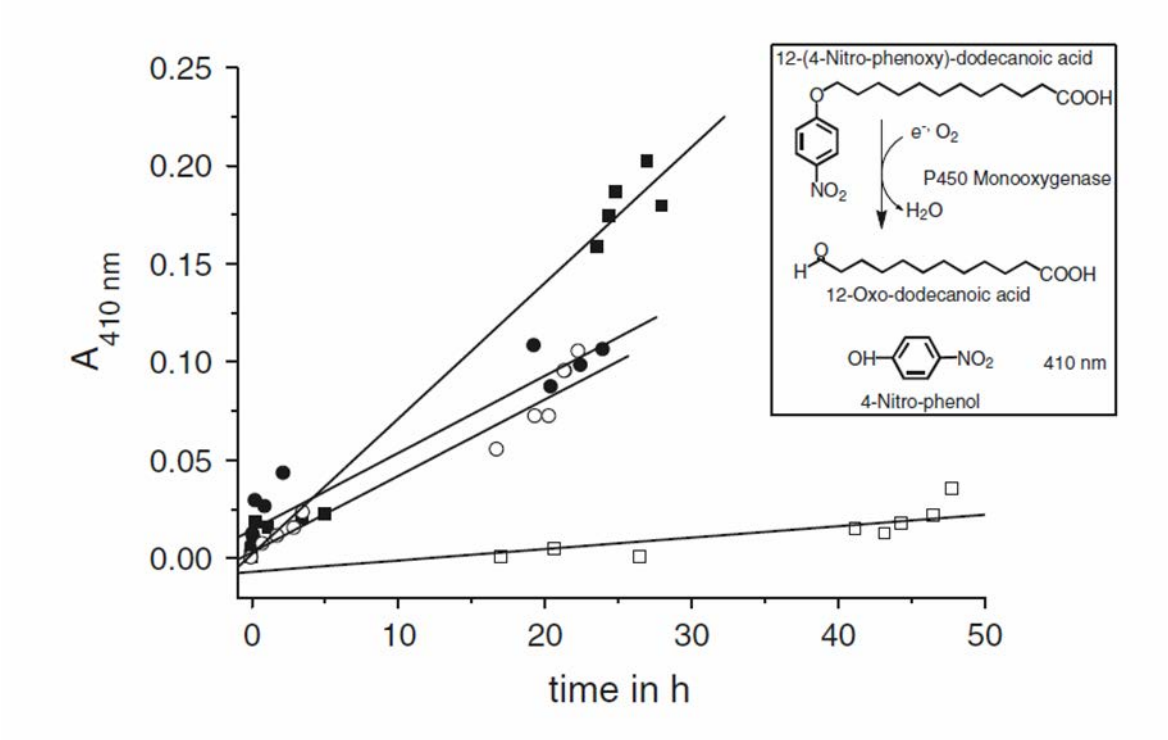

Figure 1.10. *Product (p-nitrophenolate, detected at 410 nm) formation kinetics of P450 BM-3 QM embedded in polypyrrole on platinum (■) or glassy carbon (●) electrodes with the natural cofactor NADPH (□) or by electrochemistry (○). The insert is the scheme of corresponding reaction [99].*

1.4 Immobilization of mediators

In practical electrosynthesis, the immobilization of mediators is also necessary from economic and ecological considerations. The immobilization of mediators would not only increase their reusability and simplify the product purification step, but also limit the undesirable interactions between enzymes and mediators. A huge effort has been done for immobilization of redox mediator for flavoenzymes (especially for glucose oxidase) or NAD-dependent dehydrogenases in the field of biosensors [24,72], or enzymatic fuel cells [133–135]. This topic was more rarely studied in the field of electrosynthesis and essentially for NADH regenerations which concerns two molecules methyl-viologen and (2,2'-bipyridyl)(pentamethylcyclopentadienyl)-rhodium family ($[Cp^*Rh(bpy)Cl]^+$). Here we will briefly review the immobilization of methyl-viologen and rhodium complex in relation with electrosynthesis.

1.4.1 Methyl-viologen

Methyl-viologen has been widely used as a mediator for enzymatic electroregeneration of NADH, always co-immobilized with a flavoenzyme, diaphorase [37–39], lipoamide dehydrogenase [31,39,40], ferredoxin $NAD(P)^+$ reductase [40,41] and AMAPORS [42]. Methyl-viologen immobilization was first achieved by membrane confinement [54,56,58,59,61], but these small molecules may lead to leaching. One strategy for more efficient immobilization of methyl viologen was bounding the molecule to co-flavoenzymes [55,62]. For example, in dialysis membrane reactor, when the cutoff of the membrane was larger than the molecular size of methyl-viologen, this molecule was covalently bonded with the regeneration enzyme lipoamide dehydrogenase [55]. The enzyme-mediator species were also immobilized on the electrode by a Nafion coating. The methyl-viologen species were first functionalized with amino group, followed by attaching to a lipoamide dehydrogenase by N-ethyl-N'-('t-dimethylaminopropyl)carbodiimide, then a stable membrane coated electrode was obtained by dipping the electrode into a Nafion solution [62]. Another strategy was the directly bonding to the electrode by polymerization [63] or covalent bonding [64]. Compare to physical entrapment under a Nafion membrane, electrochemical copolymerization of lipoamide dehydrogenase with oligomeric polyviologen on the electrode allowed a higher production rate in lactate production [63].

1.4.2 $[Cp^*Rh(bpy)Cl]^+$

The most efficient non-enzymatic NADH regeneration catalyst is the (2,2′-bipyridyl) (pentamethylcyclopentadienyl)-rhodium family ($[Cp^*Rh(bpy)Cl]^+$ [136]. However, low enzymatic catalytic stability has been reported in the presence of this rhodium complex due to the interaction between enzyme surface functional groups and the rhodium species. Hildebrand et al. suggested that immobilization of the rhodium complex was necessary in order to separate it from enzymes [6,7]. A membrane reactor was reported with complete separation of the proteins from the rhodium complex modified with a large size polymer modified as shown in **Figure 1.11A** [7]. This complete separation significantly improved the long-term stability of the system. A bioconversion from p-chloroacetophenone to p-chloro-(R)-phenylethanol catalyzed by *Lactobacillus brevis* alcohol dehydrogenase (Lb-ADH) was performed in this bio-reactor, a conversion rate up to 90% was achieved after 6 hours **(Figure**

1.11B), the activity of immobilized enzymes was completely kept (5.5±1 U mg^{-1} before and 6±1 U mg^{-1} after). In addition, 86% of the rhodium complex could be recovered.

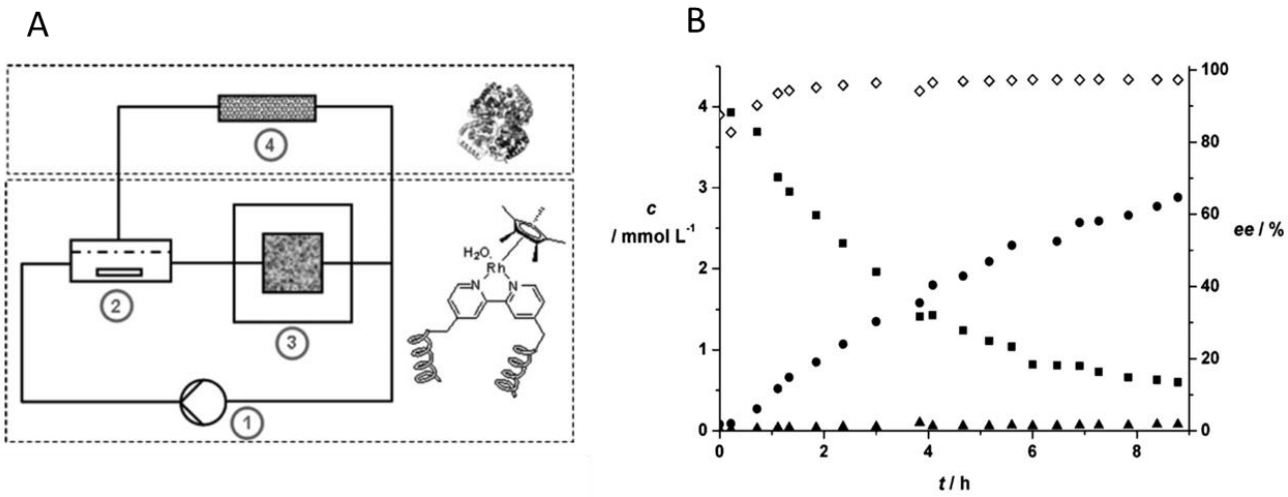

Figure 1.11. *(A) Setup of a membrane reactor with complete separation of the proteins from the large size polymer modified rhodium complex with setup: 1) pump, 2) membrane reactor, 3) electrochemical cell, 4) immobilized enzyme. (B) Conversion from 4 mM p-chloroacetophenone to p-chloro-(R)-phenylethanol by immobilized Lb-ADH with electrochemical cofactor regeneration [7].*

Some efforts have been made to immobilize the rhodium complex on the electrode. Generally, the immobilization methods can be classified into two categories. The first category is based on polymerization. Polypyrrolic rhodium (III) complex (2,2'-bipyridine or 1,10-phenanthroline ligand) films was deposited on electrodes by anodic electropolymerization of pyrrole monomers, its electrocatalytic interest for hydrogen evolution was demonstrated [137]. Rhodium(III) bis-terpyridinepyrrole complex on a reticulated vitreous carbon electrode by electropolymerization was characterized by reduction of NAD^+ into 1,4-NADH, then its enzymatic catalytic response was tested for reduction of cyclohexanone to cyclohexanol in the presence of alcohol dehydrogenase [29]. The catalytic activity of the rhodium complexes incorporated into the bilayers of vesicles formed from a polymerizable ammonium surfactant was investigated, the catalytic response was proved to depend on its position in the bilayer [138]. Despite electropolymerization, ɤ-irradiation cross-linking can also be used to obtain $[Rh^{III}(C_5Me_5)(L)C1]^+$ complex polymer-modified electrodes. Even through polymerization would provide a stable bonding, it suffered from the electron shielding effect coming from the thick porous polymer film. When the amount of immobilized polymer was doubled on the electrode, the charge calculated from the reduction

peak was only increased by a factor of less than 2. This suggested that there was some limitation in charge transfer reaction caused by the polymer layer [139].

The second immobilization strategy was based in π-π stacking effect between carbonaceous materials (graphene or carbon nanotubes) and aromatic moieties from the rhodium complex. Park and coworkers reported that a phenanthroline modified Rh complex was strongly immobilized on the graphene surface through π-π interaction and π-cation interaction the repeated usability for electrochemical NADH regeneration up to 7 cycles (each cycle lasts 2 h) was demonstrated [35]. Minteer and coworkers immobilize a rhodium complex with a pyrene-substituted phenanthroline ligand onto MWCNT via π-π stacking, good catalytic response for the regeneration of NADH and repeated usability up to 10 cycles (each cycle lasted 30 min) were achieved [34]. This route eliminated the electron shielding effect and significantly increased the usability of the catalyst. However, it could be only applied on CNT or 3D-structured graphene which has aromatic rings, as the electrode. In addition, π–π stacking which has a bond energy 0-10 kcal/mol is a kind of reversible non-covalent bond, was not as stable as covalent binding whose bond energy is 80-100 kcal/mol when applied for continuous long-term bioconversion [140,141]. Thiol-functionalized rhodium complex was also covalently immobilized by self-assembled monolayers (SAMs) on gold electrodes. The immobilized rhodium complex was electrochemically active, however, no electrocatalytic activity to addition of NAD^+ was observed. The hypothesis of the author was that the presence of thiol disturbed the complex as it was reported for the interaction of rhodium with proteins [142].

1.5 Conclusions

Enzymatic catalysis has become a central area for the synthesis/transformation of industrially important products and intermediates. They allow high regio- and stereoselectivity for the desired reactions under mild conditions. Inside this large field of research and biotechnological applications, electrochemistry is providing the possibility to regenerate efficiently the electroactive cofactor associated with redox proteins. For the community of electrochemists, electroenzymatic synthesis has a lot of similarities with enzymatic biofuel cells or biosensors. If one compares today the quantity of publications in these different domains, it appears that electrosynthesis is much less popular than other

mentioned fields. The reason is probably related to major challenges associated with bioconversion experiments, i.e., the need for long term stability of the biocatalyst, its reusability and, somehow related to the previous items, the economic competitiveness.

In general, enzymes need to be immobilized in order to increase their operational stability and eventually their recycling. In electrosynthesis, they need to be immobilized at close distance to the electrode surface in order to favor efficient electron transfer reactions between the electrode and the redox cofactors. Membrane confinement has been successfully proposed in the past for bioelectrochemical conversion but this approach has the major drawback that enzymes cannot be recycled after experiments. Surface grafting or encapsulation is probably the more suitable approaches that need to be investigated for further improvement of this biotechnology.

Electrochemical regeneration of the enzymatic cofactor implies either a mediator to shuttle electron from the redox center inside the protein to the electrode surface or a catalyst to facilitate the electrochemical conversion of nicotinamide adenine dinucleotide cofactors (NAD^+, NADH, $NADP^+$, NADPH). One of the most popular reaction in electroenzymatic synthesis is the electrochemical reduction of NAD^+ to NADH that involves either methyl-viologen as mediator in the presence of a co-enzyme, or $[Cp^*Rh(bpy)Cl]^+$ as catalyst. Methyl-viologen has the disadvantage to be highly toxic and should either be strongly immobilized on the electrode surface or simply replaced, e.g. by FAD, or removed from the bioelectrochemical pathway by exploring direct electron transfer reactions with proteins allowing regeneration of NADH, as reported for diaphorase fragments. $[Cp^*Rh(bpy)Cl]^+$ is one of the best catalyst for this reaction. Most applications in electrosynthesis with this catalyst have been performed when using it in solution. Immobilization and separation from the proteins have been proposed and this is surely one interesting area to be investigated. Recyclability of both the electrochemical catalyst and proteins should be the major objective to achieve.

The goal of this thesis was to develop a co-immobilization electrode with a stable covalent bonding to the catalyst, but a reversible bond with enzymes. As soon as the enzymes lost their enzymatic activity, they can be replaced by a new batch of active enzymes. Some preliminary work has been carried out on the immobilization of enzymes inside mesoporous silica films which has mediators or catalyst covalently immobilized on the inner surface (**Figure 1.12**). either for enzymatic assisted regeneration of nicotinamide cofactor using

mediators (eg. ferrocene or viologen) in the presence of diaphorase (**Figure 1.12A**) or non enzymatic regeneration of NADH with rhodium complex (**Figure 1.12B**).

Indeed these porous materials are good for protein immobilization for bioelectrochemistry (see **Appendix 2**). The reversible adsorption or desorption of enzymes were supposed to be controlled by pH , ionic strength or taking advantage of a histidine tag. The functionalization or dual functionalization of the silica film would have been achieved with click chemistry [143,144]. However, some difficulties we met: (1) silica film was biocompatible but its stability in aqueous solution was quite limited, making it inappropriate for long-term experiments; (2) for the materials we prepared, there was no direct evidence to prove that the enzymes were adsorbed inside the pore [145], this point is critical as only an immobilization into the pores would avoid rapid leaching with time. Moreover, immobilization of a rhodium complex in mesoporous silica film was achieved but no electrocatalytic response for NADH regeneration was observed. These preliminary results showed that it was not obvious to achieve a stable biosystem inside a mesoporous silica film (see **Appendix 1**).

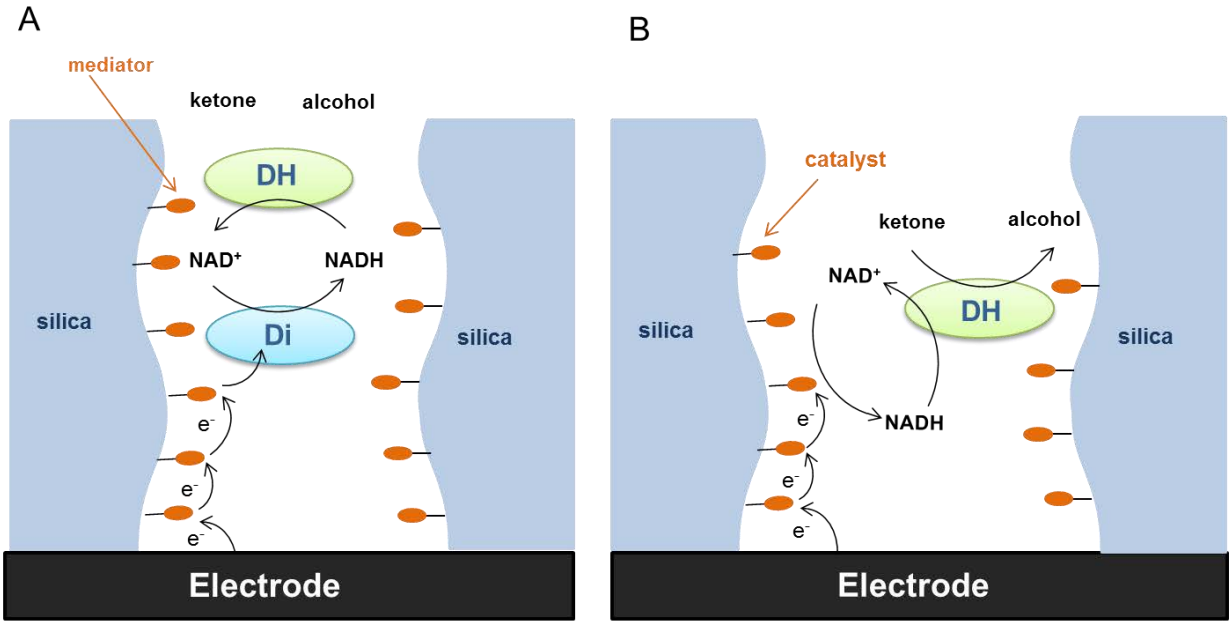

Figure 1.12 *Electrochemical process of redox proteins immobilized in mesoporous silica with (A) redox mediators and (B)catalyst covalently connected to the inner surface.*

Porous carbon electrodes were finally used instead of porous silica films. Proteins with histidine tag were also considered initially to immobilize the proteins on the electrode surface. But for improving the stability of the attachment, cysteine tag was preferred and a protocal for selective attachment of this tag on electrode was studied. $[Cp^*Rh(bpy)Cl]^+$ was covalently immobilized on the electrode surface in order to improve the recyclability and stability of NADH regeneration, and different co-immobilized electrodes for electroenzymatic synthesis were developed, keeping in mind the need for the recyclability of the rhodium catalyst and the reversible immobilization of the proteins.

This thesis is composed of 5 chapters and 2 appendices. In Chapter 1, we introduced the general principle of electroenzymatic synthesis for different classes of proteins and different immobilization methods for enzymes and catalysts which have been applied in the field of electroenzymatic synthesis. In Chapter 2, cysteine-tagged dehydrogenases were covalently immobilized onto carbon electrodes via „thiol–ene" click chemistry. In Chapter 3, we covalently immobilized rhodium complex catalyst on porous carbon electrode used for nicotinamide adenine dinucleotide reduced form (NADH) regeneration. In Chapter 4, a generic approach for heterogeneous surface functionalization of CF-CNT electrode with rhodium complex and enzymes respectively based on the azide-alkyne cycloaddition Huisgen reaction and alkene-thiol coupling was developed. In Chapter 5, a reversible packing co-immobilized electrode with rhodium complex functionalized layer and enzyme gel layer applicable to bioconversion was fabricated. Finally, the appendices include the preliminary results about mesoporous silica film and a review article describing the application of mesoporous materials in bioelectrochemistry.

Table 1: Electroenzymatic synthesis involving immobilized enzyme and/or mediator

Enzyme	Cofactor	Substrate	Product	Mediator	Co-enzymes	Electrode	Immobilization method	Bio-conversion	Ref
GOx	FAD	Glucose	Gluconic acid	O_2		Pt grid	Dialysis membrane	Transformation ratio up to 30% after 3h with membrane cut off 12–14 kDa	[87]
GOx	FAD	Glucose	Gluconic acid	O_2	-	Pt / CF	Dialysis membrane	Conversion 30% after 3h	[31]
ADH	NAD	Cyclohexanone	Cyclohexanol	MV / rhodium complex	LipDH	Pt / CF	Dialysis membrane and Ultra-filtration membranes	MV: up to 72% in continuous mode; Rhodium complex: 75% over 36 h in continuous mode 100%over70h in recycling mode	[31] [65]
ADH	NAD	Alcohol	Aldehyde	-			Ultra-filtration membrane (ADH-Al_2O_3 particles)	Continuous-flow type	[67]
ADH	NAD	Cyclohexanone	Cyclohexanol	([Rh (III) (C_2Me_5)(bpy)Cl] $^+$		CF	Dialysis membrane and Ultra- filtration membrane	92% in 45 days for D-MER and 100% in 3 days for UF-MER	[30]
ADH	NAD	p-chloroaceto-phenone	p-chloro-(R)-phenylethanol	Polymer-bound Rh(bpy)			ADH covalent on amino-epoxy carrier supports, glutaraldehyde, Rh by ultra-filtration membrane	Conversion reach 90%, Rh recovery rate 86%, TTN =214, ee =97.3%	[7]
GDH	NAD	Glucose	Gluconic acid	-	-	GF	Nafion membrane	half-life deactivation time of the enzyme $t_{1/2}$ = 24.5 h; Substrate consumption rates rs = 59 μmol min^{-1}	[68]

Table 1: continued.

Enzyme	Cofactor	Substrate	Product	Mediator	Co-enzymes	Electrode	Immobilization method	Bio-conversion	Ref
LDH	NAD	Pyruvate or α-Ketobutyrate	(L)-lactic acid (2a) or (L)-2-hydroxybutyric acid	MV	LipDH	Pt	Dialysis membrane	Reaction >95% complete after 8 days, ee > 98%	[54]
LDH	NAD	Pyruvate	Lactate	MV	LipDH	Porous graphite	Cation exchange membrane	70% in a semi-batch for 24 h, 50% in a simple batch mode for 200h	[56][61]
LDH	NAD	Pyruvate	Lactate	FAD	FDH	Gold	Proton exchange membrane	Complete transformation in batch recycling mode, TTN =1	[60]
PCMH EPMH	FAD	4-ethylphenol	1 -(4-hydroxyphenyl)-ethanol	Polyethyleneglycol modified ferrocene		CF	Ultrafiltration membrane	Conversion is 100% after 3000 minutes, ee =88% TTN =400,000	[91]
LDH	NAD	Pyruvate	Lactate	MV	LipDH	RVC	Nafion coating; LDH cross-linked by glutaraldehyde in solution	In batch: cross-linked LDH yield 70%,10% lost in stability over 25 days. Soluble LDH 50%, $t_{1/2}$ =2.5 day	[55]
LDH	NAD	Pyruvate	Lactate	FAD / pFAD	LipDH	GC	Nafion coating	TTN is 123 / 43, Stoichiometric yield is 58 / 30 %,	[57]
LDH	NAD	Pyruvate	Lactate	MV	LipDH	RVC	Nafion coating	Complete after 8 days, current efficiency is close to 100%	[58]
LDH	NAD	Pyruvate	Lactate	MV	LipDH	Porous graphite	Nafion coating	70% in a semi-batch mode for 24 h, 50% for 200 h in simple batch mode	[59]

Table 1: continued.

Enzyme	Cofactor	Substrate	Product	Mediator	Co-enzymes	Electrode	Immobilization method	Bio-conversion	Ref
LDH	NAD	Pyruvate	Lactate	MV	LipDH	Carbon	Nafion coating (MV-LipDH)	Yield is 60%, current efficiency is 660 and 107 nmol cm $^{-2}$ h $^{-1}$ for lactate and malate, active for 43 days	[62]
MDH		Oxaloacetate	Malate						
ADH	NAD	Butyraldehyde	Butanol	-	-	CF	Encapsulation in alginate–silicate gel	Faradaic efficiency ~ 40%	[132]
(S)-MDH	FMN	(S)-mandelic acid	Phenylglyoxylic acid	Ferrocenedimethanol	-	GC/ CF	Encapsulation in silica film	94% of conversion after 9 h, faradaic efficiency of 91 %	[92]
Enoate reductase	Iron-sulfur-FAD	(E)-2-methyl-3-phenyl-2-propenoate / (E)-2-methyl- 2-butenoate	3-phenyl-2-methylpropionic acid / 2-methylbutanoic acid	MV	-	CF	Encapsulated in calcium alginate gels	Conversion is 95% and 99%, half- life increase from 8h to 350h when immobilized	[129]
RDH	NAD	D / L-glucitol	D-fructose / D-sorbose	Ferrocene-dimethanol	Diaphorase	GC	Encapsulation in silica gel	Higher oxidation peak with D-glucitol	[86]
DSDH	NAD	D-sorbitol	D-fructose	Poly(methylene green)	-	MWCNTs-modified CF	Encapsulation in silica gel	TTN close to 60, conversion rate 60%, enzyme stability up to 2 weeks (in solution $t_{1/2}$ =48h)	[75]
GOx	FAD	Glucose	Gluconic acid	O_2	-	Pt / Carbon	Encapsulation in polypyrrole film	45% conversion after 8 h,	[88]
GOx	FAD	Glucose	Gluconic acid	O_2	-	Pt	Encapsulation in polypyrrole film	Different thickness give yied 23-45% after 8h	[89]

Table 1: continued.

Enzyme	Cofactor	Substrate	Product	Mediator	Co-enzymes	Electrode	Immobilization method	Bio-conversion	Ref
CYP102A1	Heme+diflavin reductase	p-nitrophenoxycarboxylic acid	p-nitrophenolate		-	Pt and GC	Encapsulation in polypyrrole	Production rate of: 0.66 μM h^{-1} cm^{-2} (Pt) 0.13 μM h^{-1} cm^{-2} (GC) 25 h bioconversion	[99]
CYP102A1	Heme+diflavin reductase	3-phenoxytoluene	Toluene and Phenol	-	-	Glassy carbon	Encapsulation in PEDOT/PSS polymer films	Reaction rate is 21.89 μM h^{-1} cm^{-2}	[98]
GOx	FAD	Glucose	Gluconic acid	Benzoquinone	-	CF	Covalent by carbodiimide	1.5 g gluconate / h; Conversion < 40%, Stability increase 50 times	[90]
Tyr	Cu	L-tyrosine	L-3,4-dihydroxyphenylalanine	-	-	Tyr /carbon NPs / polypyrrole	Carbodiimide + polymerization with pyrrole	Conversion is 95.9% in 4h and productivity 47.27mgl^{-1} h^{-1}	[107]
						CF	Nafion coating	Conversion is 44.4% in 4h and 21.93 mgl^{-1} h^{-1}	
Tyr (well-dispersed)	Cu	L-tyrosine	L-3,4-dihydroxyphenylalanine	-	-	Tyr / carbon nanopowder / polypyrrole	Covalent by carbodiimide	Conversion rate up to 77.7% in 5h, productivity is 15,300 mgl^{-1} h^{-1};	[108]
LDH	NAD	Pyruvate	L-lactate	MV derivative	VAPOR	CF	Covalent by carbodiimide	148 nmol cm^{-2} in 20 h	[64]
ADH	NADP	Acetophenone	(R)-phenylethanol	Cp*Rh(bpy)		CF	Covalent by glutardialdehyde	Complete conversion with TTN of 75,000 in one phase, twice in two-phase system, ee 99.9%. Stability of 36h in MTBE organic solvent	[33]

Table 1: continued.

Enzyme	Cofactor	Substrate	Product	Mediator	Co-enzymes	Electrode	Immobilization method	Bio-conversion	Ref
AOx	FAD	Pyruvic acid	D-alanine	ADPy		GC	Covalent by glutaraldehyde	ee~100%, current efficiency 97% in 10h, 8.9 mmol dm^{-3}, TTN more than 36000	[93]
CYP1A2 + CYP3A4	Heme	Clopidogrel	Clopidogrel carboxylic acid	-	-	Au / chitosan / RGO nanosheets	Covalent, glutaraldehyde+ carbonyldiimide	7.2% after 1h	[100]
GDH	NAD	Glucose	Gluconic acid	3,4-DHB	-	GF	Covalent by glutaraldehyde+ carbonyldiimide	TTN_{max} is 100 after 4h	[78]
G6PDH	NAD	Glucose 6-phosphate	6-phosphogluconate	PMS	-	Rotating disc graphite	Covalent by glutaraldehyde or carbonyldiimide	0.016 mol / day, current efficiency is 100%	[76]
LDH	NAD	Pyruvate	Lactate	PV	LipDH	GC	Covalent by glutaraldehyde	35% in 62 h, TTN is 38	[63]
ADH	NAD	2- and 3-methylcyclohexanone	(1 S, 2S)-(+)-2- and (lS, 3S)-(-)-3-methylcyclohexanol	Methyl viologen	Diaphorase	GF	Polyacrylic acid cross-linking	Yield (49.8 and 50.2%), current efficiency (98.6 and 96.5%) and ee % (100 and 93.1%) in 8 h	[37]
Cys-DSDH	NAD	D-fructose	D-sorbitol	$[Cp^*Rh(bpy)Cl]^+$	-	CF	Covalent by „thiol-ene" click chemistry	Conversion rate is 72%, faradaic efficiency is 77 %	[146]
Cys- GatDH	NAD	1,2-hexanediol	Hydroxyacetone	4-carboxy-2,5,7-trinitrofluorenylidene- malonnitrile	-	Gold	Self-assembled monolayers	Proof of concept with cyclic voltammetry	[77]
CYP2E1, MUT261, MUT268	Heme	p-nitrophenol	p-nitrocatechol	-	-	Gold	Self-assembled monolayers+ covalent by (DTME)	1.77 ± 0.64 (P450 2E1); 4.53 ± 0.44 (MUT261); 3.66 ± 0.35 (MUT268) µM	[97]

Table 1: continued.

Enzyme	Cofactor	Substrate	Product	Mediator	Co-enzymes	Electrode	Immobilization method	Bio-conversion	Ref
FNR	FAD	NADPH	$NADP^+$	Ferrocene	-	Gold	Self-assembled monolayers + Histidine chelated with Cu^{2+}	Orientation of the protein to favor direct electron transfer reactions	[9]
CPO	Heme	cinnamyl alcohol	cinnamic aldehyde	O_2	-	Glassy carbon	DDAB surfactant film + chitosan	Yield is 51.8% TTN is 80500, over 4 cycles	[102]
CYP119	Heme	Nitrite	ammonia	-	-	Plane pyrolytic graphite	DDAB surfactant film	Important role for protein stability in the selectivity of biocatalysts	[96]
CYP1A2 or CYP2E1	Heme	4-(Methylnitro-samino)-1-(3-pyridyl)-1-butanone	4-hydroxy-1-(3-pyridyl)-1-butanone (HPB)		Cyt P450-reductase and cyt b5	Pyrolytic graphite disk electrodes	Layer-by-layer	Turnover rate: 57±9 h^{-1} (mol HPB)$^{-1}$ (mol CYP2E1)$^{-1}$	[101]
GOx (GOx+ HPR on cathode)	FAD	Glucose	Gluconic acid	TTF		3-D cross linked carbon NPs	Gelatin+ glutaraldehyde	47% after 7h	[131]

Abbreviations: GOx, glucose oxidase; ADH, alcohol dehydrogenase; LipDH , lipoamide dehydrogenase ; PCMH, p-cresol methylenehydroxylase ; EPMH, 4-ethylphenol methylenehydroxylase; GDH, glucose Dehydrogenase ; LDH, L-lactate dehydrogenase ; FDH, formate dehydrogenase ; VAPOR, viologen accepting pyridine nucleotide oxidoreductase ; AOx, Amino acid oxidase ; G6PDH, glucose-6-phosphate dehydrogenase ; RDH, ribitol dehydrogenase ; DSDH, D-sorbitol dehydrogenase ; Cys-GatDH, cysteine-tagged galactitol dehydrogenase; S – MDH, (S)-mandelate dehydrogenase ; FNR, ferredoxin: $NADP^+$ reductase ; Cys- DSDH, cysteine-tagged dehydrogenase; Tyr, tyrosinase; CYP, cytochrome P450; CPO, chloro- peroxidase; ADPy, L-aminopropyl-1 methyl-4,4'-dipyridine ; PMS, Phenazine methosulfate ; MV, methyl viologen; PV, polyviologen; 3,4-DHB, 3,4-dihydroxybenzaldehyde ; pFAD, polymerized FAD film; DTME, dithio-bismaleimidoethane ; TTF, tetrathiafulvalene ; Pt, Platinium; CF, carbon felt; GF, graphite felt ; GC, glassy carbon; RVC, reticulated vitreous carbon; NPs, nanoparticles;

Chapter 2. Immobilization of cysteine-tagged proteins on electrode surfaces by thiol-ene click chemistry

Thiol-ene click chemistry can be exploited for the immobilization of cysteine-tagged dehydrogenases in an active form onto carbon electrodes (glassy carbon and carbon felt). The electrode surfaces have been first modified with vinylphenyl groups by electrochemical reduction of the corresponding diazonium salts generated in situ from 4-vinylaniline. The grafting process has been optimized in order to not hinder the electrochemical regeneration of NAD^+/NADH cofactor and soluble mediators such as ferrocenedimethanol and $[Cp^*Rh(bpy)Cl]^+$. Having demonstrated the feasibility of thiol-ene click chemistry for attaching ferrocene moieties onto those carbon surfaces, the same approach was then applied to the immobilization of D-sorbitol dehydrogenases with cysteine tag. These proteins can be effectively immobilized (as pointed out by XPS), and the cysteine tag (either 1 or 2 cysteine moieties at the N terminus of the polypeptide chain) was proven to maintain the enzymatic activity of the dehydrogenase upon grafting. The bioelectrode was applied to electroenzymatic enantioselective reduction of D-fructose to D- sorbitol, as a case study.

2.1 Introduction

In the field of sustainable chemistry, the exploitation of enzymes, which are likely to catalyze chemical reactions with high regio- and stereoselectivity, appears to be a powerful strategy to develop bioprocesses targeted to the synthesis of molecules for food industry, pharmacy, and cosmetics, etc [147,148]. For instance, the NADH-dependent redox proteins belonging to the dehydrogenases family can be used for the enantioselective reduction of ketone to alcohol [4], providing that regeneration of the enzymatic cofactor is ensured (e.g., by NAD^+ reduction to NADH) [149]. The effectiveness of such bioelectrochemical processes implies a durable immobilization of the protein in an active form to guarantee its long-term operational stability in the bioreactor [150], as well as efficient electrochemical regeneration of the catalyst, either by direct or mediated electron transfer [17]. Among the various methods reported for protein immobilization [150], a recent approach is based on the specific interaction between histidine-tagged proteins engineered by molecular biology [151] and porous materials holding divalent metal complexes [152]. Examples are available for enzyme immobilization on mesoporous silicates [153–155] or electrode surfaces [152], including controlled orientation [156], while keeping their catalytic activity [152,155]. The histidine tag-metal complex being reversible [157], a significant portion of the proteins can be lost upon prolonged use in solution. Attempting to circumvent this limitation, some authors suggested strengthening the enzyme-support linkage, e.g., by exploiting the thiol-gold interaction for attaching dehydrogenases or laccase to gold electrodes via their cysteine residues [77,158]. If such immobilized proteins operate in a satisfactory way in oxidation, they can, however, suffer from poor long-term stability when used for reduction reactions because of possible reductive desorption of species chemisorbed on gold via thiol moieties [159,160]. This is particularly critical when considering electroenzymatic synthesis with NAD-dependent dehydrogenases in the reduction mode, which requires the regeneration of the enzymatic catalyst at a potential more cathodic than the standard potential of the cofactor redox couple, i.e., -0.59 V vs SCE for NAD^+/NADH [161]. Going one step further to tackle these drawbacks would be the development of a method for covalent binding of cysteine-tagged proteins to other electrode materials, such as carbon surfaces, and this is what we plan to perform here by combining electrografting and click chemistry. Several click reactions are now well-established in chemical synthesis [162], materials science [163], and for the preparation of peptide conjugates [164]. The modification of proteins with azide groups was, for example, used to immobilize horseradish peroxidase on gold [165] or screen-printed

carbon electrodes [166]. Inversely, azide was immobilized on a self-assembled monolayer and used to bind a protein previously derivatized with acetylene groups [167,168]. Except in a few cases [169], these approaches are tricky as they require the preliminary functionalization of the protein (with alkyne or azide groups) before its immobilization via click-chemistry. Here, we have thus investigated the possible covalent attachment of redox proteins taking advantage of the thiol groups already available in their structure (cysteine-tagged or not), by thiol-ene click coupling on carbon surfaces previously modified with vinylphenyl groups (**Figure 2.1**). The idea is sustained by the fact that thiol-ene click coupling was previously reported for the generation of protein-polymer conjugates [170]. The carbon electrodes (either glassy carbon or carbon felt) were first functionalized with vinylphenyl groups by electrochemical reduction of 4-vinylbenzene diazonium cations and then let to react by click chemistry with thiol functionalized molecules and proteins. The approach was first tested using the 6-(ferrocenyl)hexanethiol as a model and then extended to the immobilization of redox proteins with free cysteine residues, including cysteine-tagged proteins of the polyol dehydrogenases family. It should be emphasized that if biomolecule immobilization using the aryl diazonium electro- grafting is now well-established [171], its combination to click chemistry remains uncommon [166] and it has not been yet developed in the case of cysteine-tagged proteins. The modified electrodes were characterized by X-ray photoelectron spectroscopy (XPS) and electrochemistry at the different steps of the modification procedure. The DSDH-based porous bioelectrodes were finally applied to bioconversion of D-fructose to D- sorbitol in the presence of (2-bipyridyl) (pentamethylcyclo-pentadienyl)-rhodium (III), $[Cp^*Rh(bpy)Cl]^+$, as mediator for the electrocatalytic reduction of NAD^+ to NADH in the course of the electroenzymatic processes.

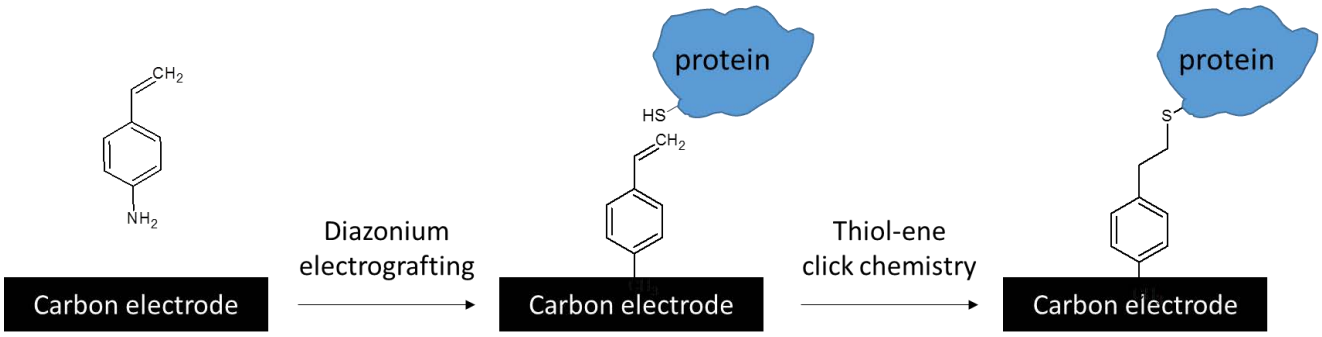

Figure 2.1. *Schematic view of the synthetic route followed for the functionalization of a carbon electrode surface with thiol-containing proteins (HS- protein) by combination of diazonium salt electrografting and thiol−ene click chemistry.*

2.2 Experimental

Chemicals and Reagents

The following chemicals were used as received: 1 M hydrochloric acid solution (Sigma), 4-vinylaniline (97%, Sigma), sodium nitrite (97%, Sigma), Tris(2-carboxyethyl)phosphine hydrochloride (TCEP, ⩾ 98%, Sigma), magnesium chloride hexahydrate (99%, Sigma), sodium dihydrogen phosphate (99.5%, Merck), Tris(hydroxylmethyl) amino-methane (Tris, Sigma), ferroce- nemethanol (97%, Sigma), ferrocenedimethanol (98%, Sigma), 6- (ferrocenyl)hexanethiol (Sigma), β-nicotinamide adenine dinucleotide (NAD^+, 98 wt %, Sigma), β-nicotinamide adenine dinucleotide, reduced dipotassium salt (NADH, 97 wt %, Sigma), D-sorbitol (98 wt %, Sigma), and D-fructose (99 wt %, Sigma). $[Cp^*Rh(bpy)Cl]^+$ was synthesized according to the reported procedure.[142] Glassy carbon electrodes were made from 1 cm × 2 cm plates (Sigradur, HTWHochtemperatur-Werkstoffe, Hochtemperatur-Werkstoffe, Germany). The carbon felt carpet (Sigratherm, GFD 4.6 EA) was supplied by SGL Group (Germany).

Cystein-Tagged DSDH

Overproduction of N-His(6) (DSDH), N-His(6)-Cys (Cys1-DSDH) and N-His(6)-Cys-Cys (Cys2-DSDH) tagged DSDH variants was done with Escherichia coli BL21GOLD (DE3) containing the corresponding expression-vectors pET-24a(+) (Novagen) and purification of the enzyme was performed with Histrap columns (GE Healthcare). The catalytic activity was determined at 340 nm in a UV/vis spectrophotometer (Ultrospec 2100pro,GE Healthcare) by adding the enzyme to 200 mM BisTris buffer (pH 9.0) containing 1.8 mM NAD^+ (final concentration) in a 1-mL cuvette. After preincubation for 2 min at 30 °C the assay was started by addition of 0.1 M D-sorbitol (final concentration). The reduction reaction was measured in 200 mM phosphate buffer (pH 6.50) containing 1.8 mM NADH (final concentration) and started by adding 0.1 M D-fructose (final concentration). Protein concentrations were determined by the method of Pierce (BCA Protein Assay) with bovine serum albumin as the standard [172]. Accessible surface area (ASA) in square Angstrom was calculated with the VADAR program (http:// vadar.wishartlab.com/), the PDB file 1K2W.pdb, and default values [173].

Apparatus

All electrochemical experiments were carried out using an Autolab PGSTAT-12 potentiostat, with a three-electrode configuration cell including an Ag/AgCl reference electrode (3 M KCl), a steel auxiliary electrode, and a carbon working electrode (glassy carbon plate or porous carbon felt). A pencil core (0.5 mm diameter) glued with silver paint to a copper wire was used for connecting the carbon felt working electrode. XPS measurements were performed using the Kratos AxisUltra DLD apparatus equipped with a monochromatic Al Kα source, aiming to prove the occurrence of the thiol-ene click reaction. Three glassy carbon electrodes were modified by 4-vinylphenyl diazonium cations by applying -0.6 V for 2, 300, and 1200 s, respectively, in order to get increasing surface density of vinylphenyl groups for reacting with 6-(ferrocenyl)hexanethiol. Meanwhile, two glassy carbon electrodes modified by 4-vinylphenyl diazonium cations by applying -0.6 V for 600 s were prepared forreacting with Cys1-DSDH or DSDH. Samples of the conversion were taken after different periods and analyzed by HPLC using a Ca^{2+}-column (Rezex RCM Mono- saccharide Ca^{2+} 300 × 7.8 mm, Phenomenex) at 80 °C, with distilled water as the mobile phase and a flow rate of 0.5 mL min^{-1}. Detection was done with a refractive index-detector at 35 °C and calibrations were performed with authentic standard substances.

Preparation and Pretreatment of Carbon Electrodes

Glassy carbon (GC) plates were wet-polished with SiC grinding paper (#4000, Struers, Denmark) for 1 min, then cleaned with ethanol and distilled water under ultrasonic treatment. Carbon felt (CF) electrodes were cut with size of 5 mm × 5 mm from the carbon felt carpet. The surface of CF was then activated via cycling potentials over the range between -0.7 and +2.5 V (20 times) in 0.1 M H_2SO_4, in order to modify the surface state from hydrophobic to hydrophilic. After this, the carbon felt was rinsed with water, followed by heat treatment at 200 °C for 1 h to remove the residual H_2SO_4.

Functionalization of Electrodes with Vinylphenyl Moieties by Electrografting

The diazonium cations were generated in situ by mixing 5 mM 4-vinylaniline and 10 mM sodium nitrite in 0.5 M HCl water solution under stirring at room temperature for 5 min, yielding the 4-vinylbenzene diazonium salt quantitatively. The electrografting on GC was carried out by cyclic voltammetry (consecutive reduction scan with the potential varying from 0 to -0.45 V). However, the electrografting on CF electrode was realized by applying -0.6 V for 1 s. After electrografting, the electrodes were rinsed with distilled water to remove the residual ungrafted compounds.

Functionalization of Electrodes with Ferrocene Moieties

Vinylphenyl functionalized electrodes were immersed into 1 mM of 6-(ferrocenyl)hexanethiol in H_2O/methanol (3/7) solution in the presence 2 mM TCEP used as catalyst for the reaction between alkene moieties and terminal thiol functionalities on ferrocene via thiol-ene "click chemistry". After reaction overnight, the electrode was thoroughly rinsed in THF and then in water to remove the possible residual 6-(ferrocenyl)hexanethiol remaining on the electrode, and subsequently dried.

Functionalization of Electrodes with Proteins

Vinylphenyl functionalized electrodes were immersed into 1 mL of aqueous PBS buffer (250 mM, pH = 7) containing 2.5 mg of proteins, 1 mM $MgCl_2$, and 0.3 mM TCEP. After reaction overnight at 4 °C, the electrodes were rinsed with water and buffer solution.

2.3 Results and discussions

2.3.1 Immobilization of ferrocene moieties on glassy carbon electrode

A two-step protocol was employed to get the modified carbon surfaces, i.e., the electrografting of vinylphenyl groups and then the thiol-ene click coupling with proteins bearing thiol groups. The feasibility of the sequential process was first demonstrated on a glassy carbon electrode with 6-(ferrocenyl)hexanethiol moieties (see scheme in **Figure 2.2**).

Electrochemical reduction of vinylaniline diazonium salts allowed the formation of arylvinyl radicals able to form a covalent bond on the electrode surface that will be available for the thiol-ene coupling with ferrocene moieties employed as a model probe. 4-Vinylaniline was let to react with two molar equivalents of sodium nitrite in 0.5 M HCl to form the corresponding diazonium cations in situ as reported in previous work [174]. The solution was subsequently used without any treatment to modify the GC plate by recording two consecutive cathodic scans in a potential range varying from 0 to -0.45 V at 100 mV s^{-1} (**Figure 2.3A**).

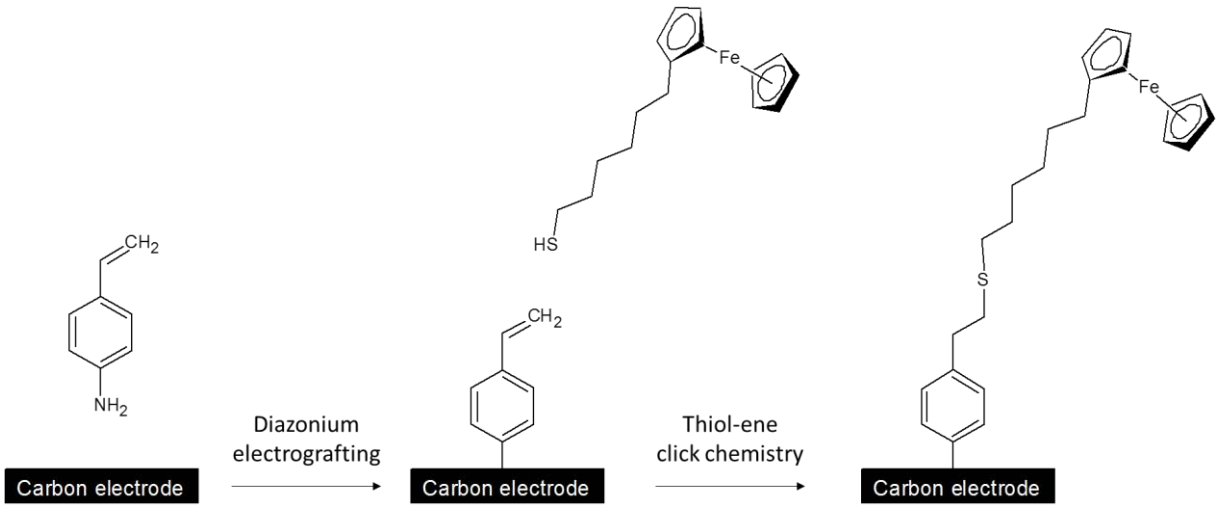

Figure 2.2. *Schematic view of the synthetic route followed for the functionalization of a carbon electrode surface with 6-(ferrocenyl)hexanethiol by combination of diazonium salt electrografting and thiol-ene click chemistry.*

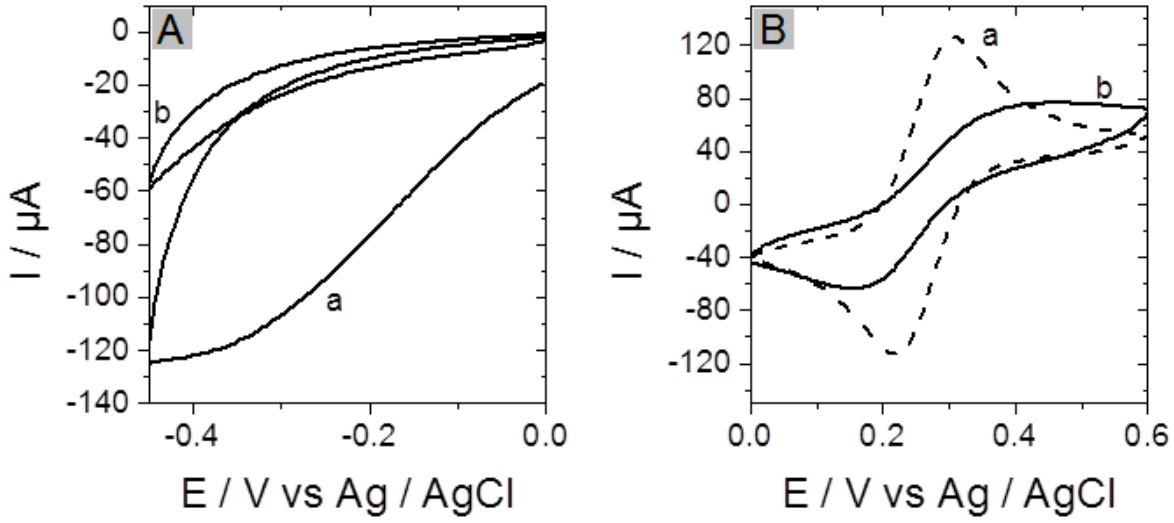

Figure 2.3. *(A) Cyclic voltammograms for the reduction of diazonium cations generated 'in situ' from 5 mM 4-vinylaniline in 0.5 M HCl, as recorded on GC electrode at 100 mV s^{-1}. (B) Cyclic voltammograms recorded at 100 mV s^{-1} in the presence of 0.5 mM ferrocenedimethanol (in 0.1 M PBS at pH 7.0) using a GC electrode (a) before (dashed line) and (b) after (solid line) electrografting with diazonium cations for 2 cycles. The geometric surface area of the electrode was 0.28 cm^2.*

A large current, more than 120 µA, was observed during the first potential cycle (**Fig. 2.3A**, curve **a**). The second reduction scan led to a dramatic decrease in the current response

(**Fig. 2.3A**, curve **b**). This decrease can be explained by the partial blocking of the surface after grafting of vinylphenyl moieties on the carbon surface. The presence of the organic layer on the carbon electrode was further evidenced by the comparison of the cyclic voltammogram of 0.5 mM ferrocenedimethanol recorded on the mentioned GC electrode before (curve a) and after electrografting (curve b) of the arylvinyl radical species. The blocking effect of the organic layer was demonstrated by an increase of the difference between anodic and cathodic peaks (ΔEp varying from 91 to 300 mV) indicative of much slower electron transfer rates on the modified electrodes (**Fig. 2.3B**). In addition, a significant decrease of the current peaks was also observed. The electrochemical reduction of the diazonium cations generated vinylphenyl radicals that can be immobilized on the glassy carbon surface by means of a covalent bond.

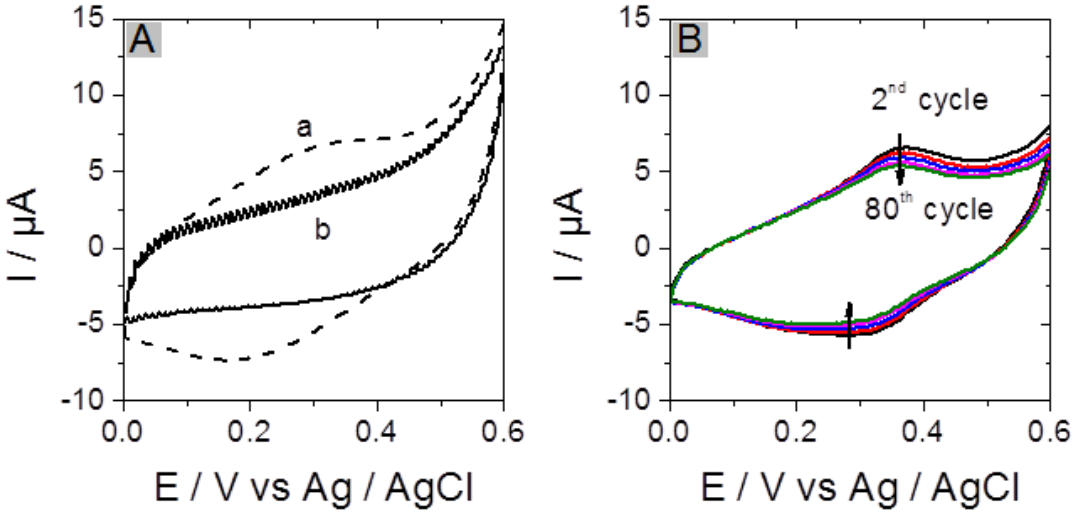

Figure 2.4. *(A) Cyclic voltammograms recorded at a potential scan rate of 100 mV s^{-1} in 0.1 M Tris-HCl buffer (pH 9.0) using vinylphenyl functionalized GC electrodes after reaction with (a) 6-(ferrocenyl)- hexanethiol (dashed line) and (b) ferrocenemethanol (solid line). (B) The 2nd, 20th, 60th, and 80th curves recorded in the same conditions as above in the course of 80 successive voltammetric cycles for ferrocene functionalized glassy carbon electrode (prepared from clicking 6-(ferrocenyl)hexanethiol). The geometric surface area of the electrode was 0.28 cm^2.*

This vinylphenyl-functionalized surface was then used to evaluate the possibility to attach ferrocene moieties by thiol-ene reaction. The electrode was let to react overnight with 6-(hexanethiol)ferrocene in the presence of TCEP and Mg^{2+} ions as reported in the literature

[170]. **Figure 2.4A** shows the typical cyclic voltammogram measured after thiol-ene reaction (curve a). A quasi-reversible electrochemical signal was observed centered at +0.25 V vs Ag/AgCl, consistently with the presence of ferrocene species at the electrode surface. The redox signal was rather stable upon successive cycling in aqueous medium (i.e., only 13% decrease observed after recording up to 80 successive cyclic voltammograms, **Figure 2.4B**). As a control experiment, it was observed that no redox peak could be observed by performing the same thiol-ene coupling experiment by replacing 6-(hexanethiol)ferrocene by ferrocenemethanol (**Figure 2.4A**, curve b), confirming the need of a thiol group on the molecule to enable click coupling and the absence of any nonspecific adsorption of the ferrocene derivative to the GC electrode.

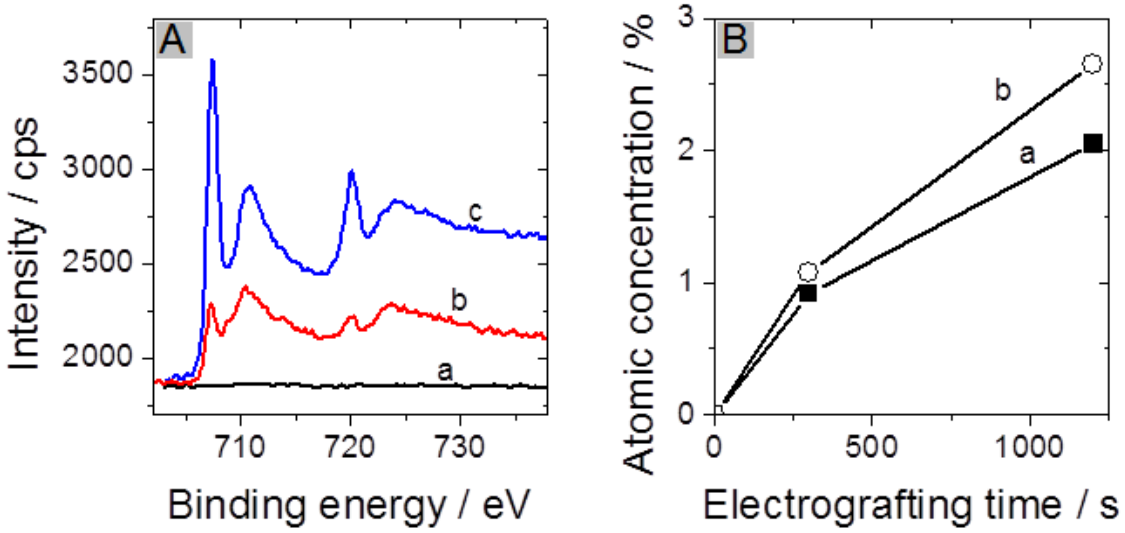

***Figure 2.5**. (A) XPS spectra of the narrow Fe2p region, as obtained for ferrocene functionalized electrodes via click chemistry for GC supports electrografted with 4-vinylaniline diazonium cations at −0.6 V for (a) 2 s, (b) 300 s, and (c) 1200 s. (B) Variation of (a) iron (■) and (b) sulfur (○) atomic concentrations measured from XPS data as a function of the electrografting time.*

The presence of ferrocene on the surface was finally evidenced from XPS measurements performed at various functionalization levels (**Figure 2.5A**). Here the diazonium electrografting was performed by applying -0.6 V for 2 s (curve a), 300 s (curve b), and 1200 s (curve c), as it is well- known that diazonium electrografting can be managed in either cyclic voltammetry or constant-potential chronoamperometry modes [175], and the

amperometric approach enables easier control of the functionalization level by tuning the deposition time. The high-resolution scan of the Fe 2p region for the ferrocene modified electrodes displays two sharp peaks with binding energies of 708.1 and 721.0 eV. These peaks can be attributed to the Fe 2p3/2 and Fe 2p1/2 respectively [176]. The intensity ratio 2:1 of the peaks is close to the data previously described in the literature for ferrocene derivatives [177]. Broader and less defined signals are observed at more positive binding energy values that could suggest the presence of small amounts of ferrocenium moieties [178]. **Figure 2.5B** shows that the atomic concentration of both iron (curve a) and sulfur (curve b, from S 2p at 163 eV) measured in this way by XPS was increasing with the time of diazonium electrografting. These results confirm that the immobilization of ferrocene on the glassy carbon surface is due to the thiol-ene reaction as schematically drawn in **Figure 2.2**.

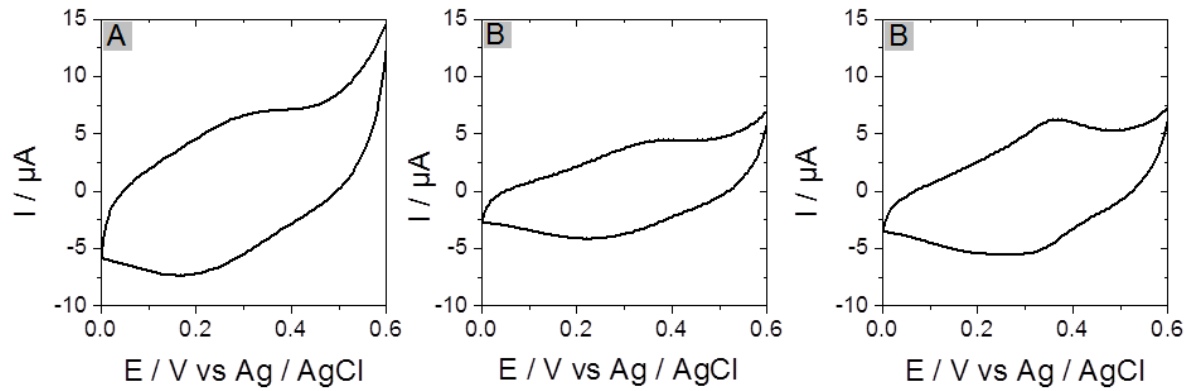

***Figure 2.6**. (A-C) cyclic voltammograms recorded at a potential scan rate of 100 mV s^{-1} in 0.1M Tris-HCl buffer (pH 9.0) using three different vinylphenyl functionalized GC electrodes after reaction with 6-(ferrocenyl)hexanethiol. The geometric surface area of the electrode was 0.28 cm^2.*

The experiment was triplicated and some variability in the voltammograms shape could be noticed, but the signal ascribed to ferrocene was always observed (**Figure 2.6**). This variability between electrode responses is probably due to the electro- grafted diazonium layer. Indeed, a disadvantage of this approach remains in that the layer structure is, in general, poorly defined. This is due to the fact that surface derivatization occurs in a process that involves highly reactive aryl radicals produced from the reduction of diazonium salts and upon expulsion of nitrogen attacking not only the flat surface but also already grafted aryl

layers to afford multilayers. The conditions employed in this work are very soft in terms of the electrografting since only one reduction scan is employed to functionalize the carbon substrates while multilayers are usually described when the reduction potential of the diazonium cations are applied for long time. Such experimental conditions, one reduction scan, can limit the formation of undesired multilayers taking advantage of the stability of the grafting, but does not fully prevent inherent variability in surface coverage.

2.3.2 Immobilization of cysteine-tagged D-sorbitol dehydrogenase on glassy carbon electrode

After its validation for ferrocene grafting, the procedure was adapted to the immobilization of proteins. Here, we have chosen to study the immobilization of NAD-dependent D-sorbitol dehydrogenase (DSDH). To this purpose, three proteins have been developed with only the N-terminal His(6)tag, or either one or two cysteine residues, positioned in front of the His(6)tag. The activity of the proteins was studied in solution and exhibited comparable values for all three variants: Km D-sorbitol 6.5 mM and Km D-fructose 49.4 mM, respectively. The stability was determined with half-life periods of 48 h at 28 °C, 5 h at 35 °C, and 0.2 h at 40 °C. If the protein is immobilized on the electrode surface in an active form, the addition of D-sorbitol in a solution containing NAD^+ must induce the production of NADH that can be electrochemically detected [179] (**Figure 2.7**).

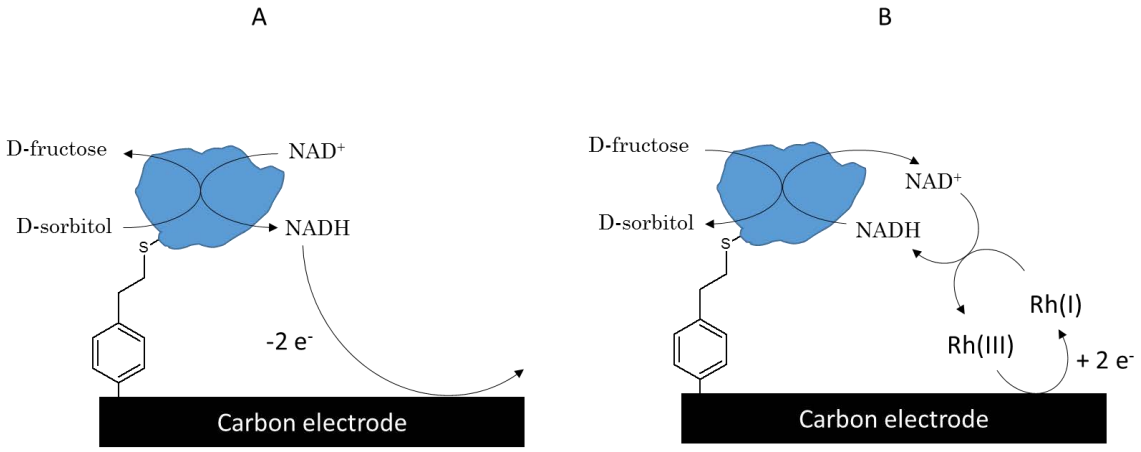

Figure 2.7. *(A) Enzymatic conversion of D-sorbitol to D-fructose and direct electrochemical oxidation of the produced NADH. (B) Enzymatic conversion of D-fructose to D-sorbitol and mediated*

electrochemical reduction of the produced NAD^+ in the presence of $Cp^*Rh(bpy)Cl^+$ mediator successively converted in Rh(I) and Rh(III) during the electrocatalytic process.

We confirmed that NADH could be detected at 0.8 V vs Ag/AgCl at glassy carbon electrode modified with the electrografted diazonium layer (**Figure 2.8**). Figure 2.8A shows the typical signal due to the direct oxidation of NADH at a bare glassy carbon electrode. A current peak was observed at 0.9 V in the presence of 1 mM NADH (curve a). This signal was significantly affected by the diazonium electrografting, as no peak was observed but still a clear current increase was evidenced upon addition of NADH in the solution (compare curves a and b in **Fig. 2.8B**). Note that direct oxidation of NADH is not considered as a valuable approach for either biosensor nor electrosynthesis applications as it happened at high potential. This reaction is usually performed in the presence of a mediator in order to decrease the overpotential of the electrochemical reaction [180]. However, this direct oxidation of NADH on the functionalized surfaces was preferred here to evaluate the activity of the immobilized proteins in order to not introduce additional complexity in the electrochemical scheme.

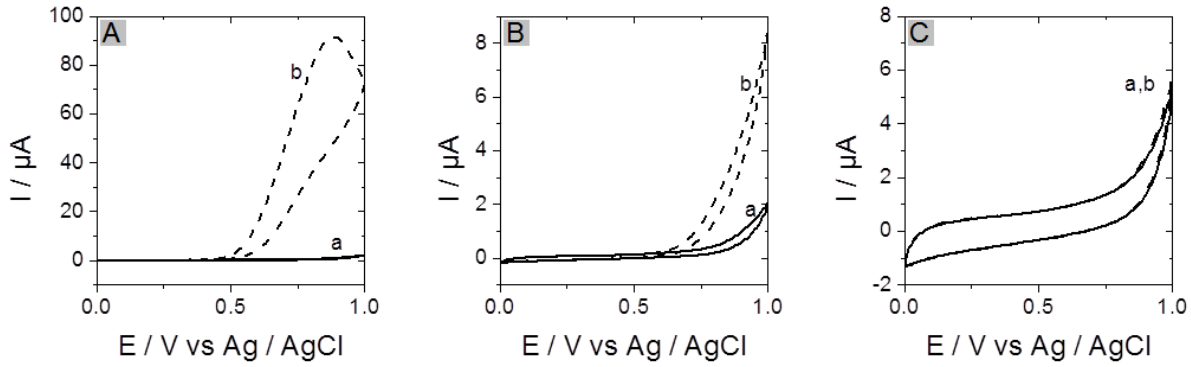

***Figure 2.8**. (A) Cyclic voltammograms recorded at a potential scan rate of 20 mV s^{-1} using a bare GC electrode in 0.1 M Tris-HCl buffer (pH 9.0) (a) in the absence and (b) in the presence of 1 mM NADH. (B) Cyclic voltammograms recorded in the same conditions as in A but using this time a vinylphenyl functionalized GC electrode (a) in the absence and (b) in the presence of 1 mM NADH. (C) Cyclic voltammograms recorded at a potential scan rate of 100 mV s^{-1} using Cys1-DSDH functionalized GC electrode in 0.1 M Tris-HCl buffer (pH 9.0) containing 1.8 mM NAD+ (a) in the absence and (b) in the presence of 1 mM D-sorbitol. The geometric surface area of the electrode was 0.28 cm^2.*

The vinylphenyl-functionalized electrode was then subjected to thiol-ene click coupling with Cys1-DSDH. However, this experiment resulted in the absence of measurable electroenzymatic production of NADH at the electrode surface as no change in the anodic signal can be noticed (**Figure 2.8C**, compare curve (a) in the absence of D-sorbitol and curve (b) in the presence of D-sorbitol). Three hypotheses can be proposed to explain this negative result: (1) a failure in the protein immobilization step, (2) a lack of activity of the proteins after immobilization, and (3) a limited amount of proteins immobilized on the flat electrode surface.

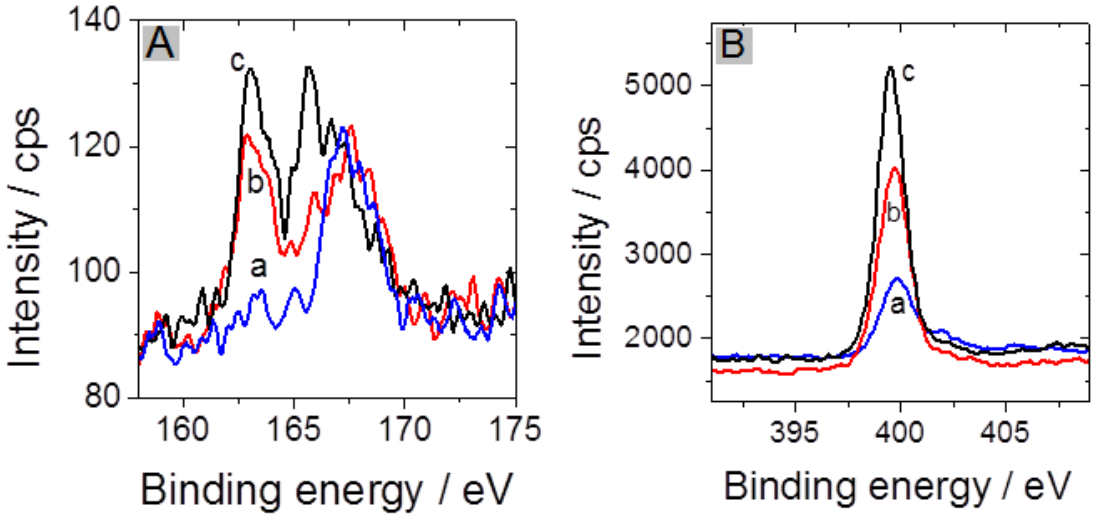

Figure 2.9. *XPS spectra of (A) S2p and (B) N1s signals obtained with GC electrodes electrografted with 4-vinylaniline diazonium cations at −0.6 V for 600 s (a) before and (b, c) after click coupling with (b) Cys1-DSDH and (c) DSDH.*

To prove the presence of proteins onto the electrode surface, XPS analysis was performed on the functionalized electrodes before and after contact with proteins under the conditions required for thiol-ene coupling reaction (**Figure 2.9**). Here, both Cys1-DSDH and DSDH (i.e., without cysteine tag) were studied. The intensity of the signal observed on the S 2p core level spectra was found to increase after the click step (0.22% atomic content, curves b and c, **Figure 2.9A**). This signal, centered at 163 eV, can be attributed to the presence of –C–S–C– linkage at the surface [181,182]. It should be also mentioned that a S2p signal located at 168 eV is observed even before the click reaction (curve a). This can be attributed

to the presence of SO_4^{2-} traces (coming from the sodium nitrite used to generate the diazonium cations from the 4-vinylaniline since the electrografting step is carried out using and excess of the nitrite source, in order to ensure quantitative conversion into the diazonium salt, and without separation of the final product). In addition, analysis of the high-resolution core level spectra for N 1s shows a peak located at 400 eV after electrografting of the diazonium salt attributed to the possible presence of *–C-N=N-C-* linkage (**Figure 2.9B**). The atomic content of nitrogen on the surface detected at 399.6 eV was found to increase by reaction with the two proteins, from 4% before (curve a) to 9% (Cys1-DSDH) or 11% (DSDH) after contact with the proteins. Overall, the clear increase of the nitrogen and sulfur contents after reaction with the proteins must result from their adsorption/attachment onto the electrode surface. These results confirm that proteins are really present on the surface of glassy carbon, but there is no clear evidence of enzyme attachment via the cysteine tag. Indeed, in the absence of cysteine tag, any cysteine residues from the protein [183,184] could react with the vinyl moieties in a comparable way as reported for cytochrome c with maleimide [185]. The structure of DSDH is shown in **Figure 2.10** and the positions of cysteine residues are pointed out. The only cysteine, which might have access to vinylphenyl, would be Cys54 with accessible surface areas (ASA) of 37.9 or 43.5 square Angstrom, respectively. Because there is no crystal structure of the protein with the His(6)-Cys(2)tag, ASA values for these cysteines cannot be given. However, the ASA of the N-terminal methionine is calculated for both chains as 106.1 or 108.5, respectively, assuming that the surface areas of the free accessible cysteines in the tag are probably even larger and therefore, click-reaction with these thiol groups should be highly preferred. We will show in the next section that there exists indeed an advantage of the cysteine tag for the immobilization of proteins on the electrode surface.

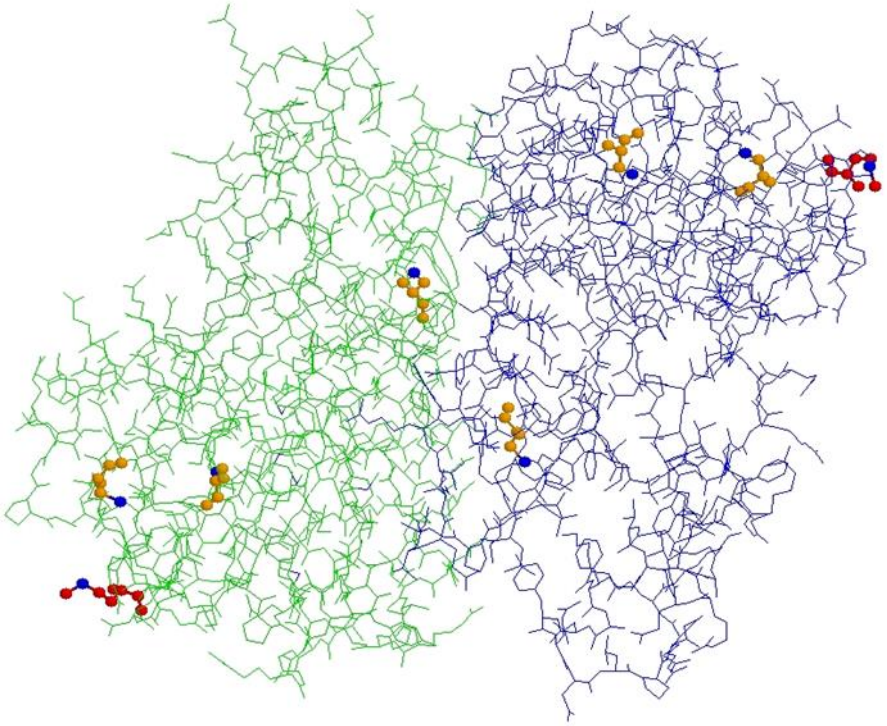

***Figure 2.10**. Structure of the D-sorbitol dehydrogenase dimer. Cysteines in orange, sulfur in blue, and N-terminal methionine in red (established with Open RasMol program).*

2.3.3 Immobilization of cysteine-tagged D-sorbitol dehydrogenase on carbon felt electrode.

At first, the electrografting reaction was optimized using NADH as a redox probe. The concentration of vinylaniline was decreased by 10 times and cyclic voltammetry was replaced by a pulse potential technique in order to limit the amount of vinylphenyl groups that can hinder NADH oxidation. **Figure 2.11A** reports the electrochemical response of an activated carbon felt electrode to NADH cofactor, showing clearly the existence of an anodic peak at 0.5 V in the presence of 1 mM NADH. After diazonium electrografting of vinylphenyl groups (performed at -0.6 V for 1s), this signal was strongly affected but the oxidation of NADH could still be observed at higher overpotentials as demonstrated by the current increase in the potential region between +0.6 V and +1.0 V after addition of NADH (compare curves a and b in **Figure 2.11B**).

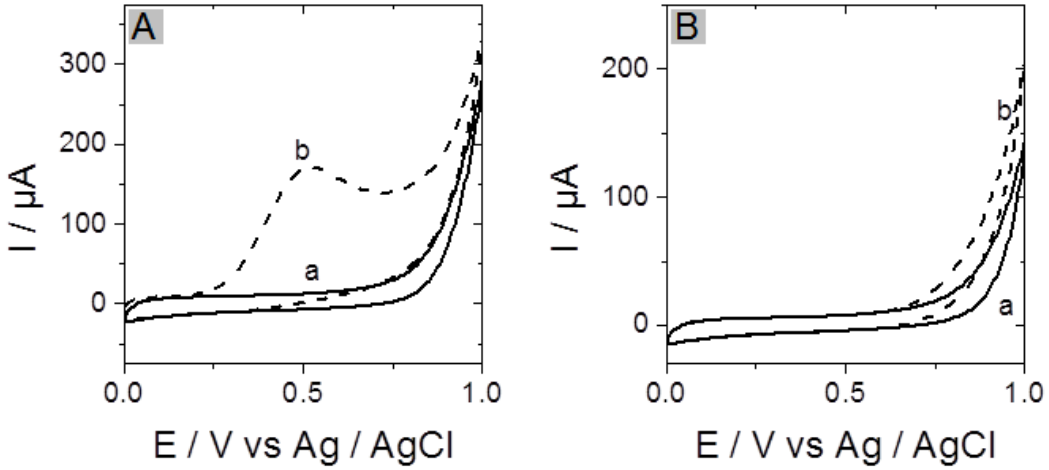

Figure 2.11. *Cyclic voltammograms recorded using (A) an activated bare carbon felt or (B) a vinylphenyl functionalized carbon felt electrode in 0.1 M Tris-HCl buffer (pH 9.0) (a) in the absence and (b) in the presence of 1 mM NADH. All curves have been recorded at a potential scan rate of 20 mV* s^{-1}*. The surface area of the carbon felt electrode was 95* cm^2.

A short electrografting time at -0.6 V (i.e., 1 s) was thereby chosen in order to provide vinylphenyl moieties on the electrode surface while maintaining an electrochemical response to NADH (see the response for 2 s electrografting in **Figure 2.12**).

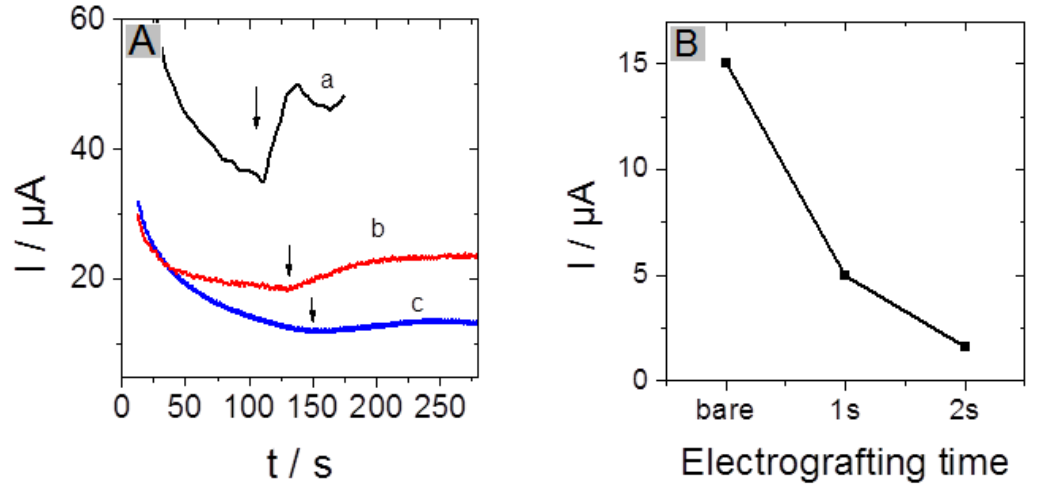

Figure 2.12. *(A) Amperometric response to the addition of 0.1 mM NADH at an applied potential of 0.8 V in 0.1 M Tris-HCl buffer at pH 9.0 for activated carbon felt electro-grafted with 4-vinylaniline diazonium cations at -0.6 V for (a) 0 s; (b) 1 s and (c) 2 s. (B) Plot of the oxidation current to 0.1 mM NADH for these different electrodes. The surface area of the carbon felt electrode was 95* cm^2.

As in the case of GC electrode (see above), the thiol-ene reaction on CF was first evaluated by reaction with 6-(hexanethiol)ferrocene and the presence of ferrocene was confirmed by cyclic voltammetry (**Figure 2.13**), so that one can also expect to be able to attach thiol-containing proteins onto vinylphenyl-functionalized CF electrodes via click chemistry.

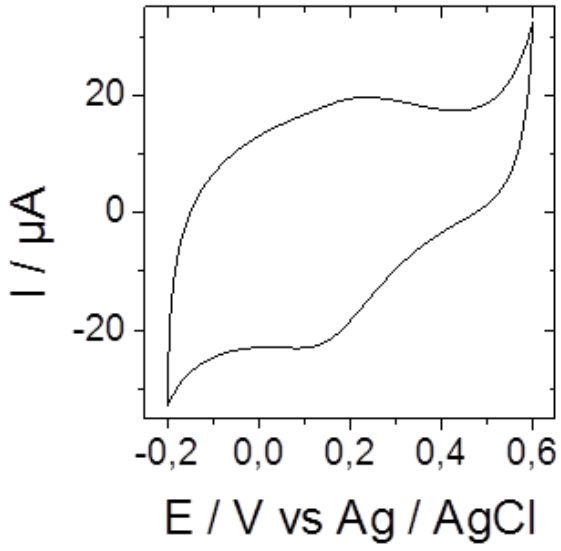

***Figure 2.13**. Cyclic voltammogram recorded in 0.1 M Tris-HCl buffer at pH 9.0 for ferrocene functionalized carbon felt electrode. Electrode potential scan rate was 20 mV s^{-1}. The surface area of the carbon felt electrode was 95 cm^2.*

Cys1-DSDH was then let to react with the carbon felt functionalized with vinylphenyl moieties, and the electrochemical response of the bioelectrode to D-sorbitol was evaluated by chronoamperometry at +0.8 V. Upon addition of D-sorbitol from 0.2 to 3 mM in the solution, the amperometric response was found to increase progressively and then tended to level off at higher concentrations (**Figure 2.14A**).

The apparent Km was evaluated from triplicate experiments, and a value of 0.9 ± 0.2 mM was found (**Figure 2.15**), which is slightly better than that for the protein in solution (6.4 mM). A similar result (apparent Km of 0.4 mM) was obtained with the tag composed of 2 cysteines (cys2-DSDH **Figure 2.16**).

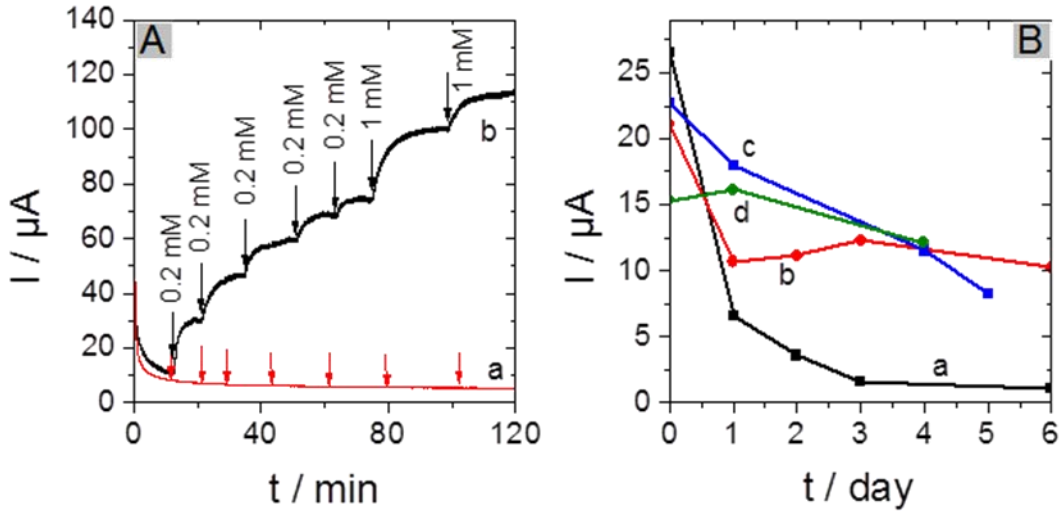

Figure 2.14. *(A) Amperometric response of (a) carbon felt electrode and (b) Cys1-DSDH functionalized carbon felt electrode to successive additions of D-sorbitol from 0.2 to 3 mM. (B) Catalytic current to the addition of 1 mM D-sorbitol measured with carbon felt electrodes modified by thio-ene click chemistry with (a) DSDH, (b and c) Cys1- DSDH, and (d) Cys2-DSDH. Both (A) and (B) were performed at +0.8 V in 20 mL of 0.1 M Tris-HCl buffer (pH 9.0) with 1.8 mM NAD^+. The surface area of the carbon felt electrode was 95 cm^2.*

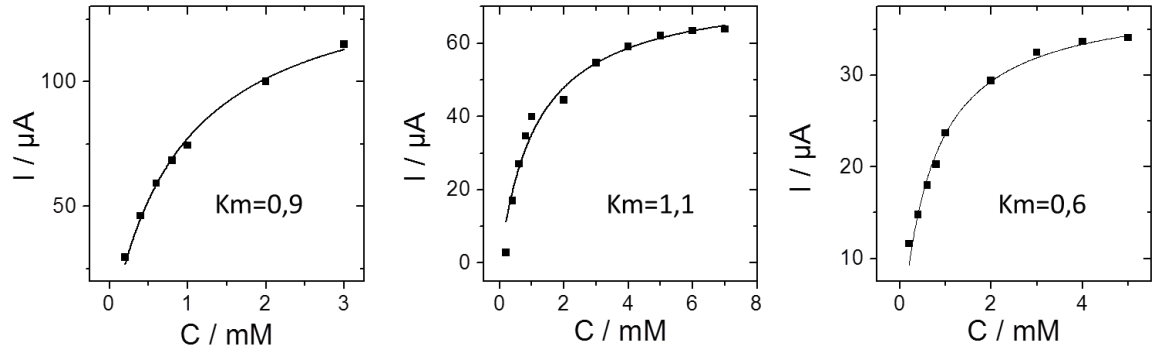

Figure 2.15. *Amperometric response of a Cys1-DSDH functionalized carbon felt electrode to successive additions of D-sorbitol. The experiment was performed at +0.8 V in 20 mL 0.1 M Tris-HCl buffer (pH 9.0) with 1.8 mM NAD^+. The surface area of the carbon felt electrode was 95 cm^2.*

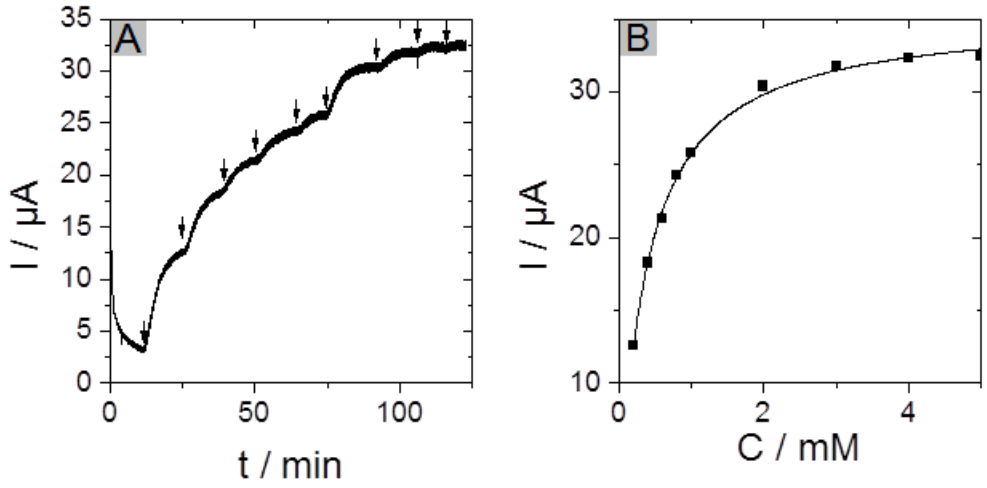

***Figure 2.16**. (A) Amperometric response of the Cys2-DSDH functionalized carbon felt at an applied potential of 0.8 V in 0.1 M Tris-HCl buffer at pH 9.0 to successive additions of D-sorbitol. The experiment was performed in the presence of 1.8 mM NAD^+. (B) Data treatment for apparent Km determination. The surface area of the carbon felt electrode was 95 cm^2.*

Therefore, the length of the cysteine tag does not affect significantly the activity of the immobilized protein. As click chemistry can involve either a cysteine tag or cysteine moieties already present in the protein, a control experiment has been performed by letting DSDH (a cysteine-tag-free protein) react with the vinylphenyl functionalized carbon felt surface. One already knows from XPS measurements that such protein can be adsorbed at the carbon surface quite similarly to the cys1-DSDH (**Figure 2.9**).

A response was also observed but was not stable with time. **Figure 2.14B** reports the catalytic current to the addition of 1 mM D-sorbitol measured with carbon felt electrodes modified by thiol-ene click chemistry with DSDH, Cys1-DSDH, and Cys2-DSDH. While the current measured with cysteine-tagged proteins was kept for several days (curves b, c, and d), it diminished rapidly with DSDH that did not possess a cysteine tag (curve a). Moreover, the more stable electrochemical response was observed with Cys2-DSDH (curve c). These results support the idea that proteins without cysteine tags are simply adsorbed on the electrode surface, without strong chemical attachment. The introduction of a tag, either one or two cysteine, improved significantly the operational stability of the electrode. The stability of the immobilized protein was not lower than the one observed with the free protein in solution

(half-life period of 48 h at 28 °C) and could be considered for application in electroenzymatic synthesis.

2.3.4 Application to the electroenzymatic reduction of D-fructose in the presence of $[Cp^*Rh(bpy)Cl]^+$

The two major fields of application of dehydrogenases are biosensing and electrosynthesis [180]. In biosensing, the oxidation reaction is most often exploited, considering different targets such as glucose, lactate, or ethanol. Detection via NADH oxidation is usually performed in the presence of an electrochemical mediator that permits decreasing significantly the anodic overpotentials in order to limit interferences. In electrosynthesis, reduction reactions are most often investigated, for example the enantioselective reduction of ketone to alcohol. In this case, NADH needs to be regenerated by reduction of NAD^+. The direct reduction of NAD^+ occurs at high overpotential and leads to the degradation of the enzymatic cofactor [17], so that long-term use of the enzyme/cofactor system and high turnover numbers require the use of a mediator. One of the most appropriate mediators for efficient NADH regeneration (**Figure 2.7B**) is the complex (2,2‟-bipyridyl)(pentamethylcyclopentadienyl)-rhodium(III), $[Cp^*Rh(bpy)Cl]^+$ [32], which will be evaluated hereafter with Cys1-DSDH proteins immobilized on carbon felt.

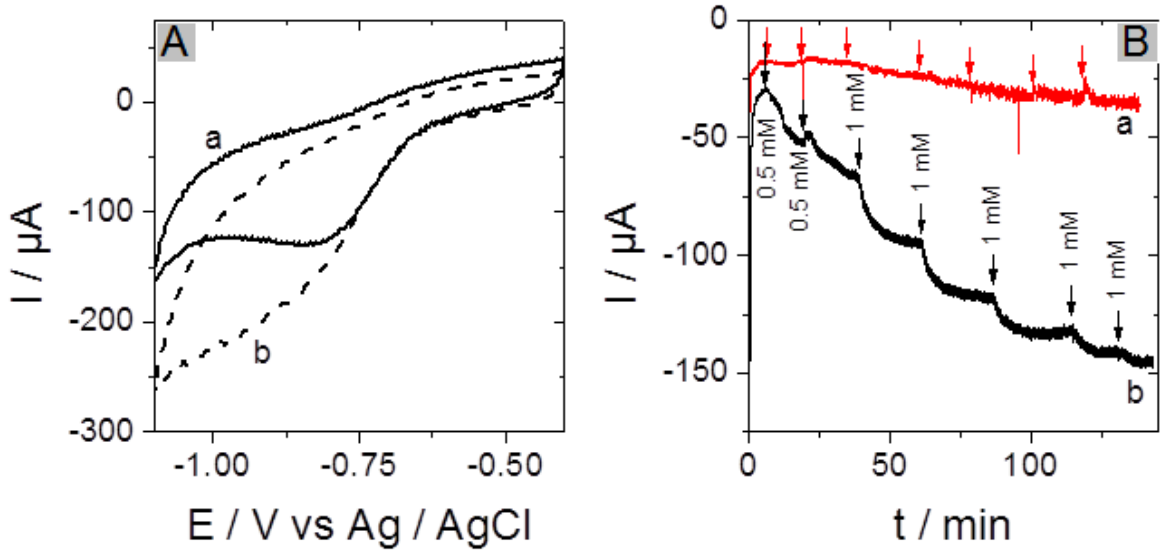

***Figure 2.17**. (A) Cyclic voltammograms recorded at a potential scan rate of 20 mV s^{-1} using a Cys1-DSDH functionalized carbon felt electrode (a) in the absence and (b) in the presence of 1 mM D-*

*fructose. (B) Amperometric response to increasing concentration of D-fructose from 0.5 to 6 mM recorded using (a) an unmodified CF electrode and (b) the same Cys1-DSDH functionalized CF electrode at an applied potential of -0.85 V. All experiments were performed under nitrogen in 20 mL of 0.1 M PBS buffer (pH 6.5) containing 1.8 mM NADH and 0.1 mM [Cp*Rh(bpy)Cl]$^+$. The surface area of the carbon felt electrode was 95 cm^2.*

Figure 2.17A depicts typical cyclic voltammograms measured with carbon felt modified by Cys1-DSDH in the presence of [Cp*Rh(bpy)Cl]$^+$. In the absence of fructose, the mediator gave rise to a well-defined reduction peak at -0.8 V (curve a), demonstrating that the diazonium electrografting does not hinder the electrochemical reduction of [Cp*Rh(bpy)Cl]$^+$. When 1 mM D-fructose was introduced in the solution (curve b), the cathodic current was almost twice as before, indicating the electrocatalytic reduction of NAD$^+$ generated by the enzymatic reaction (regeneration of NADH). A control experiment performed in the absence of [Cp*Rh(bpy)Cl]$^+$ confirmed that NAD$^+$ was not directly reduced at this potential on the carbon felt electrode, the reaction occurring at a more cathodic value (i.e., -1V, **Figure 2.18**).

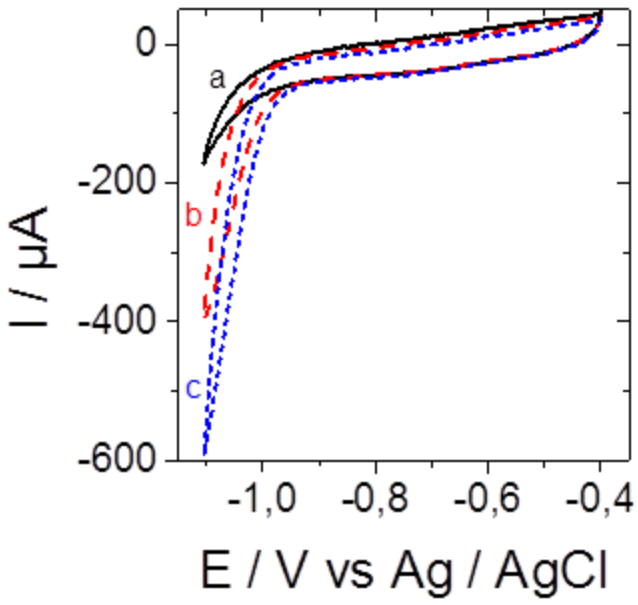

***Figure 2.18**. Cyclic voltammograms recorded under nitrogen in 0.1 M PBS buffer at pH 7.0 for activated carbon felt in the presence of increasing NAD$^+$ concentration: (a) 0 mM (solid line); (b) 0.25 mM (dashed line) and (c) 0.5 mM (short dashed line). Potential scan rate was 10 mV s^{-1}. The surface area of the carbon felt electrode was 95 cm^2.*

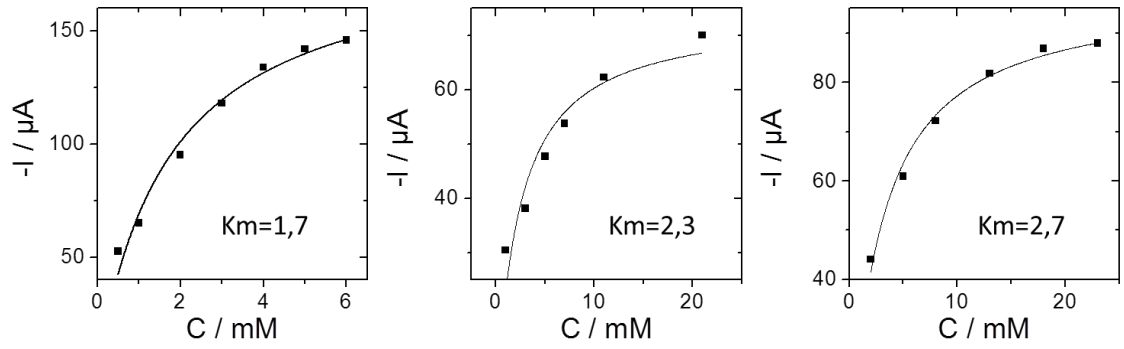

***Figure 2.19**. Amperometric responses to increasing concentration of D-fructose recorded using the same Cys1-DSDH functionalized CF electrode at an applied potential of -0.85 V, experiments were performed under nitrogen in 20 mL 0.1 M PBS buffer (pH 6.5) containing 1.8 mM NADH and 0.1 mM [Cp*Rh(bpy)Cl]$^{+}$. The surface area of the carbon felt electrode was 95 cm^{2}.*

These results demonstrate that immobilizing dehydrogenase enzymes in the form of cysteine-tagged proteins by thiol-ene click-chemistry is also a promising strategy for possible applications in the field of electrosynthesis. The bioelectrode was then analyzed by chronoamperometry (**Figure 2.17B**). The cathodic current was increasing regularly upon addition of D-fructose in the solution from 0.5 to 6 mM. The apparent Km estimated from triplicate data was 2.2 ± 0.5 mM (**Figure 2.19**), slightly higher than the one measured for oxidation reaction but still in the same range. However, as compared to the protein in solution with a Km value for fructose reduction of 49.4, this value is almost 30 fold lower, indicating that not only the stability increases with immobilization, but also the affinity of D-fructose to DSDH has improved. As a conclusion, the protein immobilized on carbon felt electrode displayed a very good activity, characterized by low Km values. The bioelectrode was finally applied for bioconversion (**Figure 2.20**). A very good relationship was found over 5 days between the catalytic current and the production of D-sorbitol from D-fructose (decrease of current proportional to the amount of transformed D-fructose). The bioconversion was found to be stoichiometric (**Figure 2.20B**) and the faradaic efficiency was 77%, which is very good in comparison of reported electrochemical bioconversion experiments form the literature [29,33,186–188].

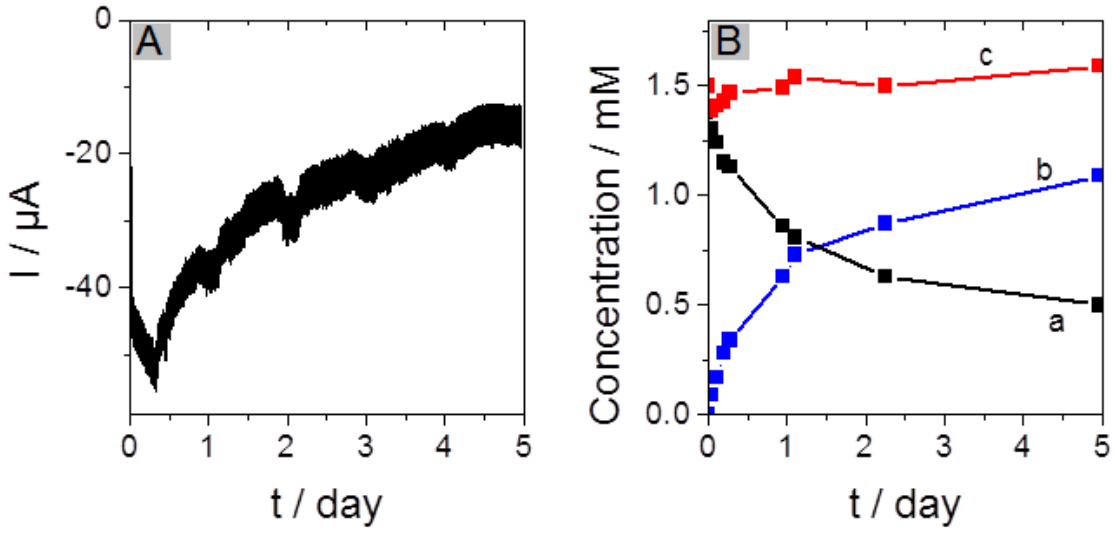

Figure 2.20. *Electroenzymatic conversion of D-fructose to D-sorbitol with (A) the current measured at −0.85 V versus Ag/AgCl and (B) evolution with time of (a) D-fructose, (b) D-sorbitol, and (c) the sum of D-fructose and D-sorbitol concentrations, determined by HPLC. The surface area of the carbon felt electrode was 380 cm*^{2}.

The current density delivered by the bioelectrode could be improved by increasing the surface area of the electrode. An attempt was done by functionalization of carbon felt with carbon nanotubes as previously reported. Three times increase in current was observed here (**Figure 2.21**). More improvement can be thus expected by further optimization of the electrode porosity and electrografting protocol in order to enhance the amount of protein immobilized on the electrode surface.

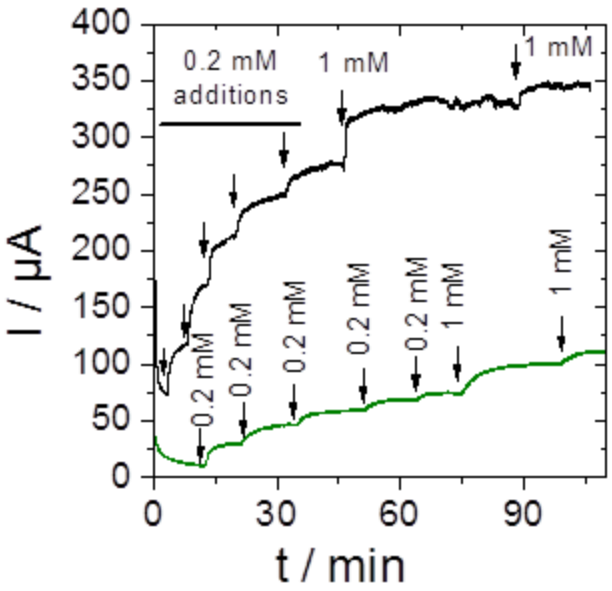

Figure 2.21. *Amperometric responses of the cys1-DSDH modified (a) MWCNT-carbon felt (0.5*0.5*0.5cm^3), (b) bare carbon felt to successive additions of D-sorbitol. The experiment was performed at +0.8 V in 20 mL 0.1 M Tris-HCl buffer (pH 9.0) with 1.8 mM NAD$^+$. The porous electrode was prepared by dipping CF into a 1 mg mL^{-1} suspension of multi-walled carbon nanotubes functionalized by carboxylic groups (MWCNT, 95%, ; 15 ± 5 nm, L 1–5 mm, Nanolab) and dried at 130°C for 30 min. This process was repeated 10 times. The modifications with cysteine-tagged DSDH were then performed following the same protocol as reported in the manuscript.*

2.4 Conclusions

Thiol-ene click chemistry was successfully applied to the immobilization of dehydrogenase-based proteins on carbon electrode surfaces for application in bioelectrochemical reactions. The combination of this reaction with diazonium electrochemistry allowed the fabrication of electrodes that did not prevent the electrochemical detection of redox probes in solution (ferrocenedimethanol, $[Cp^*Rh(bpy)Cl]^+$,and NADH). The activity of D-sorbitol dehydrogenase was kept when click coupling was made on proteins bearing a cysteine tag in front of a His(6)tag (either composed of 1 or 2 cysteine moieties). It appears very convenient to take advantage of histidine-cysteine-tagged proteins as they can easily be purified via the His(6)Tag and IMAC before immobilization on electrode. The electrocatalytic reduction of D-fructose to D-sorbitol by the immobilized DSDH was evidenced with using $[Cp^*Rh(bpy)Cl]^+$ as electron mediator. The system was applied successfully to electroenzymatic enantioselective synthesis of D-sorbitol from D-fructose. The combination of cysteine-tagged proteins with thiol-ene click reaction opens great perspectives for covalent immobilization of redox proteins in an active form on electrode surfaces for biosensing, fuel cell, and electrosynthesis applications. Moreover, positioning a cysteine tag at different locations of the polypeptide chain should allow, in principle, a controlled orientation of the protein in order to optimize direct electron transfer reactions with bound cofactor of redox proteins.

Chapter 3. Covalent immobilization of rhodium complex on porous carbon electrode for NADH regeneration

Here we report a new synthetic route for covalent immobilization of rhodium complex on porous carbon electrode in three steps as a catalyst for nicotinamide adenine dinucleotide reduced form (NADH) regeneration. The carbon electrode (carbon felt modified with multi-wall carbon nanotube, CF-CNT) was first modified with azidophenyl groups groups by diazonium electrografting generated from 4-azidoaniline. The bipyridine ligand was modified with an alkynyl group, the covalent bond between the alkynyl group from bipyridine and the azide group from the electrode was formed via azide-alkyne Huisgen cycloaddition reaction (CF-CNT-4‴4-Bpy). After a final step complexation with pentamethylcyclopentadienyl rhodium(III) chloride dimer ($(RhCp^*Cl_2)_2$), rhodium complex was functionalized on the electrode in an active form (CF-CNT-4‴4-Bpy-Rh). Different steps were confirmed by x-ray photoelectron spectroscopy. The eletrocatalytic response of CF-CNT-4‴4-Bpy-Rh to NADH regeneration from NAD^+ was evaluated and a high faradic efficiency of 87% was obtained in a 18 h chronoamperometry experiment. In comparison with the the CF-CNT electrode with simple adsorption of $[Cp^*Rh(bpy)Cl]^+$, a better long-term stability up to 14 days in solution with stirring was validated. Finally, the rhodium complex functionalized electrode was applied in electroenzymatic synthesis by depositing a silica gel layer contains NAD-dependent D-sorbitol dehydrogenase on the top, the transformation from D-fructose to D-sorbitol was achieved.

3.1 Introduction

Nowadays, NAD-dependent enzymes, especially dehydrogenases are of increasing interest for enantioselective bioconversion of a variety of compounds, eg. alcohols, acids, and sugars [4] . However, their practical applications are limited by the high price of the nicotinamide cofactors, so the regeneration of the cofactor is critical when considering to build a long-term synthesis system [18,189–192].

The regeneration of nicotinamide cofactor could be realized by enzymatic [191,193], chemical [6,194], or electrochemical methods [2,195]. Compared to chemical or enzyme-coupled cofactor regeneration, which needs a second enzyme as well as a second substrate, electrochemical regeneration methods are getting rid of the side product formation produced from the coenzyme as well as the co-substrate separation. The main advantage of mass-free electrochemical regeneration method is to offer the possibility of simplifying the processes in bioconversion. In enzymatic reduction reactions, the easiest way for electrochemical regeneration of NADH is by applying a negative potential on the electrode surface to reduce NAD^+ back to NADH. However, the negative potential needed is very high (-0.9 V, as reported in the literature [3]), at this potential, NAD^+ will be dimerized to NAD_2 instead of NADH, making the molecule unusable by the enzyme [4,27]. Therefore, to avoid the dimerization of cofactors at high potential, a catalyst who has a redox potential slightly more negative than the redox potential of cofactor NAD^+ / NADH (-0.56 V) would be favored [5]. Up to now, rhodium-based complexes $[Cp^*Rh^{III}(L)Cl]^+$ proposed by Steckhan et al. [27,28,186,196,197] was proved to be the most successful non-enzymatic regeneration catalyst for NADH regeneration [136].

However, some reports illustrate that low enzymatic catalytic stability is associated with the presence of a rhodium complex since the surface functional groups of enzymes can interact with rhodium complex, leading to degradation of rhodium complexes. The separation of the enzymes from the rhodium complex by immobilizing them separately would provide a system without losing the long-term stability [6,7,198]. Furthermore, immobilization of rhodium complex on electrodes will not only avoid the degradation problem, but also make easier the isolation of the reaction products and cofactors from the rhodium complex. Many efforts have been done to immobilize rhodium complexes onto different electrodes in order to

improve their reusability as well as their enzymatic catalytic stability in a bio-electrochemical system,

Generally, two strategies have been successfully developed to immobilize rhodium complexes on an electrode surface in an active form. The first category is based on polymers deposition onto the electrodes. Chardon-Noblat and coworkers prepared polypyrrolic rhodium (III) complex (2,2'-bipyridine or 1,10-phenanthroline ligand) films on electrode by anodic electropolymerization of pyrrole monomers. The electrocatalytic interest of this modified electrode for hydrogen evolution was demonstrated [137]. Beley and coworkers bound a rhodium (III) bis-terpyridinepyrrole complex by electropolymerization on a reticulated vitreous carbon electrode, the long-term stability of the modified electrode was characterized by reduction of NAD^+ into 1,4-NADH, and it was then applied for reduction of cyclohexanone to cyclohexanol in the presence of alcohol dehydrogenase [29]. In a report from Nolte and coworkers, rhodium complexes were incorporated into the bilayers of vesicles formed from a polymerizable ammonium surfactant by copolymerization reaction. The catalytic activity of the rhodium complexes was depending on its position in the bilayer [138]. In above cases, the porous polymerized electrode was modified by electropolymerization. Despite electropolymerization, another polymerization route by ɤ-irradiation cross-linking was also reported to obtain $[Rh^{III}(C_5Me_5)(L)C1]^+$ complex polymer-modified electrodes. Even through this method can provide a stable bonding, it suffered from the electron shielding effect caused by the thick porous polymer film. This charge transfer limitation effect caused by polymer layer was proved by the fact that when the amount of immobilized polymer was doubled on the electrode, the charge calculated from the reduction peak was only increased by a factor of less than 2 [139].

The second strategy is to take advantage of the π-π stacking effect between carbonaceous materials (graphene and carbon nanotubes) and aromatic moieties from rhodium complex. This interaction would favor a strong adsorption of the rhodium complex on the carbon support. In this route, the electrode surface was only covered with a monolayer rather than thick porous polymer films, the electron shielding effect was in principle eliminated and the electron transfer between the rhodium complex and the electrode was facilitated, a surface-confined electrochemical behavior was observed. Park and coworkers reported the synthesis of a 3D-structured graphene–Rh-complex hydrogel, on which the phenanthroline introduced Rh complex was strongly immobilized on the graphene surface through π-π interaction and π-cation interaction, the repeated usability for electrochemical

NADH regeneration up to 7 cycles (each cycle lasts 2 h) was demonstrated [35]. Later on, Minteer and coworkers synthesized a rhodium complex with a pyrene-substituted phenanthroline ligand which was immobilized onto MWCNT via π-π stacking, good catalytic response for the regeneration of NADH and repeated usability up to 10 cycles (each cycle lasting 30 min) were achieved [34]. In both cases, the immobilization of rhodium complex significantly increased the usability of the catalyst over time, making it applicable in NADH-dependent enzymatic catalytic systems. However, this method could only be applied on CNT or 3D-structured graphene that has aromatic rings as electrode, making it limited in large scale application. On the other side, π–π stacking is a kind of reversible non-covalent bond with bond energy 0-10 kcal / mol, lower than the covalent bond which is 80-100 kcal/ mol [140,141]. So in principle, the π-π stacking was not as stable as covalent binding if applied for continuous long-term bioconversion. In order to both take advantage of the stable covalent bonding and getting rid of the electron shielding effect, up to now, an attempt has been made to covalently immobilize thiol-functionalized rhodium complex by self-assembled monolayers (SAMs) on gold electrodes. There molecules could be electrochemically active but did not show any electrocatalytic activity to addition of NAD^+ [142]. This inactivation phenomena was explained by the strong coordination effect between –SH groups and the rhodium center [6,142,198]. The strategy to avoid this coordination effect could be to first immobilize covalently the bipyridine ligands on the electrode via functional groups, then to coordinate the rhodium center at the very last step.

In this study, we report a covalent immobilization of the alkynyl modified rhodium complex on an azido-functionalized CF-CNT as illustrated in **Figure 3.1**. Diazonium electrochemical reduction is a convenient way to functionalize electrode surfaces [199]. Our electrode was first functionalized with azide group by electrochemical reduction of the azidophenyl diazonium salt generated from the 4-azidoaniline electrografting, the grafting steps were shown in **Figure 3.1**. Then the covalent bond between alkynyl bipyridine (**B**) and azide groups on the electrode (CF-CNT-Az, **A**) was formed through „azide-alkyne" click chemistry, a bipyridine functionalized electrode (CF-CNT-4'4-Bpy, **C**) was obtained. After complexation of with $(RhCp^*Cl_2)_2$ in the last step, a rhodium complex immobilized electrode (CF-CNT-4'4-Bpy-Rh, **D**) was accomplished (**Figure 3.1**). The catalytic response for electrochemical regeneration of NADH from NAD^+ as well as the long-term stability of CF-CNT-4'4-Bpy-Rh were evaluated. Finally, the NAD-dependent dehydrogenases were

immobilized in a sol-gel matrix on the top of the rhodium complex modified electrode in order to study the electroenzymatic response to addition of substrate.

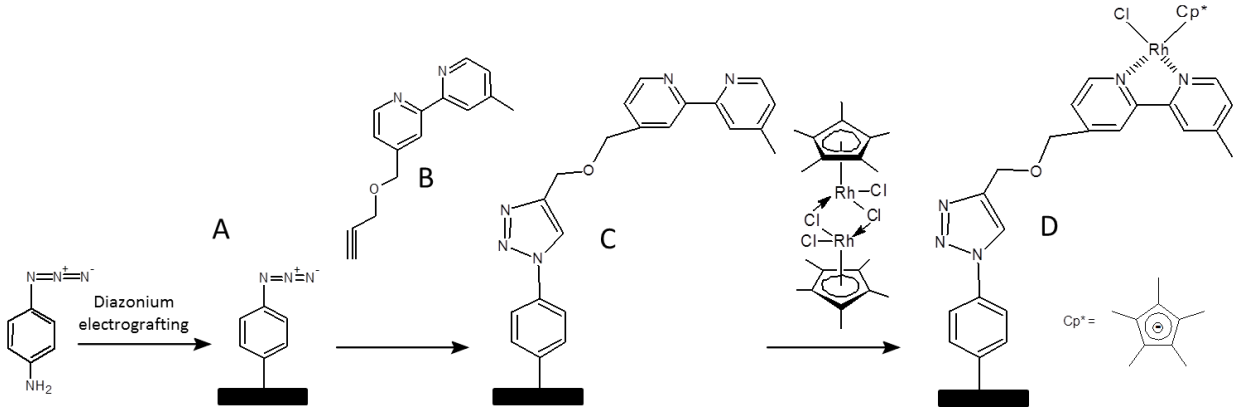

Figure 3.1. *Synthetic route followed for the functionalization of a carbon electrode surface with rhodium complex.*

3.2 Experimental

Chemicals and Enzymes

The following chemicals were used as received: tetraethoxysilane (TEOS, 98%, Alfa Aesar), 3-glycidoxypropyltrimethoxysilane (GPS, 98%, Sigma-Aldrich), β-nicotinamide adenine dinucleotide hydrate (NAD^+, ≥ 96.5%, Sigma-Aldrich), β-nicotinamide adenine dinucleotide, reduced disodium salt hydrate (NADH, ≥97%, Sigma-Aldrich), 4-azidoaniline hydrochloride (97%, Sigma-Aldrich), sodium nitrite (≥97.0% , Sigma-Aldrich), copper actate (Prolab), ascorbic acid (Prolab), pentamethylcyclopentadienylrhodium(III) chloride dimer ($(RhCp^*Cl_2)_2$, Sigma-Aldrich), D-fructose (99 wt%, Sigma), sodium dihydrogen phosphate (99.5%, Merck), hydroxyacetone (95%, Alfa Aesar), carbon felt (GFD 4.6 EA, density 0.09 g cm^{-3}, electrical resistivity 3-6 Ω mm, Sigratherm®), poly(ethylene imine) (PEI, 50% w/v in water, Mn = 60000, Fluka), carboxylic-functionalized multi-walled carbon nanotubes (MWCNT, 95%, Φ 15±5 nm, L 1-5 µm, Nanolab). Overproduction of N-His(6) D-sorbitol dehydrogenase (800U mL^{-1}) and N-His(6)-Cys-galactitol dehydrogenase (60U mL^{-1}) were done with Escherichia coli BL21GOLD (DE3) containing the corresponding expression-

vectors pET-24a(+) (Novagen) and purification of the enzyme was performed with Histrap columns (GE Healthcare).

*Sythesis of 4-[(2-propyn-1-yloxy)methyl]-4'-methyl-2,2'-bipyridine (compound **B**)*

The protocol for synthesis is following the reported literature in three steps [142].

a. 4-(carboxyaldehyde)-4‟-methyl-2,2‟-bipyridine MS (CI, CH_4) *m/z*: 213 (100) [M+1]. ^{1}H NMR (400 MHz, $CDCl_3$) δ: 2.48 (s, 3H), 7.23 (d, *J*=5.0 Hz, 1H), 7.74-7.78 (m, 1H), 8.32 (s, 1H), 8.62 (d, *J*= 4.9 Hz, 1H), 8.88 (s, 1H), 8.95 (d, *J*=4.9 *Hz,* 1H), 10.23 (s, 1H).
b. 4-(hydroxymethyl)-4‟-methyl-2,2‟-bipyridine MS (CI, CH_4) *m/z*: 201 (100) [M+1]. ^{1}H NMR (400 MHz, $CDCl_3$) δ: 2.49 (s, 3H), 5.03 (s, 2H), 7.18-7.25 (m, 1H), 7.41-7.48 (m, 1H), 8. 30-8.35 (m, 1H), 8.40-8.42 (m, 1H), 8.59 (d, *J*=4.9 Hz, 1H), 8.72 (d, *J*=5.0 Hz, 1H,)
c. 4-[(2-propyn-1-yloxy)methyl]-4‟-methyl-2,2‟-bipyridine MS (CI, CH_4) *m/z*: 239 (100) [M+1]. ^{1}H NMR (400 MHz, $CDCl_3$) δ: 2.36 (s, 3H), 2.40 (t, *J*=2.4 Hz, 2H), 4.23 (d, *J*=2.4 Hz, 2H), 4.67 (s, 2H), 7.15-7.16 (m, 1H), 7.18-7.20 (m, 1H), 8.24-8.28 (m, 1H), 8.30-8.33 (m, 1H), 8.49 (d, *J*=5.0 Hz, 1H), 8.68 (d, *J*=5.0 Hz, 1H).

MWCNT-functionalized carbon felt electrode

In order to change the surface from hydrophobic to hydrophilic, the surface of carbon felt was activated by recording up to 20 consecutive cyclic voltammetry scans over the range potential from -0.7 V to 2.5 V in 0.1M H_2SO_4. After such process of electrochemical conditioning, the carbon felt was first rinsed with water and subsequently heated up to at 200℃ for 1h to remove the remaining H_2SO_4. Afterwards, the carbon felt was cut into pieces with dimension 0.5 cm* 0.5 cm. MWCNT-functionalized carbon felt was prepared by dipping the carbon felt into 0.5 mg/mL MWCNT suspension which is dispersed in an ultrasonic bath, then let it dry in the oven at 130 ℃. The dipping/drying cycles were repeated for 10 times in order to ensure that plenty of CNT were immobilized on the carbon felt substrate.

Azido-functionalized CF-CNT electrode

The diazonium cations were generated "in situ" by mixing 1 mM 4-azidoaniline and 2 mM sodium nitrite in 0.5 M HCl water solution with stirring for 5 min. The isolation of the diazonium salt is not required and its grafting process is carried out using the same solution they were generated. The grafting process was carried out by electrochemical reduction performed by recording two consecutive cyclic voltammetry potential scans over the potential

range from 0.4 V to -0.6 V on a CF-MWCNT electrode. After electro-grafting, the carbon electrode was rinsed with distilled water to remove the remaining ungrafted compounds.

Bipyridine derivative covalent immobilization on CF-CNT-Az electrode via Huisgen cycloaddition reaction.

To a solution of molecule **B** (2.4 mg) dissolved in dimethilformamide (7 mL), a mixture of copper actate (1 mg) and ascorbic acid (2 mg) dissolved in an aqueous solution (3 mL) was added. The CF-CNT-Az electrode was immersed in this solution at room temperature for 24h in darkness. After this period the electrode was rinsed carefully with water and DMF.

Complexation reaction of rhodium with the CF-CNT-4'4-Bpy electrode.

The ability of the bipyridine ligands to coordinate transition metal was used in order to immobilize a rhodium complex. The bipyridine-functionalized CF-MWCNT electrode was then put in a dichloromethane (20 mL) solution containing $(RhCp^*Cl_2)_2$ (2 mg) with continuous stirring for 3h.

Co-immobilization of enzymes and rhodium complex on the electrode

For co-immobilization of enzymes on the Rh complex functionalized electrode, an enzyme silica sol was prepared according to a protocol that was previously described [200]. Briefly, a mixture of 0.18 g TEOS, 0.13 g GPS, together with 0.5 mL water and 0.625 mL 0.01 M HCl was pre-hydrolyzed by stirring overnight. Then, this sol was diluted 3 times and a 200 µL aliquot was mixed with 100 µL of PEI (20%), 100 µL of water and 150µL DSDH (or GatDH) stock solution. This mixture was spread over the CF-CNT-4'4-Bpy-Rh electrode and let it completely dry in the fridge for use. The CF-CNT-4'4-Bpy-Rh-gel electrode was prepared by following the same protocol but replacing the enzyme solution with same volume of water. The CF-CNT-ads-Rh-gel electrode was prepared by dipping CF-MWCNT electrode in 1mM $[Cp^*Rh(bpy)Cl]^+$ DMF / H_2O (7 : 3) solution overnight, then following the same protocol as for the CF-CNT-4'4-Bpy-Rh-gel electrode.

Procedures

All electrochemical measurements were carried out using an Autolab PGSTAT-12 potentiostat, and carried out in a sealed glass cell. A pencil core (0.5 mm diameter) connected with silver wire glued by carbon black was used for connecting the carbon felt working

electrode. Ag/AgCl (3 M KCl) was used as reference electrode, and a steel bar served as auxiliary electrode. As oxygen reduction is observed in the potential range of work the buffer solution was always purged with nitrogen for 15 min before performing the electrochemical measurement described and all the electrochemical characterizations were carried under nitrogen. During the experiment, all substrates added into the system were first purged under nitrogen, then added into the solution by a syringe.

UV-Vis spectra have been recorded on a Cary 60 Scan UV-Vis spectrophotometer.

X-Ray Photoelectron Spectroscopy (XPS) analyses were performed using a KRATOS Axis Ultra X-ray photoelectron spectrometer (Kratos Analytical, Manchester, UK) equipped with a monochromated AlKα X-ray source (hν = 1486.6 eV) operated at 150 W. The base pressure in the analytical chamber was 10^{-9} mbar during XPS measurements. Wide scans were recorded using a pass energy of 160 eV and narrow scans using a pass energy of 20 eV (instrumental resolution better than 0.5 eV). Charge correction was carried out using the C(1*s*) core line, setting adventitious carbon signal (H/C signal) to 284.6 eV.

3.3 Results and discussions

3.3.1 Characterization of the alkynyl functionalized rhodium complex in solution

A bipyridine molecule was first functionalized with an alkynyl group (molecule **B**) following the reported protocol [142]. After modification, the complexation of the molecule with $(RhCp^*Cl_2)_2$ was studied by UV spectroscopy. Sprectrum a in **Figure 3.2A** displays the UV-Vis spectrum of the molecule **B** alone in DMF/H_2O (7/3) solution. A single absorption peak was observed at 282 nm which was ascribed to the bipyridine ligand. After addition of an excess amount of $(RhCp^*Cl_2)_2$ in the solution, the peak at 282 nm decreased as a result of the complexation of the bipyridine ligand with the Rh. The structure of alkynyl functionalized $[Cp^*Rh(bpy)Cl]^+$ **(**compound **E)** was shown in **Figure 3.3**. Three new absorption bands appeared at 299 nm, 310 nm and 380 nm (Sprectrum **c** in **Figure 3.2A**). These absorption peaks from curve **a→b→c** was the evolution of complexation process in a time scale of approximately 20 min.

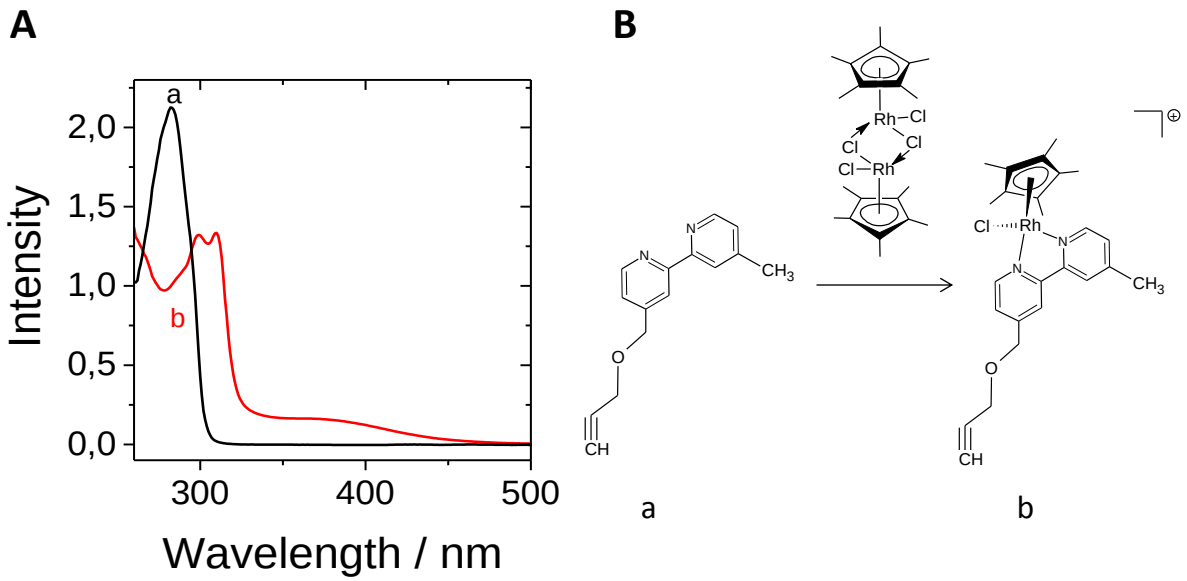

Figure 3.2. *(A)UV-vis spectra recorded for 4-[(2-propyn-1-yloxy)methyl]-4'-methyl-2,2'-bipyridine in DMF/H_2O (7/3) solution (a) before and (b) after complexation in the presence of a molar excess of (RhCp*Cl2)2. (B) Corresponding illustration of the complexation process.*

Since the catalytic activity of $[Cp^*Rh(bpy)Cl]^+$ has been proved to be influenced by the functional groups modified on the bipyridine ligand [142,197,201], the complex functionalized with alkynyl group had to be evaluated for NADH regeneration in comparasion with the original rhodium complex reported in the literature (molecule structure was show as **Figure 3.3** compound **F**). The experiment was performed at pH 6.5 i.e. in the optimol pH window determined previously [142]. **Figure 3.4A** shows the electrocatalytic response of alkynyl-functionalized $[Cp^*Rh(bpy)Cl]^+$ complex to NAD^+ reduction using a CF-CNT electrode in PBS buffer at pH 6.5. A reduction peak, attributed to compound **E** appears at -0.680 V, which was only -0.005 V negatively shifted compared to the classical unmodified compound **F** (**Figure 3.4B)**. There was no oxidation peak appear with compound **E**, but a small oxidation peak was observed with compound **F.** The appearance of an anodic peak could be explained by the lack of protons availability to form electrocatalytically active rhodium hydride complex, the unprotonated Rh(I) was oxidize back to Rh(III) on the electrode surface [136,142].

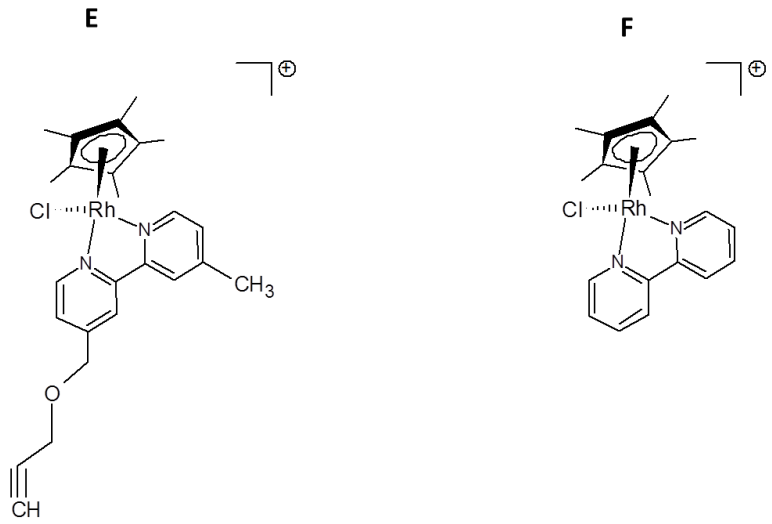

Figure 3.3. *Structures of alkynyl functionalized rhodium complex (compound* ***E****) and original unmodified rhodium complex (compound* ***F****).*

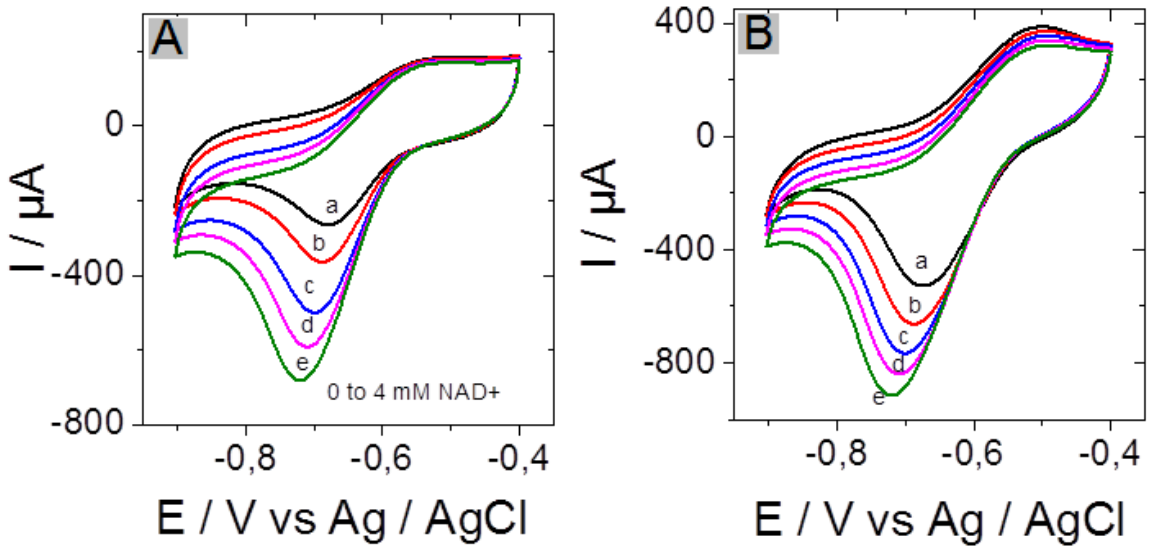

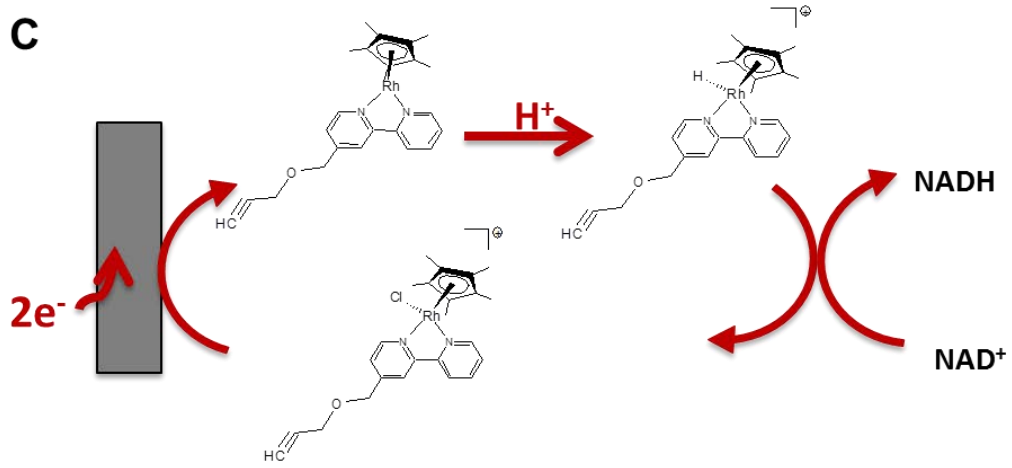

Figure 3.4. *(A) Cyclic voltammograms recorded using a CF-CNT electrode at a potential scan rate of 5 mV s^{-1} with 0.1 mM compound* ***E*** *to gradual addition of NAD^+ (a) 0 mM (b) 1 mM (c) 2 mM (d) 3 mM (e) 4 mM ; (B) Cyclic voltammograms recorded using a CF-CNT electrode at a potential scan rate of 5 mV s^{-1} with 0.1 mM compound* ***F*** *to gradual addition of NAD^+ (a) 0 mM (b) 1 mM (c) 2 mM (d) 3 mM (e) 4 mM . Both experiments were carried out in 50 mM PBS (pH 6.5) under nitrogen. (C) Mechanism of electrocatalytic regeneration of NADH by rhodium catalyst. The geometric surface area of the electrode was 0.25 cm^2.*

Furthermore, the capacitive current in the two experiments was different, this may explained by the dissimilarity of surface area for individual CF-CNT electrode. However, the evolution of the catalytic responses to the addition of NAD^+ with compound **E** from 1 mM to 4 mM was found similar to compound **F**, the catalytic current in a solution with 4 mM of NAD^+ reaching a value close to 400 µA. So the electrochemical catalytic property of the alkynyl functionalized rhodium complex **E** was not much influenced by the presence of the alkynyl functionalities.

3.3.2 Covalent immobilization of rhodium complex on the electrode

3.3.2.1 Diazonium electrografting

CF-CNT electrode was functionalized with azide group by diazonium grafting. It was achieved by mixing 1 mM 4-azidoaniline with 2 mM sodium nitrite in 0.5 M HCl water solution to generate arylazide radicals, which could form covalent bond on CF-CNT by

electro-reduction. The surface concentration of grafted organic had to be controlled, in order not to block the electrode surface with an insulated organic layer. Here, the grafting process was carried out by two reduction scans from 0.4 V to -0.6 V in 1mM 4- azidophenyl diazonium cations, in order to obtain only a partial coverage of the surface. During the electrografting process **(Figure 3.5A)**, the first cyclic voltammogram exhibited an irreversible peak located around -0.3 V (**curve a**). During the second scan, the cathodic wave vanished and reduction current decreased (**curve b**). This decrease was attributed to the presence of grafted azidophenyl groups on the electrode.

The permeability of the organic layer was examined using a 0.1 mM ferrocenedimethanol pH 6.5 aqueous solution as electroactive redox probe. **Figure 3.5B** shows cyclic voltammograms for a CF-CNT electrode before (**curve a**) and after (**curve b**) grafting of 4-azidophenyl groups. The presence of the organic layer induced decrease of peak current and slight increase of the ΔEp between anodic and cathodic peaks. This experiment proved that the electrode surface was functionalized without preventing electron transfer reactions from occury.

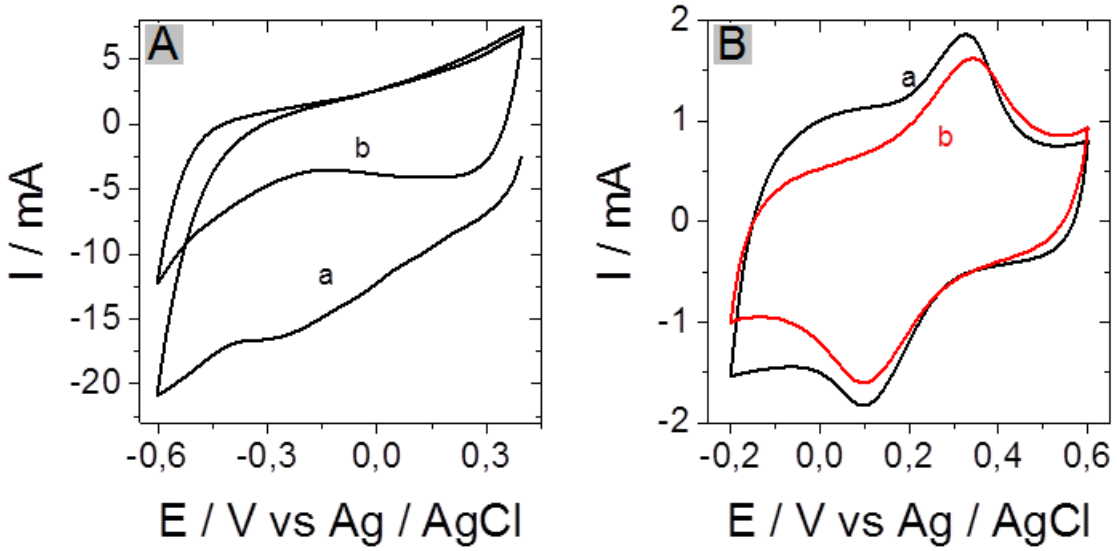

Figure 3.5. *Cyclic voltammograms recorded on CF-CNT electrode at 100 mV s^{-1} for the reduction of diazonium cations generated ''in situ'' from 1mM 4-azidoaniline in 0.5 M HCl. (B) Cyclic voltammograms recorded at 50 mV s^{-1} in the presence of 0.1 mM ferrocenedimethanol (in 50 mM PBS*

at pH 6.5) using a CF-CNT electrode (a) before and (b) after diazonium electrografting. The geometric surface area of the electrode was 0.25 cm^2.

The attachment of the azidophenyl groups was then evidenced in the XPS survey spectrum of the azido-functionalized substrate by the appearance of a peak at 400 eV attributed to the presence of N1s in addition to the main C1s and O1s peaks at 285 eV and 532 eV respectively from the underlaying substrate. The high-resolution XPS spectrum in the N1s region (**Figure 3.6A**) has been analyzed showing two main contributions with binding energies of 404 and 400 eV. An azide group was expected to present two peaks with a ratio 1:2 in this region. The central nitrogen, positively charged, exhibited a higher binding energy than the two other terminal nitrogen atoms. The higher energy component was fixed at 404.1 eV with a width of 2 eV. However, fitting the N1s region for the azido-modified substrate resulted in a ratio of 1:3.3, suggesting the presence of other nitrogen species in addition to the azide groups. In summary, the ratio between of the two N1s component should be 1:2, but the area of the first peak was slightly higher than expected likely due to the contribution of the C-N=N-C bonds coming from the electrografting of the diazonium cations. The component at 400 eV can be fitted as a result of two peaks, one of them due to the terminal atoms of the azide groups located at 400.5 eV and another which was due to the electrochemical reduction of diazonium cations at 399.3 eV.

3.3.2.2 Huisgen cycloaddition

The azido-functionalized electrode was then derivatized with bipyridine ligands via cycloaddition Huisgen reaction. The azido-functionalized electrode was reacting with alkynyl functionalized bipyridine in the presence of Cu (I) acting as a catalyst in this azide-alkyne coupling reaction leading to the formation of a triazole core substituted by a bipyridine ligand in at the 4 position.

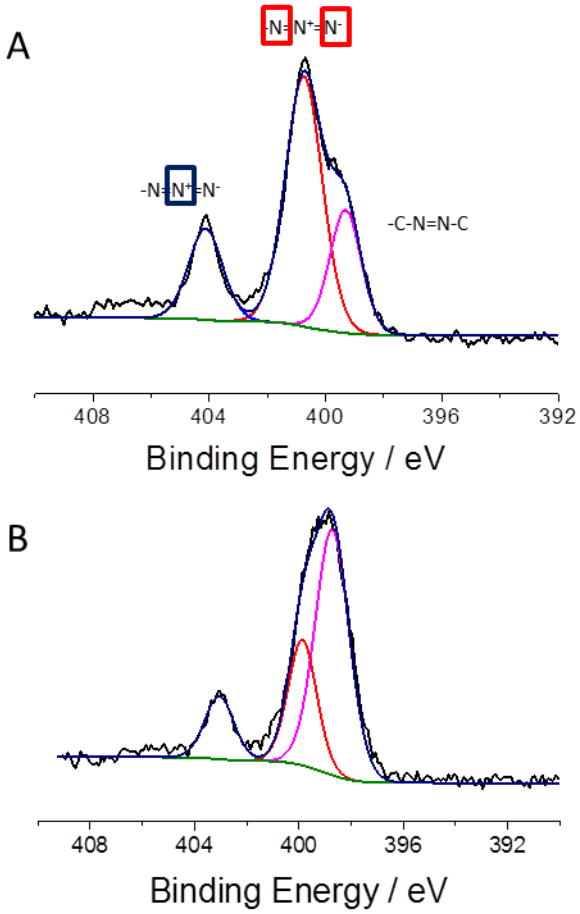

Figure 3.6. *XPS spectra of the N1s region obtained from the azido-functionalized substrate. (A) before and (B) after 'click' reaction with the bipyridine ligands.*

Evolution of the high resolution nitrogen spectra from XPS was employed to monitor the effectiveness of the chemical reaction. After quantitative click reaction, the triazole cores formed as a result of the azide-alkyne coupling and the incorporated bipyridine ligands should be the only species responsible of the nitrogen signal. The N1s spectrum (**Figure 3.6B**) displays a signal at 399.1 eV corresponding to uncharged species mainly attributed to the triazole cores and bipyridine ligands appearing at very close binding energies. A small shoulder at higher binding energies was observed indicating that some azide groups could remain unreacted. Analysis of the atomic concentration corresponding to each N1s from the area peaks indicates that 10-15% of the starting azide functionalized groups have not been converted after click reaction. **Figure 3.6B** shows the clear decrease of the main signal due to the azide groups.

3.3.2.3 Rhodium complexation

The bipyridine –functionalized substrates were finally derivatized by coordination with a Rh complex. ($(RhCp^*Cl_2)_2$) was complexed with the immobilized bipyridine by stirring in dichloromethane to form $[Cp^*Rh\ (bpy)Cl]^+$ complex on the electrode.

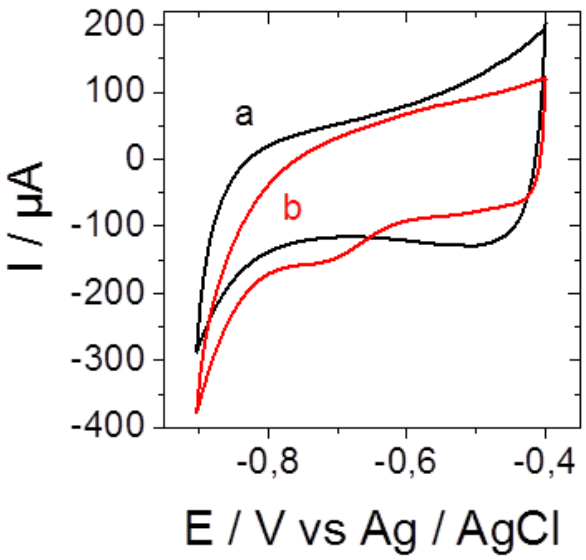

Figure 3.7. *Cyclic voltammograms of the bipyridine immobilized electrode (CF-CNT-4'4-Bpy) (a) before and (b) after complexation with ($(RhCp^*Cl_2)_2$). Experiment was carried out in 50mM PBS (pH6.5) under nitrogen. Scanning rate is 5 mV s^{-1}. The geometric surface area of the electrode was 0.25 cm^2.*

Figure 3.7 shows the cyclic voltammograms of the bipyridine immobilized electrode (CF-CNT-4'4-Bpy) before and after complexation with ($(RhCp^*Cl_2)_2$) in dichloromethane for 3h under continuous gentle stirring at room temperature. Before complexation, no redox peak was observed in the CV range from -0.4 to -0.9V, which means bipyridine itself was not electrochemically active in this potential window under the experimental conditions employed (**Figure 3.7a**). From the CV after the formation of rhodium complex (**Figure 3.7b**) on the electrode (CF-CNT-4'4-Bpy-Rh), a reduction peak was observed around -0.7 V, but no oxidation peak appeared. This was explained by the pH-dependent property of this rhodium complex. Indeed, in neutral or slightly acidic media, Rh(III) complex is first reduced to Rh(I) complex before being protonated in the solution to form protonated-Rh(I), and protonated-Rh(I) cannot be oxidized electrochemically back to Rh(III) [142].

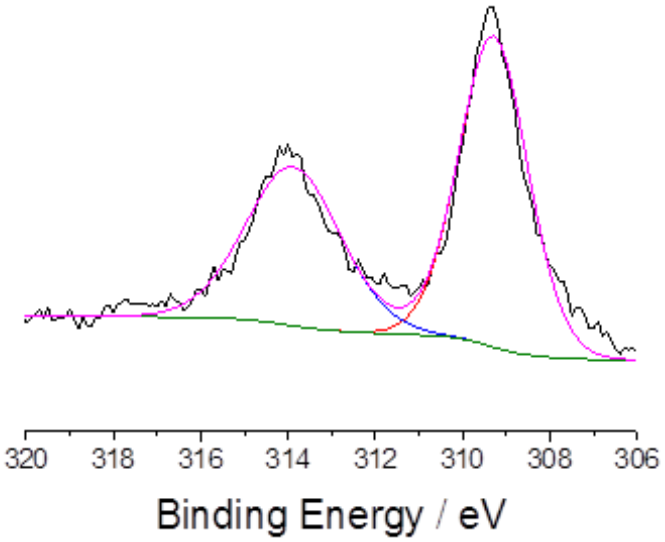

Figure 3.8. *XPS Rh 3d core-level spectrum of a CF-CNT-Rh electrode.*

The XPS survey spectrum also indicates the presence of Rh with the appearance of two new peaks located at 390 and 494 eV assigned to Rh3d and Rh3p respectively. **Figure 3.8** shows the Rh3d core-level spectrum. The binding energy observed for Rh3d spectrum shows a doublet at 309.28 and 314.5 eV corresponding to $3d_{5/2}$ and $3d_{3/2}$ respectively.

3.3.3 NADH regeneration

The catalytic activity of CF-CNT-4‟4-Bpy-Rh electrode for NADH regeneration was then tested. Since protonated Rh(I) complex can transfer a proton to NAD^+ to regenerate NADH and return to Rh(III) species, **Figure 3.9A** shows the electrochemical response to NAD^+ of CF-CNT-4‟4-Bpy-Rh electrode measured by cyclic voltammetry in PBS buffer. By successive addition of NAD^+ into the solution, the cathodic current measured at -0.7 V was increasing up to saturation when the final concentration of NAD^+ reached 4 mM. The potential reduction peak was simultaneously slightly shifted to more negative potential because of limited heterogeneous electron transfer kinetics [142]. It should be highlighted that the catalytic current increased proportionally to the concentration of NAD^+ at low

concentration. However, no significant current increase was detected when reaching the concentration of 4 mM, suggesting that the availability of rhodium species on the electrode surface was near to the saturation.

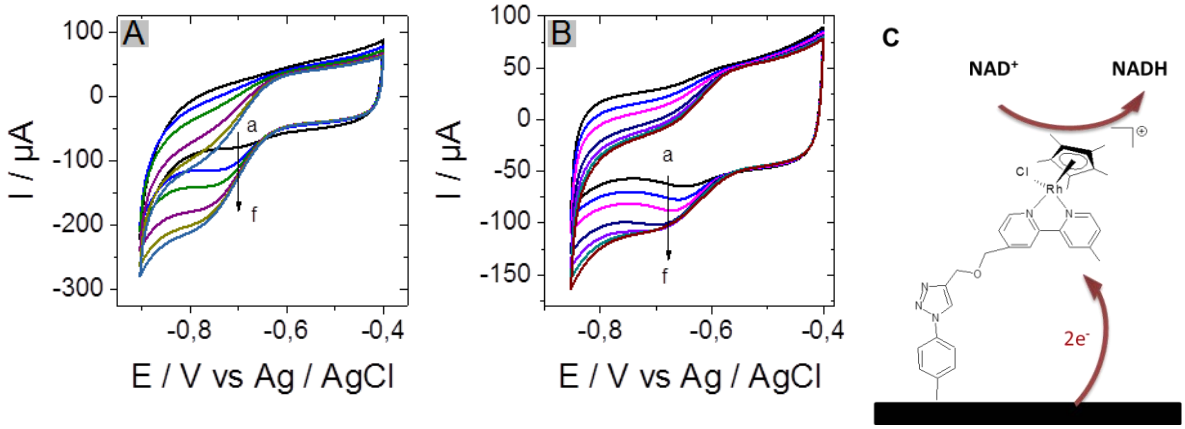

Figure 3.9. *Cyclic voltammograms recorded using a (A) CF-CNT-4'4-Bpy-Rh and (B) CF-CNT-4'4-Bpy-Rh-gel electrode at a potential scan rate of 5 mV* s^{-1} *in 50 mM PBS buffer (pH 6.5) under nitrogen to gradual addition of* NAD^+ *(a) 0 mM (b) 0.5 mM (c) 1 mM (d) 2 mM (e) 3 mM (f) 4 mM. (C) Schematic representation of NADH regeneration mediated by a rhodium catalyst functionalized electrode. The geometric surface area of the electrode was 0.25* cm^2.

After the catalytic response was confirmed, the functionalized electrode was applied to electrochemical conversion. The final bioelectrochemical system will include NAD-dependent dehydrogenase. To avoid the interaction between the rhodium complex and the functional group of the enzymes which might cause their degradation, here we used a sol-gel method was used to encapsulate the redox enzymes on the top of the functionalized electrode [75,202]. In that way, the enzymes could be in principle physically separated but relatively close to the rhodium complex. As the gel was composed of silane and polyethylenimine polymer, the influence of the layer on the electrocatalytic activity of the rhodium complex was first evaluated in the absence of enzymes. Silica gel prepared by replacing the enzyme solution with water was deposited on CF-CNT-4'4-Bpy-Rh, a CF-CNT-4'4-Bpy-Rh-gel electrode was obtained. **Figure 3.9B** shows the electrochemical behavior of CF-CNT-4'4-Bpy-Rh-gel by cyclic voltammetry in PBS buffer at pH 6.5. Similar to the CF-CNT-4'4-Bpy-Rh electrode without gel, catalytic response was observed upon addition of NAD^+ with saturation of the catalytic current when NAD^+ concentration reached 5 mM. It was also

noticed that the current was lower compared to the electrode without gel (**Figure 3.9A**). This could be explained by a more limited diffusion of NAD^+ towards the Rh complex when passing through the gel.

Here we were also wondering if the chemical attachment of the Rh complex really provides an advantage compare to the simple adsorption of the molecule as reported before [142]. So we prepared an electrode by simple adsorption of compound **F** onto CF-CNT for 24 h in DMF/ H_2O (7/3) solution, then covered with silica gel (CF-CNT-ads-Bpy-Rh-gel). The stability of this CF-CNT-4‟‟4-Bpy-Rh-gel electrode without enzyme was first compared with a CF-CNT-ads-Bpy-Rh-gel electrode employed as a blank electrode. Both electrodes were introduced separately in a volume of 500 mL 50 mM PBS (500 mL) buffer (pH 6.5) with a continuous vigorous stirring. The electrochemical behavior of each electrode was repetitively tested with time. **Figure 3.10A** shows the evolution of the cathodic peak current attributed to the reduction of rhodium species measured for both electrodes, a different stability depending on the immobilization method employed in each case (either covalently immobilized or adsorbed rhodium complex) was observed. The CF-CNT-ads-Bpy-Rh-gel electrode has a relatively higher peak current at the beginning of the experiment. However, after one day in the buffer solution, the current dropped from 15 μA to 5.5 μA, which means almost 63% of the adsorbed species were leaching out from the electrode to the buffer solution. After 7 days, the peak current of the CF-CNT-ads-Rh-gel electrode was almost null. In comparison, the covalently immobilized CF-CNT-4‟‟4-Bpy-Rh-gel electrode had only 18% current decrease after one day. This could be explained by desorption of a small amount of unreacted rhodium complex remaining adsorbed on the surface after functionalization. The truly covalently immobilized CF-CNT-4‟‟4-Bpy-Rh-gel electrode was then stable for at least 14 days in solution, with only 8% decrease of the catalytic current.

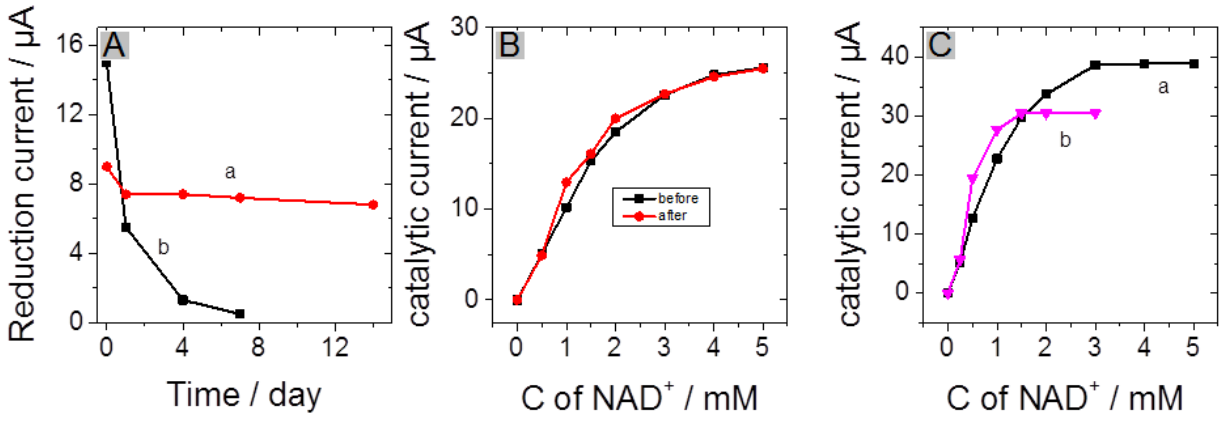

Figure 3.10. *(A) Evolution of 0.5 mM NAD^+ reduction catalytic current measured with (a) CF-CNT-4'4-Bpy-Rh-gel and (b) CF-CNT-ads-Bpy-Rh-gel electrode. (B) Catalytic current measured from CV versus NAD^+ concentration using a CF-CNT-4'4-Bpy-Rh-gel electrode (a) before and (b) after running a 39 h chronoamperometry at a potential of -0.73 V. (C)) Catalytic current measured from CV versus NAD^+ concentration using a CF-CNT-4'4-Bpy-Rh-gel electrode after stirring in buffer (a) for 4 days (b) for 21 days. All experiments were carried out in 50 mM PBS buffer at pH 6.5 under nitrogen. The geometric surface area of the electrode was 0.25 cm^2.*

In addition to the reduction peak of rhodium complex, the stability of its catalytic activity was also confirmed by performing NADH regeneration tests. **Figure 3.10B** shows the evolution of the catalytic current of the CF-CNT-4'4-Bpy-Rh-gel electrode to the addition of NAD^+ before and after running a 39 h chronoamperometry (at applied potential of -0.73 V) experiment. The catalytic response to NAD^+ remained almost unchanged. After 3 weeks stirring, one observed the dissolution of the silica gel layer and loss of CNTs. The rhodium complex reduction peak current decreased up to 60% compared to the initial signal, but the saturated catalytic current in the presence of 5 mM NAD^+ still reached 78% of the initial value (**Figure 3.10C**). These tests indicate that the CF-CNT-4'4-Bpy-Rh-gel electrode was very stable in solution even under stirring conditions and the immobilized rhodium complex would not be influenced by either depositing gel on the top or long-term electrochemistry experiment, making it a suitable potential candidate for bioconversion processes in the presence of the enzymes. The main limitation would not come from the chemical functionalization but from the electrode assembly.

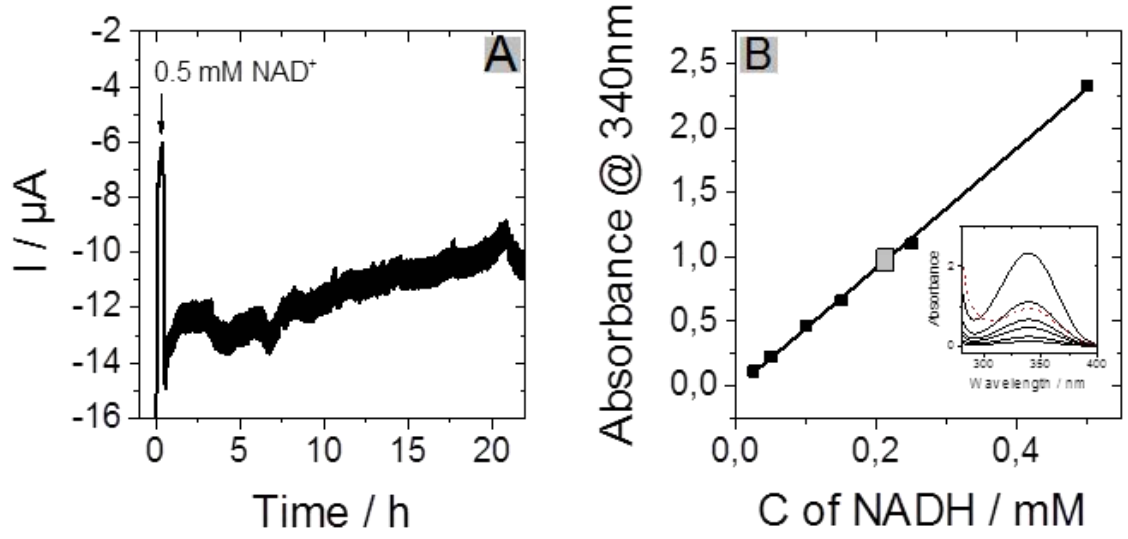

Figure 3.11. *(A) Amperometric response to 0.5 mM NAD^+ measured with a CF-CNT-4'4-Bpy-Rh-gel electrode at an applied potential of -0.73 V in 20 mL 50 mM PBS buffer (pH 6.5) under nitrogen. (B) Calibration curve of NADH in 50mM PBS buffer (pH 6.5) and corresponding UV-vis spectroscopy (inset), the square point correspond to the NADH formed from NAD^+ at the end of the chronoamperometry experiment. The geometric surface area of the electrode was 0.25 cm^2.*

Furthermore, the current efficiency of CF-CNT-4'4-Bpy-Rh-gel electrode for regeneration of NADH was evaluated by chronoamperometry (**Figure 3.11A**). A potential of -0.73V (50 mV overpotiential) was applied on the CF-CNT-4'4-Bpy-Rh-gel electrode and a catalytic current of 8 µA was observed upon addition of 0.5 mM NAD^+, then the conversion was performed for 23 h. At the end, the absorbance of NADH at 340 nm was detected by UV-Vis spectroscopy corresponding to a NADH concentration of 0.216 mM **(Figure 3.11B).** Since the long-term experimental condition (in PBS buffer at room temperature) will influence the stability of NADH [203], this value did not take into account the degraded NADH which was UV inactive. The estimation of the concentration done from the charge involved in the electrocatalytic process leading to a theoretical concentration of 0.248 mM NADH, which resulted in a faradic efficiency of at least 87%, higher than the value reported (23–36%) with immobilized rhodium complex on CNT by ‚π- π'' stacking [34].

3.3.4 Bioelectrocatalytic amperometric responses of co-immobilized electrodes

After confirming the stability as well as the efficiency of the electrode, NAD-dependent dehydrogenases were introduced into the gel and both rhodium complex and enzymes were co-immobilized on the electrode. The bioelectrocatalytic amperometric response of CF-CNT-4′4-Bpy-Rh-DSDH gel electrode was first demonstrated (**Figure 3.12A**) by injecting D-fructose substrate into 50 mM PBS buffer containing 1mM NADH cofactor. DSDH reduces D-fructose to D-sorbitol and consumes NADH to generate NAD^+, which can then be reduced by the rhodium complex at the electrode surface. The regenerated NADH could be recycled in this electro-reduction synthesis system to maintain constant catalytic activity. The apparent Km estimated from the chronoamperometric experiment was 1.0 ± 0.2 mM, much lower than the Km of free DSDH in buffer solution (Km is 49.4 mM [204]).

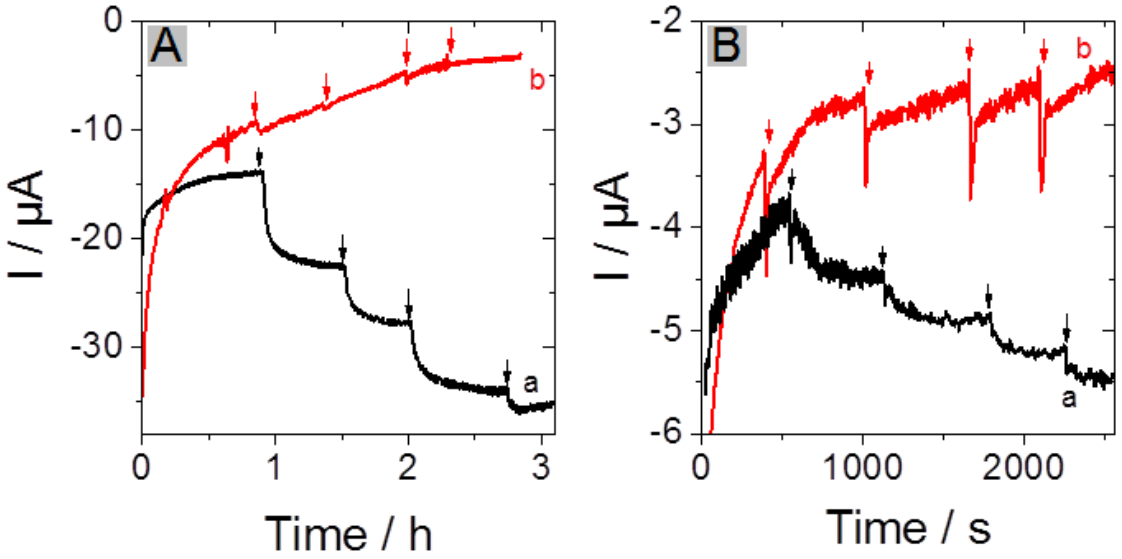

C

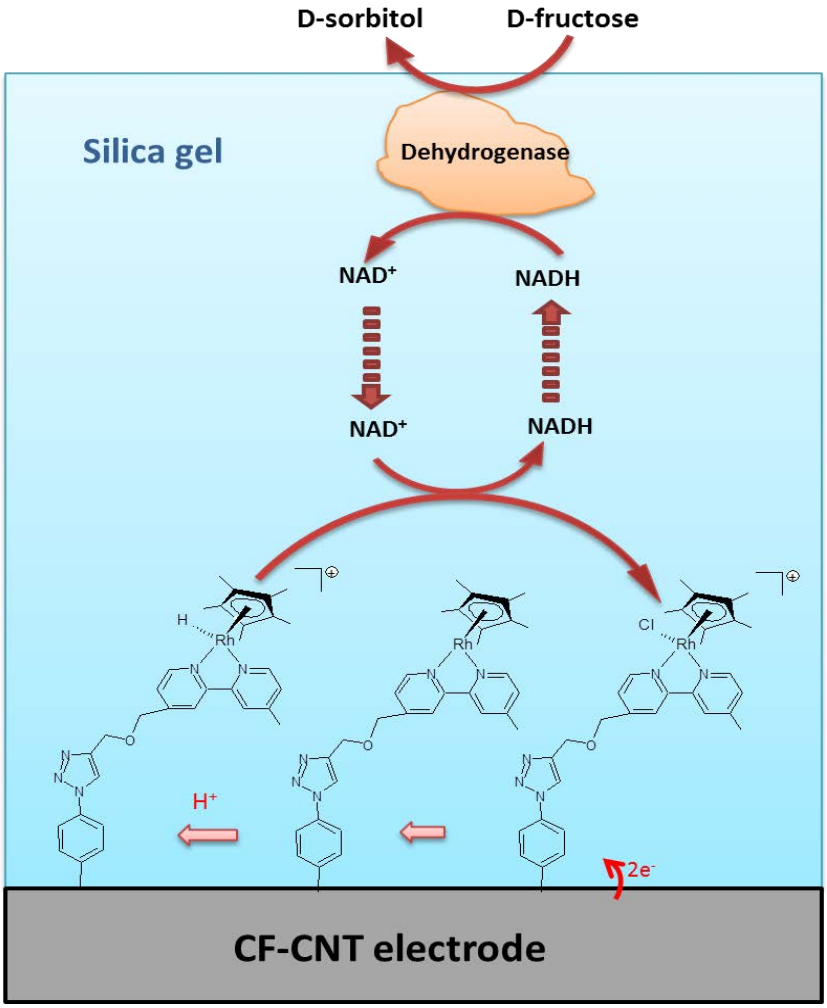

Figure 3.12. *(A) Amperometric response to increasing concentration of D-fructose from 0.5 to 3mM recorded using (a) CF-CNT-4'4-Bpy-Rh-DSDH-gel electrode (b) CF-CNT-4'4-Bpy-Rh-gel electrode measured in 50 mM PBS (pH 6.5) contains 1 mM NADH at an applied potential of -0.74 V. (B) Amperometric response to increasing concentration of hydroxyacetone from 1 to 4 mM recorded using (a) CF-CNT-4'4-Bpy-Rh-GatDH-gel (b) CF-CNT-4'4-Bpy-Rh-gel electrode measured in 50 mM PBS (pH 6.5) contains 1 mM NADH and 1mM $MgCl_2$ at an applied potential of -0.72 V. Both experiments were carried out under nitrogen. (C) Schematic representation of the electroenzymatic synthetic process for CF-CNT-4'4-Bpy-Rh-DSDH-gel electrode. The geometric surface area of the electrode was 0.25 cm^2.*

To test the applicability of CF-CNT-4‟4-Bpy-Rh electrode with other NAD-dependent redox enzymes, Galactitol dehydrogenase (GatDH) was also encapsulated into the gel layer instead of DSDH. GatDH is a multifunctional enzyme that can catalyze broad substrates [205], here we choose hydroxyacetone as the substrate to investigate its electroenzymatic property. **Figure 3.12B** shows the amperometric response against the addition hydroxyacetone substrate in 50 mM PBS buffer containing 1 mM NADH cofactor and 1 mM $MgCl_2$ on a CNT-Rh-GatDH gel electrode which contained GatDH instead of DSDH. Even through the response was lower than with DSDH electrode due to its low enzymatic activity, it indicated that this co-immobilized electrode was able to be applied on different kinds of NAD-dependent enzymes which is promising for bio-electrochemical synthesis of a variety of valuable products.

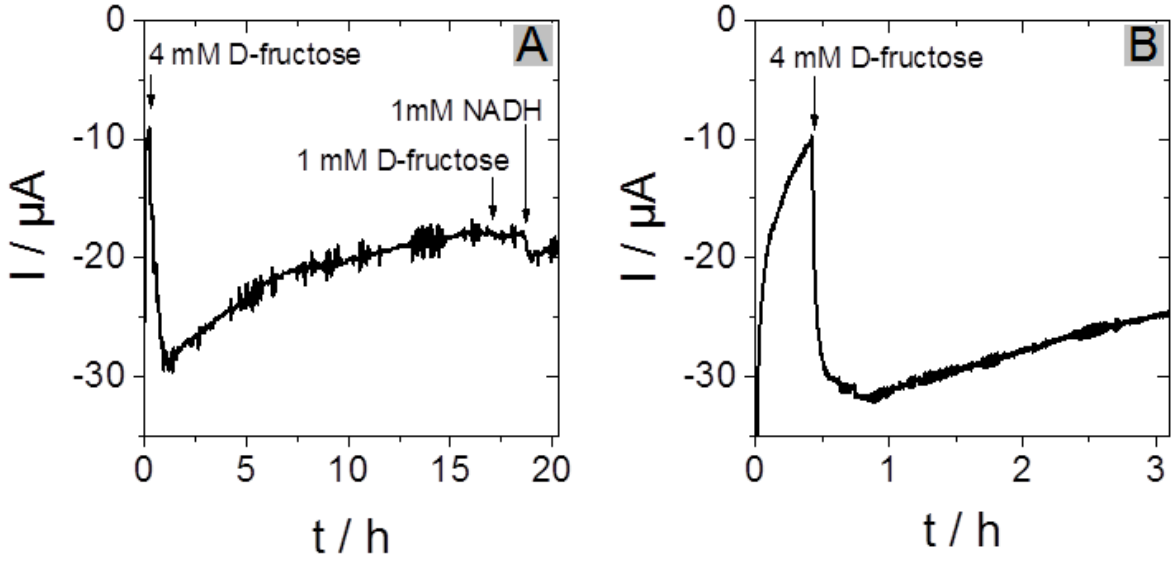

Figure 3.13. *(A) Amperometric response recorded using CF-CNT-4'4-Bpy-Rh-DSDH gel electrode to addition of 4 mM of D-fructose in the beginning, 1 mM of D-fructose and 1 mM NADH in the end after 18 h in 50 mM PBS (pH 6.5) contains 1 mM NADH. (B) Amperometric response to addition of 4 mM of D-fructose using the same CF-CNT-4'4-Bpy-Rh-DSDH gel electrode in fresh 50 mM PBS (pH 6.5) contains 1 mM NADH. Applied potential was -0.73 V. The geometric surface area of the electrode was 0.25 cm^2.*

However, it was noticed that enzyme activity was inhibited during long-term electroenzymatic operations. **Figure 3.13A** showed the amperometric response of a CF-CNT-4′4-Bpy-Rh-DSDH gel electrode to addition of D-fructose for 18 h in 50 mM PBS (pH 6.5) buffer contained 1 mM NADH. At the beginning of the experiment, the catalytic current to addition of 4 mM of D-fructose was around 20 µA. The current was then half decreased after 18 h. The estimation of the D-Fructose conversion was done from the charge involved in the electrocatalytic process leading to a theoretical D-Fructose conversion concentration of only 0.7 mM (18% of consumption from initial value), indicating that the decrease of catalytic current was not caused by substrate comsumption. At the end of the chronoamperometry experiment, 1 mM of D-Fructose was added into the solution, but no catalytic response was observed. Then 1 mM NADH was finally added into the solution leading to a small increase of catalytic current of 1.5 µA, this indicates that small amount of NADH degraded after 18 h experiment at room temperature, but the decrease of catalytic current was not caused only by degradation of NADH. Surprisingly, if we put the electrode into fresh PBS buffer contained 1 mM NADH, the catalytic current to addition of 4 mM D-fructose was almost the same value with the first chronoamperometry experiment. This confirmed that the activity of enzyme was inhibited at the end of the first long-term chronoamperometry experiment, but was recovered in the fresh solution. A possible explanation could be the change of local pH during the electroenzymatic process, protons need to be continuously supplied from buffer solution through the gel layer, reaching the rhodium complex at the electrode interface. Under a long-term operation, if the proton consumption was faster than the proton supply, the local pH inside the CF-CNT electrode will slowly increase. As the activity of the enzymes was sensitive to pH, the increase of pH may inhibit the activity of enzymes, half activity was observed when the pH changed from 6.5 to 7.5, as reported in the previous literature [206]. This experiment showed that the enzyme was kept active in the bioelectrode. The similar current was also an indication of the good stability of the immobilized Rh(III) catalyst.

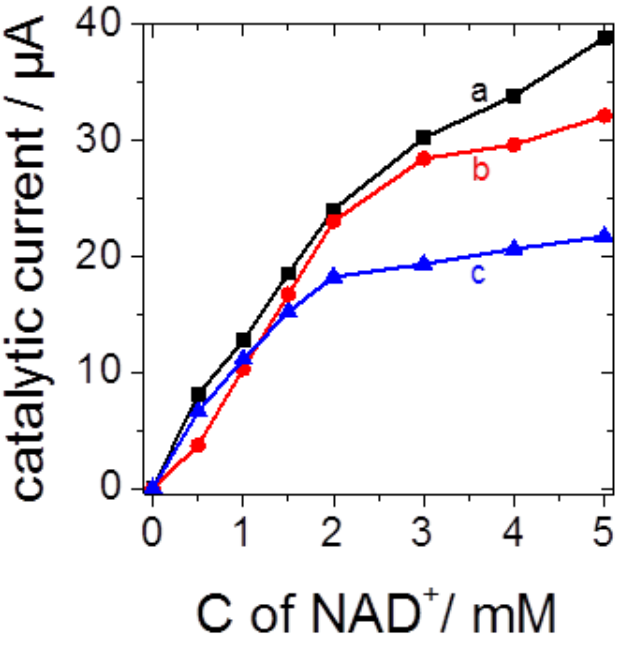

Figure 3.14. *Catalytic current measured from CV versus NAD^+ concentration using a CF-CNT-4'4-Bpy-Rh-DSDH-gel electrode to gradual addition of NAD^+ (a) before and after running a (b)25 h , (c) 90 h chronoamperometry in 50 mM PBS (pH 6.5) contains 1 mM NADH at a potential of -0.73V under nitrogen. The geometric surface area of the electrode was 0.25 cm^2.*

To confirm the stability of the rhodium complex on the CF-CNT-4'4-Bpy-Rh-DSDH-gel electrode, chronoamperometry was applied on the CF-CNT-4'4-Bpy-Rh-DSDH-gel electrode at an applied potential of -0.73 V. **Figure 3.14** shows the evolution of the catalytic current of the CF-CNT-4'4-Bpy-Rh-DSDH-gel electrode to addition of NAD^+ before and after running a chronoamperometry for 25 h and 90 h. After 25h, only a small loss of catalytic current (**b**) was observed compared to the initial catalytic response (**a**), which further indicated that the decrease of the electrochemical response was mainly due to enzymes inhibition and not to inactivation after interaction with rhodium complex. After 90 h continuous operation, 44% current with 5 mM NAD^+ in the buffer solution were observed (**c**). The loss of catalytic response was detected compared to the electrode in the absence proteins (**Figure 3.10B**). However, this degradation of rhodium complex reactivity was slow, indicating that even though this enzymes gel deposition method did not provide unfortunately a 100% complete separation between both components, it provide a rhodium complex functionalized electrode stable enough for NADH regeneration.

3.4 Conclusion

$[Cp^*Rh(bpy)Cl]^+$ was successfully immobilized on a CF-CNT electrode by covalent bonding. Azido-functionalized electrodes were prepared by electrochemical reduction of 4-azidophenyl diazonium cations that could be used later on to incorporate bipyridine ligands via cycloaddition Huisgen reaction. A final post-functionalization step was based on the ability of bipyridine ligands to coordinate with rhodium centers such as $(RhCp^*Cl_2)_2$ dimer under mild conditions yielding CF-CNT-4‴4-Bpy-Rh electrode. The catalytic response of this CF-CNT-4‴4-Bpy-Rh electrode towards transformation from NAD^+ to NADH was evaluated, a faradic efficiency of 87% was measured. The application of the CF-CNT-4‴4-Bpy-Rh electrode was demonstrated by combining NAD-dependent enzymes encapsulated in silica gel on the top of the electrode (D-sorbitol dehydrogenase and galactitol dehydrogenase). However, enzyme inhabitation was observed that was probably caused by the local environment of the enzymes (pH, sorbitol accumulation). Moreover, a slow degradation of rhodium complex was still observed.

Chapter 4. Functionalization of carbon felt supported carbon nanotubes by combining diazonium chemistry and a sequential dual click chemistry approach

Concerning the enzyme inhibition effect in Chapter 3, a more opened functionalized surface of electrode was built in this chapter. A generic approach has been developed for heterogeneous surface modification of carbon felt/carbon nanotubes (CF-CNT) electrode composites. Such strategy, applicable for a wide range of functional groups, provides a versatile methodology to yield multifunctionalized carbon surfaces that can employed in a variety of applications. The sequential method is consisting of two main steps. In the first step, azide-alkene bifunctionalized CF-CNT electrodes (CF-CNT-AzVi) are achieved by electrochemical reduction of a mixture of the corresponding diazonium salts generated in situ from 4-azidoaniline and a 4-vinylaniline. Reactive sites available for further functionalization, azide and alkene moieties, are incorporated in the carbon surfaces during the first step. Two consecutive „click reactions" can be subsequently used to immobilize the targeted molecules. In that way, we provide reactive sites that are available for further functionalization in a sequential process based on the azide-alkyne cycloaddition Huisgen reaction and alkene-thiol coupling. The concept by sequentially combining the diazonium chemistry and robust chemical reactions („click chemistry") allows versatile, simple, and environmentally friendly heterogeneous modification of CF-CNT substrates. The methodology has been employed first to co-immobilize cobaltocenium and ferrocene moieties on the CF-CNT-AzVi which can be characterized by cyclic voltammetry and X-ray photoelectron spectroscopy measurements. This pair of compounds has been used as a model to demonstrate the feasibility of the generic approach developed. After proving the possibility to use this method to introduce various functional groups in a selective way, the work has been extended to the co-immobilization of a molecule catalyst $[Cp^*Rh(bpy)Cl]^+$ and a NAD-dependent dehydrogenase that were proved to act simultaneously in electroenzymatic conversion of D-fructose to D-sorbitol.

4.1 Introduction

In the early 90s, the most widely used system for modifying surfaces with monolayers containing multiple components was initially the alkanethiol chemistry, where thiol groups spontaneously adsorb onto gold. However, a number of disadvantages arising from the low strength of the interaction between the thiol and the substrates [207], such as thermal instability [208], evidence of the changing structures over time [209] and limited potential window (typically -0.8 to +0.8 V versus Ag/AgCl) [207] justified the growing interest in alternative processes overcoming some of the mentioned disadvantages. Later on, several methods have been reported in the literature describing the modification of surfaces by means of covalent bonding (electrochemical reduction of aryl diazonium salts [210–246], electrochemical oxidation of alkyl amines [247], for instance). Among them, the electrochemical reduction of aryl diazonium salts, firstly reported by Pinson and co-workers [210], has been extensively used to prepare modified electrodes. Such electrografting method was based on the electrochemical generation of highly reactive aryl radicals concerted with the loss of N_2. These aryl radicals are able to attack the electrode surface resulting on the formation of an organic monolayer covalently attached to the substrate. The method can be applied to a wide range of substrates such as carbon, silicon and metal surfaces [210–254]. The generation of organic monolayers by means of a covalent bond provides functionalized surfaces which are highly stable, resistant to heat, ultrasonication and chemical degradation.

However, depending on the application considered, the high reactivity of these aryl radicals could be less convenient since they can further react with phenyl groups already grafted on the electrode surface and multilayers can be obtained. The formation of organic multilayers can result in the formation of insulating coatings that usually are not favorable for electrochemical applications. In this sense, the control of the compacting degree of the organic layer is mandatory.

Since the introduction of several organic functions at the electrode surface would be advantageous in a large variety of applications, including surface wetting, cell biology, chemical sensing, biosensing and photosynthesis, multifunctionalized surfaces based on covalent bonds have been already prepared by electrochemical reduction of mixtures of aryl diazonium cations [246,248–252]. The main drawback of such modification approach to obtain multiple organic functions on the substrate is the low degree of selectivity due to the high reactivity of the aryl radicals generated, making difficult their use to obtain mixed

organic layers with a controlled composition. Different experimental approaches have been described in the literature in order to get a precise control over the composition of binary monolayers deposited at the electrode surface. Applying a constant cathodic potential negative enough to reduce all the different diazonium cations present in solution was a first strategy employed. The results obtained when working in solutions of different composition suggested that changing the composition of the starting mixture in solution do not make a significant difference in the final composition of the organic layers deposited on the electrode surface. This fact could be rationalized taking into account that, even in the most optimal situations, where the peak potential separation for the reduction of two different diazonium salts can be up to 1V, the efficiency of the grafting is not the same for all the species of different nature [253–255]. Another factor influencing the final composition of the deposited organic layer is the potential required to reduce the aryldiazonium cations involved in the grafting which leads to a most important surface concentration for the species which are easy to reduce even if its concentration in the starting solution is lower.

The demand/requirement of more selective modification processes that could address the difficulties encountered in the control of the composition of binary layers prepared by electrochemical reduction of diazonium cations has opened the door to the development of novel methods to incorporate organic functions in a variety of substrates by means of covalent bonds. In this sense, more recently new indirect and versatile methods have been developed in order to get functionalized substrates providing new functional platforms which allow the selective incorporation of a variety of organic groups. Among them, “click chemistry” approaches are attracting increasing attention in the field of materials science [11–13], being an easy and powerful mean for joining molecular species to each other in rather mild conditions as first reported in 2001 [256]. The mild reaction conditions of the copper (I)-catalyzed azide-alkyne cycloaddition (CuAAC), producing 1,2,3-triazoles and its very high yield makes this reaction particularly suitable for the functionalization of a large variety of substrates[257]. Lately, other reactions are classified as click-type reactions since they accomplished the requirements established by *Kolb et al.* [256]. (that is modular, wide in scope, gives close to quantitative yields, generates inoffensive (if any) byproducts that are easily removed by non-chromatographic methods and stereospecific.) The required processes use to take place under simple and mild experimental reaction conditions (insensitive to oxygen and water), readily accessible starting materials and reagents, the use of no solvent or an environmentally friendly solvent (such as water) which should be easily removed and

simple product isolation. For this reason, thiol-ene coupling reaction has been extensively exploited to prepare dendrimers and for the post-functionalization of polymers [12]. In this paper we described a generic approach for the functionalization of CF-CNT based on a synthetic strategy in a two-steps process via the combination of the electrochemical reduction of diazonium salts and sequential double click reactions. This process was schematically represented in **Figure 4.1**. The first derivatization step is based on a one-pot bifunctionalization process based on the electrochemical reduction of a mixture of diazonium salts, 4-azidobenzene and 4-vinylbenzene diazonium cations, which enables the formation of binary functional CF-CNT-AzVi. The CF-CNT-AzVi can be used as a real platform to introduce sequentially a variety of functional groups by taking advantage of the Huisgen cycloaddition and the thiol-ene click reaction.

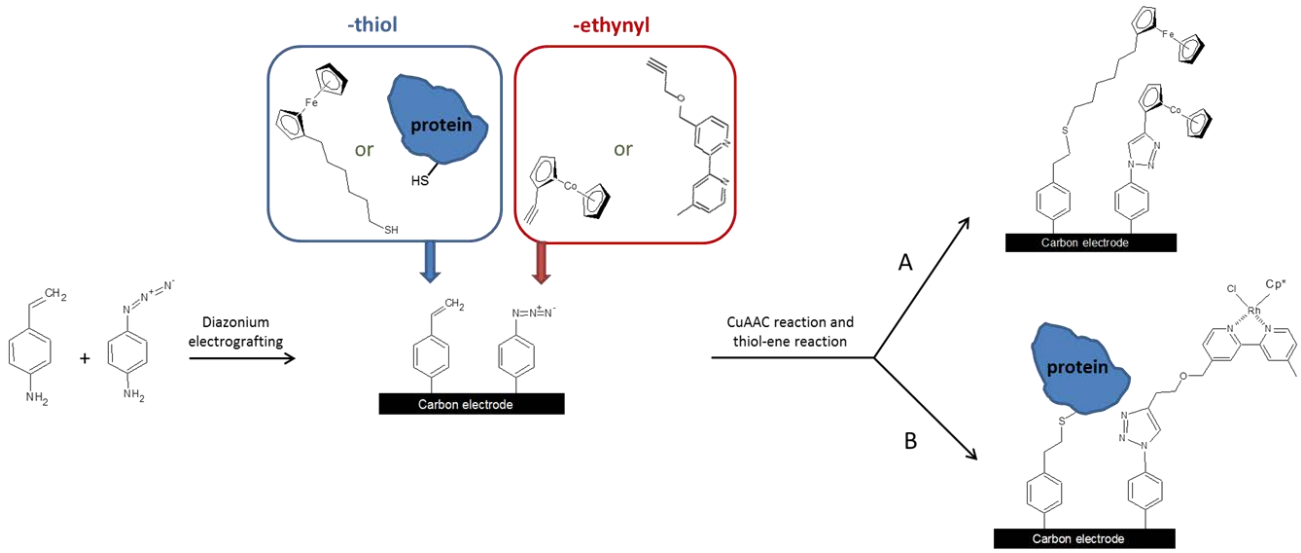

Figure 4.1. *Schematic representation of the synthetic route followed for the bi-functionalization of a carbon electrode surface with thiol-containing molecule and ethynyl-containing molecule by combination of diazonium salt electrografting and click chemistry.*

4.2 Experimental

Chemicals and enzymes

The following chemicals were used as received: sodium nitrite (97%, Sigma), 4-vinylaniline (97%, Sigma), 4-Azidoaniline hydrochloride (97%, Sigma-Aldrich), 1 M

hydrochloric acid solution (Sigma), β-Nicotinamide adenine dinucleotide hydrate (NAD^+, ≥ 96.5%, Sigma-Aldrich), β-Nicotinamide adenine dinucleotide, reduced disodium salt hydrate (NADH, ≥97%, Sigma-Aldrich), 6-(ferrocenyl)hexanethiol (Sigma), D-fructose (99 wt%, Sigma), sodium dihydrogen phosphate (99.5%, Merck), Tris(2-carboxyethyl)phosphine hydrochloride (TCEP, 98%, Sigma), Carboxylic-functionalized multi-walled carbon nanotubes (MWCNT, 95%, Φ 15±5 nm, L 1-5 μm, Nanolab), the carbon felt carpet (Sigratherm®, GFD 4.6 EA) was supplied by SGL Group (Germany), Overproduction of N-His(6)-Cys (Cys-DSDH) tagged DSDH variants was done with Escherichia coli BL21GOLD (DE3) containing the corresponding expression-vectors pET-24a(+) (Novagen) and purification of the enzyme was performed with Histrap columns (GE Healthcare)

Synthesis of ethynylcobaltocenium (Cc^+)

Ethynylcobaltocenium was synthesized by following an experimental procedure slightly modified from the literature. The synthetic procedure is based on the introduction of a suitable carbanion and subsequent hydride abstraction by nucleophilic attack into a cationic sandwich as cobaltocenium. In a first step of the synthetic procedure, to a suspension of cobaltocenium hexafluorophosphate in THF at 0°C was added lithium ethynylide complex. The reaction mixture was stirred for 30 min at 4-5°C and the solvent was evaporated under vacuum. The solid residue was dissolved in cyclohexane. The solution was filtered through Celite and evaporated and the compound obtained was purified.

In the second step of the synthesis, the compound previously obtained was dissolved in dichloromethane and trityliumhexafluorophosphate was added. The mixture was stirred at room temperature for 10 minutes. Afterwards the solvent was removed under vacuum and the compound was purified by chromatography.

Procedures

All electrochemical experiments were performed using an Autolab PGSTAT-12 potentiostat, with a three-electrode configuration cell including an Ag/AgCl reference electrode (3 M KCl), a steel auxiliary electrode, and a working electrode. A pencil core (0.5 mm diameter) glued with a copper wire was used for connecting the carbon felt as working electrode. All the electrochemical measurements performed in negative potential window are under nitrogen flow, and substrates were purged under nitrogen for 15 min before adding into the electrochemical cell, in order to eliminate the influence of oxygen.

X-ray Photoelectron Spectroscopy (XPS) measurements.

The surface chemical composition of the samples was evaluated by using X-Ray Photoelectron Spectroscopy (XPS). The measurements were performed using a KRATOS Axis Ultra X-Ray Photoelectron spectrometer (Kratos Analytical, Manchester, UK) equipped with a monochromated AlKα X-Ray source (hν = 1486.6 eV) operated at 150 W. The low pressure in the analytical chamber was 10^{-9} mbar during XPS measurements. Wide scans were recorded using an analyzer pass energy of 160 eV and narrow scans using a pass energy of 20 eV (instrumental resolution better than 0.5 eV). Charge correction was carried out using the C1s core line, setting adventitious carbon signal (H/C signal) to 284.6 eV.

Preparation of multi-wall carbon nanotube functionalized electrode

The surface of carbon felt was first activated by running 20 cyclic voltammetry scans over the range from -0.7 V to 2.5 V in 0.1M H_2SO_4 solution. Then the carbon felt was rinsed carefully with water followed by heat treatment at 200 ℃ for 1h to eliminate the H_2SO_4 residues. Subsequently, the MWCNT-functionalized carbon felt was prepared by repeating the dipping/drying process for 10 cycles. The dipping step was carried out in 0.5 mg/mL MWCNT suspension, and the drying step is at 130℃ in the oven.

Azido and vinyl groups functionalized electrode (CF-CNT-AzVi)

Bi-functionalized electrodes CF-CNT-AzVi were prepared from solution containing a mixture of the corresponding diazonium cations. To a solution containing 0.3 mM 4-vinylaniline and 0.7 mM 4-azidoaniline in 0.5 M HCl was added 2 mM sodium nitrite with continuous stirring for 5 min at room temperature. Then the grafting process was applied immediately on the CF-MWCNT electrode by running two successive scans from 0.4 V to -0.6 V, after rinsing with water, the vinyl and azido groups functionalized electrode was obtained.

Ferrocene and cobaltocenium co-functionalized electrode (CF-CNT-Cc^{+}Fc)

A sequential dual click chemistry approach was used in order to carry out the post-functionalization of the CF-CNT-AzVi composite electrodes. Such sequential process has been performed primarily using a couple of electroactive molecules, ethynylcobaltocenium and 6-(ferrocenyl)hexanethiol to exemplify the feasibility of such strategy. The advantage of using the ethynylcobaltocenium and 6-(ferrocenyl)hexanethiol, having active sites allowing

the sequential post-functionalization is based on their characteristic electrochemical behavior that can be studied by cyclic voltammetry. The post-functionalization process consists of the combination of two different consecutive click reactions, copper (I)-catalyzed „alkyne-azide" cycloaddition (CuAAC) and „thiol-ene" click coupling, for which it has been previously proves that they can be accomplished in a stepwise procedure without interaction between the reactants. The reaction sequence employed was as follows: the electrode was first dipped into a mixture of DMF/H_2O (70/30) solution containing 0.1 mM copper acetate, 0.3 mM ascorbic acid and 1mM ethynylcobaltocenium. The reaction mixture was left for 24 h at room temperature in the darkness. Afterwards, the electrode was thoroughly rinsed with DMF and water to remove residual species that could remain adsorbed on the substrate. After drying, the sequence was completed in a second step by a thiol-ene click reaction. The electrode was dipped in methanol/H_2O (70/30) mixture in the presence of 1 mM TCEP and 1 mM 6-(ferrocenyl)hexanethiol overnight. After completion of reaction, the ferrocene /cobaltocenium functionalized electrodes were washed with water and methanol before use.

DSDH and rhodium complex co-functionalized electrode (CF-CNT-Rh/DSDH)

After proving the possibility to perform a double post-functionalization on the CF-CNT-AzVi via the sequential dual click chemistry process, this generic and versatile approach has been used to co-immobilize DSDH and rhodium complex. The co-functionalization process involves two steps. The CF-CNT-AzVi electrode was first put into a DMF/H_2O (70/30) solution consisting of 4-[(2-propyn-1-yloxy)methyl]-4'-methyl-2,2'-bipyridine (1 mM)(synthetic procedure was following the reported literature [142]), and copper acetate (0.3 mM) and ascorbic acid (0.9 mM) for 24 h in the darkness. The modified electrode was thoroughly rinsed with water, DMF and followed by a last rinsing in dichloromethane (DCM). A complexation step of the bipyridine ligand to immobilize a rhodium complex was then carried out. The electrode was then immersed in a DCM (20 mL) solution containing $(RhCp^*Cl_2)_2$ (2 mg) with continuous stirring for 3h and the CF-CNT-RhVi electrode was obtained. Thiol-ene click reaction was subsequently used to co-functionalize the electrode with cysteine-tagged DSDH taking advantage of the availability of the alkene functional groups present on the substrate. The CF-CNT-RhVi electrode was immersed into 1 mL of aqueous PBS buffer (250 mM, pH=7) containing 2.5 mg protein, 0.3 mM TCEP and 1 mM $MgCl_2$. The mixture was allowed to react at 4 ℃ overnight. The resulting CF-CNT-Rh/DSDH electrode was rinsed carefully with water and buffer solutions before use.

4.3 Results and discussions

4.3.1 Electrochemical behavior of 4-azidobenzene and 4-vinylbenzene diazonium salts individually and its corresponding mixture.

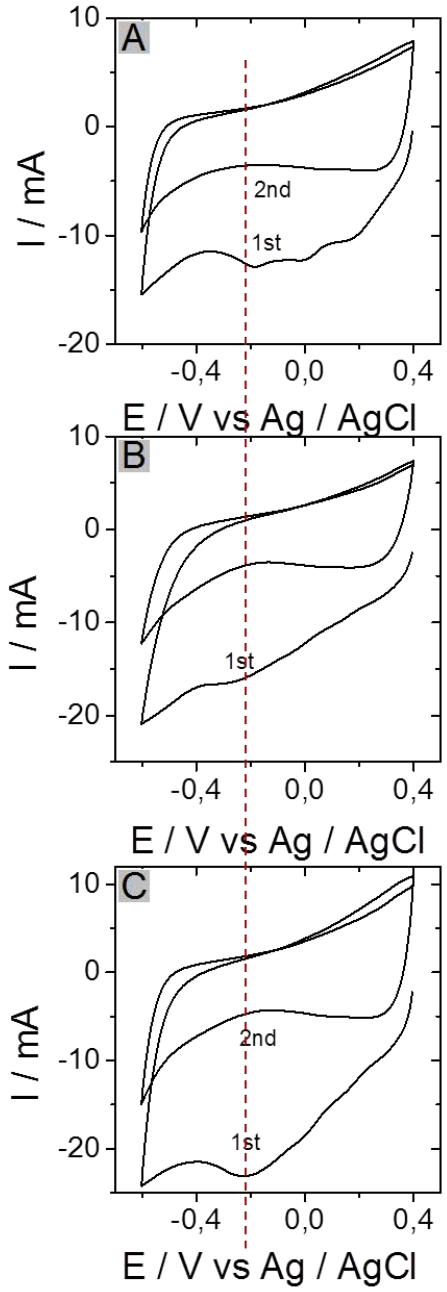

Figure 4.2. *Cyclic voltammograms on a CF-CNT electrode of electrochemical reduction of (A) 1mM 4-vinylaniline, (B) 1 mM 4-azidoaniline, and (C) 0.3 mM 4-vinylaniline and 0.7 mM 4-azidoaniline*

diazonium cations generated with 2 mM sodium nitrite at in 0.5 M HCl solution at scan rate of 100 mV s^{-1}. The geometric surface area of the electrode was 0.25 cm^2.

Prior to the modification of the CF-CNT composite electrodes, the electrochemical behavior of the diazonium cations involved in the electrografting process, 4-azidobenzene and 4-vinylbenzene diazonium cations has been investigated separately. A typical cyclic voltammogram of 1mM 4-vinylaniline diazonium cations in 0.5 M HCl containing various equivalents of $NaNO_2$, showed during the first reduction scan an irreversible cathodic peak at 0.15 V (**Fig. 4.2A**). Furthermore, the presence of minor peaks, the origin of which was still unknown was observed at more negative potentials. 4-azidobenzene diazonium cations show a voltammetric signal close to -0.3 V (**Fig. 4.2B**). The passivation of the electrode due to the presence of organic functions was demonstrated by the significant decrease of the current observed during the second potential scan in both cases. **Fig 4.2C** presents the electrochemical response of a solution containing 0.3 mM 4-vinylbenzene and 0.7 mM 4-azidobenzene diazonium salts. A broad and irreversible cathodic peak was observed located at -0.2 V. A significant increase was observed in the current peak which was attributed to the simultaneous reduction of the mixture of diazonium salts due to the proximity of the cathodic potential values of the species in solution.

4.3.2 Bi-functionalization of the electrode by diazonium electrografting

The preparation of the CF-CNT bi-functionalized composite electrodes containing azide and alkene functionalities was carried out by electrochemical reduction in a solution containing a mixture of the corresponding diazonium salts that were generated in situ from 4-azidoaniline and 4-vinylaniline respectively in 0.5 M HCl in the presence of 2 equivalents of $NaNO_2$. Two different approaches could be employed to modify the carbon composites. A first approach could be to apply a constant negative potential and change the composition of the solution depending on the cathodic potential values determined for each diazonium salt involved in the modification step. The second approach could be to work with a solution containing always the same concentration of the diazonium cations used to modify the electrode substrate and applying a negative potential which will be gradually changed from the more positive to the more negative potentials. Furthermore, depending on the desired

application, the surface concentration achieved after the grafting is an important parameter that needs to be considered before proceeding to the modification. According to these premises and taking into account that we were not interested in a fully covering of the carbon composites, we have chosen to carry out the modification process in a solution containing 0.3 mM 4-vinylbenzene and 0.7 mM 4-azidobenzene diazonium cations generated in situ from a mixture of 4-vinylaniline and 4-azidoaniline respectively in 0.5 M HCl in the presence of an excess of $NaNO_2$. The electrografting was performed recording a single reduction scan starting from 0.5 V to -0.5 V.

The one step bi-functionalization of the electrode was carried out by electrochemical reduction performed in solution with diazonium salt cations generated from a mixure solution of 4-vinylaniline and 4-azidoaniline. The cathodic peak potential values of each diazonium salt employed for the electrografting procedure are very close. In order to get a reasonable ratio between the two kinds of compound, typical cyclic voltammograms recorded upon reduction of individual 1mM 4-vinylaniline **(Figure 4.2A)** and 1 mM 4-azidoaniline **(Figure 4.2B)** were first carried out as references. In both cases, irreversible reduction peaks were observed during the first scan and vanished during the subsequent sweep, indicating the formation of an organic layer onto the electrode surface. The reductive peak potential values for the two kinds of diazonium cations are quite similar, the 4-vinylaniline cation has a slightly smaller reduction potential. In order to get a relatively equivalent amount of the two species on the electrode, a compromise ratio of 4-vinylaniline / 4-azidoaniline (3/7) was finally used. As shown in **Figure 4.2C**, a similar electrografting process for diazonium salt mixture was observed compared to the mono species, reductive peak in the 1st cycle appeared in the same range of potential window, and the disappearing of reduction peak in the 2nd cycle indicated the blocking effect of the organic layers formed from the first scan.

The influence of the presence of the organic layer on the electrochemical response of the CF-CNT-AzVi modified composite electrodes was evaluated by using ferrocenedimethanol as an electrochemical redox probe. **Figure 4.3** showed the electrochemical response recorded in a solution containing 0.1 mM ferrocenedimethanol in 50 mM PBS (pH 6.5) at 50 mV s^{-1} before the electrografting of the azidophenyl and vinylphenyl groups (**a**) on CF-CNT electrode and after the electrochemical modification on a CF-CNT-AzVi (**b**). The cyclic voltammogram obtained on the modified electrode showed a clear decrease in the anodic and cathodic peak currents demonstrating the blocking effect of the active surface by the presence of the organic groups. The blocking effect was also supported

by the increase in the difference between the anodic and cathodic peak potentials values compared to the electrochemical response obtained on a bare CF-CNT suggesting that the substrate is partially covered by the organic layer that makes the electron transfer slower.

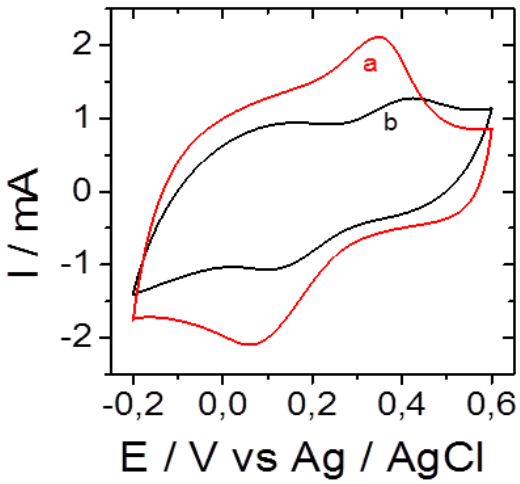

***Figure 4.3**. Cyclic voltammograms recorded using a CF-CNT electrode in the presence of 0.1 mM ferrocenedimethanol (in 50 mM PBS at pH 6.5) at 50 mV s^{-1} (a) before and (b) after (solid line) electrografting with diazonium cations for 2 cycles. The geometric surface area of the electrode was 0.25 cm^2.*

4.3.3 Evaluation of click chemistry reactions on the bi-functionalized electrode

Before using the CF-CNT-AzVi to immobilize the $[Cp^*Rh(bpy)Cl]^+$ and the enzyme, the sequential dual click chemistry approach has been tested with a pair of compounds that can be used as a model in order to analyze the efficiency and evolution of the click reaction. The compounds employed to this aim are the ethynylcobaltocenium and the 6-(ferrocenyl)hexanethiol which exhibit a characteristic electrochemical behavior and that can be readily detected by cyclic voltammetry. The azide functionalities will react with the alkyne terminal groups present in the ethynylcobaltocenium structure through the copper-catalyzed azide-alkyne cycloaddition whereas the vinyl moieties will be able to react with the thiol functions of the 6-(ferrocenyl)hexanethiol through the thiol-ene click reaction. The overall sequential post-functionalization process was presented in **Figure 4.1A.** The feasibility of similar functionalization methodologies, allowing selective incorporation of organic moieties,

has been previously described in the literature for other substrates and combining different click reactions types. However, the main aim of using the pair ethynylcobaltocenium/vinylferrocene to carry out the sequential post-functionalization process is to demonstrate that the azide- and vinyl functionalities remained accessible after their incorporation in the carbon composites for further functionalization. After confirming not only that the azido- and alkene functional groups remained available for further functionalization but also the success of such double sequential click reaction such method was subsequently extended to co-immobilize covalently cysteine-tagged enzymes and mediators on the CF-CNT-AzVi substrates. The CuAAC click reaction used for mediator immobilization was performed in a first step since involves the use of organic solvents that would be able to deactivate the enzymes (**Figure 4.1B**).

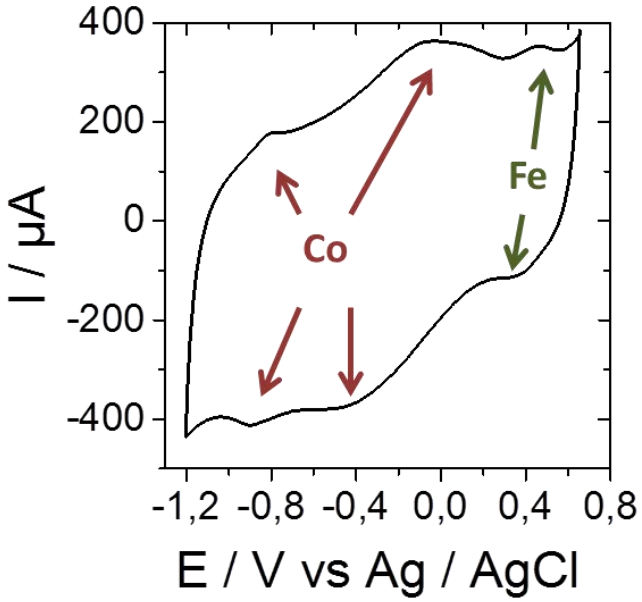

Figure 4.4. *Cyclic voltammograms recorded using CF-CNT-CoFc in 50 mM PBS buffer (pH 6.5) electrode at a scanning rate of 20 mV* s^{-1}*. The geometric surface area of the electrode was 0.25* cm^2*.*

Figure 4.4 shows a typical cyclic voltammogram recorded on CF-CNT after co-immobilization of ferrocene and cobaltocenium (*CF-CNT-*Cc^{+}*Fc*) performed in PBS buffer solution. From the cyclic voltammogram, three pairs of redox peaks were observed, the one located in positive potential region was derived from the Fe^{2+}/Fe^{3+} couple, its oxidative

voltammetric signal was located at +0.46 V. Another two pairs of redox peaks in the negative potential window was due to cobaltocenium reduction, corresponding to Co^{3+}/Co^{2+} and Co^{2+}/Co^{+} redox pairs. Their reductive voltammetric signal was located around -0.45 V and -0.9 V, respectively. The electroactive behavior of the electrode not only indicates the successful coupling of the two reactions with vinyl and azido groups, but also proves the facility in electron transfer from molecular to the electrode after organic layer grafting.

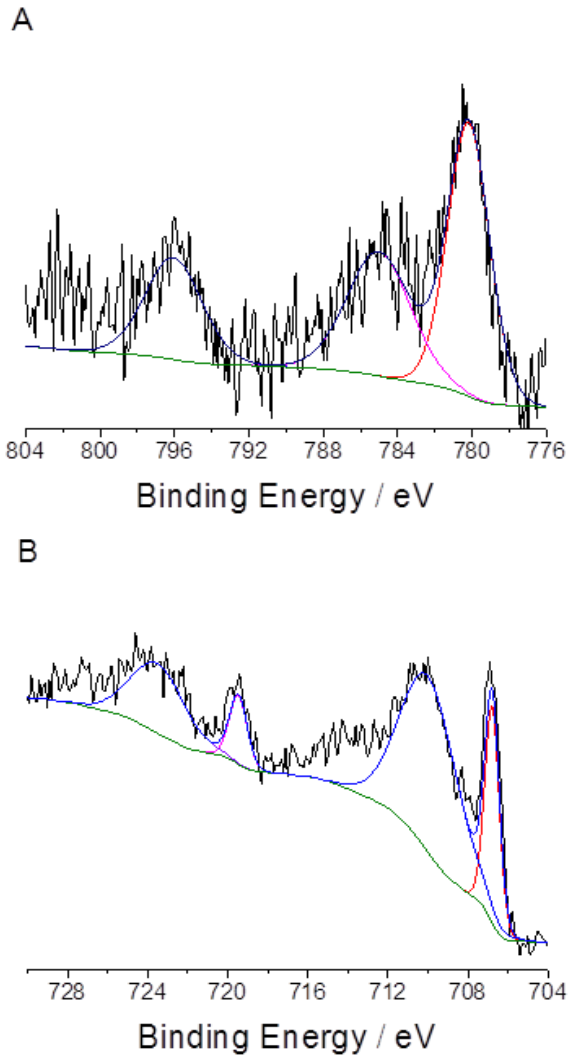

Figure 4.5. *XPS spectra of the (A) Co 2p and (B) Fe 2p core level spectrum from the cobaltocenium and ferrocene functionalized sunbstrate.*

X-Ray Photoelectron Spectroscopy measurements were performed to confirm the uptake of cobaltocenium and ferrocene moieties on ITO modified electrodes. The

functionalization was carried out on ITO plates by following the same experimental procedure previously described for CF-CNT-AzVi electrodes since the purpose it was mainly to evidence the feasibility of the generic modification process. The survey XPS spectrum recorded at the end of the functionalization process shows the presence of the C 1s, O 1s, N 1s, Fe 2p and Co 2p. Deconvolution of the high-resolution Co 2p XPS spectrum (**Figure 4.5A**) displays two characteristics peaks centered at 780.6 and 796.1 eV corresponding to Co 2p3/2 and Co 2p1/2 spin orbits peaks respectively. Furthermore, the Fe 2p core level spectrum (**Figure 4.5B**) shows two main sharp components centered at 709.9 and 724.6 eV respectively assigned to Fe 2p3/2 and Fe 2p1/2 spin orbits peaks respectively for Fe^{2+}. The high resolution spectrum also displays peaks at slightly higher binding energies which are attributed to 2p3/2 and 2p1/2 in the case of the oxidation state Fe^{3+}. These peaks are broadened due to spin-orbit coupling between the 2p3/2 and 2p1/2 core holes and the unpaired 3d electrons which induces multplet components [258]. Moreover, in addition to multiplet structures, satellite shake-up structures associated with 2p3/2 and 2p1/2 appear.

4.3.4 Co-immobilization of $[Cp^*Rh(bpy)Cl]^+$ and enzymes on the electrode

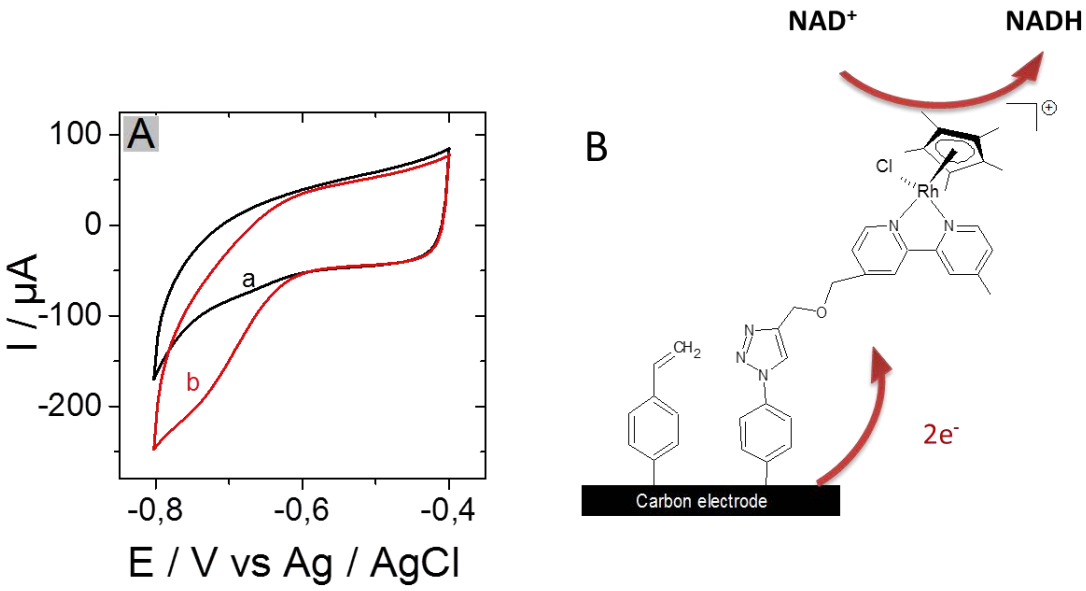

Figure 4.6. *(A) Cyclic voltammograms recorded using a CF-CNT-RhVi electrode in 50mM PBS buffer (pH 6.5) at a potential scan rate of 5 mV s^{-1} (a) in the absence and (b) in the presence of 1 mM NAD^+. (B) Schematic representation of NADH regeneration by a CF-CNT-RhVi electrode. The geometric surface area of the electrode was 0.25 cm^2.*

The co-immobilization procedure on the electrode was operated in two steps. Initial immobilization of rhodium complex was performed by azide-alkyne Huisgen reaction to incorporate bipyridine ligands on the electrodes which subsequently underwent a complexation reaction followed by a complexation with $(RhCp^*Cl_2)_2$. Its electrocatalytic activity towards NADH regeneration was checked before carrying out the enzymes immobilization. **Figure 4.6A** shows the cyclic voltammogram of CF-CNT-RhVi electrode performed in 50 mM PBS buffer (pH 6.5). Before addition of NAD^+, a reduction peak was observed around -0.69 V (**curve a**), which was the typical reductive potential value for rhodium complex. This value is similar to that of rhodium complex functionalized electrode fabricated through only one kind of diazonium salt electrografting, showing that the appearance of other functionalized groups on the electrode doesn not influence the electrocatalytic behavior of rhodium complex. After addition of 1mM NAD^+ into the buffer, the reductive peak current was significantly increased from 100 µA to 200 µA (**curve b**). The increase of peak current indicated that the NADH regeneration process was catalyzed by the rhodium complex (**Figure 4.6B**): By applying a negative potential, Rh(III) was reduced to Rh(I), the Rh(I) was then protonated in the buffer solution and re-oxidized by transferring a hydride ion to NAD^+ to regenerate NADH. In the meantime, the increase of anodic peak current was observed, suggesting the decrease of the protons availability to form protonated Rh(I).

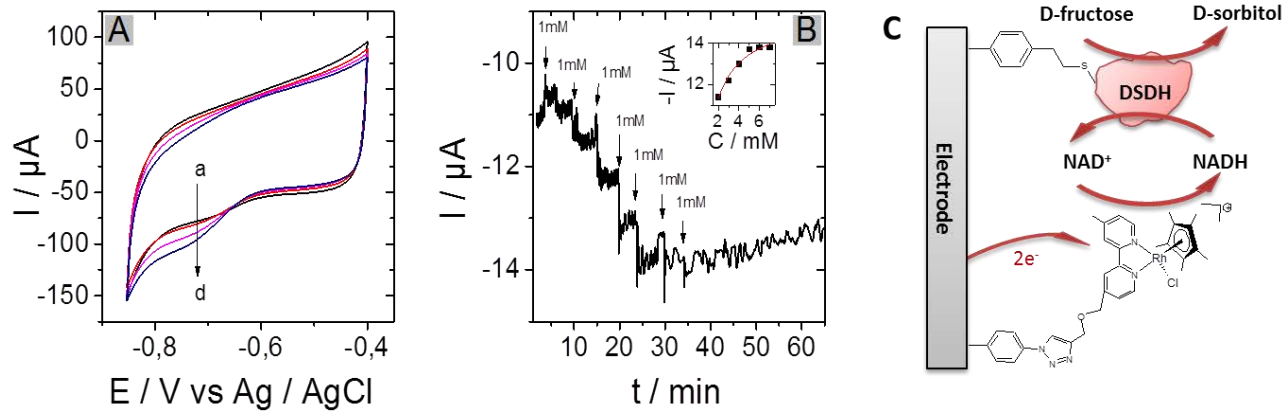

Figure 4.7. (A) *Cyclic voltammograms recorded using a CF-CNT-Rh/DSDH electrode at a potential scan rate of 5 mV s^{-1} to addition of (a) 0 mM (b) 1 mM (c) 3 mM (d)5 mM oxygen free D-fructose (B) Amperometric response to successive addition of 1mM D-fructose up to 7mM using a CF-CNT-*

Rh/DSDH electrode at an applied potential of -0.75 V. Both experiments are carried out in 50mM PBS buffer (pH 6.5) with the presence of 1mM NADH. (C) Schematic representation of the electroenzymatic synthetic process for CF-CNT-Rh/DSDH electrode. The geometric surface area of the electrode was 0.25 cm^2.

After confirming the catalytic activity of the immobilized rhodium complex, cysteine-tagged DSDH was covalently attached to the CF-CNT-RhVi electrode taking advantage of the thiol groups from cysteine tages by „thiol-ene" click chemistry. The bioelectrocatalytic response of the CF-CNT-Rh/DSDH electrode was demonstrated by introducing the oxygen free D-fructose into buffer solution containing 1 mM NADH. **Figure 4.7A** shows the cyclic voltammograms measured with CF-CNT-Rh/DSDH electrode. In the absence of D-fructose, the reduction peak of rhodium complex was observed around -0.69 V (curve a), which was comparable to that before attaching DSDH, demonstrating that the immobilization of enzymes does not hinder the electron transfer or deactivate the rhodium complex. When D-fructose was gradually introduced into the solution (**curve b, c and d**), the cathodic current was gradually increased. In this bioelectrocatalytic process, D-fructose was reduced to D-sorbitol by DSDH in the presence of NADH, in the same time, NADH was oxidized to NAD^+. The formed NAD^+ can be transformed back to electroactive NADH catalyzed by rhodium complex at the electrode surface. The bioelectrocatalytic amperometric response of CF-CNT-Rh/DSDH electrode was also tested (**Figure 4.7B**). The cathodic current was increasing upon successively addition of 1 mM D-fructose in the solution. The apparent Km estimated for D-fructose reduction was around 1 mM, in the same range of immobilized cys-DSDH on carbon felt electrode (Km is 2.2 ± 0.5 mM), and much lower than that of DSDH in solution (Km is 49.4). The Km value indicated that the affinity of D-fructose to DSDH on this co-immobilized electrode was improved. From the bioelectrocatalytic response discussed above, it was confirmed that the cys-DSDH and rhodium complex can be co-immobilized on an electrode keeping their catalytic properties.

4.4 Conclusion

A versatile approach has been developed in order to get bi-functionalized CF-CNT electrodes. The sequential modification method is based on the combination of two well-established and robust functionalization processes, the electrochemical reduction of

diazonium cations and a double consecutive click reactions process. In situ electrografting of a mixture of diazonium salts (4-azidobenzene and 4-vinylbenzene diazonium salts). The cathodic peak potentials of the species involved in the functionalization step are very close and the modification of the CF-CNT electrodes was achieved by recording a single scan towards negative potentials by cyclic voltammetry. The co-functionalized electrodes allow selective covalent bonding of alkyne and thiol organic moieties, via two „click" immobilization steps. The combination of these reactions with diazonium electrochemistry in fabrication of electrodes did not hinder the electron transfer between redox probes and electrode. The electron mediator $[Cp^*Rh(bpy)Cl]^+$ was immobilized by first coupling vinyl 2,2"-bipyridine on the electrode via CuAAC reaction, followed a complexation step with $(RhCp^*Cl_2)_2$. Taking advantage of the thiol groups from cysteine tags, the cys-DSDH was then coupled to vinyl groups on the electrode via thiol-ene click reaction. The activity of both rhodium complex and D-sorbitol dehydrogenase were kept after click couplings were made. The electrocatalytic reduction of D-fructose to D-sorbitol by the immobilized DSDH using rhodium complex as mediator was evidenced by both cyclic voltammetry and chronoamperometry. This facile co-immobilization route could be further used for other bio-systems with different redox enzymes and mediators in the field of biosynthesis, biosensing and fuel cell applications.

Chapter 5. Co-immobilization of rhodium complex and NAD-dependent dehydrogenase in an electrochemical bioreactor for enantioselective bioconversion

Here we report a simple immobilization method for covalent bounding of rhodium complex ($[Cp^*Rh(bpy)Cl]^+$) onto carbon electrode (CF-CNT, carbon nanotube functionalized carbon felt or BP, „bucky paper"). The bipyridine ligand was first grafted on the electrode by electro-reduction of bipyridyl diazonium cations generated from 4-amino-2,2'-bipyridine compound. After a mild complexation step with rhodium dimer ($((RhCp^*Cl_2)_2)$), the rhodium complex functionalized electrode was obtained. Their electrocatalytic property towards NADH regeneration was investigated for rhodium functionalized CF-CNT electrode. Taking advantage of the thin layer structure of BP electrode, a separated glassy filter layer with D-sorbitol dehydrogenase in the gel was overlaid on the top of the rhodium functionalized electrode, the enzyme layers could be easily changed, the reusability of BP-Bpy-Rh electrode was significantly improved. Finally, a bioconversion experiment for electroenzymatic enantioselective reduction of D-fructose to D- sorbitol was carried out, a conversion rate of 87%, faradic effciency up to 83% and a high total turnover number (TTN) up to 12500 for rhodium complex was achieved.

5.1 Introduction

As mentioned in Chapter 3, $[Cp^*Rh(bpy)Cl]^+$ has been proved to be the most efficient non-enzymatic catalyst for NADH regeneration [136]. The presence of $[Cp^*Rh(bpy)Cl]^+$ not only reduced the overpotential needed for NAD^+ reduction, but also avoided the unfavorable formation of inactive NAD_2 dimer [5,259,260]. So in the field of electroenzymatic synthesis, $[Cp^*Rh(bpy)Cl]^+$ has been used as NADH regeneration agent in combination with NAD-dependent redox enzymes [5–9]. To be really applied in bioconversion, rhodium complex need to be immobilized on the electrode due to the following reasons: firstly, in large scale synthesis, the purification of reaction products can be facilitated if the catalyst is not involved in the final mixture solution; secondly, the immobilization of rhodium complex can increase the reusability of the catalyst, which is economically desirable [72]; thirdly, the rhodium complex was observed to interact with some surface functional groups of the proteins, leading to degradation of its catalytic responses. Separation of rhodium complex from enzymes will significantly increase the stability of rhodium complex as well as the lifetime of the system [6,7,198]. The degradation problem can be avoided by immobilization of rhodium complex and enzymes separately. Despite the efforts made on rhodium complex immobilization by growing conductive polymers [29,137–139] on electrode, or by non-covalent π-π interactions between carbon materials (eg. carbon nanotube [34] or graphene [35]) and rhodium complex, a new synthetic route for covalent immobilization of rhodium complex has been discussed in Chapter 3. This synthetic route combined a surface modification step on CF-MWCNT electrode, a post-functionalization step to „click" bipyridine ligand, and eventually a metal coordination step. Even through the rhodium complex functionalized electrode showed good catalytic activity and stability, some limitations were observed and some improvements can be made.

On one hand, the fabrication route could be simplified. Among the methods for transition metal complex immobilization, the diazonium grafting was the most convenient method for carbon surface functionalization [262]. As the coordination ligand of our target molecular $[Cp^*Rh(bpy)Cl]^+$ contained a bipyridine, instead of post-grafting the bipyridine onto the azide-functionalized carbon surface, this bipyridyl diazonium can be directly electrografted onto carbon electrode if the bipyridine ligand was modified with an amino group [263]. The bipyridyl diazonium salt grafting method has been used for immobilization

of some other transition metal complex (eg. Mn, Re, Fe, Co, Ni, or Cu) on graphene for water oxidation or syngas generation [263,264]. In this work, taking advantage of the diazonium property of 4-amino-2,2'-bipyridine, a more simple and rapid immobilization route for rhodium complex was proposed as shown in **Figure 5.1.** 4-amino-2,2'-bipyridine (compound **A**) was first activated to obtain bipyridyl diazonium cation (compound **B**), then a negtive potential was applied to promote the release of N_2, resulting in the covalent functionalization on electrode surface. After a complexation step with rhodium dimer $((RhCp^*Cl_2)_2$ (compound **C**), $[Cp^*Rh(bpy)Cl]^+$ (compound **D**) was covalently immobilized on the electrode. Compared to the rhodium functionalized electrode prepared in Chapter 3, not only the preparation process was simplified, but the distance between rhodium complex and electrode surface are shortened, the electron transfer reaction was expected to be improved.

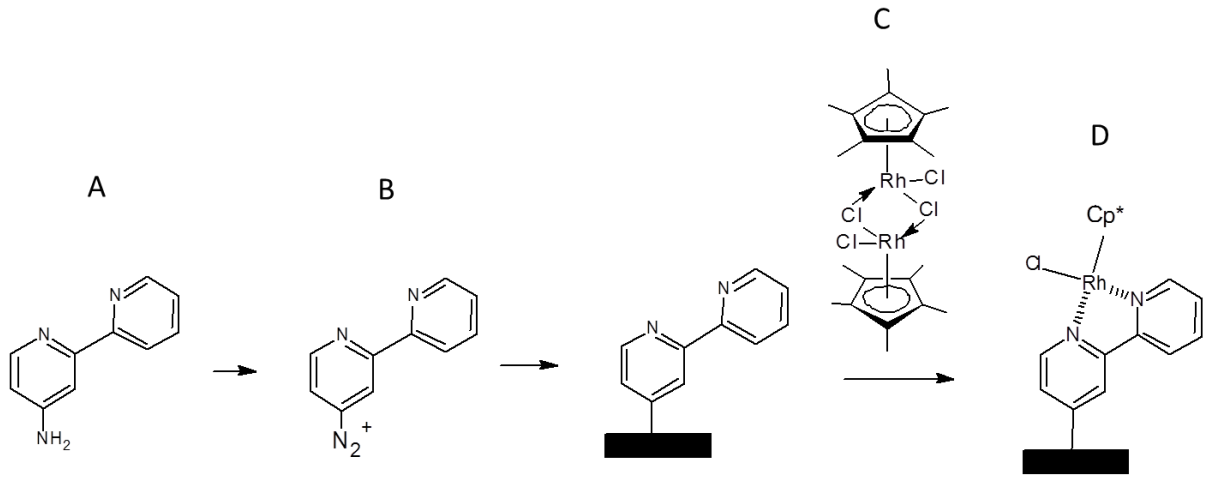

Figure 5.1. *Schematic representation of synthetic route followed for the functionalization of carbon electrode with* $[Cp^*Rh(bpy)Cl]^+$ *by combination of diazonium salt electrografting and complexation process.*

On the other hand, the configuration of the CF-CNT electrode influenced the efficiency of the system. Since the CF-CNT electrode was a thick layer, in the enzymatic electrocatalytic process in combination with NAD-dependent enzymes as performed in Chapter 3, the reduced Rh(I) need to receive protons from buffer solution to form hydrid Rh(I) for NAD^+ reduction [5,6,136], we assumed that if the proton consumption speed is higher than the proton diffusion speed from bulk solution to the interface, the local pH inside the

porous electrode can increase, significantly influencing the activity of enzymes [206], leading to decrease of conversion efficiency of the system [142]. To get rid of the potential local pH inhibition, thinner electrodes would be preferred, so another kind of thinner layered „bucky paper" electrode could be employed. It was fabricated from stable suspensions of carbon nanotubes (CNT), by controlling the volume of the suspension in the filtration process, the thickness was controlled within hundred micrometers, this highly mesoporous layer was mechanically robust, flexible, stable and electrically conductive [265]. „Bucky paper" has been widely applied as working electrode in the field of bio-sensing [266] or bio-fuel cells [265,267], it will also be a good candidate in electroenzymatic synthesis.

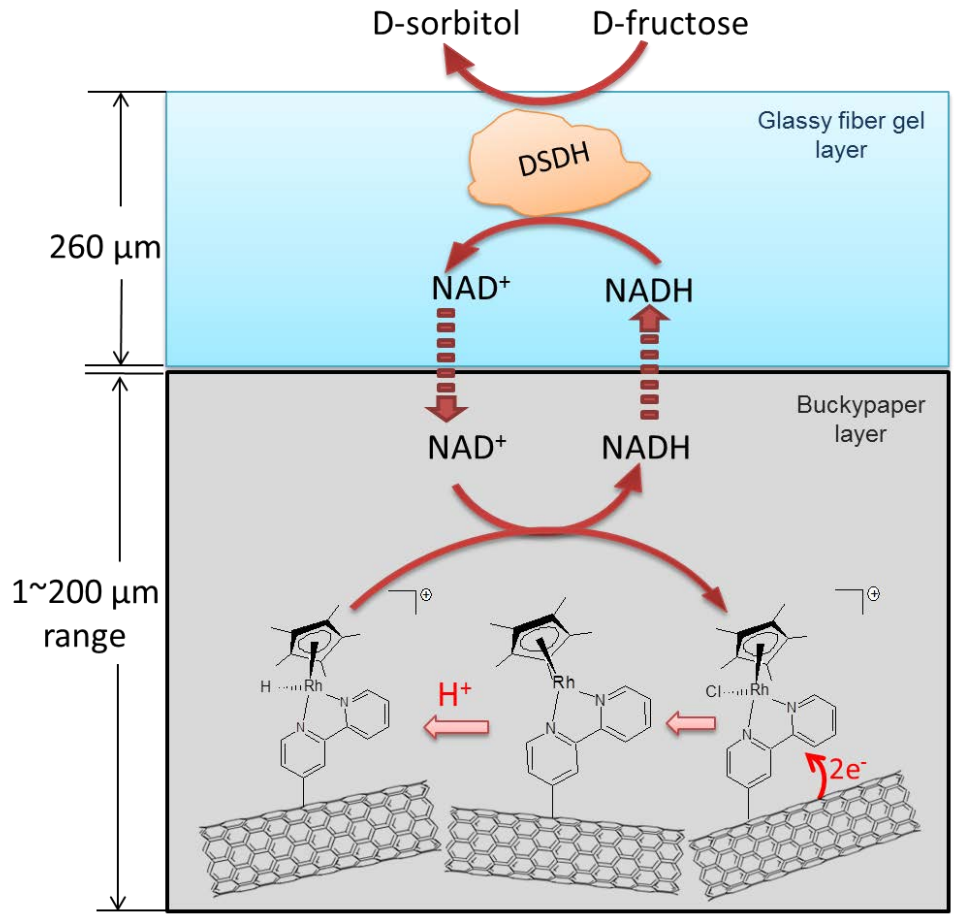

Figure 5.2. *Configuration and electroenzymatic process involved of the packing electrode with separated D-sorbitol dehydrogenase gel layer and rhodium functionalized BP layer. BP can be prepared in the thickness range of 1~200 µm according to the reported literature* [265].

Furthermore, the rhodium complex functionalized CF-CNT electrode with enzyme gel layer deposited on the top showed good electroenzymatic catalytic response, however, a long-term stability experiment show 40% decrease of catalytic current to NAD^+ reduction at their saturated concentrations over 90h continuous electrochemical operation (Chapter 3), indicating that this enzymes immobilization method did not provide complete prevention of interactions between the immobilized rhodium complex and enzyme in the gel. On the other hand, the enzymes and the rhodium complex have different range of lifetime, the enzyme has a quite limited one (eg. DSDH has a half-life period of 48 h at 28°C, 5 h at 35°C and 0.2 h at 40°C in solution) [204], while the $[Cp^*Rh(bpy)Cl]^+$ immobilized on CF-CNT was stable at least for 2 weeks under continuous stirring in solution (Chapter 3). As soon as the enzymes lost their activity, the gel deposited co-immobilized electrode has to be discarded. The objective of the work in this chapter was to build an electrode which could be applied in bioconversion without suffering from the above problems. If we physically separated the long-term stable BP-Bpy-Rh layer with the lifetime-limited enzyme layer, we could build the co-immobilized electrode by simple packing, in this way, the BP-Bpy-Rh electrode can be reused with new enzyme gel layers, practically and economically improved the life-time of the BP-Bpy-Rh electrode in system. In this work, as shown in **Figure 5.2**, we prepared an individual enzyme gel layer by depositing enzyme gel on a piece of microfiber filter, then it was overlaid on the top of BP-Bpy-Rh layer. The distance between enzymes and rhodium complexes was close but physically restricted in two layers, the interaction between rhodium complex and enzymes should be completely prevented, and the pH inhibition should also be avoided due to their thin layer structures. The reusability of this rhodium functionalized BP electrode will be studied, and the packed co-immobilized electrode will be applied to bioconversion of D-fructose to D-sorbitol.

5.2 Experimental

Chemicals and Enzymes

β-Nicotinamide adenine dinucleotide hydrate (NAD^+, ≥ 96.5%, Sigma-Aldrich) , β-nicotinamide adenine dinucleotide, reduced disodium salt hydrate (NADH, ≥97%, Sigma-Aldrich), 4-azidoaniline hydrochloride (97%, Sigma-Aldrich), sodium nitrite (≥97.0% , Sigma-Aldrich), 1,1‟-ferrocenedimethanol (97%, Sigma-Aldrich), 97% D-fructose (99 wt%,

Sigma), sodium dihydrogen phosphate (99.5%, Merck), pentamethylcyclo-pentadienylrhodium (III) chloride dimer ($(RhCp^*Cl_2)_2$, Sigma-Aldrich), dimethylformamide (≥99.8%, Sigma-Aldrich), dichloromethane (Carlo Erba), 1M hydrochloric acid solution (Sigma-Aldrich), carboxylic-functionalized multi-walled carbon nanotubes (MWCNT-COOH, 95%, Φ 15±5 nm, L 1-5 µm, Nanolab), multi-walled carbon nanotubes (MWCNT, 95%, Φ 6-9nm, L 5µm, Sigma), glassy microfibre filters (thickness is 0.26 mm, diameter is 70 mm, Whatman®), PVDF membrane filter (pore size is 0.45 µm, diameter is 47 mm, Durapore ®). Overproduction of N-His(6) D-sorbitol dehydrogenase (800 U mL^{-1}) was done with Escherichia coli BL21GOLD (DE3) containing the corresponding expression-vectors pET-24a(+) (Novagen) and purification of the enzyme was performed with Histrap columns (GE Healthcare).

Synthesis of 4-amino-2,2'-bipyridine

4-amino-2,2‟-bipyridine was synthesized following the reported protocol [263,268,269], the scheme of synthetic route was shown in **Figure 5.3**:

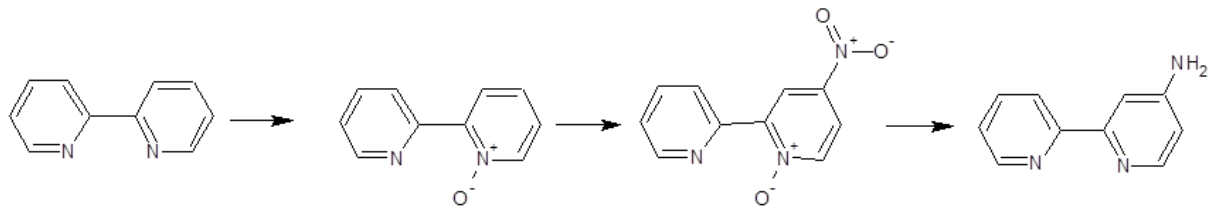

Figure 5.3. *Schematic representation of synthetic route for 4-amino-2,2'-bipyridine.*

2,2'-bipyridine-N-oxide : 5 g 2,2‟-bipyridine was dissolved in 25 mL trifluoroacetic acid, then 5.32 mL of 30% H_2O_2 slowly added into the solution under stirring. After the solution stirring at room temperature for 4h, its pH was adjusted by addition of 25% NaOH aqueous solution, then extracted with $CHCl_3$ (30 mL ×5). The organic phase was gathered and dried over Na_2SO_4, filtered and vacuum evaporated. The product was obtained as pale yellow oil.

4-nitro-2, 2'-bipyridine-1-oxide: 2.1 g of 2, 2‟-bipyridine-N-oxide and 6.7 g potassium nitrate dissolved in 16.3 mL concentrated sulfuric acid, keep stirring for 30 h at 95 ℃. Then the resulting solution was poured into 50 g ice and adjusted pH to 9.0 by 25% NaOH. The yellow

precipitate formed was collected by vacuum filtration and washed with plenty of cold water. After drying the solid in the air, it was dissolved in DCM, filtered off and the then DCM was removed by vacuum evaporation, the product was obtained as yellow solid.

4-amino-2, 2'-bipyridine: 500 mg of 4-nitro-2, 2‟-bipyridine-1-oxide was dissolved in 100 mL methanol, 115 mg 10% Pd/C was added under nitrogen atmosphere with vigorously stirring. The solution was incubated in the ice bath, 1.25 g sodium borohydride was slowly added. Stirring was continued at 4 ℃ overnight until the gas evolution ceased. The catalyst was removed by Gravity filtration, and the methanol was removed from the filtrate by vacuum evaporation. 30 mL water was added to dissolve the solid, extracted with DCM (50 mL×5), the organic phase was dried with $NaSO_4$ and then removed the solvent to get product as white solid.

MWCNT-functionalized electrode (CF-CNT)

The surface of carbon felt was activated by cyclic voltammetry scans from -0.7 V to 2.5 V for 20 cycles in 0.1M H_2SO_4, in order to change the surface from hydrophobic to hydrophilic. After treatment, the carbon felt was rinsed with water, followed by heat treatment at 200 ℃ for 1 h to remove the residue H_2SO_4. Then the carbon felt was cut into pieces with dimension of 0.5 cm*0.5 cm. The carbon felt was dipped into 0.5 mg mL^{-1} MWCNT-COOH suspension which was dispersed by ultrasonic for 1 h, then let it dry in the oven at 130 ℃. The dipping and drying process was repeated for 10 times in order to get enough CNT on the carbon felt.

'Bucky paper' electrode (BP)

The electrode was prepared following the reported literature[265]. 10 mg MWCNT was dispersed in 50 mL ethanol by ultrasonication for 5 h. Afterwards, the MWCNTs solution were decanted and vacuum filtered using a PVDF membrane filter (Durapore ®, pore size is 0.45 μm, diameter is 47 mm), then it was dried at 50 ℃ overnight. Finally, the electrode was cut into suitable size for use (1 cm* 1 cm or 2 cm* 2 cm).

2, 2'-bipyridine functionalized electrode

1 mM 4-amino-2, 2‟-bipyridine was mixed with 2 mM sodium nitrite in 0.5 M HCl aqueous solution with stirring for 5 min to generate 2, 2‟-bipyridine cations, the grafting was achieved by running 2 cycles of cyclic voltammograms from 0.4 V to -0.8 V on the electrode

inside the 2, 2‟-bipyridine diazonium cations solution. After grafting, the electrode was rinsed carefully with water and left dry for use.

$[Cp^*Rh(bpy)Cl]^+$ functionalized electrode

The 2,2‟-bipyridine functionalized electrode was put into 0.15 mM $((RhCp^*Cl_2)_2$ dichloromethane solution with gentle stirring for 4 h. Then the electrode was first rinsed with DCM and then immersed inside clean DCM for 5 min to remove the unreacted residue.

DSDH- $[Cp^*Rh(bpy)Cl]^+$ co-immobilized CF-CNT-gel electrode

The sol was prepared following the reported protocol[75]. 0.18 g TEOS, 0.13 g GPS, together with 0.5 mL water and 0.625 mL 0.01 M HCl was pre-hydrolyzed by stirring overnight. Then, this sol was diluted 3 times and a 40 µL aliquot was mixed with 20 µL PEI (20%), 20 µL of water and 30 µL DSDH stock solutions. This mixture was spread over the $[Cp^*Rh(bpy)Cl]^+$ functionalized electrode and let it completely dry at 4 ℃ for use.

Preparation of DSDH gel layer packed electrode

A piece of glassy microfibre filter was cut into certain size and then spread over by the same DSDH sol as mentioned above, keep it suspend in a bottle and dried at 4 ℃ over night for use. For electroenzymatic experiment, this DSDH gel layer was overload on the top of the $[Cp^*Rh(bpy)Cl]^+$ functionalized bucky paper electrode, then four corners were fixed by cotton thread.

Apparatus

All electrochemical experiments were conducted with an Autolab PGSTAT-12 potentiostat. The three-electrode configuration cell included an Ag/AgCl reference electrode (3 M KCl), a steel auxiliary electrode, and a carbon working electrode (CF-CNT or BP). A pencil core (0.5 mm diameter) glued by carbon black to a copper wire was used for connecting the CF-CNT working electrode. A steel clip was used for connecting with the BP electrode.

UV-Vis spectra have been recorded on a Cary 60 Scan UV-Vis spectrophotometer

X-Ray Photoelectron Spectroscopy (XPS) analyses were performed using a KRATOS Axis Ultra X-ray photoelectron spectrometer (Kratos Analytical, Manchester, UK) equipped with a monochromated AlKα X-ray source ($h\nu$ = 1486.6 eV) operated at 150 W. The base

pressure in the analytical chamber was 10^{-9} mbar during XPS measurements. Wide scans were recorded using a pass energy of 160 eV and narrow scans using a pass energy of 20 eV (instrumental resolution better than 0.5 eV). Charge correction was carried out using the C(1*s*) core line, setting adventitious carbon signal (H/C signal) to 284.6 eV.

5.3 Results and discussions

In order to evaluate the electrochemical properties of the immobilized rhodium complex between new synthetic route and the old one in Chapter 3, rhodium complex was first immobilized on CF-MWCNT electrode, then applied to „bucky paper" electrode with the same protocol.

5.3.1 Covalent immobilization of rhodium complex on CF-CNT electrodes by bipyridyl diazonium electrografting

A two-step protocol was applied to covalently immobilize the rhodium complex on the CF-CNT electrode. The bipyridine ligand was first immobilized on electrode surface by electrografting of bipyridyl diazonium cations generated from 1 mM 4-amino-2,2"-bipyridine activated with the presence of $NaNO_2$ in 0.5 mM HCl aqueous solution (CF-CNT-Bpy). The covalent attachment to the electrode surface was realized by running 2 successive cyclic voltammograms in a potential range from 0.4 V to -0.8 V (**Figure 5.4A**). During the first scan, an irreversible peak located around -0.7 V was observed (curve a), in which process the grafting of bipyridine radical occurred along with the release of N_2. When carrying out the second scan, the cathodic reduction current was significantly decreased (curve b). This decrease was attributed to the presence of grafted bipyridyl groups on the electrode, partially blocking the surface. The presence of the organic layer on the CF-CNT electrode was further evidenced by the comparison of the cyclic voltammograms of 0.1 mM ferrocenedimethanol recorded on the CF-CNT electrode before and after electrografting of the bipyridine layer (**Figure 5.4B**). We observed a slight decrease in peaks current in both oxidation and reduction after electrografting of bipyridine groups demonstrating the blocking effect of the organic layer, but the remained peak current showed that the electrode after functionalization still kept in a good condition for electron transfer. The bipyridine functionalized electrode was

further complexed with $((RhCp^*Cl_2)_2$ in dichloromethane with stirring for 4 h to form rhodium complex on the electrode surface (CF-CNT-Bpy-Rh).

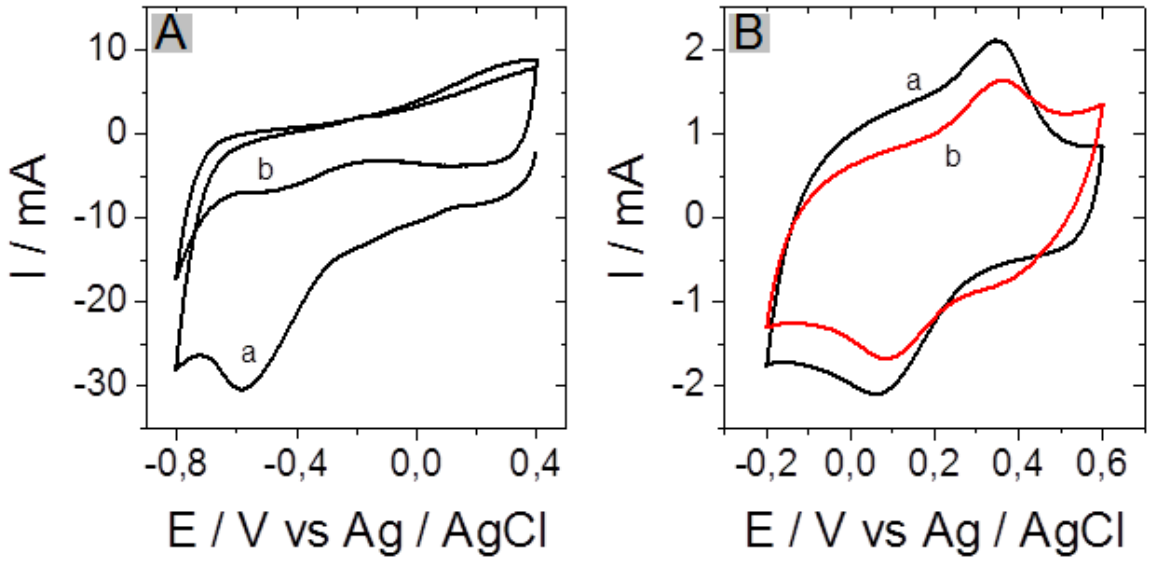

Figure 5.4. (A) *Cyclic voltammograms for the reduction of diazonium cations generated 'in situ' from 1 mM 4-amino-2, 2'-bipyridine in 0.5 M HCl, as recorded on CF-CNT electrode at 100 mV* s^{-1}. ***(B)*** *Cyclic voltammograms recorded at 50 mV* s^{-1} *in the presence of 0.1 mM ferrocenedimethanol (in 50 mM PBS at pH 6.5) using a CF-CNT electrode (a) before and (b) after electrografting with diazonium cations for 2 cycles. The geometric surface area of the electrode was 0.25* cm^2.

The catalytic response of CF-CNT-Bpy-Rh electrode for NADH regeneration was checked by cyclic voltammetry in 50 mM PBS (pH 6.5). When a negative potential was applied on the electrode, the Rh(III) at the electrode surface will be reduced to Rh(I) , then it will receive a proton from the buffer solution to form protonated Rh(I), the protonated Rh(I) species were not able to be re-oxidized by electron transfer reactions from the electrode, but can be re-oxidized by transferring a hydride ion to NAD^+ to regenerate NADH [3,197], so the catalytic response of CF-CNT-Bpy-Rh electrode was tested by addition of NAD^+ into the solution. **Figure 5.5A** showes the catalytic response of CF-CNT-Bpy-Rh electrode to gradual addition of NAD^+. Before adding NAD^+, a cathodic peak was observed around -0.71 V, this value was similar to the previously reported value (-0.7 V) for CF-CNT-4'4-Bpy-Rh electrode fabricated by CuAAC click reaction in Chapter 3. The cathodic peak current increased with successive addition of NAD^+, the peak current stopped increasing when the NAD^+

concentration reached 3 mM. Meanwhile, the cathodic peak was also gradually shifted to negative potential, which was related to the limitation of the heterogeneous electron transfer kinetics [142]. If we compared the catalytic current at saturated concentration of NAD^+ between CF-CNT-Bpy-Rh and the CF-CNT-4‟4-Bpy-Rh electrode made via „click reaction‟ in the same buffer solution, the catalytic current was 292 µA versus137 µA, the electrode made in this work showed a significant increasing up to 210%. Moreover, the catalytic cathodic peak of CF-CNT-Bpy-Rh was better defined than that of CF-CNT-4‟4-Bpy-Rh demonstrating faster electron transfer rate [138].

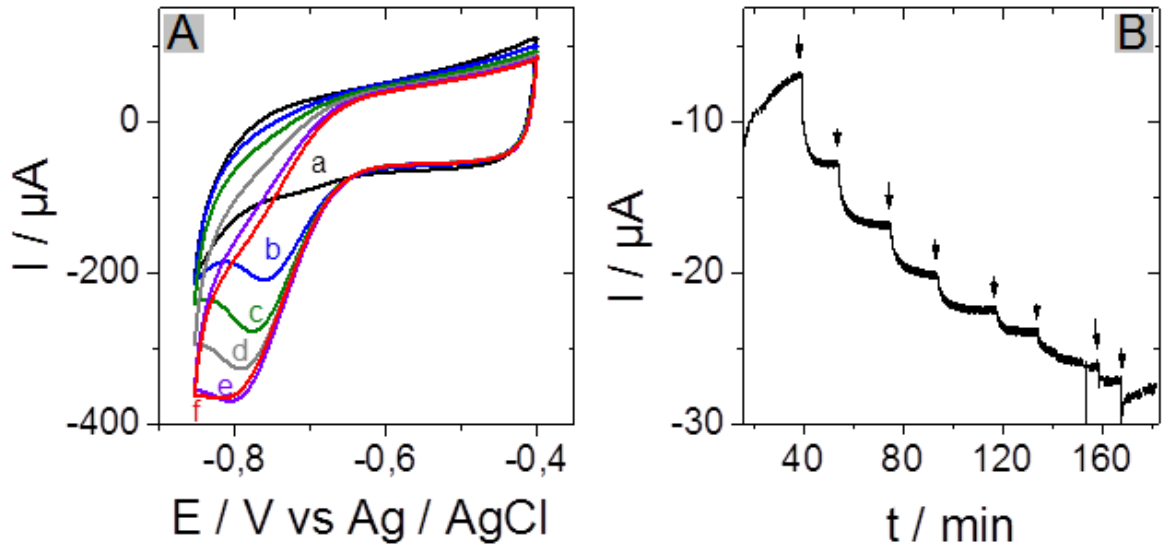

Figure 5.5. *(A) Cyclic voltammograms recorded at a potential scan rate of 5 mV s^{-1} using a $[Cp^*Rh(bpy)Cl]^+$ functionalized CF-CNT electrode in 50mM PBS buffer at pH 6.5 to gradual addition of NAD^+ (a) 0 mM (b) 0.5 mM (c) 1 mM (d) 1.5 mM (e) 2 mM (f) 3 mM. (B) Amperometric response to gradual addition of 0.5 mM NAD^+ recorded using CF-CNT-Bpy-Rh -gel electrode (0.5 *0.5cm^2) in 10 mL 50 mM PBS (pH 6.5) at an applied potential of -0.78 V. Both experiments are carried out under nitrogen.*

As the amino-group on bipyridine has been reported to suppressed catalytic reduction of NAD^+ [142], here the observation of catalytic response was a further evidence of covalent bonding of bipyridyl ligand, because the amino group on bipyridine was removed upon covalently grafting on the electrode.

Since the rhodium functionalized CF-CNT electrode showed a good catalytic response towards NADH regeneration, a long-term NAD^+ transformation experiment was carried out. To be comparable with the NADH regeneration experiment with CF-CNT-4‟4-Bpy-Rh-gel electrode, a similar silica gel layer was deposited on the top of the electrode (CF-CNT-Bpy-Rh -gel), a chronoamperometry experiment with applied potential of -0.78 V was performed on the CF-CNT-Bpy-Rh-gel electrode. As shown in **figure 5.5B**, the catalytic current was increasing by gradual addition of 0.5 mM NAD^+, saturation was reached at a concentration of 4 mM. After 18 h continuous electrochemical operation, 0.412 mM NADH was detected by checking the final solution with UV spectroscopy at absorbance of 340 nm. Since the experiment was carried out in PBS buffer at room temperature, the buffer type and temperature was influencing the stability of NADH [203], the degraded NADH was not UV active, the concentration of NADH really formed should be more than measured. By estimating the concentration of NADH from the charge involved in the electrocatalytic process, a faradic efficiency of at least 74% was obtained. Compared to CF-CNT-4‟4-Bpy-Rh-gel electrode, faradic efficiency was slightly lower, but the NADH formation rate was greater.

5.3.2 Immobilization of rhodium complex on ‘bucky paper’ electrode by bipyridyl diazonium electrografting

To covalently immobilize rhodium complex on bucky paper (BP) electrode, the same protocol previously used for the modification of CF-CNT was applied on the BP electrode. **Figure 5.6A** was the diazonium electrografting by cyclic voltammetry in a potential range from 0.4 V to -0.8 V for BP electrode in 1 mM bipyridyl diazonium salt solution (BP-Bpy). During the first scan, an irreversible peak located around -0.3 V was observed (**curve a**). The reductive peak potential of electrografting process on BP electrode was less negative than that on CF-CNT, the difference in potential was attributted to the different property of carbon materials. Meanwhile, similar to that of CF-CNT, the tendency of decrease in cathodic reduction current when carrying out the second scan (**curve b**) indicated the successful grafting of bipyridyl groups and partial blocking on the surface. The modified BP electrode (BP-Bpy) has been analyzed by XPS after electrografting of the diazonium cation generated in situ from the amino-bipyridine. The N1s high resolution spectrum obtained after modification shows a main component located at 398.8 eV attributed to the presence of bipyridine functions immobilized on the electrode surface (**Figure 5.7A**).

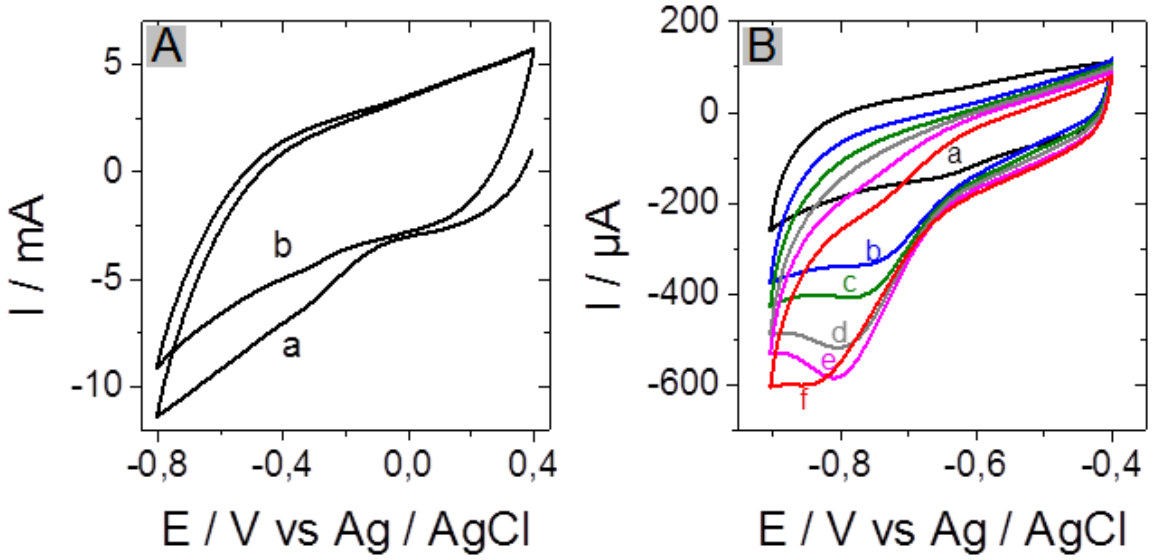

Figure 5.6. (A) *Cyclic voltammograms for the reduction of diazonium cations generated 'in situ' from 1mM 4-amino-2, 2'-bipyridine in 0.5 M HCl, as recorded on BP electrode at 100 mV* s^{-1}. ***(B)*** *Cyclic voltammograms recorded at a potential scan rate of 5 mV* s^{-1} *using a* $[Cp^*Rh(bpy)Cl]^+$ *functionalized bucky paper electrode in 50 mM PBS buffer at pH 6.5 under nitrogen to gradual addition of* NAD^+ *(a) 0 mM (b) 0.5 mM (c) 1 mM (d) 1.5 mM (e) 2 mM (f) 3 mM. The geometric surface area of the electrode was 1* cm^2.

After complexation with $((RhCp^*Cl_2)_2$ using the same experimental condition previously described, rhodium complex functionalized „bucky paper" electrode (BP-Bpy-Rh) was obtained. The Rh is observed at 312 eV in the XPS survey spectrum of the BP-Bpy-Rh recorded after complexation in addition to the C1s (285 eV), O1s (532 eV) and N1s (400 eV) peaks. The main envelope of the Rh 3d core level spectrum (**Figure 5.7C**) has been curve-fitted with Rh $3d_{5/2}$ and $Rh3d_{3/2}$ peaks centered at 308.1 and 312.6 eV respectively associated to the presence of Rh^+. Changes have been also observed for the N1s core level spectrum with the main component slightly shifted up to 400.5 eV as a result of the complexation with Rh (**Figure 5.7B).**

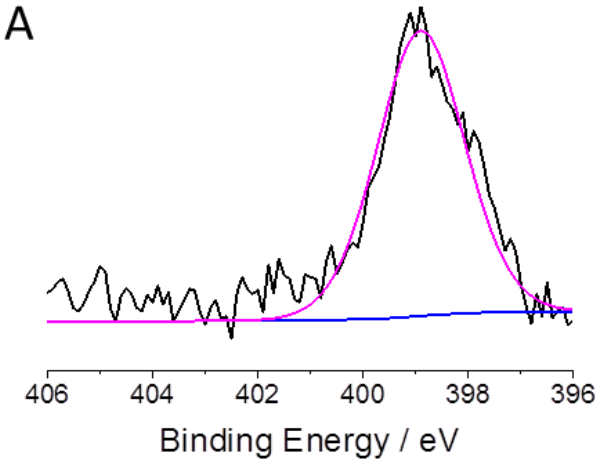
A
406
404
402
400
398
396
Binding Energy / eV

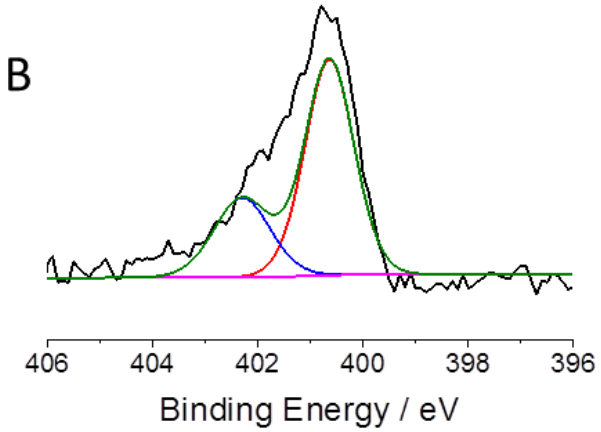
B
406
404
402
400
398
396
Binding Energy / eV

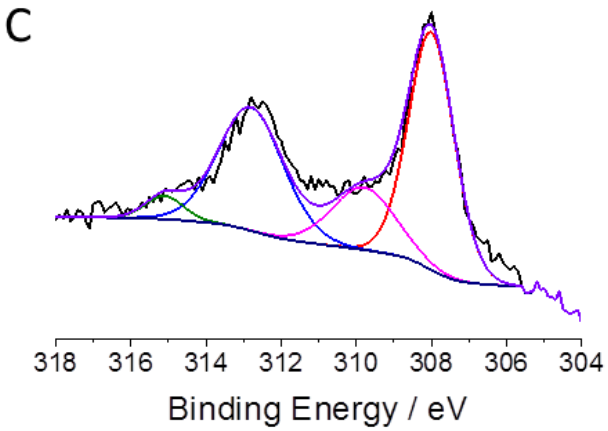
C
318
316
314
312
310
308
306
304
Binding Energy / eV

Figure 5.7 *N1s core level spectrum for (A) BP-Bpy electrode and (B) BP-Bpy-Rh. (C) Rh 3d core level spectrum for the BP-Bpy-Rh.*

The catalytic response of BP-Bpy-Rh electrode for NADH regeneration was evaluated by cyclic voltammetry (**Figure 5.6B**). Without the presence of NAD^+, the cathodic peak was observed around -0.65 V, which was positively shifted compared to the CF-CNT-4‟4-Bpy-Rh electrode. The potential shift can be ascribed to the influence of different electrode on electron density of the rhodium complex center [197]. To gradual addition of NAD^+, we observed the typical catalytic response of Rh complex with increasing cathodic current and negatively shifted cathodic peak as reported in the literature [142]. The catalytic current saturation was also observed at the concentration of 3 mM. After comfirming the catalytic response of the thin BP-Bpy-Rh electrode, its application in elctroenzymatic synthesis was further explored.

5.3.3 The combination of BP-Bpy-Rh electrode with enzymes

5.3.3.1 Co-immobilization with enzymes gel on the top

The electroenzymatic catalytic response was first tested with a co-immobilized BP-Rh-DSDH-gel electrode with both enzymes and rhodium complexes prepared by directly depositing the D-sorbitol dehydrogenase (DSDH) gel on the top of the BP-Bpy-Rh electrode. In this bioelectrochemical system, D-fructose was reduced to D-sorbitol by DSDH in the presence of NADH, in the same time, the NAD^+ formed through this enzymatic reaction could be reduced back to NADH by the rhodium complex at the electrode surface. The regenerated NADH could be recycled in this electro-synthetic system to keep constant catalytic activity. The bioelectrocatalytic amperometric response of BP-Bpy-Rh-DSDH-gel electrode was demonstrated by gradually adding 1 mM of D-fructose substrate into 50 mM PBS buffer contains 0.5 mM NADH as cofactor. All the experiments were performed in the absence of oxygen.

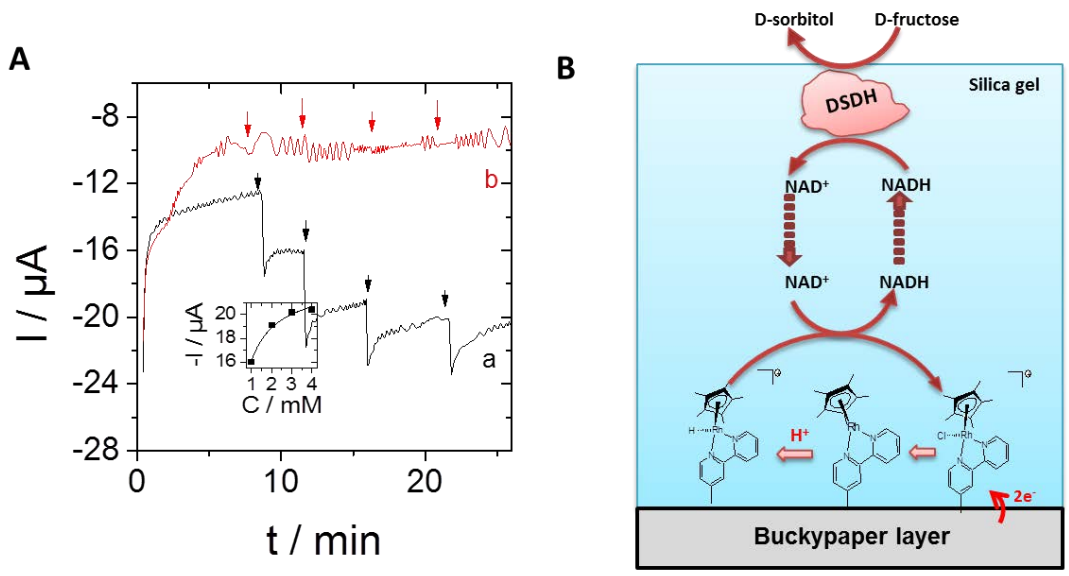

Figure 5.8. *(A) Amperometric response to gradual addition 1mM D-fructose recorded using (a) BP-Bpy-Rh-DSDH gel electrode and (b) Bucky-Rh-gel electrode in 50 mM PBS (pH 6.5) with the presence of 0.5 mM NADH at an applied potential of -0.72 V. (B) Schematic representation of the electroenzymatic synthetic process for BP-Bpy-Rh-DSDH gel electrode. The geometric surface area of the electrode was 1 cm^2.*

As shown in **Figure 5.8** (curve a), the increase of catalytic current followed the Michaelis–Menten kinetics, an apparent Km was estimated to be 0.4 mM, much less than the Km obtained from free DSDH in the solution (Km is 49.4 mM [204]). As the BP electrode has a thin layer configuration, we observed faster response to the addition of substrate on BP-Bpy-Rh compared to that on CF-CNT-Bpy-Rh electrode, as a result of easier mass transport of cofactors between enzymes and rhodium complex. A control experiment without the presence of DSDH in the gel was also carried out, as shown in **Figure 5.8** (curve b), no increase of catalytic current to addition of D-fructose was observed.

5.3.3.2 Co-immobilization with replaceable enzyme layer

To achieve the final target in preparation of enzymes and rhodium complex in two different layers, a separate DSDH gel layer (tailored into the same size with BP-Bpy-Rh electrode was overlaid on the top of BP-Bpy-Rh electrode, the 4 corners of the double layer were simply fixed by cotton thread. The electrode configuration was shown in **figure 5.2,** DSDH was encapsulated inside a 260 μm thick gel layer, and the rhodium complexes were immobilized at the interface of porous buckypaper layer, the combination of enzymatic

reaction convert D-fructose to D-sorbitol and electrochemical cofactor regeneration process was realized by transferring of cofactors through the two layers. The bioelectrocatalytic amperometric response of this double layer electrode was tested in PBS buffer with the presence of 1 mM NADH by applying a potential at -0.72 V. As shown in **figure 5.9,** the catalytic current to addition of D- fructose substrate was kept at the same level with the BP-Rh-DSDH-gel electrode, an apparent Km of 0.25 mM was obtained. This pointed out that the bioelectrode with separated layer was still efficient for NADH regeneration in combination with enzymatic reactions. The reusability of BP-Bpy-Rh electrode was then investigated.

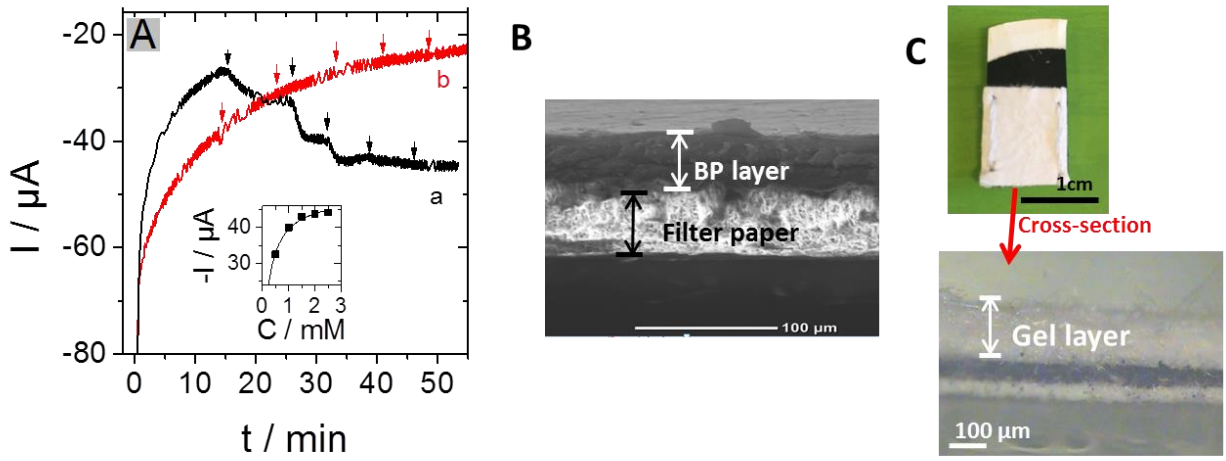

Figure 5.9. *(A) Amperometric response to gradual addition of 0.5 mM D-fructose recorded using a combined electrode (1 cm * 1 cm) of (a) separate BP-Bpy-Rh and DSDH gel layer (b) separate BP-Bpy-Rh and blank gel layer in 50 mM PBS (pH 6.5) with the presence of 1 mM NADH at an applied potential of -0.72 V under nitrogen.(B) SEM picture for the cross-section of the buckypaper layer on filter paper electrode.(C) Optical image illustrating the assembly of the packing electrode, as well as its cross-section under optical microscopy.*

After each experiment, the DSDH layer could be easily removed from BP-Bpy-Rh electrode by cutting the threads, and a new active enzyme layer could be then packed on BP-Bpy-Rh to continue the bioconversion. The reusability of one BP-Bpy-Rh electrode was proved by checking the amperometric response to 3 mM D-fructose with three different DSDH gel layers, each experiment lasted 30 min. The catalytic current of the three enzyme layers stabilized at current of 37 ± 1 µA for the same BP-Bpy-Rh electrode, showing good repeatability and stability (**Figure 5.10**).

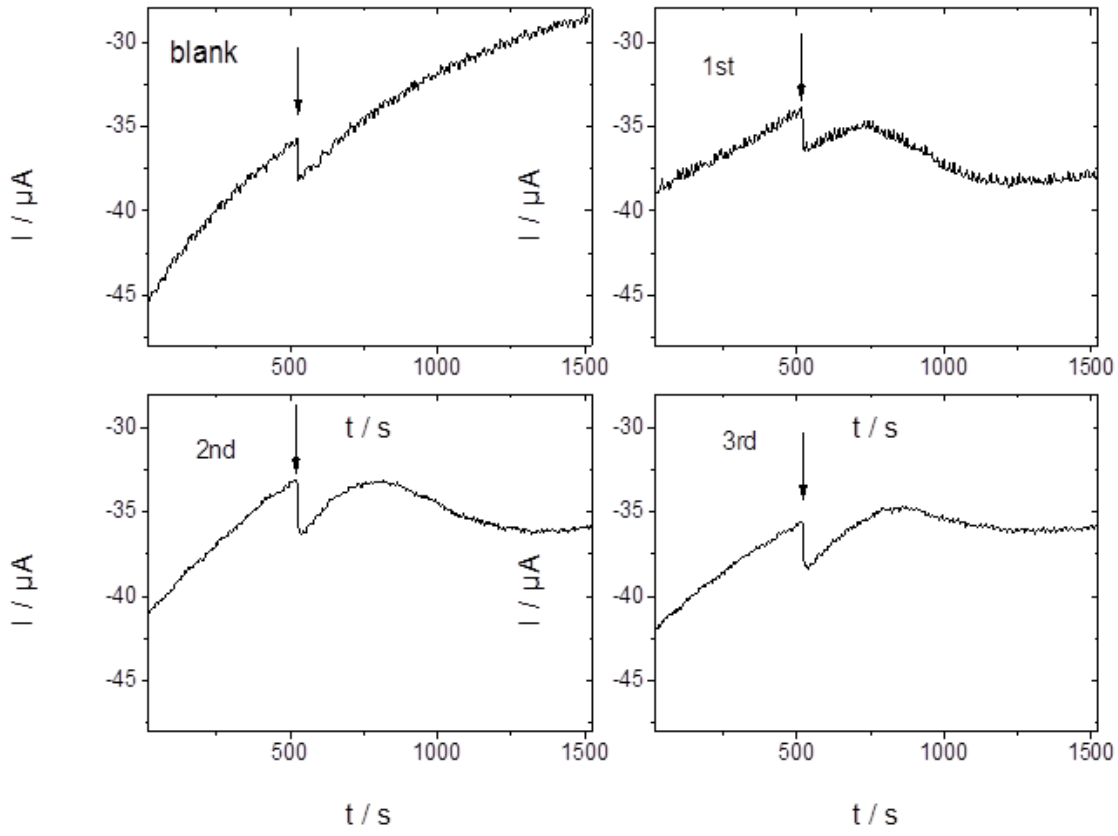

Figure 5.10. *Amperometric responses to gradual addition of 3 mM D-fructose recorded using A BP-Bpy-Rh electrode (1 cm * 1 cm) packing with (A) gel layer without enzyme; (B) 1st DSDH layer; (C) 2nd DSDH layer; (D) 3rd DSDH layer at an applied potential of -0.72 V under nitrogen.*

The electrode was finally applied for bioconversion from D-fructose to D-sorbitol in combination with NAD-dependant DSDH (**Figure 5.11**). A larger piece (2 cm* 2 cm) of BP-Bpy-Rh layer and DSDH gel layer were packed in a batch reactor containing 1 mM NADH in 30 mL 50 mM PBS buffer (pH 6.5). After adding 90 µmol D-fructose (correspond to 3 mM in concentration), a potential of -0.72 V was applied over 95 h**,** the catalytic current is decreasing corresponding to the transformation of D-fructose to D-sorbitol (**Figure 5.11A)**. The molar mass evolution for substrate and product during the bioconversion was shown in **Figure 5.11B,** after 95 h, 87% of D-fructose was transformed to D-sorbitol, a high faradic effciency of 83% was obtained. The amount of rhodium complex on BP electrode was roughly estimated (6.5×10^{-9} mol) from cylic voltammogram by integrating the cathodic peak. A TTN up to 12500 was obtained for rhodium complex, which was the highest value obtained with

rhodium complex applied in electroenzymatic synthesis. This electrode is thus promising to be applied in large scale bioconversion experiment by simply increasing the size of the bioelectrode.

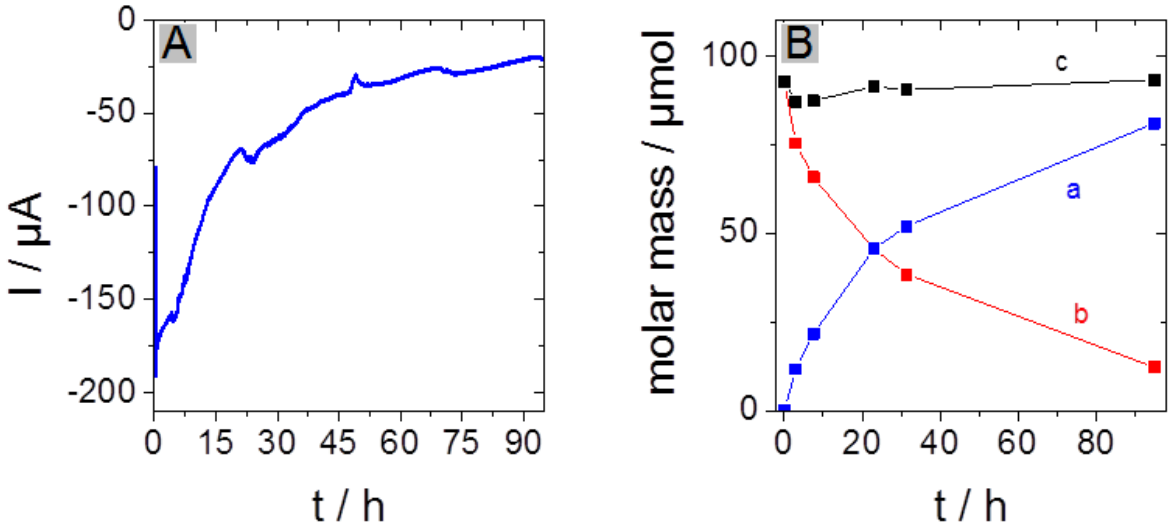

Figure 5.11. *(A) Amperometric response of bioconversion of 3 mM D-fructose to D-sorbitol in 30 mL 50 mM PBS (pH 6.5) contains 1 mM NADH using a combined electrode of separate BP-Rh and DSDH gel layer (2 cm* 2 cm) at −0.72 V under nitrogen. (B) Evolution with time of (a) D-fructose, (b) D-sorbitol, and (c) the sum of D-fructose and D-sorbitol number of mole, determined by HPLC.*

5.4 Conclusions

$[Cp^*Rh(bpy)Cl]^+$ was covalently immobilized onto carbon electrode surfaces (CF-CNT or BP electrode) via diazonium coupling and complexation processes. The immobilized $[Cp^*Rh(bpy)Cl]^+$ showed good catalytic activity towards NADH regeneration. The reusability of the $[Cp^*Rh(bpy)Cl]^+$ functionalized BP electrode was demonstrated by packing replaceable layers who contain DSDH gel on the top, comparable catalytic response was observed. Finally, the double layered electrode was applied in bioconversion of D-fructose to D-sorbitol in the presence of cofactor NADH, a high conversion rate of 87% and faradic effciency of 83% was obtaind after 95 h, showing promising prospect in electroenzymatic production of valuable products with other NAD-dependent redox enzymes.

Conclusions and perspectives

In this thesis, different chemical routes have been employed to immobilize enzymes and rhodium complex catalyst in order to apply them to enzymatic electrosynthesis. Experiments have been performed with D-sorbitol dehydrogenase (DSDH) catalyzing the reduction of D-fructose to D-sorbitol. Some experiments were also done with galactitol dehydrogenase (GatDH) having a wider range of substrate.

The electrode functionalization was mainly performed via electrochemical reduction based on the generation of highly reactive aryl radical species from diazonium salts. A variety of functional groups have been grafted depending on the final usage. 4-vinylaniline was used to obtain a vinly functionalized surface, 4-azidoaniline was used to obtain an azido functionalized surface, and 4-amino-2,2"-bipyridine was used to obtain bipyridyl functionalized surface. In addition, the simultaneous introduction of two functions at the electrode surface was achieved by electrochemical reduction of mixtures of diazonium salts to create selectively mixed monolayers with a controlled chemical composition. These functional groups offered the possibility for further reactions steps including „dick" chemistry or metal-ligand complexation. In all above cases, the coverage of the organic layer on the electrode was controlled, in order to allow electron transfer reactions.

„Click" chemistry was applied in covalent immobilization of proteins or catalysts due to their simple and mild experimental reaction conditions. There were two types of „dick" reactions employed to these works. „Thiol-ene" click chemistry was applied to the immobilization of dehydrogenase-based proteins on carbon electrode surfaces, the thiol group from cysteine residue of enzymes was reacting with the vinyl groups on the electrode. In this way, the activity of DSDH was kept when click coupling was made on proteins bearing a cysteine tag. This method was also applied to the immobilization of GatDH. Copper (I)-catalyzed azide-alkyne cycloaddition reaction (Huisgen coupling) was then used to immobilize covalently (2,2'-bipyridyl)(pentamethylcyclopentadienyl)-rhodium as catalyst on carbon electrode surface, a better long-term stability for NADH regeneration was achieved by using this covalent bond compared to the molecule only adsorbed. The combination of the two click types was finally evaluated. The co-functionalization involved electrochemical reduction of diazonium cations and a double consecutive click reactions process, after

diazonium electrografting process, the co-functionalized electrodes allow selective incorporation of rhodium complex and DSDH, via two „click" immobilization steps. Co-immobilization was also achieved by combining click chemistry and sol-gel immobilization of molecules.

Several problems were met when fabricating the bioelectrode for electroenzymatic synthesis. Firstly, the enzymes were inhibited during long-term experiments, but the activity was recovered after replacing the used solution by a fresh buffer. We assumed that this inhibition may due to the change of local environment eg. increase of local pH at the electrode interface or product accumulation. Secondly, a slow degradation of rhodium complex was also observed when depositing silica gel containing enzyme directly on the top of the rhodium complex functionalized electrode. Since no degradation was observed in the same condition in the absence of enzyme, we can conclude that the slow degradation originated from possible interaction between enzyme and rhodium complex after long-term experimental operation.

In order to fulfill the demand for long-term stability, the enzyme and the rhodium complex had to be better separated while still keeping close distance for NADH regeneration. This was achieved by using a bioelectrode consisting of two separated layers. A rhodium complex functionalized „buckypaper" layer on one side and a glassy fiber layer with gel immobilized DSDH on the other side. The bioelectrode was obtained by assembling these two materials. The enzyme gel glassy fiber layer could be easily replaced when losing their activity. Good reusability with three different enzyme layers and stable electrocatalytic response were observed with a rhodium complex functionalized electrode. Not only the degradation of rhodium complex was avoided benefiting from the complete separation, but also the enzymatic inhibition effect observed previousely was avoided. This co-immobilized bioelectrode must simplify the purification steps and show promising prospect in electroenzymatic production of chiral valuable products with NAD-dependent redox enzymes. Actually this system could be applied to regeneration of NADPH for other enzymes such as P450 cytochrome.

If considering larger size of bioelectrodes that could be applied in large-scale electroenzymatic synthesis, the proton consumption at the electrode interface has to be considered. We assume that the local pH control will be a key parameter. For long-terms operation with layer structured flow-cell system, the pH of buffer solution may increase due to the proton consumption. Since in some tests, we observed that the elecrocatalytic response

was not observed in high buffer concentration (0.5 M), the proton supplement cannot be provided simply by increasing the concentration of buffer. The production of protons from water oxidation at the counter electrode would also produce O_2 in the solution which should be avoided. A solution to keep constant pH would be the combination of the bioelectrode with a gas diffusion electrode to continuously produce H^+ from H_2 without production of O_2.

In a more general thinking, when we started these PhD studies, the rhodium complex was, and is still, the most efficient non-enzymatic NADH regeneration catalyst. However the metal is rather rare, expensive and toxic. Direct electron transfer with flavoenzymes allowing NADH regeneration is certainly one topic to be further investigated in the coming years for electroenzymatic synthesis. Developing stable and recyclable bioelectrodes leading to long-term enzymatic activity and direct electron transfer reactions, would allow significant steps forward for major industrial developments with lower environmental impact.

Finally, another direction to improve the electrochemical regeneration in this electroenzymatic synthesis would be the application of NAD analogs, which would avoid the limited stability of the original biomolecule [270] that could eventually be immobilized on the electrode surface as suggested before [202] with the goal to build optimal and stable electronic pathway usable in bioelectrochemical conversions.

Conclusion générale et perspectives

Dans cette thèse, différentes voies chimiques ont été employées pour immobiliser ensemble des enzymes et un complexe de rhodium afin de les appliquer en électrosynthèse enzymatique. Les expériences ont été menées avec la D-sorbitol déshydrogénase (DSDH) catalysant la réduction du D-fructose en D-sorbitol. Certaines expériences ont également été menées avec la galactitol déshydrogénase (GatDH) ayant un spectre de substrat plus large.

La fonctionnalisation des électrodes a principalement été faîte par génération électrochimique de radicaux aryle hautement réactifs à partir de sels de diazonium. Une grande variété de groupes fonctionnels a été utilisée pour différents usages. La 4-vinylaniline a été utilisée pour obtenir une surface fonctionnalisée par des groupements vinyles. La 4-azidoaniline a été utilisée pour obtenir une surface fonctionnalisée par des groupements azoture. Enfin, la 4-amino-2,2‟-bipyridine a été utilisée pour préparer une surface fonctionnalisée par des groupements pyridine. Finalement, l‟introduction simultanée de deux groupements fonctionnels a été obtenue par électrogreffage d‟un mélange de sels de diazonium. Ces groupements fonctionnels ont ensuite été utilisés pour des réactions de chimie click ou de complexation métal-ligand. Dans tous les cas, le dépôt organique a été optimisé afin d‟autoriser des réactions de transfert d‟électron avec des espèces en solution ou greffées en surface.

La chimie “click” a été appliquée à l‟immobilisation covalente de protéines ou de catalyseurs en raison des conditions simples et douces qu‟elle permet. Deux types de chimie click ont été utilisés dans ce travail. Le couplage « thiol-ène » a été appliqué à l‟immobilisation de déshydrogénases à la surface d‟électrodes de carbone. Dans ce cas, le groupement thiol de résidus cystéine pouvait réagir avec le groupe vinyle greffé à la surface de l‟électrode. De cette manière, l‟activité de la DSDH était conservée plus longtemps à la surface de l‟électrode lorsque le couplage était fait avec des protéines portant un tag cystéine. La réaction de cyclo-addition azoture-alcène catalysée par le cuivre(I) (couplage de Huisgen) a ensuite été utilisée pour immobiliser de manière covalente le complexe (2,2'-bipyridyl)(pentamethylcyclopentadienyl)-rhodium à la surface d‟électrodes carbonées. Une meilleure stabilité pour la régénération de NADH a été observée avec le complexe immobilisée qu‟avec ce complexe simplement adsorbé à la surface de l‟électrode. La combinaison de ces deux chimies click a ensuite été étudiée. La co-fonctionnalisation

impliquait la réduction électrochimique de cations diazonium et deux réactions de chimie click consécutives permettant l'incorporation sélective du complexe de rhodium et de la DSDH. La co-fonctionnalisation a également obtenue par combinaison d'une première étape de couplage par chimie click pour l'immobilisation du complexe de rhodium et une seconde étape d'encapsulation des protéines dans une matrice de silice par voie sol-gel.

Plusieurs problèmes ont été rencontrés lorsque nous avons testés ces électrodes en électrosynthèse enzymatique. Tout d'abord, une inhibition de l'activité enzymatique a été observée au cours de l'expérience, mais cette activité était retrouvée lorsque la solution était remplacée par une solution fraîche. Nous supposons que cette inhibition pouvait être causée un environnement local dans l'électrode poreuse, par exemple une augmentation de pH ou une accumulation du produit de la réaction enzymatique. Ensuite, la dégradation lente de l'activité du complexe de rhodium a été observée lorsque le gel de silice contenant les enzymes était déposé au contact de l'électrode fonctionnalisée par le complexe de rhodium. Cette dégradation n'a pas été observée en absence d'enzymes et serait causée par l'interaction entre les enzymes et les complexes de rhodium après des temps de réactions longs qui favorise une dissolution partielle de la silice.

Afin d'améliorer la stabilité de la bioélectrode dans le temps, les enzymes et les complexes métalliques doivent être mieux séparés tout en conservant une faible distance pour permettre la régénération de NADH. Ceci a été obtenu en combinant deux couches séparées, une première sur laquelle était greffée le complexe de rhodium et une seconde sur la quelle était immobilisée l'enzyme. La bioélectrode était alors obtenue par l'assemblage de ces deux matériaux. Le matériau (un filtre en fibres de verre) permettant l'immobilisation de l'enzyme pouvait être facilement remplacée. Ainsi, il fut possible de réutiliser le complexe de rhodium avec trois couches enzymatiques différentes. De plus, la dégradation du complexe de rhodium n'a pas été observée. Enfin, cette configuration de bioélectrode a permis de supprimer l'inhibition enzymatique observée précédemment. Cette voie de co-immobilisation devrait donc simplifier la purification des produits de synthèse et pourrait conduire à de nouvelles applications en électrosynthèse enzymatique. Par exemple, ce système pourrait être appliqué à la régénération du cofacteur NADPH pour d'autres enzymes redox comme les cytochromes P450.

Si nous considérons l'utilisation d'électrodes de grande taille dans des dispositifs d'électrosynthèse en continu, la consommation des protons à l'électrode de travail risque

d'être un paramètre limitant de la réaction. Nous supposons que le pH local à proximité de l'enzyme est un paramètre essentiel permettant de favoriser la plus grande activité enzymatique. Ces protons pourraient être apportés par l'oxydation de l'eau, mais cette réaction conduit également à la production d'oxygène, qui devrait être évité pour conserver une bonne efficacité pour la réaction de régénération de NADH. Une solution technologique pourrait être l'utilisation d'une électrode à diffusion de gaz pour produire en continu des protons à partir de l'oxydation de H_2, sans production d'O^2.

D'un point de vue plus général, lorsque cette thèse a commencé, le complexe de rhodium que nous avons de rhodium que nous avons immobilisé était, et est encore, le catalyseur le plus efficace pour la régénération non-enzymatique de NADH. Cependant ce métal est relativement rare, cher et toxique. Les réactions de transfert d'électron directes avec une flavoenzyme permettant la régénération de NADH est certainement un sujet à explorer encore dans les années à venir pour application en électrosynthèse enzymatique. Le développement de bioélectrodes stables et recyclables permettant de conserver l'activité enzymatique sur des temps longs tout en autorisant des réactions de transfert d'électron serait un grand pas vers un développement industriel ayant un impact environnemental limité.

Finalement, une autre direction de recherche pour améliorer la régénération électrochimique dans cette réaction d'électrosynthèse serait l'étude des analogues de NAD qui permettent de dépasser les limites en stabilité de la molécule naturelle [270] qui pourrait alors être immobilisée à la surface de l'électrode comme cela a été suggéré auparavant [202] pour construire un chemin de transfert électronique optimal et stable utilisable en dans des réactions de conversion bioélectrochimique.

References

[1] K. Drauz, H. Waldmann, eds., *Enzyme Catalysis in Organic Synthesis: A Comprehensive Handbook, Second Edition*, Wiley-VCH, Veinheim, **2002**.

[2] P. Kornberger, F. Giffhorn, G.-W. Kohring, *Encycl. Ind. Biotechnol.* **2009**, 1.

[3] E. Steckhan, *Top. Curr. Chem.* **1994**, 170, 83.

[4] C. Kohlmann, W. Märkle, S. Lütz, *J. Mol. Catal. B: Enzym.* **2008**, 51, 57.

[5] L. Gorton, E. Dominguez, *Encycl. Electrochem.* **2002**, 9, 67.

[6] M. Poizat, I.W.C.E. Arends, F. Hollmann, *J. Mol. Catal. B: Enzym.* **2010**, 63, 149.

[7] F. Hildebrand, S. Lütz, *Chem. Eur. J.* **2009**, 15, 4998.

[8] L. Cao, in *Carrier-bound Immobilized Enzymes*, Wiley-VCH Verlag GmbH & Co. KGaA, Weinheim, **2006**, pp. 169–316.

[9] J. Madoz-gurpide, J.M. Abad, J. Fernandez-Recio, M. Velez, *J. Am. Chem. Soc.* **2000**, 122, 9808.

[10] C. Ley, D. Holtmann, K.-M. Mangold, J. Schrader, *Colloids Surf. B* **2011**, 88, 539.

[11] J. Hodac, L. Raehm, J.D. Michel, W. Chi, *J. Sol-Gel Sci. Technol.* **2014**, 70, 245.

[12] P.M.G. Finn, V. Fokin, *Chem.Soc.Rev.* **2010**, 39, 1355.

[13] C.E. Hoyle, T.A.I.Y. Lee, T. Roper, *J. Polym. Sci. Part A Polym. Chem.* **2004**, 42, 5301.

[14] A. Schmid, J.S. Dordick, B. Hauer, A. Kiener, M. Wubbolts, B. Witholt, *Nature* **2001**, 409, 258.

[15] V. Uppada, S. Bhaduri, S.B. Noronha, *Curr. Sci.* **2014**, 106, 946.

[16] T.R. Besanger, J.D. Brennan, *J. Sol-Gel Sci. Technol.* **2006**, 40, 209.

[17] F. Hollmann, I.W.C.E. Arends, K. Buehler, *ChemCatChem* **2010**, 2, 762.

[18] R. Wichmann, D. Vasic-Racki, *Adv Biochem Engin/Biotechnol* **2005**, 92, 225.

[19] W. Andrea, G. Harald, H. Werner, *Adv Biochem Eng Biotechnol.* **2010**, 120, 195.

[20] V. Urbanova, G.-W. Kohring, T. Klein, Z. Wang, O. Mert, M. Emrullahoglu, K. Buran, A.S. Demir, M. Etienne, A. Walcarius, *Z. Phys. Chem.* **2013**, 227, 667.

[21] H. Wu, C. Tian, X. Song, C. Liu, D. Yang, Z. Jiang, *Green Chem.* **2013**, 15, 1773.

[22] U. Hanefeld, L. Gardossi, E. Magner, *Chem. Soc. Rev.* **2009**, 38, 453.

[23] Xochitl, S. Srikanth, Y. Satyawali, K. Vanbroekhoven, D. Pant, *J Microb. Biochem Technol* **2013**, S6, 007.

[24] L. Gorton, P.N. Bartlett, in *Bioelectrochemistry*, P.N. Bartlett (Ed.), John Wiley & Sons, Ltd, Chichester, **2008**, pp. 157–198.

[25] M. Rasmussen, S. Abdellaoui, S.D. Minteer, *Biosens. Bioelectron.* **2016**, 76, 91.

[26] P.J. Elving, C.O. Schmakel, K.S. V Santhanam, P. Zuman, *C R C Crit. Rev. Anal. Chem.* **1976**, 6, 1.

[27] B.E. Steckhan, S. Herrmann, R. Ruppert, *Angew. Chem. Int. Ed.* **1990**, 29, 388.

[28] R. Wienkamp, E. Steckhan, *Angew. Chem. Int. Ed.* **1982**, 21, 782.

[29] M. Beley, J.-P. Collin, *J. Mol. Catal.* **1993**, 79, 133.

[30] K. Délécouls-Servat, R. Basséguy, A. Bergel, *Chem. Eng. Sci.* **2002**, 57, 4633.

[31] K. Délécouls-Servat, R. Basséguy, A. Bergel, *Bioelectrochemistry* **2002**, 55, 93.

[32] E. Steckhan, *Top. Curr. Chem.* **1994**, 170, 83.

[33] F. Hildebrand, S. Lu, *Tetrahedron: Asymmetry* **2007**, 18, 1187.

[34] B. Tan, D.P. Hickey, R.D. Milton, F. Giroud, S.D. Minteer, *J. Electrochem. Soc.* **2015**, 162, H102.

[35] J.S. Lee, S.H. Lee, J. Kim, C.B. Park, *J. Mater. Chem. A* **2013**, 1, 1040.

[36] A.A. Karyakin, O.A. Bobrova, E.E. Karyakina, *J. Electroanal. Chem.* **1995**, 399, 179.

[37] Y. Kashiwagi, Y. Yanagisawa, N. Shibayama, K. Nakahara, F. Kurashima, J. Anzai, T. Osa, *Electrochim. Acta* **1997**, 42, 2267.

[38] Y.W. Kang, C. Kang, J.S. Hong, S.E. Yun, *Biotechnol. Lett.* **2001**, 23, 599.

[39] M.H. Kim, S.E. Yun, *Biotechnol. Lett.* **2004**, 26, 21.

[40] R. DiCosimo, C.-H. Wong, L. Daniels, G.M. Whitesides, *J. Org. Chem.* **1981**, 46, 4622.

[41] R. Yuan, S. Watanabe, S. Kuwabata, H. Yoneyama, *J. Org. Chem.* **1997**, 3263, 2494.

[42] M. Schulz, H. Leichmann, H. Günther, H. Simon, *Appl. Microbiol. Biotechnol.* **1995**, 42, 916.

[43] A. Bergel, M. Comtat, *J. Electroanal. Chem.* **1991**, 302, 219.

[44] T. Tzedakis, K. Cheikhou, R. Jerome, G.S. Karine, R. Olivier, *Electrochim. Acta* **2010**, 55, 2286.

[45] Y. Ogino, K. Takagi, K. Kano, T. Ikeda, *J. Electroanal. Chem.* **1995**, 396, 517.

[46] P. Gros, C. Zaborosch, H.G. Schlegel, A. Bergel, *J. Electroanal. Chem.* **1996**, 405, 189.

[47] K. Délécouls, P. Saint-Aguet, C. Zaborosch, a. Bergel, *J. Electroanal. Chem.* **1999**, 468, 139.

[48] J. Cantet, A. Bergel, M. Comtat, *J. Mol. Catal.* **1992**, 73, 371.

[49] J. Cantet, A. Bergel, M. Comtat, *J. Electroanal. Chem.* **1992**, 342, 475.

[50] J. Cantet, A. Bergel, M. Comtat, *Enzyme Microb. Technol.* **1996**, 18, 72.

[51] H.A. Reeve, L. Lauterbach, P.A. Ash, O. Lenz, K.A. Vincent, *Chem. Commun.* **2012**, 48, 1589.

[52] H.A. Reeve, L. Lauterbach, O. Lenz, K.A. Vincent, *ChemCatChem* **2015**, 7, 3480.

[53] S. Shipovskov, A. Bonamore, A. Boffi, E.E. Ferapontova, *Chem. Commun.* **2015**, 51, 16096.

[54] M.T. Grimes, D.G. Drueckhammer, *J. Org. Chem.* **1993**, 58, 6148.

[55] S.B. Sobolov, M.D. Leonida, A. Bartoszko-Malik, K.I. Voivodov, F. McKinney, J. Kim, A.J. Fry, *J. Org. Chem.* **1996**, 61, 2125.

[56] M.E. Zawalich, R.J. Fisher, in *Bioengineering Conference, 1998. Proceedings of the IEEE 24th Annual Northeast*, **1998**, pp. 85–87.

[57] M.D. Leonida, S.B. Sobolov, A.J. Fry, *Bioorganic Med. Chem. Lett.* **1998**, 8, 2819.

[58] A.J. Fry, S.B. Sobolov, M.D. Leonida, K.I. Voivodov, *Tetrahedron Lett.* **1994**, 35, 5607.

[59] R.J. Fisher, J.M. Fenton, J. Iranmahboob, *J. Memb. Sci.* **2000**, 177, 17.

[60] C. Kane, T. Theodore, *AIChE J.* **2008**, 54, 1365.

[61] X. Chen, J.M. Fenton, R.J. Fisher, R.A. Peattie, *J. Electrochem. Soc.* **2004**, 151, 56.

[62] K.I. Voivodov, S.B. Sobolov, M.D. Leonida, A.J. Fry, *Bioorg. Med. Chem. Lett.* **1995**, 5, 681.

[63] M.D. Leonida, A.J. Fry, S.B. Sobolov, V.K. 1, *Bioorg. Med. Chem. Lett.* **1996**, 6, 1663.

[64] H. Günther, A.S. Paxinos, M. Schulz, C. van Dijk, H. Simon, *Angew. Chemie Int. Ed.* **1990**, 29, 1053.

[65] K. Delecouls-Servat, A. Bergel, R. Basseguy, *Bioprocess Biosyst. Eng.* **2004**, 26, 205.

[66] E. Siu, K. Won, B.P. Chan, *Biotechnol. Prog.* **2007**, 23, 293.

[67] R.W. Coughlin, M. Aizawa, F. Bruce, M. Charles, *Biotechnol. Bioeng.* **1975**, XVII, 515.

[68] J.M. Obón, P. Casanova, A. Manjón, V.M. Fernández, J.L. Iborra, *Biotechnol. Prog.* **1997**, 13, 557.

[69] A. Radoi, D. Compagnone, *Bioelectrochemistry* **2009**, 76, 126.

[70] Y. Dilgin, L. Gorton, G. Nisli, *Electroanalysis* **2007**, 19, 286.

[71] D.G. Dilgin, D. Gligor, H.I. Gökçel, Z. Dursun, Y. Dilgin, *Microchim. Acta* **2011**, 173, 469.

[72] S. Kochius, A.O. Magnusson, F. Hollmann, J. Schrader, D. Holtmann, *Appl. Microbiol. Biotechnol.* **2012**, 93, 2251.

[73] G. Hilt, E. Steckhan, *J. Chem. Soc* **1993**, 1706.

[74] J. Komoschinski, E. Steckhan, *Tetrahedron Lett.* **1988**, 29, 3299.

[75] I. Mazurenko, M. Etienne, G. Kohring, F. Lapicque, A. Walcarius, *Electrochim. Acta* **2016**, 199, 342.

[76] O. Miyawaki, T. Yano, *Enzyme Microb. Technol.* **1993**, 15, 525.

[77] P. Kornberger, J. Gajdzik, H. Natter, G. Wenz, F. Giffhorn, G.W. Kohring, R. Hempelmann, *Langmuir* **2009**, 25, 12380.

[78] A. Manjón, J.M. Obón, P. Casanova, V.M. Fernández, J.L. Ilborra, *Biotechnol. Lett.* **2002**, 24, 1227.

[79] I. Schröder, E. Steckhan, A. Liese, *J. Electroanal. Chem.* **2003**, 541, 109.

[80] Y. Kashiwagi, T. Osa, *Chem. Lett.* **1993**, 4, 677.

[81] T. Osa, Y. Kashiwagi, Y. Yanagisawa, *Chem. Lett.* **1994**, 23, 367.

[82] Z. Wang, M. Etienne, S. Pöller, W. Schuhmann, G.-W. Kohring, V. Mamane, A. Walcarius, *Electroanalysis* **2012**, 24, 376.

[83] S. Itoh, H. Fukushima, M. Komatsu, Y. Ohshiro, *Chem. Lett.* **1992**, 8, 1583.

[84] E. Steckhan, T. Arns, W.R. Heineman, G. Hilt, D. Hoormann, J. Jörissen, L. Kröner, B. Lewall, H. Pütter, *Chemosphere* **2001**, 43, 63.

[85] D. Degenring, I. Schroder, C. Wandrey, A. Liese, L. Greiner, *Org. Process Res. Dev.* **2004**, 8, 213.

[86] S. Gauer, Z. Wang, H. Otten, M. Etienne, M.J. Bjerrum, L. Lo Leggio, A. Walcarius, F. Giffhorn, G.-W. Kohring, *Appl. Microbiol. Biotechnol.* **2014**, 98, 3023.

[87] R. Basseguy, K. Delecouls-Servat, A. Bergel, *Bioprocess Biosyst. Eng.* **2004**, 26, 165.

[88] R. Devaux-Basseguy, G. Pierre, A. Bergel, *J. Chem. Tech. Biotechnol* **1997**, 68, 389.

[89] P. Gros, A. Bergel, *AIChE J.* **2005**, 51, 989.

[90] C. Bourdillon, R. Lortie, J.M. Laval, *Biotechnol. Bioeng.* **1988**, 31, 553.

[91] B. Brielbeck, M. Frede, E. Steckhan, *Biocatalysis* **1994**, 10, 49.

[92] I. Mazurenko, W. Ghach, G. Kohring, C. Despas, *Bioelectrochemistry* **2015**, 104, 65.

[93] S. Kawabata, N. Iwata, H. Yoneyama, *Chem. Lett.* **2000**, 29, 110.

[94] S. Krishnan, J.B. Schenkman, J.F. Rusling, *J. Phys. Chem. B* **2011**, 115, 8371.

[95] B.D. Fleming, D.L. Johnson, A.M. Bond, L.L. Martin, *Expert Opin. Drug Metab. Toxicol.* **2006**, 2, 581.

[96] C.E. Immoos, J. Chou, M. Bayachou, E. Blair, J. Greaves, P.J. Farmer, *J. Am. Chem. Soc.* **2004**, 126, 4934.

[97] L.H. Mak, S.J. Sadeghi, A. Fantuzzi, G. Gilardi, *Anal. Chem.* **2010**, 82, 5357.

[98] G. Güven, *ECS Trans.* **2011**, 35, 9.

[99] D. Holtmann, K.M. Mangold, J. Schrader, *Biotechnol. Lett.* **2009**, 31, 765.

[100] J. Lu, D. Cui, H. Li, Y. Zhang, S. Liu, *Electrochim. Acta* **2015**, 165, 36.

[101] S. Krishnan, D. Wasalathanthri, L. Zhao, J.B. Schenkman, J.F. Rusling, *J. Am. Chem. Soc.* **2011**, 133, 1459.

[102] H. Tian, S. Mu, H. Li, X. Wu, Z. Lu, *ChemCatChem* **2012**, 4, 1850.

[103] T. Krieg, S. Hüttmann, K.-M. Mangold, J. Schrader, D. Holtmann, *Green Chem.* **2011**, 13, 2686.

[104] A.E.W. Horst, K.M. Mangold, D. Holtmann, *Biotechnol. Bioeng.* **2015**, 113, 260.

[105] D. Holtmann, T. Krieg, L. Getrey, J. Schrader, *Catal. Commun.* **2014**, 51, 82.

[106] L. Getrey, T. Krieg, F. Hollmann, J. Schrader, D. Holtmann, *Green Chem.* **2014**, 16, 1104.

[107] K. Min, D. Park, Y. Je, *J. Biotechnol.* **2010**, 146, 40.

[108] K. Min, T. Kathavarayan, K. Park, Y. Je, *J. Mol. Catal. B. Enzym.* **2013**, 90, 87.

[109] T. Krieg, A. Sydow, U. Schröder, J. Schrader, D. Holtmann, *Trends Biotechnol.* **2014**, 32, 645.

[110] R. Szamocki, S. Reculusa, S. Ravaine, P.N. Bartlett, A. Kuhn, R. Hempelmann, *Angew. Chem. Int. Ed.* **2006**, 45, 1317.

[111] Y.B. Saint Côme, H. Lalo, Z. Wang, G.-W. Kohring, R. Hempelmann, M. Etienne, A. Walcarius, A. Kuhn, *Electroanalysis* **2013**, 25, 621.

[112] F. Qu, R. Nasraoui, M. Etienne, Y.B. Saint Côme, A. Kuhn, J. Lenz, J. Gajdzik, R. Hempelmann, A. Walcarius, *Electrochem. Commun.* **2011**, 13, 138.

[113] I. Ali, A. Gill, S. Omanovic, *Chem. Eng. J.* **2012**, 188, 173.

[114] I. Ali, T. Khan, S. Omanovic, *J. Mol. Catal. A Chem.* **2014**, 387, 86.

[115] Y.H. Kim, Y.J. Yoo, *Enzyme Microb. Technol.* **2009**, 44, 129.

[116] N. Ullah, I. Ali, S. Omanovic, *Mater. Chem. Phys.* **2015**, 149, 413.

[117] R.L. Mccreery, *Chem. Rev.* **2008**, 108, 2646.

[118] W. Zhang, S. Zhu, R. Luque, S. Han, L. Hu, G. Xu, *Chem. Soc. Rev.* **2016**, 45, 715.

[119] P. Taylor, I. Švancara, K. Vyt, I. Svancara, *Crit. Rev. Anal. Chem.* **2010**, 31, 311.

[120] B.J. Sanghavi, A.K. Srivastava, *Electrochim. Acta* **2010**, 55, 8638.

[121] M. Merino, L.J. Nunez-Vergara, J.A. Squella, *Electroanalysis* **1999**, 11, 1285.

[122] S.-H. Shuo-Han, J. Zhang, X. Gao, H. Ying, *J. Mater. Chem. B* **2015**, 3, 6626.

[123] P. Zucca, E. Sanjust, *Molecules* **2014**, 19, 14139.

[124] S.Y.R. Pugh, in *Enzymes as Catalysts in Organic Synthesis*, M.P. Schneider (Ed.), Springer Netherlands, Cranfield, **1986**, pp. 217–232.

[125] J. Krenková, F. Frantisek, *Electrophoresis* **2004**, 25, 3550.

[126] F. Hildebrand, S. Lütz, *Tetrahedron Asymmetry* **2006**, 17, 3219.

[127] J.G. Vos, R.J. Forster, T.E. Keyes, in *Interfacial Supramolecular Assemblies*, John Wiley & Sons, Ltd, Chichester, **2003**, pp. 87–152.

[128] E. Nouri-Nigjeh, R. Bischoff, A.P. Bruins, H.P. Permentier, *Curr. Drug Metab.* **2011**, 12, 359.

[129] I.C.G. Thanos, H. Simon, *J. Biotechnol.* **1987**, 6, 13.

[130] H.R. Luckarift, J.C. Spain, R.R. Naik, M.O. Stone, *Nat. Biotechnol.* **2004**, 22, 211.

[131] M. Varni, T. Vidakovi c-Koch, K. Sundmacher, *Electrochim. Acta* **2015**, 174, 480.

[132] S. Schlager, H. Neugebauer, M. Haberbauer, G. Hinterberger, N.S. Sariciftci, *ChemCatChem* **2015**, 7, 967.

[133] D. Membreno, L. Smith, B. Dunn, *J. Sol-Gel Sci. Technol.* **2014**, 70, 203.

[134] M.J. Moehlenbrock, S.D. Minteer, *Chem. Soc. Rev.* **2008**, 37, 1188.

[135] E. Lojou, *Electrochim. Acta* **2011**, 56, 10385.

[136] F. Hollmann, B. Witholt, a. Schmid, *J. Mol. Catal. B: Enzym.* **2002**, 19-20, 167.

[137] S. Chardon-Noblat, S. Cosnier, A. Deronzier, N. Vlachopoulos, *J. Electroanal. Chem.* **1993**, 352, 213.

[138] J.H. van Esch, M. a M. Hoffmann, R.J.M. Nolte, *J. Org. Chem.* **1995**, 60, 1599.

[139] H. Eva, E. Steckhan, R. Brigitte, W.R. Heineman, *J. Electroanal. Chem.* **1996**, 402, 115.

[140] L. Qin, K. Lv, Z. Shen, M. Liu, in *Soft Matter Nanotechnology*, X. Chen, H. Fuchs (Eds.), Wiley-VCH Verlag GmbH & Co. KGaA, Weinheim, **2015**, pp. 21–94.

[141] T. Schlick, *MolecularModeling and Simulation An Interdisciplinary Guide*, Springer-Verlag New York, **2010**.

[142] A. Walcarius, R. Nasraoui, Z. Wang, F. Qu, V. Urbanova, M. Etienne, M. Göllü, A.S. Demir, J. Gajdzik, R. Hempelmann, *Bioelectrochemistry* **2011**, 82, 46.

[143] N. Vilà, J. Ghanbaja, E. Aubert, A. Walcarius, *Angew. Chem. Int. Ed. Engl.* **2014**, 53, 2945.

[144] N. Vilà, J. Ghanbaja, A. Walcarius, *Adv. Mater. Interfaces* **2016**, 3, 1500440.

[145] L. Bayne, R. V Ulijn, P.J. Halling, *Chem. Soc. Rev.* **2013**, 42, 9000.

[146] L. Zhang, N. Vilà, T. Klein, I. Kohring, Gert-Wieland Mazurenko, A. Walcarius, M. Etienne, *ACS Appl. Mater. Interfaces* **2016**, 8, 17591.

[147] M.C.R. Franssen, P. Steunenberg, E.L. Scott, H. Zuilhof, J.P.M. Sanders, *Chem. Soc. Rev.* **2013**, 42, 6491.

[148] T. Hudlicky, J.W. Reed, *Chem. Soc. Rev.* **2009**, 38, 3117.

[149] P. Kornberger, F. Giffhorn, G.W. Kohring, in *Encyclopedia of Industrial Biotechnology: Bioprocess, Bioseparation, and Cell Technology*, M.C. Flickinger (Ed.), John Wiley & Sons, Inc, Hoboken, NJ, USA, **2010**, pp. 1888–1898.

[150] R.A. Sheldon, S. van Pelt, *Chem. Soc. Rev.* **2013**, 42, 6223.

[151] E. Hochuli, W. Bannwarth, H. Döbeli, R. Gentz, D. Stüber, *Nat. Biotechnol.* **1988**, 6, 1321.

[152] C. Ley, D. Holtmann, K.-M. Mangold, J. Schrader, *Colloids Surf. B* **2011**, 88, 539.

[153] D. Gaffney, J. Cooney, E. Magner, *Top. Catal.* **2012**, 55, 1101.

[154] D.A. Gaffney, S. O'Neill, M.C. O'Loughlin, U. Hanefeld, J.C. Cooney, E. Magner, *Chem. Commun.* **2010**, 46, 1124.

[155] Y.-C. Lin, M.-R. Liang, Y.-C. Lin, C.-T. Chen, *Chem. Eur. J.* **2011**, 17, 13059.

[156] M. Mielecki, J. Wojtasik, M. Zborowska, K. Kurzątkowska, K. Grzelak, W. Dehaen, J. Radecki, H. Radecka, *Electrochim. Acta* **2013**, 96, 147.

[157] D.S. Waugh, *Trends Biotechnol.* **2005**, 23, 316.

[158] Y. Li, J. Zhang, X. Huang, T. Wang, *Biochem. Biophys. Res. Commun.* **2014**, 446, 201.

[159] A.C. Widrig, C. Chung, M.D. Porter, *J. Electroanal. Chem.* **1991**, 310, 335.

[160] M.W.J. Beulen, M.I. Kastenberg, F.C.J.M. van Veggel, D.N. Reinhoudt, *Langmuir* **1998**, 14, 7463.

[161] A.A. Karyakin, *Electrochem. Commun.* **2003**, 5, 677.

[162] J.E. Moses, A.D. Moorhouse, *Chem. Soc. Rev.* **2007**, 36, 1249.

[163] D.P. Nair, M. Podgórski, S. Chatani, T. Gong, W. Xi, C.R. Fenoli, C.N. Bowman, *Chem. Mater.* **2014**, 26, 724.

[164] W. Tang, M.L. Becker, *Chem. Soc. Rev.* **2014**, 43, 7013.

[165] Q. Ran, R. Peng, C. Liang, S. Ye, Y. Xian, W. Zhang, L. Jin, *Anal. Chim. Acta* **2011**, 697, 27.

[166] A. Hayat, J.-L. Marty, A.-E. Radi, *Electroanalysis* **2012**, 24, 1446.

[167] L. Wang, Q. Ran, Y. Tian, J. Xu, Y. Xian, R. Peng, L. Jin, *J. Colloid Interface Sci.* **2010**, 350, 544.

[168] G. Bayramoglu, O. Celikbicak, M.Y. Arica, B. Salih, *Ind. Eng. Chem. Res.* **2014**, 53, 4554.

[169] M.H. Stenzel, *ACS Macro Lett.* **2013**, 2, 14.

[170] M.W. Jones, G. Mantovani, S.M. Ryan, X. Wang, D.J. Brayden, D.M. Haddleton, *Chem. Commun.* **2009**, 5272.

[171] S. Abdellaoui, B.C. Corgier, C. a. Mandon, B. Doumèche, C. a. Marquette, L.J. Blum, *Electroanalysis* **2013**, 25, 671.

[172] P.K. Smith, R.I. Krohn, G.T. Hermanson, A.K. Mallia, F.H. Gartner, M.D. Provenzano, E.K. Fujimoto, N.M. Goeke, B.J. Olson, D.C. Klenk, *Anal. Biochem.* **1985**, 150, 76.

[173] L. Willard, A. Ranjan, H. Zhang, H. Monzavi, R.F. Boyko, B.D. Sykes, D.S. Wishart, *Nucleic Acids Res.* **2003**, 31, 3316.

[174] N. Vilà, M. Van Brussel, M. D'Amours, J. Marwan, C. Buess-Herman, D. Bélanger, *J. Electroanal. Chem.* **2007**, 609, 85.

[175] D. Bélanger, J. Pinson, *Chem. Soc. Rev.* **2011**, 40, 3995.

[176] J.F. Moulder, W.F. Stickle, P.E. Sobol, K.D. Bomben, *Handbook of X-Ray Photoelectron Spectroscopy: A Reference Book of Standard Spectra for Identification and Interpretation of XPS Data*, Physical Electronics, Eden Prairie, **1995**.

[177] M.R. Das, M. Wang, S. Szunerits, L. Gengembre, R. Boukherroub, *Chem. Commun. (Camb).* **2009**, 2753.

[178] A.W. Taylor, P. Licence, *ChemPhysChem* **2012**, 13, 1917.

[179] Z. Wang, M. Etienne, G.-W. Kohring, A. Walcarius, *Electroanalysis* **2010**, 22, 2092.

[180] L. Gorton, P.N. Bartlett, in *Bioelectrochemistry: fundamentals, experimental techniques and applications*, P.N. Bartlett (Ed.), John Wiley & Sons, Ltd, Chippenham, **2008**, pp. 157–198.

[181] Z. Yang, Z. Yao, G. Li, G. Fang, H. Nie, Z. Liu, X. Zhou, X. Chen, S. Huang, *ACS Nano* **2012**, 6, 205.

[182] C.D. Bain, H.A. Biebuyck, G.M. Whitesides, *Langmuir* **1989**, 5, 723.

[183] J. Johansson, L. Fleetwood, H. Jesrnvall, *FEBS Lett.* **1992**, 303, 5.

[184] J. Jeffery, L. Cummins, M. Carlquist, H. Jornvall, *Eur. J. Biochem.* **1981**, 120, 229.

[185] E.J. Wright, M. Sosna, S. Bloodworth, J.D. Kilburn, P.N. Bartlett, *Chem. Eur. J. 2014,* **2014**, 20, 5550.

[186] R. Ruppert, S. Herrmann, E. Steckhan, *Tetrahedron Lett.* **1987**, 28, 6583.

[187] C. Caix, S. Chardon-noblat, A. Deronzier, *J. Electroanal. Chem.* **1997**, 434, 163.

[188] S. Kim, G.Y. Lee, J. Lee, E. Rajkumar, J.-O. Baeg, J. Kim, *Electrochim. Acta* **2013**, 96, 141.

[189] T. Quinto, V. Köhler, T.R. Ward, *Top. Catal.* **2014**, 57, 321.

[190] W. Liu, P. Wang, *Biotechnol. Adv.* **2007**, 25, 369.

[191] H. Zhao, W. a. Van Der Donk, *Curr. Opin. Biotechnol.* **2003**, 14, 583.

[192] C. Rodriguez, I. Lavandera, V. Gotor, *Curr. Org. Chem.* **2012**, 16, 2525.

[193] H.K. Chenault, G.M. Whitesides, *Appl. Biochem. Biotechnol.* **2007**, 14, 147.

[194] M.M. Grau, M. Poizat, I.W.C.E. Arends, F. Hollmann, *Appl. Organomet. Chem.* **2010**, 24, 380.

[195] L. Campanella, T. Ferri, M.P. Sammartino, W. Marconi, A. Nidola, *J. Mol. Catal.* **1987**, 43, 153.

[196] F. Hollmann, A. Schmid, E. Steckhan, *Angew. Chem. Int. Ed.* **2001**, 40, 169.

[197] E. Steckhan, S. Herrmann, R. Ruppert, E. Dietz, M. Frede, *Organometallics* **1991**, 10, 1568.

[198] J. Lutz, F. Hollmann, T.V. Ho, A. Schnyder, R.H. Fish, A. Schmid, *J. Organomet. Chem.* **2004**, 689, 4783.

[199] N. Vilà, M. Van Brussel, M. D'Amours, J. Marwan, C. Buess-Herman, D. Bélanger, *J. Electroanal. Chem.* **2007**, 609, 85.

[200] Z. Wang, M. Etienne, V. Urbanova, G.-W. Kohring, A. Walcarius, *Anal. Bioanal. Chem.* **2013**, 405, 3899.

[201] D. Sivanesan, S. Yoon, *Polyhedron* **2013**, 57, 52.

[202] Z. Wang, M. Etienne, F. Quilès, G.-W. Kohring, A. Walcarius, *Biosens. Bioelectron.* **2012**, 32, 111.

[203] L. Rover Júnior, J.C. Fernandes, G. de Oliveira Neto, L.T. Kubota, E. Katekawa, S.H. Serrano, *Anal. Biochem.* **1998**, 260, 50.

[204] S. Schauder, K.H. Schneider, F. Giffhorn, *Microbiology* **1995**, 141, 1857.

[205] P. Kornberger, J. Gajdzik, H. Natter, G. Wenz, F. Giffhorn, G.W. Kohring, R. Hempelmann, *Langmuir* **2009**, 25, 12380.

[206] Z. Wang, M. Etienne, G.-W. Kohring, Y. Bon-Saint-Côme, A. Kuhn, A. Walcarius, *Electrochim. Acta* **2011**, 56, 9032.

[207] R.L. Garrell, J.E. Chadwick, D.L. Severance, N.A. Mcdonald, D.C. Myles, *J. Am. Chem. Soc.* **1995**, 117, 11563.

[208] E. Delamarche, B. Michel, H. Kang, C. Gerber, *Langmuir* **1994**, 10, 4103.

[209] M.H. Schoenfisch, J.E. Pemberton, *J. Am. Chem. Soc.* **1998**, 120, 4502.

[210] M. Deiamar, R. Hitmi, J. Pinson, J.M. Savbnt, *J. Am. Chem. Soc.* **1992**, 114, 5883.

[211] P. Allongue, M. Delamar, B. Desbat, O. Fagebaume, R. Hitmi, J. Pinson, J. Save, *J. Am. Chem. Soc.* **1997**, 119, 201.

[212] D. Matcriaux, *Carbon N. Y.* **1997**, 35, 801.

[213] A. Adenier, M. Bernard, M.M. Chehimi, E. Cabet-deliry, B. Desbat, O. Fagebaume, J. Pinson, F. Podvorica, *J. Am. Chem. Soc.* **2001**, 123, 4541.

[214] A. Chausse, M.M. Chehimi, N. Karsi, J. Pinson, F. Podvorica, C. Vautrin-ul, *Chem. Mater.* **2002**, 14, 392.

[215] A. Adenier, E. Cabet-deliry, T. Lalot, J. Pinson, *Chem. Mater.* **2002**, 14, 4576.

[216] J. Pinson, F. Podvorica, J. Pinson, *Chem. Soc. Rev.* **2005**, 34, 429.

[217] D. Belanger, J. Pinson, *Chem. Soc. Rev.* **2011**, 40, 3995.

[218] A.J. Downard, D.J. Garrett, E.S.Q. Tan, *Langmuir* **2006**, 22, 10739.

[219] A.C. Cruickshank, E.S.Q. Tan, P.A. Brooksby, A.J. Downard, *Electrochem. Commun.* **2007**, 9, 1456.

[220] Y. Liu, R.L. Mccreery, *J. Am. Chem. Soc.* **1995**, 117, 11254.

[221] H. Yang, R.L. Mccreery, *Anal. Chem.* **1999**, 71, 4081.

[222] B.L. Hurley, R.L. Mccreery, *J. Electrochem. Soc.* **2004**, 151, B252.

[223] F. Anariba, U. Viswanathan, D.F. Bocian, R.L. Mccreery, *Anal. Chem.* **2006**, 78, 3104.

[224] C. Saby, B. Ortiz, G.Y. Champagne, D. Be, *Langmuir* **1997**, 13, 6805.

[225] B. Ortiz, C. Saby, G.Y. Champagne, D. Be, *J. Electroanal. Chem.* **1998**, 455, 75.

[226] D. Be, *J. Phys. Chem. B* **2003**, 107, 4811.

[227] D. Cations, *J. Phys. Chem. B* **2005**, 109, 24401.

[228] A. Laforgue, T. Addou, D. Be, *Langmuir* **2005**, 21, 6855.

[229] J. Lyskawa, D. Belanger, *Chem. Mater.* **2006**, 18, 4755.

[230] J.L. Bahr, J.M. Tour, *Chem. Mater.* **2001**, 13, 3823.

[231] M.P. Stewart, F. Maya, D. V Kosynkin, S.M. Dirk, J.J. Stapleton, C.L. Mcguiness, D.L. Allara, J.M. Tour, V. Pennsyl, S. Uni, U. V Park, V. Pennsyl, *J. Am. Chem. Soc.* **2004**, 126, 370.

[232] J.L. Hudson, H. Jian, A.D. Leonard, J.J. Stephenson, J.M. Tour, N. Science, R.U. V, M. Street, R. V January, V. Re, M. Recei, V. March, *Chem. Mater.* **2006**, 18, 2766.

[233] N. Nair, W. Kim, M.L. Usrey, M.S. Strano, *J. Am. Chem. Soc.* **2007**, 129, 3946.

[234] K. Roodenko, M. Gensch, J. Rappich, K. Hinrichs, N. Esser, R. Hunger, D. Elektronen-synchrotron, H. Berlin, *J. Phys. Chem. B* **2007**, 111, 7541.

[235] D. Pandey, D.Y. Zemlyanov, K. Bevan, R.G. Reifenberger, S.M. Dirk, S.W. Howell, D.R. Wheeler, *Langmuir* **2007**, 23, 4700.

[236] C.E. Banks, T.J. Davies, G.G. Wildgoose, R.G. Compton, *Chem. Commun.* **2005**, 829.

[237] G.G. Wildgoose, C.E. Banks, R.G. Compton, *Small* **2006**, 2, 182.

[238] W. Yang, S.E. Baker, J.E. Butler, C. Lee, J.N. Russell, L. Shang, B. Sun, R.J. Hamers, *Chem. Mater.* **2005**, 17, 938.

[239] B.P. Corgier, C.A. Marquette, J. Blum, C.B. Lyon, *J. Am. Chem. Soc.* **2005**, 127, 18328.

[240] B.P. Corgier, F. Li, J. Blum, C.A. Marquette, L. Icbms, *Langmuir* **2007**, 23, 8619.

[241] J.C. Harper, R. Polsky, D.R. Wheeler, S.M. Dirk, S.M. Brozik, *Langmuir* **2007**, 23, 5883.

[242] A. Hermans, A.T. Seipel, C.E. Miller, R.M. Wightman, C. Hill, N. Carolina, *Langmuir* **2006**, 22, 11254.

[243] J. Wang, J.A. Carlisle, *Diam. Relat. Mater.* **2006**, 15, 279.

[244] D. Guo, H. Li, *Electroanalysis* **2005**, 17, 869.

[245] J. Marwan, T. Addou, D. Be, C. Postale, C. Hc, *Chem. Mater.* **2005**, 17, 2395.

[246] M. Van Brussel, M.D. Amours, J. Marwan, C. Buess-Herman, D. Be, *J. Electroanal. Chem.* **2007**, 609, 85.

[247] A. Adenier, M.M. Chehimi, I. Gallardo, J. Pinson, *Langmuir* **2004**, 20, 8243.

[248] N. Vilà, D. Bélanger, *Electrochim. Acta* **2012**, 85, 538.

[249] L. Santos, A. Mattiuzzi, I. Jabin, N. Vandencasteele, O. Reinaud, P. Hapiot, Y. Leroux, C. Lagrost, *J. Phys. Chem. C* **2014**, 118, 15919.

[250] A. Mattiuzzi, I. Jabin, C. Mangeney, C. Roux, O. Reinaud, L. Santos, J. Bergamini, P. Hapiot, C. Lagrost, *Nat. Commun.* **2012**, 3, 1130.

[251] Y.R. Leroux, F. Hui, J. No, A.J. Downard, P. Hapiot, D. Rennes, C. De Beaulieu, *Langmuir* **2011**, 27, 11222.

[252] A.L. Gui, H.M. Yau, D.S. Thomas, M. Chockalingam, J.B. Harper, J.J. Gooding, *Langmuir* **2013**, 29, 4772.

[253] S. Mei, G. Liu, C. Fairman, S.G. Iyengar, J.J. Gooding, *Biosens. Bioelectron.* **2011**, 26, 2038.

[254] G. Liu, M. Chockalingham, S.M. Khor, A.L. Gui, J.J. Gooding, *Electroanalysis* **2010**, 22, 918.

[255] C. Louault, M.D. Amours, D. Bølanger, *ChemPhysChem* **2008**, 9, 1164.

[256] H.C. Kolb, M.G. Finn, K.B. Sharpless, *Angew. Chem. Int. Ed.* **2001**, 40, 2004.

[257] P.M.G. Finn, V. Fokin, M.G. Finn, V. V Fokin, *Chem.Soc.Rev.* **2010**, 39, 1231.

[258] P. Re, *Phys. Rev. B* **1974**, 10, 71.

[259] F. Hildebrand, C. Kohlmann, A. Franz, S. Lütz, *Adv. Synth. Catal.* **2008**, 350, 909.

[260] J. Gajdzik, J. Lenz, H. Natter, A. Walcarius, G.W. Kohring, F. Giffhorn, M. G ll , A.S. Demir, R. Hempelmann, *J. Electrochem. Soc.* **2012**, 159, F10.

[261] K. Vuorilehto, S. Lütz, C. Wandrey, *Bioelectrochemistry* **2004**, 65, 1.

[262] M.R. Axet, O. Dechy-Cabaret, J. Durand, M. Gouygou, P. Serp, *Coord. Chem. Rev.* **2016**, 308, 236.

[263] X. Zhou, T. Zhang, C.W. Abney, Z. Li, W. Lin, *ACS Appl. Mater. Interfaces* **2014**, 6, 18475.

[264] X. Zhou, D. Micheroni, Z. Lin, C. Poon, Z. Li, W. Lin, *ACS Appl. Mater. Interfaces* **2016**, 8, 4192.

[265] L. Hussein, G. Urban, M. Krüger, *Phys. Chem. Chem. Phys.* **2011**, 13, 5831.

[266] A. Le Goff, F. Moggia, N. Debou, P. Jegou, V. Artero, M. Fontecave, B. Jousselme, S. Palacin, *J. Electroanal. Chem.* **2010**, 641, 57.

[267] C.W. Narváez Villarrubia, R. a. Rincón, V.K. Radhakrishnan, V. Davis, P. Atanassov, *ACS Appl. Mater. Interfaces* **2011**, 3, 2402.

[268] M. Zalas, M. Ceglowski, G. Schroeder, *Chem. Pap.* **2012**, 66, 733.

[269] M. Sprecher, R. Breslow, O. Uziel, T.M. Link, *Org. Prep. Proced. Int.* **1994**, 26, 696.

[270] H.J. Lee, S.H. Lee, C.B. Park, K. Won, *Chem. Commun.* **2011**, 47, 12538.

[271] F. Krohm, H. Didzoleit, M. Schulze, C. Dietz, R.W. Stark, C. Hess, B. Stühn, A. Brunsen, *Langmuir* **2013**, 30, 369.

[272] N. Vilà, J. Ghanbaja, E. Aubert, A. Walcarius, *Angew. Chem. Int. Ed. Engl.* **2014**, 53, 2945.

Appendix 1

Section 1. Immobilization of diaphorase in mesoropous silica film

The target of this section was to immobilize diaphorase inside a mediator functionalized mesopore by adsorption which could be used for NAD cofactor regeneration. Since the dimension of diaphorase was estimated to be $(4\sim5)^3$ nm^3, the size of mesopore should be larger than the size of enzyme, but shouldn‟t be too large in order to avoid the rapid leaching.

A mesoporous silica film who has 15% (3-aminopropyl)triethoxysilane (APTES) and 85% TEOS in the starting sol give good pore size for adsorption of diaphorase [271]. In addition, pI of diaphrase is 4.7, when we work at neutral buffer solution, the enzyme was negtively charged. The pure silica film was also negatively charge, the introduction of amino group was expected to change the silica surface more positive, favourable for the interaction between diaphorase and silica film.

The adsorption of diaphorase was first tested with mesoporous silica film obtained by calcination (amino functional groups was removed during the calcination process) (**Figure A1)**.

A **B**

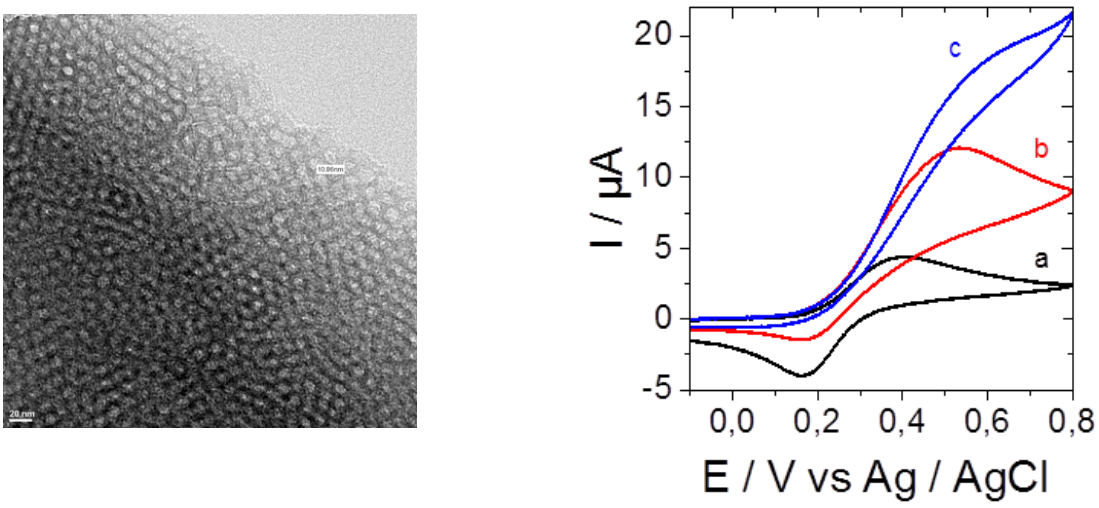

Figure A1. *(A) TEM image of mesoporous silica film prepared by dip-coating, pore size is around 10 nm. (B) Cyclic voltammograms of the diaphorase adsorbed mesoporous silica film (obtained by calcination) on FTO electrode (0.28 cm^2) to addition of (a) 0 mM (b) 0.1 mM (c) 0.5 mM NADH in 0.1M PBS solution at pH=7 containing 0.1 mM ferrocenedimethanol as electron mediator. Scanning rates is 100 mV s^{-1}. The functionalized silica film was prepared following a reported protocal* [271].

In order to remain the functionalized group after template removal, extraction methods were expolored.

Extraction solution	0.01 M HCl in EtOH	0.01 M HCl in EtOH	1 M HCl in EtOH	0.06 M H_2SO_4	0.6 M H_2SO_4	6 M H_2SO_4
Temprature	Room T	90℃	90℃	90℃	90℃	90℃
Time	72 h	24 h	18 h	16 h	8 h	6 h
Result	Template kept				Template partly removed	Template removed

Table A1. *Different template extraction conditions used for silica films on FTO electrode which has 15% APTES and 85% TEOS in the starting sol.*

The influence of APTES amount in the starting silica sol to permeability and catalytic response of adsorbed diaphorase was studied. It seems the permeability was decreasing with increasing amount of APTES moieties (**Figure A2A)**. However, the increase of amino group from 10% to 30% in the silica pore will improve the catalytic current. The sudden decease at 40% may due to the loss of mesostructures (**Figure A2B)**.

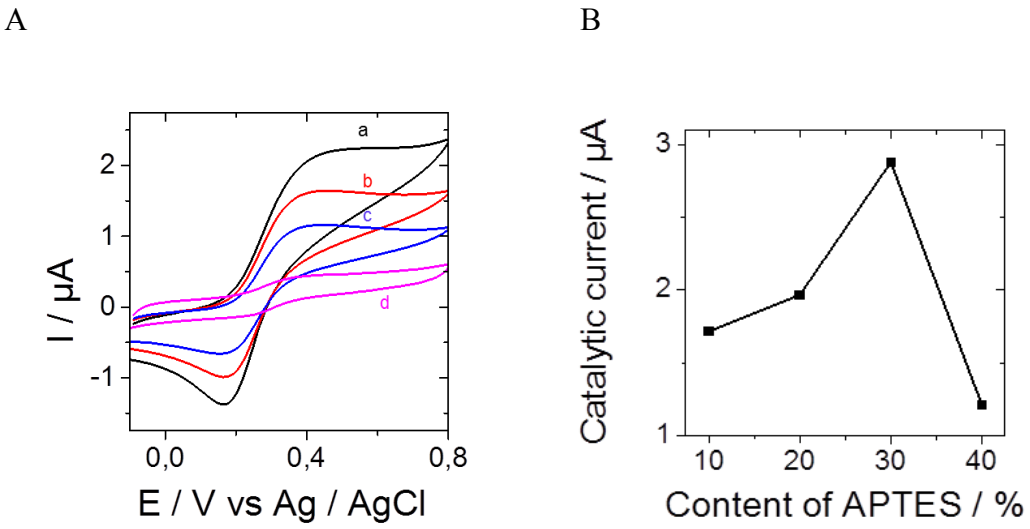

Figure A2. *(A) Permeability tests with 0.1mM ferrocenedimethanol for mesoporous silica films with (a) 10% (b) 20% (c) 30% (d) 40% APTES in the starting sol in 0.1M PBS at pH 7.0. (B) Evolution of catalytic current to addition of 0.1 mM NADH for the diaphorase adsorbed mesoporous silica mesoporous films on FTO electrode (0.28 cm^2) with different percentage of APTES in the starting sol in 0.1M PBS at pH 7.0 containing 0.1 mM ferrocenedimethanol.*

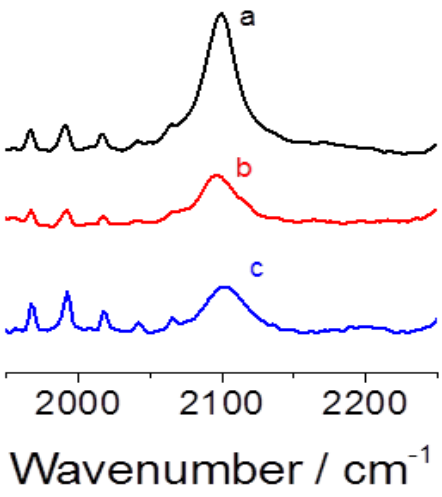

***Figure A3**. Infrared spectrum of an azide functionalized mesoporous silica film obtained from a sol prepared with 10% AzPTMS,15% APTES and (a) with template, (b) after extraction of template by 6M H_2SO_4 at 90 ℃ for 6h, (c) after click with Fc*

Then 10% 3-azidopropyltrimethoxysilane (AzPTMS) as well as 15% APTES was introduced into the starting sol. The azide group was used for covalent immobilization of mediators (here we use ferrocene as a model) via Azide-alkyne Huisgen cycloaddition. However, no ferrocene was detected, this was comfirmed by IR (-N_3 peak at 2100 cm^{-1} was not decreased after click reaction). The possible explaination could be the degredation of azide group under harsh extraction condition or the change of film structure during the click reaction.

Section 2. Immobilization of $[Cp^*Rh(bpy)Cl]^+$ in highly ordered mesoporous silica films.

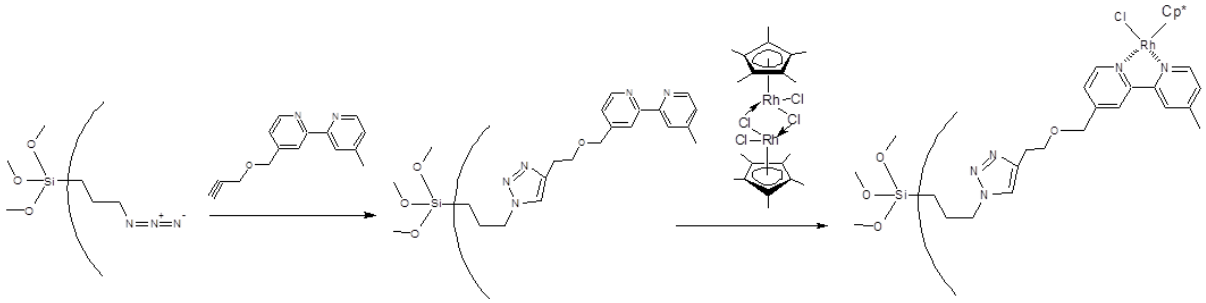

Figure A4. *Synthetic route followed for covalent immobilization of* $[Cp^*Rh(bpy)Cl]^+$ *in the silica film with mesopore structure vertical to the FTO electrode surface generated by electrochemical assisted method. The azide functionalized silica was prepared by following the reported protocol* [272].

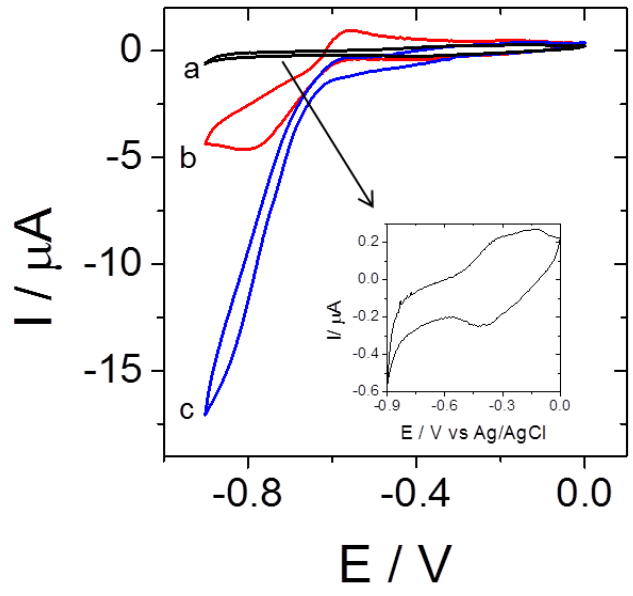

Figure A5. *Cylic voltammograms applied on a bare FTO electrode (0.28* cm^2*) in (a) buffer solution at pH 7.0 (b) buffer solution containing 0.1 mM* $[Cp^*Rh(bpy)Cl]^+$ *and (c) buffer solution containing 0.1 mM* $[Cp^*Rh(bpy)Cl]^+$ *and 0.5 mM* NAD^+ *in PBS. The inset is the zoom in of curve (a).*

The electrocatalytic response of $[Cp^*Rh(bpy)Cl]^+$ in solution for NADH regeneration was tested with bare FTO electrode.

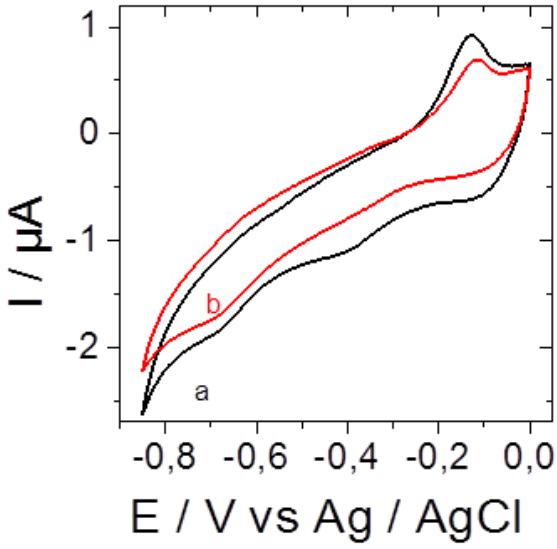

Figure A6. *Cylic voltammograms applied on a* $[Cp^*Rh(bpy)Cl]^+$ *functionalized mesoporous silica film on FTO electrode (0.28* cm^2*) in 50 mM PBS at pH 7.0 (a) without presence and (b) in presence of 0.5 mM* NAD^+.

After covalent immobilization of $[Cp^*Rh(bpy)Cl]^+$ inside the mesoporous film, the reduction peak of rhodium was observed, but no electrocatalytic response was observed for NAD^+ reduction.

Appendix 2

Review

Wiley Online Library

ELECTROANALYSIS

DOI: 10.1002/elan.201500172

Mesoporous Materials-Based Electrochemical Enzymatic Biosensors

Mathieu Etienne,[a] Lin Zhang,[a] Neus Vilà,[a] and Alain Walcarius*[a]

Abstract: This review (239 references) is dealing with the use of mesoporous materials in the field of electrochemical enzymatic biosensors. After a brief discussion on the interest of mesoporous materials for electrochemical biosensing, a presentation of the various types of inorganic and organic-inorganic hybrid mesostructures used to date in the elaboration of enzymatic bioelectrodes is given and the main bioelectrode configurations are described. The various biosensor applications are then summarized on the basis of a comprehensive table and some representative illustrations. The main detection schemes developed in the field are based on amperometry and mediated electrocatalysis, as well as some on spectroelectrochemistry.

Keywords: Ordered mesoporous materials · Mesoporous silica · Organic-inorganic hybrids · Mesoporous carbon · Mesoporous metals · Mesoporous metal oxides · Self-assembly · Surfactant template · Mediator · Thin films · Composite electrodes · Biomolecule immobilization · Electrochemical detection · Enzymatic biosensors · Heme proteins · Oxidases · Dehydrogenases · Tyrosinase

1 Introduction

Ordered mesoporous materials exhibiting a regular, periodic organization made of mesopores of uniform size distribution, and characterized by very high specific surface areas and pore volumes, as well as possible tuning of reactivity via suitable modification, have inspired prominent research interest in the past two decades due to their unique properties and functionalities [1–27]. They have indeed potential applications in adsorption [28–31], separation [32–34], catalysis [35–37], electrochemistry [38,39], sensors [39–46] and biosensors [44,47–53], drug delivery and other biomedical fields [54–58], immobilization of biomolecules and biocatalysis [59–64], environmental processes [28,30,31,65,66], energy conversion and storage [39,66–69], and so on [70,71]. Nowadays, effective synthesis procedures have been developed to generate various types of ordered mesoporous materials, such as silica and silica-based organic-inorganic hybrid materials [1–8,72], metal oxides other than silica [1,9–12,73–75], mesoporous non-oxide materials [13,14,76], ordered porous metals [1,11,15,16], ordered mesoporous carbons [1,17–26,77,78], or mesostructured organic polymers [22,26,27]. Many of them are particularly attractive for being used in electrochemical sensing and biosensing devices, in which one can take advantage of their support/hosting properties (i.e., for immobilization of biomolecules, catalysts, or charge transfer mediators), their intrinsic (electro)catalytic and/or conductivity properties (mainly mesoporous metal and carbon), their widely open, highly ordered and mechanically stable inorganic mesostructure (ensuring fast transport of reactants throughout highly porous and accessible spaces), and their ease of functionalization with huge amounts of diverse reactive moieties that can be attached to mesopore walls over wide surface areas (mainly on mesoporous silica), for instance.

Here, we provide a comprehensive overview of electrodes modified with mesoporous materials bearing enzymes or other redox biomolecules applied in biosensing applications, as a follow-up of a very recent review on the (non-enzymatic) electrochemical sensors based on ordered mesoporous materials [47]. In the field of enzymatic electrochemical biosensors, there are several crucial points that could be addressed with the aid of ordered mesoporous materials. An electrochemical biosensor is an integrated device combining a biological recognition element (e.g. antibodies, enzymes or whole cells), and an electronic signal transducer (i.e., potentiometry, amperometry, conductometric or surface charge using field effect transistors) [79]. To be effective, the biomolecule(s) should be immobilized under an active form, in sufficient amounts, and in a durable way. This can be achieved by encapsulation in the course of the sol-gel process [80] or through the precipitation of 2D-inorganic materials, i.e. clays [81], LDH [82]. Following a different pathway, the hosting properties of preformed mesoporous matrices, associated to their extremely large surface areas, are likely to provide promising approaches for protein immobilization [59–64].

Electronic signal transduction of the biological recognition event is usually made by the electrochemical detection of one product of the enzymatic reaction (first generation biosensors), or via the use of a redox mediator acting as an electron shuttle between the active site of the biomolecule and the electrode surface (second gener-

[a] M. Etienne, L. Zhang, N. Vilà, A. Walcarius
Laboratoire de Chimie Physique et Microbiologie pour l'Environnement, UMR 7564, CNRS – Université de Lorraine
405 rue de Vandoeuvre, F-54600 Villers-lès-Nancy, France
*e-mail: alain.walcarius@univ-lorraine.fr

ation, which is often used to decrease the high overpotentials usually observed for various bioelectrochemical systems), or by direct electronic wiring of redox enzymes (third generation biosensors) [83–88]. In this respect, it became recently evident that nanomaterials (such as carbon nanotubes or graphene, metal nanoparticles, or nanostructured solids, for instance) are likely to improve the bioelectrocatalytic performance of electrochemical biosensing devices [89–96]. The ordered mesoporous materials belong to this category and offer attractive features, such as intrinsic catalytic and/or conductivity properties or large surface area to support huge amounts of redox mediators, which can be exploited in the field of electrochemical biosensors.

Actually, some reviews are already available, dealing entirely or in part with the use of mesoporous materials for electrochemical biosensing. They include the application of mesoporous silica-based materials for sensors and biosensors [46,49] or immunosensors [51], or the use of mesoporous silica for enzyme immobilization and application in biosensor technology [48,50], or the interest of mesoporous carbon for electrocatalysis and electrochemical sensing [43,44]. A general overview on bioanalysis based on nanoporous materials is also available [52]. To date, however, no comprehensive review including all kinds of ordered mesoporous materials (silica-based, non-siliceous metal oxide, metal, carbon, etc.) being used in designing enzyme-based electrochemical biosensors, has appeared. This is what we describe in this paper, on the basis of an extensive table, after having discussed briefly the interest of mesoporous materials for electrochemical biosensing and mentioned the various types of mesoporous materials used in enzymatic bioelectrodes and their most usual configurations. This constitutes a follow-up and actually a complement of our previous report on mesoporous materials-based electrochemical sensors (non bio) [47].

Mathieu Etienne received his PhD in Electroanalytical Chemistry from University Henri Poincaré Nancy I (France) in 2001 before to work with Prof. Wolfgang Schuhmann at Ruhr-Universität Bochum (Germany). In 2004, he joined the Laboratory of Physical Chemistry and Microbiology for the Environment (France) as CNRS researcher where he is currently developing researches on textured and functionalized materials for bioconversion and energy storage. He is also involved in the development of shearforce-regulated scanning electrochemical microscopy. He is the co-author of about 90 papers.

Neus Vilà received her PhD degree in chemistry in 2005 at the Universitat Autonoma de Barcelona under the guidance of Pr. Iluminada Gallardo. Between 2005 and 2012, she held several postdoctoral positions in different research groups (Pr. Daniel Bélanger, Université du Quebec, Montréal; Pr. Héctor D. Abruña, Cornell University, New York; Dr. Alain Deronzier, Université Joseph Fourier, Grenoble; Dr. Israël Mbomekallé, Institut Lavoisier, Versailles). Since 2012, she is a lecturer at the Université de Lorraine working in the Electrochemistry and Analytical Chemistry group headed by Dr. Alain Walcarius in the Laboratory of Physical Chemistry and Microbiology for the Environment (Nancy). She is currently working on the functionalization and characterization of mesoporous silica-based materials.

Lin Zhang received her B.Sc. in Chemistry from Henan University (China) in 2010. Then, in the frame of an 'Erasmus Mundus' program, she received two M.Sc., one in 'Advanced Functional Materials' from Augsburg University (Germany) and one in 'Chemistry and Physical Chemistry of Materials' from Bordeaux University (France) in 2013. She is curently PhD student at Lorraine University, working in the Electrochemistry and Analytical Chemistry group headed by Dr. Alain Walcarius in the Laboratory of Physical Chemistry and Microbiology for the Environment (Nancy) since 2013, under the supervision of Dr. Mathieu Etienne and Dr. Neus Vilà. Her research is focusing on functionalization of electrodes and immobilization of redox proteins on porous electrodes.

Alain Walcarius received his Ph.D. from the University of Namur (Belgium) in 1994. After a postdoctoral stay in the Joe Wang's group in New Mexico State University, he joined the CNRS (France) as a Research Associate. He is currently CNRS Research Director and Head of the Laboratory of Physical Chemistry and Microbiology for the Environment (Nancy). His analytical and electroanalytical chemistry group works in the area of reactions at solid/liquid interfaces. Among his actual research interests is the intersection between the chemistry of silica-based organic-inorganic hybrid materials and electroanalysis, nanostructuration of electrode surfaces with mesoporous thin films, and bioelectrocatalysis. He has published over 200 peer-reviewed manuscripts, 8 book chapters, and one book.

2 The Various Mesoporous Materials Used in Electrochemical Enzymatic Biosensors

Mesoporous materials applied to electrochemical biosensors can be classified in three main categories, silica-based materials [97–137], carbon-based materials [113,138–178,76,179–184] and metal oxides other than silica [121,130,185,73,186–198,75,74,199–202]. A mesoporous polymer, i.e., polyacrylamide, was also namely reported [203], but in this latter example, the organic template was kept in the membrane and no information on the porosity was given.

The general and basic principle that guides the preparation of an ordered mesoporous material by the template route is shown in Figure 1. Organic or inorganic precursors (salts, alkoxides, organosilanes, organic monomers, nanobuilding blocks such as clusters or nanoparticles, etc.) are allowed to self-assemble with a template or a texturing agent (ionic and nonionic surfactants, amphiphilic block copolymers, biopolymers, ionic liquids, dendrimers, polymer or inorganic colloids, etc.), to form ordered mesoporous and/or macroporous materials in the form of particles, monoliths, thin films or micropatterns [204]. The topic of this review is strictly limited to mesoporous materials, i.e., with pore sizes comprised between 2 and 50 nm as defined by IUPAC. However one needs to keep in mind that both ordered and nonordered macroporous materials (pore sizes >50 nm) can have also some interest in electroanalysis and bioelectrochemistry [44].

The story of ordered mesoporous materials really started in 1992, with the report on the synthesis of a new family of silicate/aluminosilicate mesoporous molecular sieves designed as M41S [205]. Since then, the field of mesoporous materials has virtually exploded (close to 50 000 papers according to WoS). The preparation of mesoporous silica powders involves either precipitation or gelation [206]. Inorganic monomers are hydrolyzed and oligomers are progressively formed upon condensation, to build an organized silica structure (1) around preformed liquid crystal mesophases or (2) by a self-assembly cooperative process occurring between the templates and the silica precursors. The exact mechanism of mesostructuration that is involved for a specific synthesis is depending on the experimental conditions (sol composition and processing) and could be a combination of (1) and (2). The mesostructures that can be produced depend strongly on the organic template. Cetyltrimethylammonium halides were first used to elaborate MCM-41 (hexagonal phase), MCM-48 (cubic phase), and MCM-50 (lamellar phase). Other classes of materials (MSU, HSM, SBA, KIT, …) have been synthesized later on, by using nonionic organic templates (alkylamine, block copolymers P123 or F127, Brij, KLE, ionic liquids, etc.) to tune the porosity of the materials in a wider range of pore size (typically from 2 to 30 nm) [206]. This template can then be removed by calcination or solvent extraction to give the resulting mesoporous open structure that can then be used, e.g., in the present case for protein or electrocatalyst immobilization. The processing of the material has also been addressed to obtain particles with the desired shape and size, films with controllable porosity and thickness [207], and micropatterns or monoliths [208]. A large variety of oxides have been considered by direct or repeated templating [209].

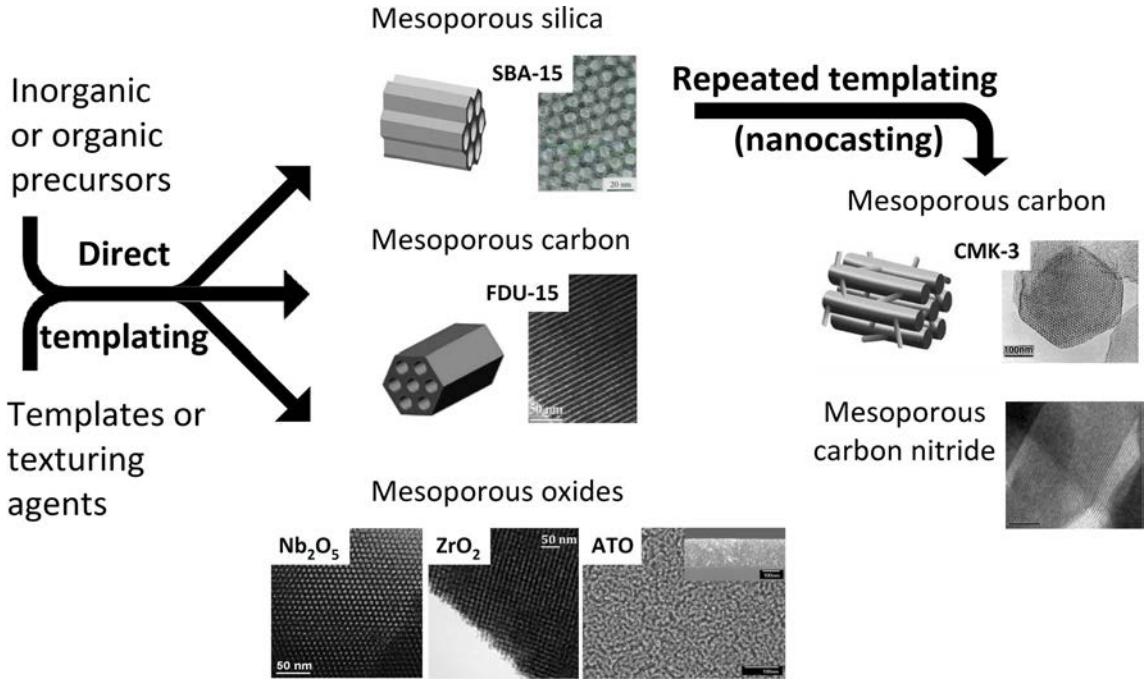

Fig. 1. Schematic view of the preparation of mesoporous materials by direct or repeated templating. TEM micrographs are given for mesoporous silica (SBA-15 [72]), mesoporous carbons (FDU-15 [77] and CMK-3 [78]), mesoporous carbon nitride [76], mesoporous Nb_2O_5 [73], mesoporous ZrO_2 [74], and mesoporous antimony-doped tin oxide (ATO [75]).

The silica-based materials used to date in electrochemical biosensors are mainly MCM-41 [99,102,117,118,121,124,128–132,134,136,137], SBA-15 [101,104,107,110,112,114,122,133], HMS [97,98,100] and FSM8 [111,125,126]. MSU [109], bimodal mesoporous silica [103], mesocellular foams [108,157], mesoporous silica hollow sphere [115], and vesicle-like mesoporous particles [119], were also applied in this field of research. Most of the works have been developed with mesoporous materials in the form of particles [97–104,107–115,117–122,124–126,128–134,136,137], sometimes as nanospheres [129,131]. Only few examples of electrodes modified with mesoporous silica films are reported [105,123].

Oxide materials other than silica that have been applied to electrochemical biosensing are mesoporous Nb_2O_5 [185,73,199], Al_2O_3 [188], SnO_2 [191,193] and doped SnO_2, i.e., antimony-doped tin oxide (ATO) [75] and indium-doped tin oxide (ITO) [192,195], ZrO_2 [194,74], ZnO [201], TiO_2 [186,190,191,196,200], MnO_2 [189,197], or Fe_3O_4 [121,198]. Hydroxyapatite was also used [196,202]. These materials are prepared by the direct templating approach depicted in Figure 1, e.g., Nb_2O_5 [73,185], ATO [75], ITO [192], ZrO_2 [74,194] or MnO_2 [189], or by other routes, e.g., self-assembly of nanoparticles generating a mesoporosity defined by the space present between NPs, e.g., TiO_2 [191], SnO_2 [193] or hydroxyapatite [210]; the mesoporous material can be otherwise produced by electrodeposition of ZnO [201] or MnO_2 [197] in the presence of a surfactant template.

Carbon materials can be prepared either by nanocasting using preformed mesoporous silica templates, leading to carbon replica mesostructures. CMK-1 (as obtained from a MCM-48 silica template [211]) and CMK-3 (as obtained from SBA-15 [78]) were the most widely used for bioelectrochemical purposes. Replication is not the only route for the preparation of mesoporous carbon materials. A direct templating method was reported by Zhao's group [77,212]. The synthesis involved an organic-organic assembly of triblock copolymers with soluble, low-molecular-weight phenolic resin precursors (resols) by an evaporation induced self-assembly strategy. Controlling the ratio of phenol/template or poly(ethylene oxide)/poly(propylene oxide) in the templates enables one to get various materials, e.g., FDU-15 displaying a hexagonal mesoscopic organization. After formation of a regular three-dimensional arrangement of these block copolymers, the mesoporous carbon was obtained by pyrolysis of this skeleton at temperature above 600 °C for graphitization.

Carbon materials applied to electrochemical biosensors are essentially prepared by nanocasting from mesoporous silica hard templates such as SBA-15 [130,132,135,138,140,141,145,147,152–154,160,168,173] or some others [152,153,159,166,167]. Silica or calcium carbonate NPs were also used as hard template for the fabrication of mesoporous carbon material with pore diameter ranging from about 10 nm [155,213] to several tens of nm [139,162,173,182]. Finally, some research works have been performed using FDU-15 carbon materials prepared by direct templating [150,160,161]. Other works illustrate also the application of mesoporous carbon nanoparticles [175] or nanospheres [170] for the construction of biosensors.

From this literature survey, one can conclude that mesoporous materials used to develop electrochemical biosensors display a large range of porosity, from few nm to several tens of nm, variable composition, and several types of mesostructure. Application of these materials in electrochemical biosensors can involve their electrochemical/electrocatalytic properties and/or their large porosity to immobilize redox proteins. The next Section will provide a critical discussion on these different aspects.

3 Interest of Mesoporous Materials for Electrochemical Biosensing

Ordered mesoporous materials offer attractive features that can be basically useful in elaborating electrochemical biosensors, including large specific surface area and high pore volume (great hosting capacity) with tunable pore diameters (size selectivity), regular and widely open mesostructure (for fast transport of reactants), and in some cases intrinsic catalytic and/or conductivity properties (mainly for carbon and metal oxides, which can be useful to promote charge transfer reactions and/or lowering the overpotentials often observed in electrochemical biosensing). Their surface can be also engineered by attaching organo-functional groups (mainly for silica-based materials), which is likely to extend the range of their properties. The interest of mesoporous materials for electrochemical biosensing especially relies on their hosting properties, with the aim at accomplishing the requirements of promoting electron transfer, improving long-term stability, increasing sensitivity, ensuring fast response, and opening the way to miniaturization. This is briefly discussed hereafter, by distinguishing enzyme immobilization onto/into mesoporous materials and the use of mesoporous supports for mediators and catalysts. In addition, one has to mention that mesoporous materials (especially silica-based ones, possibly bearing an enzyme and a mediator) can also serve as a support to antibodies, for being integrated in electrochemical immunosensors, but this aspect is not treated here as it has been reviewed specifically elsewhere [51].

3.1 Enzyme Immobilization in Mesoporous Materials

Several well-documented reviews are available dealing with the immobilization of biomolecules (and among them, enzymes) in mesoporous materials [59–64], and the interested reader is directed to them for details. Only some general trends are given hereafter, focusing on systems used for biosensing purposes.

In order to get successful enzyme-based biosensing devices, enzymes should be immobilized onto suitable solid supports while maintaining their biological activity. If possible, this could also contribute to increasing the catalytic

activity and the recyclability of the enzyme towards harsh conditions. Ordered mesoporous materials are good candidates for hosting enzymes thanks to their unique advantages such as large pore volume and high specific surface area, uniform pore size distribution and tunable pore size, as well as defined pore geometry [60,214,215], which could also contribute to enable fast transport of substrates and products to and from the biologically-active sites in the material.

To improve the biocompatibility of materials with proteins, the surface hydrophilicity, surface charge and mesoporous structure become main factors to manipulate [216]. To reach this goal, the surface of mesoporous silica was modified by selected functional groups to increase the interaction between the enzymes and the silica walls. This was realized either by post-grafting of pure silica [119,133] or from one-step synthesis by co-condensation of organosilanes and tetraalkoxysilane [105]. For example, the introduction of amino groups into a mesoporous silica film allowed increasing its interaction with cytochrome c, which was claimed to be higher on amino-functionalized films than on the pure silica films [105]. For mesoporous carbon materials, their surface can be modified by hydrophilic –COOH groups through sulfuric acid treatment [141]. These carboxylic groups not only improve the hydrophilicity of the carbon material, but also introduce negative charges on the carbon surface, favoring thereby the immobilization of the positively-charged hemoglobin in the conditions of the experiment [147].

Basically, protein immobilization can be achieved by physical adsorption or covalent binding. Zhou et al. compared the performance of glucose biosensors with glucose oxidase immobilized on mesoporous silica by physical adsorption and by covalent binding, showing that the latter approach resulted in higher enzyme loading but lower detection sensitivity than for physical adsorption [119].

Besides the interfacial properties of the mesoporous material, pore characteristics also influenced the enzyme loadings. Bayne et al. have summarized some trends that can be drawn between pore characteristics and protein loadings on the basis of 182 experiments in total, involving many porous materials classified according to three categories of pore diameters [217]. They report a decrease in protein loadings for mesopores with diameters less than 10 nm, as explained by physical restrictions limiting the protein molecules to access the internal volume/surface of so small mesopores. For pore sizes larger than 100 nm, the protein loading declines due to the decrease of available surface area, but this belongs no more to mesoporous materials. Meanwhile, pore sized in the range of 40–70 nm seems to be the optimum for getting the best protein loadings [217]. However, there is still not enough work to systematically certify the definite conclusion within whole ranges and this is expected to be strongly dependent on the nature and structure of the host and the type and size of proteins.

The relative size of the protein compared to the mesopore aperture affects necessarily the immobilization behavior. Different mesoporous materials have been applied to immobilize glucose oxidase, not only because this enzyme is particularly stable and can thus be used as a model protein but also regarding the great importance of electrochemical glucose biosensors [74]. However, among these experiments, some mesoporous materials exhibited a pore diameter smaller than the size of glucose oxidase ($7.0 \times 5.5 \times 8.0$ nm^3), meaning that it should not be possible for the protein to enter the internal pore volume of the hosting material. In such case, the adsorption/immobilization should mainly occur at the outer surface of the mesoporous particles, which would basically not prevent the biosensor application, but without taking advantage of the mesostructure of the material. Full exploitation of the pore volume and high specific surface areas of the hosting solid requires the use of larger pore mesoporous materials. For example, immobilization of glucose oxidase in SBA-15 functionalized with amino groups (11.4 nm pore diameter) gave a higher normalized absolute activity than for the same protein adsorbed onto the outer surface of microporous silica particles (pore diameter <2 nm), an advantage that was also evidenced in their application for glucose biosensing in terms of extended linear concentration range (0.4–13.0 mM instead of 0.4–3.1 mM) [133].

Comparative studies revealed also that a material with mesopore diameter similar to the size of the protein (i.e., 6 nm, Figure 2A) could have significant advantages over a material with larger pore size (i.e., 13 nm, Figure 2B) in facilitating the direct electron transfer of entrapped biomolecule (as pointed out with hemoglobin [155]) and improving thereby the performance of the corresponding biosensor. It has been suggested that the "entrapment" immobilization mode and "interspace confinement effect", which would restrain the unfolding or conformational change of enzyme molecules from inactivation, could result in pore-size-dependent enzymatic stability and bioactivity, which might be a crucial factor for the superior biosensing performance. On the other hand, one has to mention that large pores can be beneficial for the preparation of nanoscale enzyme reactors (NERs), as exemplified for mesoporous carbon with a bottleneck pore structure (mesocellular pores of 26 nm connected with window mesopores of 17 nm), which was applied to prevent the cross-linked glucose oxidase enzymes from leaching through the smaller window mesopores (Figure 2C). This NER approach improved the enzyme stability and favored electron transfer reaction between the enzyme and the conductive mesoporous carbon by maintaining a short distance between them. The comparison with redox proteins simply adsorbed without cross-linking, allowed to prove that the NER approach was effectively improving the sensitivity of glucose biosensors [182,218].

Mesoporous conductive or semi-conductive and transparent matrices constitute another attractive family of solids useful to enzyme immobilization and offering the advantage to allow the spectroelectrochemical investigation of redox proteins and the elaboration of spectroelec-

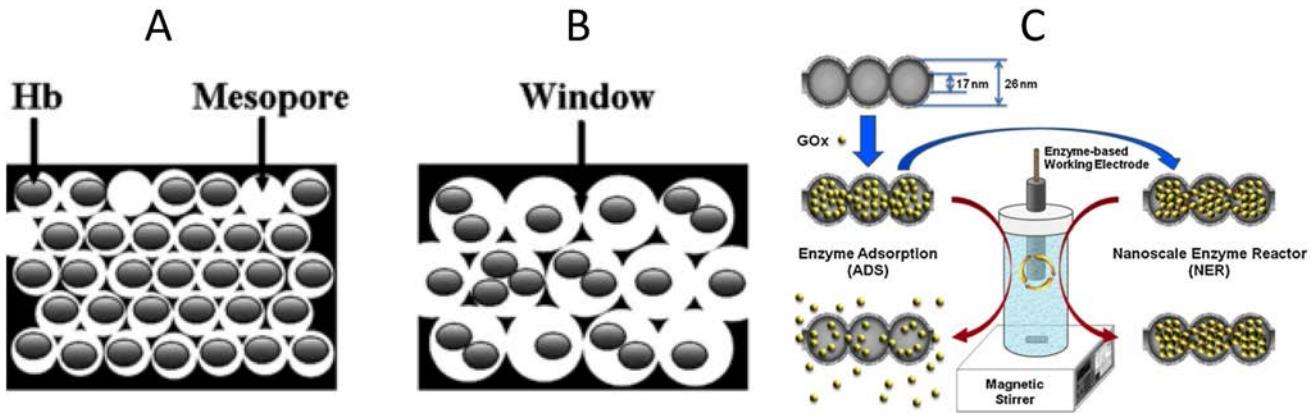

Fig. 2. Schematic diagram of hemoglobin, Hb ($6.4\times5.5\times5.0\ nm^3$), immobilized on ordered graphitized mesoporous carbon with pore sizes of (A) 6 nm and (B) 13 nm [155]. (C) Illustration of the enzyme adsorption and the nanoscale enzyme reactor (NER) in the mesoporous carbon (MSU-F-C). The enzyme in NER was cross-linked in the bottleneck structure of MSU-F-C by treating the adsorbed enzyme with glutaraldehyde, which prevented their leaching (ship-in-a-bottle encapsulation) [218].

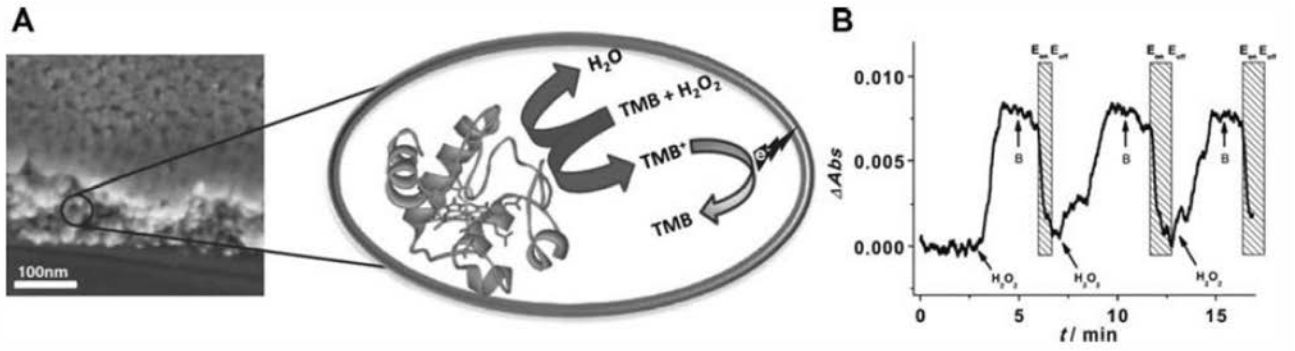

Fig. 3. (A) Side-view of a mesoporous indium tin oxide (mpITO) film obtained by scanning electron microscopy and schematic representation of a nanoreactor consisting of a cytochrome c molecule entrapped in an ITO pore. The catalytic oxidation of 3,30,5,50-tetramethylbenzidine (TMB) in the presence of hydrogen peroxide is also depicted, as well as the electrochemical regeneration of the dye by electron exchange with the conductive ITO pore wall. (B) Absorbance changes at 370 nm of a TMB/cyt c-modified mpITO. The moment of H_2O_2 addition and the applied potential are marked. The experiment is performed in 5 mM potassium phosphate buffer, pH 7.0; the added H_2O_2 solution was 10 mM; the moments when a potential of −0.5 V vs. Ag/AgCl was switched on and off is indicated with "Eon" and "Eoff"; B arrows indicate the moments when a fresh H_2O_2-free buffer was flown. Reprinted from [195]. Anodic current was defined by convention positively in this work.

trochemical biosensing devices. Examples are available for transparent electrode materials such as TiO_2 [186,191], SnO_2 [191,193], ITO [192,195,219], or ATO [75]. Figure 3 illustrates an example of such film with the schematic draw of one of them, based on cytochrome c (Cyt c) immobilized in the porous structure of a transparent and conducting ITO film (Figure 3A). Cyt c is likely to catalyze the oxidation of a color-developing dye, the 3,30,5,50-tetramethylbenzidine (TMB), by hydrogen peroxide, and the reaction was monitored by UV–Vis spectroscopy and direct electrochemistry. Monitoring the adsorption of TMB at 370 nm versus time for successive injections of H_2O_2 enabled the rapid detection of hydrogen peroxide due to the reaction with the dye catalyzed by the protein (Figure 3B). The sensor was regenerated by applying a reducing potential at the mesoporous ITO electrode, as a result of TMB reduction back to the uncolored form.

3.2 Mesoporous Supports for Mediator/Catalyst

In addition to being an attractive host for proteins, mesoporous materials can also provide possibilities for the immobilization of mediators and/or electrocatalytic compounds, as discussed by family of materials in the next Section.

3.2.1 Silica-Based Materials

A strategy employed to overcome the insulating properties of mesoporous silica, which might be a limitation for electrochemical applications, consists in the incorporation of metal nanoparticles (NPs) into the material. In addition to their excellent conductivity properties, NPs can also exhibit catalytic activities and good biocompatibility. A variety of biomolecules have been co-immobilized with metal NPs such as gold, platinum or palladium, among

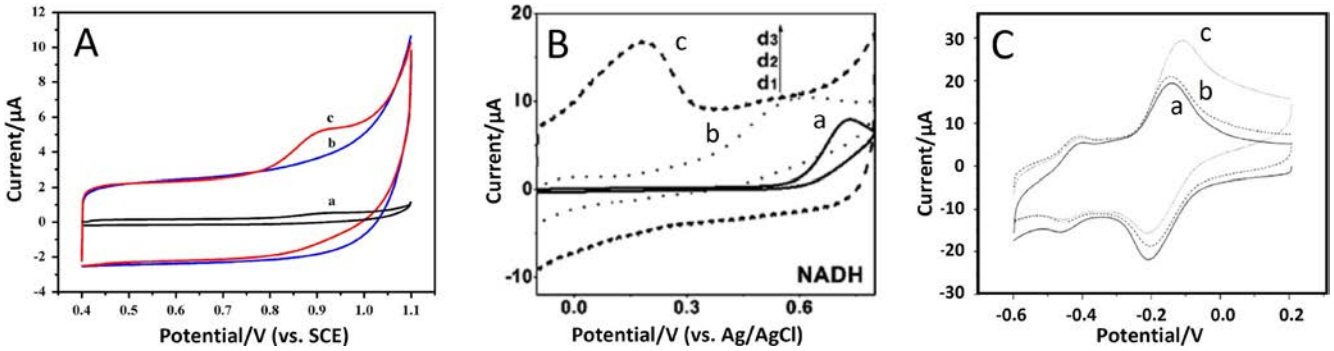

Fig. 4. (A) Cyclic voltammograms recorded with (a) organophosphorus hydrolase (OPH)-bacteria/GCE in 10 μM paraoxon, (b) OPH-bacteria/OMCs/GCE in blank buffer solution, and (c) OPH-bacteria/OMCs/GCE in 10 μM paraoxon (all curves have been obtained in 0.1 M phosphate buffer at pH 7.4; GCE = glassy carbon electrode; OMC = ordered mesoporous carbon) [176]. (B) Cyclic voltammograms recorded using (a) GCE, (b) graphene on GCE, and (c) ordered mesoporous carbons on GCE, in 1 mM NADH (in 0.1 M phosphate buffer at pH 7.0) [164]. (C) Cyclic voltammograms recorded using GCE/OMC loaded with meldola's blue (in 0.05 M phosphate buffer at pH 6.85) in the absence (a) and presence of 1 mM (b) and 5 mM (c) NADH (potential scan rate = 50 mV s^{-1}) [153]. Anodic current was defined by convention positively in these works.

others, including glucose oxidase [104,114,124,136], horseradish peroxidase [114], or hemoglobin [101,110]. MCM-41 [99,102,112,114,117,128], SBA-15 [101,104] and SBA-16 [105] have been mainly used as supports for metal NPs. The presence of NPs in the material was often discussed in terms of affecting the immobilization of the desired biomolecules or enhancing electron transfer processes occurring with the underlaying electrode surface. One can cite the example of a glassy carbon electrode modified by a hybrid system of mesoporous silica particles bearing glucose oxidase incorporating poly(amidoamine) dendrimer encapsulated platinum NPs showing high catalytic activity to the reduction of H_2O_2, which was exploited for glucose determination [120]. In another example, the immobilization of hemoglobin in SBA-15 has been reported to exhibit an improved catalytic activity towards H_2O_2 reduction when gold NPs were incorporated into the mesoporous material [101]. Yet much less developed in electrochemical biosensors, mesoporous silica was also used to immobilize redox mediators, as reported for methylene blue on MCM-41, which was then applied to the detection of catechol using laccase as the protein [117].

3.2.2 Ordered Mesoporous Carbon (OMC) Materials

Compared to mesoporous silica, OMC materials possess the advantage of being electronically conductive, while maintaining the same attractive features of high surface area and pore volume, as well as highly interconnected mesopores facilitating the diffusion of products. They also exhibit intrinsic electrocatalytic properties ascribed to edge-plane graphite sites on the OMC material, which can be exploited to lower the overpotentials and to enhance the sensitivity associated to the electrochemical detection of target analytes [44]. An illustrative example is the microbial biosensor developed for the rapid monitoring of p-nitrophenyl-substituted organophosphates (OPs) [176]. Such biosensor enables the detection of *p*-nitrophenol on glassy carbon electrode during the microbial conversion of paraoxon, which was found to be very limited on the bare electrode and dramatically improved in the presence of OMC (compare curves a for bare electrode and c for OMC on Figure 4A). Meanwhile, the large conductive surface area of OMC resulted in huge capacitive currents (see blank curve b on Figure 4A, as recorded without biomolecule), indicating that full exploitation of such conductive mesoporous materials for electroanalytical purposes would be possible only in case of kinetically-limited electron transfer processes or applying pulsed detection techniques [41]. Another example is the detection of NADH, as reported by Wang et al. [164] who have compared the decrease in overpotential for the oxidation of NADH at a glassy carbon electrode before and after modification with graphene or mesoporous carbon (Figure 4B). As it can be observed on the cyclic voltammograms, the detection of NADH on bare glassy carbon is observed at high potential around +0.7 V (curve a), whereas its modification with graphene (curve b) and mesoporous carbon (curve c) permitted to reduce this overpotential by ~200 mV and ~500 mV, respectively. This effect is critical in order to prevent the detection of interfering species in biosensor based on NAD-dependant dehydrogenases, e.g., alcohol dehydrogenase [145].

In addition to their intrinsic electrocatalytic properties, OMC can be modified with either charge transfer mediators or metal and metal oxides nanoparticles to further facilitate the electron transfer between the electrode surface and the active site of the enzyme or its cofactor. For instance, the immobilization of a mediator such as Meldola's blue on mesoporous carbon facilitates the oxidation of NADH, which was observed at −0.1 V vs. Ag/AgCl (see curves b and c in Figure 4C) instead of +0.2 V on unmodified mesoporous carbon (see curve c in Fig. 4B) [153]. When applied in a device comprising alcohol dehydrogenase, such NADH-sensitive material constitutes an

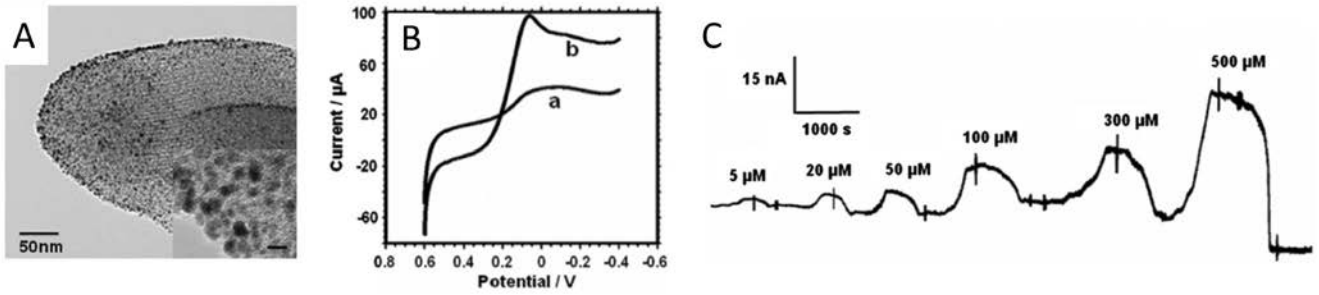

Fig. 5. (A) TEM micrograph of a Pt/PDDA-CMM nanocomposite loaded with 30% Pt (PDDA = poly(diallyldimethylammonium chloride); CMM = carbon mesoporous material). (B) Linear sweep voltammetric responses of the 30% Pt/PDDA-CMM electrodes to (a) 1 mM H_2O_2 in artificial cerebrospinal fluid (pH 7.4) and (b) 1 mM H_2O_2 solution (potential scan rate = 100 mV s^{-1}). (C) Amperometric response for different standard solutions of glucose obtained at 30% Pt/PDDA-CMM/GOx/Nafion modified electrode in the on-line microdialysis system (flow rate = 2.0 mL min^{-1}; applied potential = −200 mV). Reprinted from [172]. Cathodic current was defined by convention positively in this work.

ethanol biosensor exhibiting excellent analytical performance [153]. OMC can be decorated with catalytic nanoparticles, such as gold [165,171,177], platinum [120,143,151,167,172] or palladium [181], but also quantum dots [106], iron oxide [168] or $NiFe_2$ [183]. For example, platinum or gold NPs deposited onto OMC have been reported to catalyze the oxidation and especially the reduction of hydrogen peroxide, which is exploitable for the development of amperometric glucose biosensors by immobilization of glucose oxidase on the nanocomposite [151,165,167]. The addition of such NPs catalysts is particularly useful to lower the overpotentials at values compatible with the selective glucose analysis in real samples, such as blood sugar levels in human serum, which can contain other redox-active species that are likely to interfere with the detection of hydrogen peroxide [167]. More sophisticated nanocomposites have been designed recently for the simultaneous detection of glucose and L-lactate in the central nervous system, based on Pt-loaded OMC [172]. Studies of the influence of increased loadings of Pt from 5% to 50%, and size-dependence of the electrochemical behavior of positively charged polyelectrolyte (diallyldimethylammonium chloride (PDDA)) attached to the carbon material *via* electrostatic interaction, have been carried out for the electrochemical detection of H_2O_2. The presence of Pt NPs was clearly evidenced from TEM imaging (Figure 5A) and the functionalized OMC material displays well-defined electrocatalytic detection of H_2O_2 (see curve b in Figure 5B). This was applied to the determination of glucose or lactate through the detection of H_2O_2 produced by glucose oxidase or L-lactate oxidase (glucose detection is illustrated in Figure 5C).

4 Electrode Configurations

About two third of the enzymatic biosensor applications involving mesoporous materials, as reported to date in the literature, involve a film-based configuration, typically made of particles deposited onto an electrode surface (essentially glassy carbon). The principle is to drop-cast in one or several steps a small volume of solution containing the mesoporous material as a dispersed powder and the protein dissolved in the suspension. Most often, a polymeric binder was useful to ensure mechanical stability (Figure 6A). The polymer can be incorporated into the film or deposited onto the top of the particle/protein assembly [204]. The protocol is very versatile and allows application of many different material particles having submicrometric or micrometric dimensions, in the presence of various proteins. One possible drawback could be the complexity of the resulting electrode assembly that does not allow, sometimes, identifying clearly the relevance of mesoporous materials for protein immobilization since the polymer can also play a significant role in maintaining the protein on the electrode surface. Some films made of particles are prepared without binders [101,110,128,132,153,161,165,190], but most of the reported works are performed with a polymeric binder to favor the mechanical stability of the biosensing layer. The most frequently used polymers are Nafion [102,112,115,120,131,136,137,140,145,147,150–152,154–157,159,160,166,173,176,181,182,187,199], polyvinyl alcohol (PVA) [97–100,104,106,108,117,121,143,188] and chitosan [103,122,129,130,163]. Other polymers have been used, such as gelatin [189], L-lysine [171], poly(dimethyldiallyl ammonium) (PDDA) [172], poly(vinyl butyral) (PVB) [119], or a silicate matrix [107,114]. In another example, polypyrrole was electrochemically deposited into a particle film for protein immobilization [167] and was expected to participate to the stabilization of the assembly. Finally, the additional use of glutaraldehyde, in the presence of bovine serum albumin [153] or not [76,124,196], has been also reported.

Another approach to deposit the mesoporous materials on solid electrode surfaces was via the Layer-by-Layer (LbL) technique [109,141,170] (Figure 6B). The assembly of the bioelectrode involved successively dipping of the electrode in the suspension containing the mesoporous

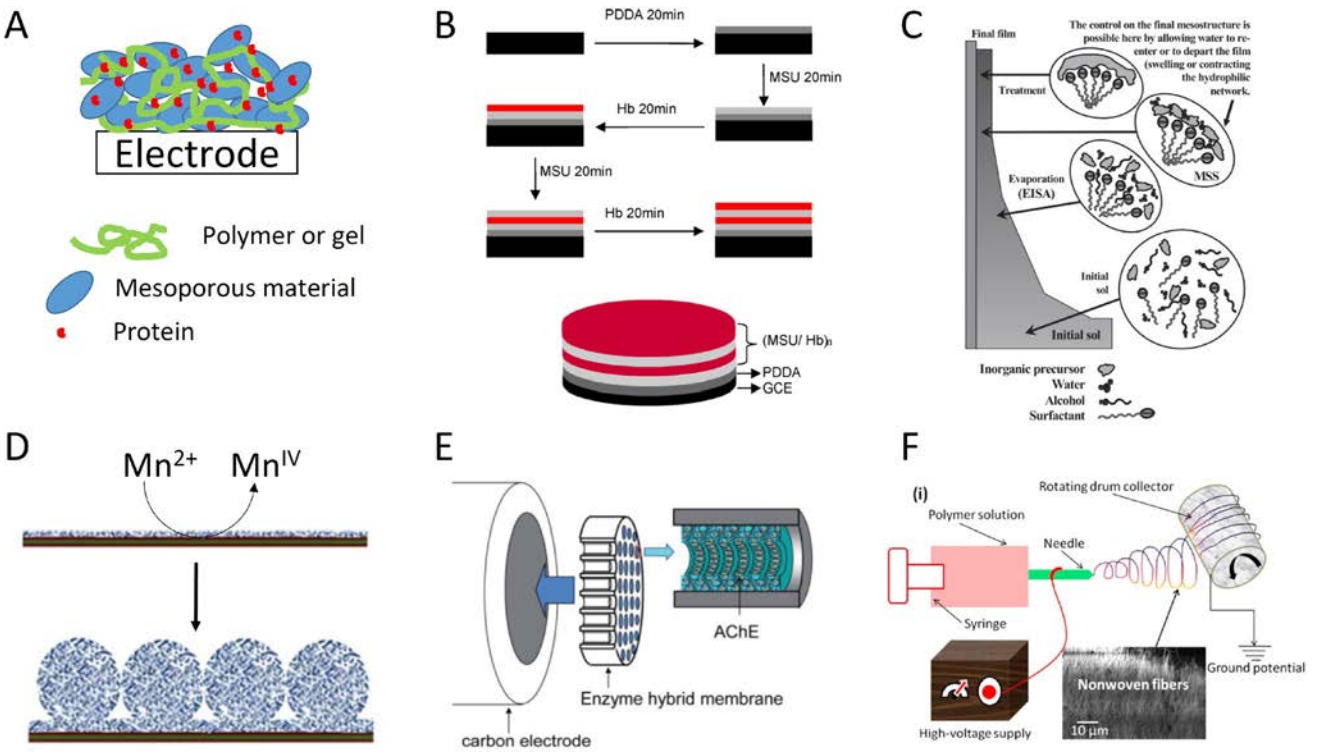

Fig. 6. Illustration of various approaches for preparing electrodes modified with mesoporous materials (used for biosensing purposes): (A) film of mesoporous particles deposited on an electrode surface by drop-casting suspension containing the mesoporous material and the protein (along with a polymeric binder); (B) layer-by-layer deposition of a mesoporous material [109]; (C) Mesostructured thin film prepared by evaporation induced self-assembly (EISA) [221]; (D) Anodic deposition of MnO_2 hierarchical spheres on ITO substrate[197]; (E) AChE–(F127-MST) enzyme hybrid membrane on nylon mesh [135]; (F) synthesis of aligned TiO_2 nanofibers by electrospinning [200].

material and a redox protein [109,141], or a polyelectrolyte (in this latter example the protein was adsorbed into the film after LbL deposition [170]).

Carbon paste electrodes [118,146,168,198] and screen printed electrodes [113,125,126], or cavity microelectrode [149], are other electrode configurations that are popular in electroanalysis and that have been applied for the development of enzymatic biosensors with mesoporous materials. In such case, the mesoporous material bearing the enzyme was simply incorporated as dry powder in the composite carbon paste or ink matrix (or accommodated to the cavity electrode).

Other strategies exploit a particular way to prepare mesoporous materials, i.e., the deposition of few amount of material as thin film onto an electrode surface by controlled evaporation. First the mesoporosity can be introduced by the assembly of nanoparticles, as illustrated for TiO_2 and SnO_2 transparent mesoporous films [186,191,193]. In this configuration, a μm-thick mesoporous film is prepared by "doctor blade" deposition of the aqueous suspension of nanoparticles. This technique is the one usually employed for the deposition of TiO_2 layer in the well-known Grätzel cell [220]. The resulting mesoporous material is however not ordered.

Continuous ordered mesoporous thin films can be prepared by evaporation induced self-assembly (EISA, Figure 6C) [221]. In the field of enzymatic biosensors, niobium films of that type were the first ones reported for protein immobilization [185,73]. Afterwards, amino-functionalized mesoporous silica thin films [105], mesoporous ITO [192], ATO [75], and zirconia thin films [74], have been exploited for the immobilization and the electrochemical investigation of redox proteins, as well as their application for biosensing. One great interest of this configuration is the opportunity that is gives to perform not only electrochemical but also coupled spectroscopic detections [195]. EISA was otherwise applied for the modification of alumina [111,116,135] or polycarbonate [127] membranes. In this case the mesoporous materials, silica-based, fill the larger pores of the membrane, leading to an enzyme hybrid membrane after protein immobilization [135] (Figure 6E). All-organic mesoporous materials can be also used as hosting supports for biomolecules, as exemplified for polyacrylamide-P123 (PAM-P123) composite film immobilizing hemoglobin [203]. An alternative to EISA is the electrodeposition of mesoporous inorganic materials [222]. Mesoporous MnO_2 spheres were prepared by anodic deposition of Mn^{IV} species from a Mn^{2+} solution [197] (Figure 6D). Electrochemistry was also involved in the deposition of hemoglobin/ZrO_2 composite coatings by cycling the potential of a gold electrode in a potential range between −1.1 V and +1.6 V for 25

sweeps [194], and for the deposition of enzyme-integrated phospholipid-templated mesoporous ZnO films [201]. Finally, an alternative approach for the preparation of textured materials is the electrospinning method (Figure 6F). The high voltage applied between a metallic needle of a syringe (filled with the titania starting sol) and an electrode collector allows the formation of mesoporous electrospun TiO_2 nanofiber suitable for bio-functionalization [200].

5 Applications: Biosensors and Analytes

Table is providing an overview of the various enzyme biosensors developed with mesoporous materials. About 25 analytes are summarized there by alphabetical order, from the ascorbic acid to the uric acid. The porous materials, the immobilized biomolecules, the electrode configuration and the analytical performance of the biosensors are reported.

Two target analytes were massively studied, i.e., H_2O_2 [97,98, 100, 101, 103, 105–110,113,115, 118, 122, 127, 130, 141, 144, 147, 154, 155, 157, 160, 161, 170, 180, 183, 185, 73, 188, 190, 191, 193, 194, 199, 203] and glucose [91, 93, 101, 103, 108, 109, 113, 117, 120, 122, 125, 129, 132, 134, 135, 138–141, 145, 154–157, 161, 162, 164, 170–173, 180, 187, 188, 191, 194, 195], H_2O_2 being also in some cases the electroactive species detected in glucose biosensors [103, 108, 109, 113, 117, 122, 125, 132, 135, 140, 141, 156, 157, 161, 162, 170, 172, 173, 180, 191], as well as a series of other analytes (see Table 1).

The detection of these targets involves proteins with distinct characteristics. First, are the heme proteins, i.e., hemoglobin [86, 90, 92, 96–99, 107, 130, 136, 143, 144, 149, 150, 170, 177, 179, 181, 185, 189, 192, 196], myoglobin [98, 106, 113, 157], cytochrome c (Cyt c) [94, 133, 159, 175, 176, 183], microperoxidase from Cyt c [193] and horseradish peroxidase (HRP) [99, 100, 114, 115, 122, 127, 128, 130, 137, 73, 191, 223]. They contain an iron porphyrin complex allowing in many cases a direct electron transfer to occur between this cofactor and the electrode surface. Second, are the oxidases, including the glucose oxidase, that are flavoproteins containing a flavin adenine dinucleotide (FAD) or a flavin adenine mononlucleotide (FMN) cofactor. For the specific example of glucose oxidase, FAD cofactor is located inside the protein and direct electron transfer reactions are difficult to achieve [224]. Other target analytes of concern in this review using oxidases are lactate [125, 126, 172], choline [116] and cholesterol [132, 200]. Other proteins have also been immobilized on electrode surface taking advantage of mesoporous materials, i.e., acethylcholine [135] and cholesterol esterases [200], alcohol [145, 153, 187, 201] and formaldehyde dehydrogenases [111], tyrosinase [99, 121, 171, 76, 213], laccase [117, 163], human sulfite oxidase [75], uricase [137] superoxide dismutase [129] and organophosphorus hydrolase [159,176].

The interest of mesoporous supports in biosensing is either related to the stabilization of the enzyme in its active form or to the capability of the hosting material to favor the electrochemical detection of redox species involved in the enzymatic reaction or the direct electron transfer with the redox proteins. If looking carefully at the information on stability for the various biosensors reported in Table 1, it appears clearly that better stability was achieved with mesoporous silica materials [98, 99, 102, 111, 116, 125, 126, 168] than with others, at least when the information was provided. This quite clear trend was observed with various proteins, such as lactate oxidase [125,126], myoglobin [98], tyrosinase and horseradish peroxidase [99], glucose oxidase [102,168], formaldehyde dehydrogenase [111], choline oxidase [116], or acethylcholine esterase [135]. Concerning the analytical characteristics of the biosensors, the interest of one material versus another one is more difficult to analyze since no clear trend is appearing from the data collected in Table 1. Beside the detection limit or the concentration range that can be reached, the advantage of some material, e.g., mesoporous carbon (either functionalized with organic groups or metal nanoparticle, or not) is to decrease the overpotential for detection of some analytes or to help in the observation of direct transfer reactions with the redox proteins (see Section 3.2). The consequence is here more related to the ability to detect the target analyte in the presence of potential interfering species, e.g., by decreasing the overpotential of NADH oxidation for ethanol analysis [145,153].

The next sections will provide a discussion on the basis of chosen illustrations of the various biosensors that have been reported in the literature with the goal to take advantage of the attractive/unique properties of mesoporous materials to improve the electrochemical detection of the target analyte. The discussion is organized by reference to the proteins immobilized in the biosensor platform, firstly the heme enzymes, secondly the oxidases, and other proteins in a third section.

5.1 Heme Proteins

5.1.1 Cytochrome c and Related Proteins

Cytochrome c (Cyt c, 12.5 kDa) is a quite small size protein ($2.6 \times 3.2 \times 3.0$ nm^3 [225]), thus being a good candidate for immobilization in mesopores, including those of rather small dimensions. The first report on the immobilization of a redox protein in mesoporous materials for biosensing application was implemented with a niobium oxide film deposited on a conducting glass (Figure 7) [73,185]. The film was deposited by dip-coating (see an illustration of this method in Figure 6C) using triblock copolymer Pluronic P123 ($EO_{20}PO_{70}EO_{20}$) as structuring agent and $Nb(Cl_5)/Nb(OC_2H_5)_5$ as the inorganic precursors. The material displayed a uniform pore size centred at about 6.0 nm and a relatively high specific surface area (190 $m^2 g^{-1}$) favorable for the adsorption of Cyt c. Cyt c is sufficiently small for allowing direct electron transfer between the electroactive heme and the electrode surface. Figure 7B displays the electrochemical characterization of

Table 1. Enzymatic electrochemical biosensors based on ordered mesoporous materials.

Analyte	Porous materials		Immobilized biomolecule(s)	Electrode configuration [c]	Analytical performance		Stability	Refs.
	Type [a]	Modifier [b]			Concentration range	Detection limit		
Ascorbic acid	SBA-16	–Pr–NH_2	Cytochrome c (Cyt c)	ITO/(SBA-16-NH_2 + Cyt c)	1×10^{-6}–1.5×10^{-3} M	5×10^{-7} M	20 days	[105]
Catechol	CMK-3 (SBA-15/sucrose)	Cu	Laccase (Lac)	Au/(OMC-Cu/Lac + chitosan)	6.7×10^{-7}–1.57×10^{-5} M	$6.7\times10^{-}$ M	30 days (95 %)	[163]
Catechol	OMC	Au NPs	Tyrosinase(Tyr)	GCE/Au/(L)-lysine/OMC-Au/Tyr	4×10^{-7}–8×10^{-5} M	2.5×10^{-8} M	1 month (85 %)	[171]
Catechol	MCM-41	Methylene Blue (MeB)	Laccase (Lac)	Au/MCM-41-MeB/PVA/lac	4×10^{-6} M–8.8×10^{-5} M	3.31×10^{-7} M	–	[117]
Catechol	MCM-41	–	Tyrosinase (Tyr) + horseradish peroxidase (HRP)	GCE/(MCM-41-Tyr-HRP + PVA)	2×10^{-7}–4.8×10^{-4} M	7.8×10^{-10} M	–	[99]
Catechol	MCN	–	Tyrosinase(Tyr)	GCE/MCN/Tyr	5×10^{-7}–9.5×10^{-6} M	1.5×10^{-8} M	1 month (87 %)	[76]
Catechol	Mg-MCM-41	–	Laccase (Lac)	Au/Mg-MCM-41/PVA/Lac	9.4×10^{-7}–1.02×10^{-5} M	5.3×10^{-9} M	1 month (91 %)	[134]
Catechol	OMC	Au NPs	Tyrosinase(Tyr)	Au/(L)-lysine/OMC-Au/Tyr	1×10^{-7}–1.7×10^{-4} M	2.5×10^{-8} M	–	[177]
Catechol	OMC	Co_3O_4 nanorods	Tyrosinase(Tyr)	GCE/OMC-Tyr-Co_3O_4/chitosan	5.0×10^{-8}–1.3×10^{-5} M	2.5×10^{-8} M	–	[213]
Choline	F127-M	–	Choline oxidase (ChOx)	Pt/F127-M–ChOx	5×10^{-6}–$8\times10^{-}4$ M	5×10^{-6} M	80 days (85 %)	[116]
Cholesterol oleate	TiO_2-NF	–COOH, –CHO	Cholesterol esterase (ChEt) + Cholesterol oxidase (ChOx)	ITO/TiO_2-NF/ChEt-ChOx	25–400 mg/dL	$4.9\times10^{-}4$ M	3 weeks (95 %)	[200]
Cholesterol	Fe_3O_4@SiO_2–Au@mp-SiO_2 microspheres	–	Cholesterol oxidase (COx)	GCE/Fe_3O_4@SiO_2–Au@mp-SiO_2/COx	8.3×10^{-4}–2.62×10^{-3} M	2.8×10^{-7} M	1 weeks (90 %)	[132]
Dichlorvos	F127-MST	–	Acetylcholinesterase (AChE)	GCE/(F127-MST)-AChE	Up to 100 ppb	14 ppb	2 months (90 %)	[135]
Ethanol	CMK-3 (SBA-15/sucrose)	Meldola's Blue (MB)	Alcohol dehydrogenase (ADH)	GCE/OMC-MB/(ADH + BSA + GluA)	Up to 6×10^{-3} M	1.9×10^{-5} M	15 days (22 %)	[153]
Ethanol	Mesop. TiO_2	–	Alcohol dehydrogenase (ADH)	GCE/TiO_2-Nafion/ADH	4.0×10^{-5}–1×10^{-1} M	1.0×10^{-5} M	2 weeks (75 %)	[187]
		CNT		GCE/CNT-TiO_2-Nafion/ADH	1.0×10^{-5}–1×10^{-1} M	5.0×10^{-6} M		
Ethanol	CMK-3 (SBA-15/sucrose)	-	Alcohol dehydrogenase (ADH)	GCE/OMC/(ADH + BSA)/GluA/Nafion	3.0×10^{-4}–1.3×10^{-2} M	1.0×10^{-4} M	1 month (91 %)	[145]
Ethanol	Mesop. ZnO film	–	Alcohol dehydrogenase (ADH)	Au/ZnO/DPGP-ADH	1×10^{-5}–6.5×10^{-4} M	2.1×10^{-6} M	20 days (93 %)	[201]
Formaldehyde	FSM-8	–	Formaldehyde dehydrogenase (FDH)	GCE/FSM-8–FDH	1.2×10^{-6}–6.17×10^{-4} M	1.2×10^{-6} M	80 days (100 % and 90 %)	[111]
	P123-M			GCE/(P123-M)–FDH		1.1×10^{-6} M		
Glucose	CMK-3 (SBA-15/sucrose)	–	Glucose oxidase (GOD)	GCE/OMC/(GOD + BSA)/GluA/Nafion	5.0×10^{-4}–1.5×10^{-2} M	1.5×10^{-4} M	–	[145]
Glucose	2D-OMC (SBA-15/sucrose)	–	Glucose oxidase (GOD)	GCE/(OMC-GOD + Nafion)	Up to 7.94×10^{-3} M	1.0×10^{-5} M	45 days (86 %)	[152]
	3D-OMC (FDU-5/sucrose)				Up to 9.90×10^{-3} M	1.0×10^{-5} M		
Glucose	CMK-3 (SBA-15/furfuryl alcohol)	Iron oxide	Glucose oxidase (GOD)	Pt/(OMC-Fe_3O_4 + GOD)/Nafion	2×10^{-4}–1.0×10^{-2} M	8×10^{-5} M	1 week (90 %)	[156]

Table 1. (Continued)

Analyte	Porous materials		Immobilized biomolecule(s)	Electrode configuration [c]	Analytical performance		Stability	Refs.
	Type [a]	Modifier [b]			Concentration range	Detection limit		
Glucose	CMK-3 (SBA-15/sucrose)	Pt NPs	Glucose oxidase (GOD)	GCE/(OMC-Pt + gelatin + -GOD + GluA)	4×10^{-5}–1.22×10^{-2} M	1×10^{-6} M	30 days (95 %)	[143]
Glucose	CMK-3 (SBA-15/sucrose)	Pt NPs	Glucose oxidase (GOD)	GCE/(OMC-Pt + Nafion) imp. GOD	Up to 7.94×10^{-3} M	1×10^{-6} M	27 days (31 %)	[151]
Glucose	CMK-3 (SBA-15/sucrose)	Pt NPs	Glucose oxidase (GOD)	Au/OMC-Pt/PPy-GOD	5×10^{-5}–3.7×10^{-3} M	5×10^{-5} M	15 days (50 %)	[167]
Glucose	CMK-3 (SBA-15/sucrose)	Au NPs	Glucose oxidase (GOD)	GCE/OMC-Au/GOD	5.0×10^{-5}–2.2×10^{-2} M	–	30 days (88 %)	[165]
Glucose	FDU-15	–	Glucose oxidase (GOD)	GCE/(OMC-GOD + Nafion)	1×10^{-4}–1.0×10^{-3} M	9×10^{-5} M	–	[150]
Glucose	MCM-41	–	Glucose oxidase (GOD)	GCE/(MCM-41-GOD + Nafion)	3.2×10^{-4}–1.5×10^{-2} M	1.8×10^{-4} M	3 month (89 %)	[102]
Glucose	SBA-15	–Pr-NH_2, Au NPs	Glucose oxidase (GOD)	GCE/(amine SBA-15 + GOD + Au NPs)	2×10^{-5}–1.4×10^{-2} M	1.5×10^{-5} M	1 month (90 %)	[104]
Glucose	MSCF	–	Glucose oxidase (GOD)	GCE/(MSCF/GOD + Nafion)	5.0×10^{-5}–5.0×10^{-3} M	3.4×10^{-5} M	2 weeks (94 %)	[140]
Glucose	IFMC	Pd NPs	Glucose oxidase (GOD)	GCE/Pd NPs-IFMC/GOD/Nafion)	5×10^{-4}–10^{-2} M	1.9×10^{-4} M	2 weeks (91 %)	[181]
Glucose	PMS	Au NPs	Glucose oxidase (GOD)	GCE/RGO-PMS-AuNPs-GOD	1×10^{-5}–8×10^{-3} M	2.5×10^{-6} M	1 month (92 %)	[136]
Glucose	LMC	Co(salen)	Glucose oxidase (GOD)	GCE/LMC/Co(salen)/GOD	5×10^{-4}–1.3×10^{-2} M	2×10^{-4} M	10 days (92 %)	[173]
Glucose	Hierarchical MnO_2 spheres	–	Glucose oxidase (GOD)	GCE/Nafion/MnO_2/GOD	3.5×10^{-7}–3.15×10^{-3} M	3.5×10^{-7} M	–	[197]
Glucose	MSN	–	Glucose oxidase (GOD)	GCE/GOD–MSN/Nafion	4×10^{-5}–4.8×10^{-3} M	2×10^{-5} M	20 days (93.5 %)	[131]
Glucose	MCM-41	–	Glucose oxidase (GOD) + Horseradish peroxidase (HRP)	GCE/MCM-41/(GOD + HRP)/Nafion	2×10^{-5}–1×10^{-3} M	8.6×10^{-6} M	25 days	[128]
Glucose	CMM	Pt NPs/PDDA	Glucose oxidase (GOD)	GCE/$Pt_{30\,\%}$/PDDA-CMM/GOD/Nafion	5×10^{-7}–5×10^{-5} M	2.5×10^{-6} M	2 weeks (88 %)	[172]
Glucose	Mesop. HAP + TiO_2 +	MWCNTs	Glucose oxidase (GOD)	GCE/MWCNTs/TiO_2/HAP/GOD	1×10^{-5}–1.52×10^{-2} M	2×10^{-6} M	1 month (86 %)	[196]
Glucose	OMC	Iron oxide	Glucose oxidase (GOD)	CPE/OMC-Fe_3O_4/GOD	0.5×10^{-3}–10×10^{-3} M	0.2×10^{-3} M	2 months (90 %)	[168]
Glucose	SBA-15	–Pr–NH_2	Glucose oxidase (GOD)	GCE/amine SBA-15/GOD	4×10^{-4}–1.3×10^{-2} M	–	–	[133]
Glucose	Mesop. ZnO film	–	Glucose oxidase (GOD)	Au/ZnO/DPGP-GOD	1×10^{-3}–5×10^{-2} M	3.6×10^{-6} M	–	[201]
Glucose	Rod-like SiO_2	–	Glucose oxidase (GOD)	Pt/(rod-like SiO_2 + GOD)	2×10^{-5}–7.5×10^{-3} M	3.2×10^{-6} M	–	[119]
				Pt/(GOD/rod-like SiO_2)	1×10^{-5}–7.5×10^{-3} M	3.2×10^{-6} M		
	Vesicle-like SiO_2	–		Pt/(vesicle-like SiO_2 + GOD)	2×10^{-5}–7.5×10^{-3} M	1.35×10^{-5} M	–	
				Pt/(GOD/vesicle-like SiO_2)	1×10^{-5}–7.5×10^{-3} M	1.6×10^{-6} M		
	Vesicle-like SiO_2	–NH_2		Pt/(vesicle-like SiO_2-NH_2 + GOD)	1×10^{-4}–7.5×10^{-3} M	1.44×10^{-5} M	–	
				Pt/(GOD/vesicle-like SiO_2-NH_2)	1×10^{-5}–7.5×10^{-3} M	5.2×10^{-6} M		

Table 1. (Continued)

Analyte	Porous materials		Immobilized biomolecule(s)	Electrode configuration [c]	Analytical performance		Stability	Refs.
	Type [a]	Modifier [b]			Concentration range	Detection limit		
Glucose	MSN	Pt NPs	Glucose oxidase (GOD)	GCE/MSN–Pt–GOD	1×10^{-6}–2.6×10^{-5} M	8×10^{-7} M	1 month (90 %)	[124]
Glucose	OMS	Pt NPs	Glucose oxidase (GOD)	GCE/OMS/Pt-DENs/GOD	2×10^{-5}–1×10^{-2} M	4×10^{-6} M	1 month (73.5 %)	[120]
Glucose	BGMC	–	Glucose oxidase (GOD)	GCE/BGMC/GOD	Up to 7.49×10^{-3} M	1.0×10^{-5} M	30 days (95 %)	[166]
Glucose	OMC	–	Glucose oxidase (GOD)	Pt-cUME/(OMC + GOD + IL)	1×10^{-5}–8×10^{-5} M	–	3 weeks (93 %)	[149]
Glucose	SBA-15	Au NPs	Glucose oxidase (GOD) + Horseradish peroxidase (HRP)	GCE/SBA-15-Au–HRP + GOD	1×10^{-6}–4.8×10^{-5} M	5×10^{-7} M	2 weeks (91 %)	[114]
Glucose	SBA-15	–	Glucose oxidase (GOD)	GCE/SBA-15-GOD/Nafion	2×10^{-4}–1×10^{-3} M	7×10^{-5} M	–	[112]
Glucose	Mesop. MnO_2	–	Glucose oxidase (GOD)	GCE/gelatin–MnO_2–GOD	9×10^{-7}–2.73×10^{-3} M	1.8×10^{-7} M	1 week (90 %)	[189]
Glucose	OMC	–	Glucose oxidase (GOD)	OMCPE/GOD	Up to 15×10^{-3} M	7.2×10^{-5} M	–	[146]
Glucose	MCF	–	Pyranose oxidase (POx)	GCE/MCF/POx	Up to 1×10^{-3} M	–	–	[182]
			Glucose oxidase (GOD)	GCE/MCF/GOD	Up to 8×10^{-3} M	–		
Glucose	OMC	$NiFe_2$ NPs	Glucose oxidase (GOD)	GCE/$NiFe_2$-OMC/Nafion/GOD/Nafion	4.86×10^{-5}–1.25×10^{-2} M	2.7×10^{-6} M	4 weeks (95 %)	[183]
Glucose	Mesop. ZrO_2	Platinum	Glucose oxidase (GOD)	FTO/Pt@MZF/GOD	2.5×10^{-5}–1.1×10^{-3} M & 2.1×10^{-3}–6.8×10^{-3} M	–	–	[74]
Glucose	CNPs	Fc-MeOH	Glucose oxidase (GOD)	GCE/CNP-GOD/Fc-MeOH	Up to 6×10^{-2} M	–	–	[175]
Hydrogen peroxide	HMSM	–	Horseradish peroxidase (HRP)	GCE/HMSM/HRP	Up to 3.5×10^{-2} M	–	–	[127]
Hydrogen peroxide	SBA-16	–Pr–NH_2	Cytochrome c (Cyt c)	ITO/(amine-MS + Cyt c)	5×10^{-6}–2×10^{-3} M	5×10^{-6} M	20 days	[105]
Hydrogen peroxide	HMS	–	Horseradish peroxidase (HRP)	GCE/(HMS-HRP + PVA)	2×10^{-7}–4.2×10^{-5} M	1.7×10^{-9} M	1 month (95 %)	[100]
Hydrogen peroxide	SBA-15	–	Hemoglobin (Hb)	GCE/(SBA-15-Hb + silica sol)	1×10^{-8}–1×10^{-7} M	2.3×10^{-9} M	20 days	[107]
Hydrogen peroxide	SBA-15	Au NPs	Hemoglobin (Hb)	GCE/(SBA-15-Hb-Gold)	5×10^{-6}–1×10^{-2} M	1×10^{-6} M	–	[101]
Hydrogen peroxide	BMS-CS	–	Hemoglobin (Hb)	GCE/(BMS-CS-Hb)	5×10^{-6}–2.1×10^{-4} M	1.7×10^{-6} M	1 month	[103]
Hydrogen peroxide	MCFs	QDs	Myoglobin (Mb)	GCE/(MCFs-Mb-QDs)/PVA	2.5×10^{-6}–6.0×10^{-5} M	0.7×10^{-6} M	1 month (96 %)	[106]
Hydrogen peroxide	HMS	–	Hemoglobin (Hb)	GCE/(HMS-Hb + PVA)	4×10^{-7}–6×10^{-6} M	1.86×10^{-9} M	1 month (96 %)	[97]
Hydrogen peroxide	HMS	–	Myoglobin (Mb)	GCE/(HMS-Mb + PVA)	4×10^{-7}–1.24×10^{-4} M	6.2×10^{-8} M	3 month (92 %)	[98]
Hydrogen peroxide	CMK-3 (SBA-15/sucrose)	–COOH	Hemoglobin (Hb)	GCE/{Chitosan/OMC-Hb}$_n$	1.2×10^{-6}–5.7×10^{-5} M	6×10^{-7} M	30 days	[141]
Hydrogen peroxide	GMC-6 (SiO_2 pellets/PS)	–	Hemoglobin (Hb)	GCE/(OMC-Hb + Nafion)	1×10^{-6}–1.84×10^{-4} M	1×10^{-7} M	16 days (97 %)	[155]

Table 1. (Continued)

Analyte	Porous materials		Immobilized biomolecule(s)	Electrode configuration [c]	Analytical performance		Stability	Refs.
	Type [a]	Modifier [b]			Concentration range	Detection limit		
Hydrogen peroxide	GMC-380	–	Hemoglobin (Hb)	GCE/(OMC-Hb + Nafion)	1×10^{-6}–2.67×10^{-4} M	1×10^{-7} M	21 days (90 %)	[154]
Hydrogen peroxide	Macroporous carbon	–COOH	Cytochrome *c* (Cyt *c*)	OMC-Cyt *c* monolith	2.0×10^{-5}–2.4×10^{-4} M	1.46×10^{-5} M	1 month (86 %)	[144]
Hydrogen peroxide	MCWC	–COOH	Hemoglobin (Hb)	GCE/OMC-Hb/Nafion	1.0×10^{-5}–8.0×10^{-5} M	–	weeks	[147]
Hydrogen peroxide	FDU-15	–	Hemoglobin (Hb)	GCE/OMC film imp. Hb	2×10^{-6}–3×10^{-4} M	8×10^{-7} M	30 days (90 %)	[161]
Hydrogen peroxide	OMCN	–	Cytochrome c (Cyt c)	ITO/(MCNs/PDDA)/Cyt c	5×10^{-6}–1.5×10^{-3} M	1×10^{-6} M	20 days (82 %)	[170]
Hydrogen peroxide	Polyacrylamide (PAM)-P123 composite film	–	Hemoglobin (Hb)	GCE/PAM-P123/Hb/Nafion	1×10^{-6}–3×10^{-5} M	4×10^{-7} M	1 month (90 %)	[203]
Hydrogen peroxide	Mesop. ZrO_2	–	Hemoglobin (Hb)	Au/ZrO_2-Hb	1.75×10^{-7}–4.9×10^{-3} M	1×10^{-7} M	–	[194]
Hydrogen peroxide	(CNTs)-SBA-15	–	Horseradish peroxidase (HRP)	Au-chitosan/CNTs-SBA-15-HRP	1×10^{-6}–7×10^{-3} M	5×10^{-7} M	1 month (83 %)	[122]
Hydrogen peroxide	Mesop. SnO_2	–	Microperoxidase (MP-11)	ITO/SnO_2-PLL/MP-11	5×10^{-8}–3×10^{-5} M	5×10^{-8} M	–	[193]
Hydrogen peroxide	MCFs	–	Myoglobin (Mb)	GCE/MCFs–Mb	3.5×10^{-6}–2.45×10^{-4} M	1.2×10^{-6} M	20 days (95 %)	[157]
Hydrogen peroxide	FDU-15	Platinum	Hemoglobin (Hb)	GCE/PDDA/FDU-15-Pt/Hb/Nafion	2×10^{-6}–6×10^{-2} M	1.0×10^{-6} M	20 days (96 %)	[160]
Hydrogen peroxide	Mesop. ITO	–	Cytochrome c (Cyt c)	ITO/mpITO/Cyt-c	1.3×10^{-7}–6.7×10^{-7} M	–		[192]
Hydrogen peroxide	MCM-41	–	Hemoglobin (Hb)	CILE – MCM/Hb	5×10^{-6}–3.1×10^{-4} M	5×10^{-8} M	2 weeks (100 %)	[118]
Hydrogen peroxide	Mesop. TiO_2	–	Horseradish peroxidase (HRP)	CG/TiO_2/HRP	–	4×10^{-8} M	–	[191]
	Mesop. SnO_2			CG/SnO_2-PLL/HRP	1×10^{-6}–2×10^{-5} M	1×10^{-6} M		
Hydrogen peroxide	MSHS	–	Horseradish peroxidase (HRP)	GC/Nafion/MSHS/HRP	3.9×10^{-6}–1.4×10^{-4} M	1.2×10^{-6} M	20 days	[115]
Hydrogen peroxide	SBA-15	Pd NPs	Hemoglobin (Hb)	GCE/SBA-15/Pd/Hb	1.8×10^{-6}–1.19×10^{-4} M	8×10^{-7} M	20 days (95 %)	[110]
Hydrogen peroxide	Mesop. Nb_2O_5 spheres	–	Hemoglobin (Hb)	GCE/Nb_2O_5-Hb	5×10^{-6}–1.1×10^{-2} M	–	–	[199]
Hydrogen peroxide	MSFs	–	Hemoglobin (Hb)	GCE/PVA–MSF–BMIM PF6-Hb	2×10^{-7}–2.8×10^{-5} M	8×10^{-8} M	15 days (96 %)	[108]
Hydrogen peroxide	Mesop. TiO_2	–	Hemoglobin (Hb)	GCE/TiO_2/Hb	2×10^{-6}–2.75×10^{-5} M	1×10^{-6} M	1 month	[190]
Hydrogen peroxide	Al-MSU-S	–	Hemoglobin (Hb)	GCE/PDDA/(Al-MSU/Hb)$_n$	1.0×10^{-6}–1.86×10^{-4} M	5.0×10^{-7} M	15 days (92 %)	[109]
Hydrogen peroxide	Mesop. Al_2O_3	–	Hemoglobin (Hb)	GCE/PVA-Al_2O_3-Hb	1.95×10^{-7}–2.05×10^{-5} M	1.95×10^{-8} M	2 weeks	[188]

Table 1. (Continued)

Analyte	Porous materials		Immobilized biomolecule(s)	Electrode configuration [c]	Analytical performance		Stability	Refs.
	Type [a]	Modifier [b]			Concentration range	Detection limit		
Hydrogen peroxide	Mesop. Nb_2O_5	–	Cytochrome c (Cyt c)	ITO/Nb_2O_5/Cyt-c	–	1.0×10^{-5} M	1 month (90 %)	[73]
			Horseradish peroxidase (HRP)	ITO/Nb_2O_5/HRP	1×10^{-7}–1×10^{-4} M	–		
Hydrogen peroxide	Mesop. Nb_2O_5	–	Cytochrome c (Cyt c)	ITO/Nb_2O_5/Cyt-c	7×10^{-5}–5×10^{-3} M	–	–	[185]
Hydrogen peroxide	KIT-6	–	Myoglobin (Mb)	SPE/Mb-KIT-6/Nafion	1.0×10^{-6}–8.96×10^{-6} M	–	–	[113]
Hydrogen peroxide	CNPs	Methylene Blue (MeB)	Horseradish peroxidase (HRP)	GCE/CNP-MeB-HRP	Up to 1.5×10^{-2} M	–	–	[175]
Hydrogen peroxide	MCC	–	Hemoglobin (Hb)	MCCE/Hb	1×10^{-6}–2.2×10^{-4} M	4×10^{-7} M	2 weeks (95 %)	[180]
Hydroquinone	OMC	Au NPs	Tyrosinase(Tyr)	GCE/Au/(L)-lysine/OMC–Au/Tyr	4×10^{-7}–8×10^{-5} M	5×10^{-8} M	–	[171]
Hydroquinone Catechol	OMC	Au NPs	Tyrosinase(Tyr)	GCE/Au/(L)-lysine/OMC–Au/Tyr	1×10^{-7}–1.1×10^{-4} M	2.5×10^{-8} M 5×10^{-8} M	–	[177]
Lactic acid	FSM-8	–	Lactate oxidase (LOD)	SPCE-PB/FSM-8-LOD/HPM	1.5×10^{-7}–1.1×10^{-3} M	1.5×10^{-7} M	200 days	[126]
L-Lactate	FSM-8	–	Lactate oxidase (LOD)	SPCE-CoPC/Nafion/FSM-8-LOD	1.83×10^{-5}–1.5×10^{-3} M	1.8×10^{-5} M	9 month (98 %)	[125]
L-Lactate	CMM	Pt NPs/PDDA	Lactate oxidase (LOD)	GCE/$Pt_{30\%}$/PDDA-CMM/LOD/Nafion	5×10^{-7}–5×10^{-5} M	1.7×10^{-6} M	–	[172]
Methyl parathion	OMC	–	Organophosphorus hydrolase (OPH)	GCE/OMC/bacteria-OPH-	8×10^{-8}–3×10^{-5} M	1.5×10^{-8} M	–	[176]
Nitrite	HMS	–	Hemoglobin (Hb)	GCE/(HMS-Hb + PVA)	2×10^{-7}–3.8×10^{-6} M	6.11×10^{-7} M	1 month (93 %)	[97]
Nitrite	HMS	–	Myoglobin (Mb)	GCE/(HMS-Mb + PVA)	8×10^{-6}–2.16×10^{-4} M	8.0×10^{-7} M	3 month (89 %)	[98]
Nitrite	Mesop. Al_2O_3	–	Hemoglobin (Hb)	GCE/PVA-Al_2O_3-Hb	2×10^{-7}–1×10^{-2} M	3×10^{-5} M	20 days	[188]
Nitric oxide	Mesop. TiO_2	–	Hemoglobin (Hb)	FTO/TiO_2/Hb	1×10^{-6}–1.5×10^{-5} M (electrochemistry)	4×10^{-9} M (optical)	–	[186]
Nucleic acid	MCN	Au NPs	Streptavidin-horseradish peroxidase (SA-HRP)	GCE/MCN-Au/SA-HRP-scaffolded-GNCs	1×10^{-17}–1×10^{-9} M	8×10^{-18} M	–	[223]
Paraoxon	OMC	–	Organophosphorus hydrolase (OPH)	GCE/CB/OMC/OPH	2×10^{-7}–8×10^{-6} M	1.2×10^{-7} M	–	[159]
Paraoxon	OMC	–	Organophosphorus hydrolase (OPH)	GCE/OMC/bacteria-OPH	5×10^{-8}–2.5×10^{-5} M	9×10^{-9} M	1 month (70 %)	[176]
Parathion	OMC	–	Organophosphorus hydrolase (OPH)	GCE/OMC/bacteria-OPH	5×10^{-8}–2.5×10^{-5} M	1×10^{-8} M	–	[176]
Phenol	MCM-41	–	Tyrosinase (Tyr) + horseradish peroxidase (HRP)	GCE/(MCM-41-Tyr-HRP + PVA)	2×10^{-7}–2.3×10^{-4} M	4.1×10^{-9} M	3 month (90 %)	[99]
p-Cresol	MCM-41	–	Tyrosinase (Tyr) + horseradish peroxidase (HRP)	GCE/(MCM-41-Tyr-HRP + PVA)	2×10^{-7}–2.0×10^{-4} M	3.9×10^{-9} M	–	[99]
Phenol	MCN	–	Tyrosinase(Tyr)	GCE/MCN/Tyr	5×10^{-7}–9.5×10^{-6} M	1.02×10^{-8} M	–	[76]
Phenol	Fe_3O_4@SiO_2 microspheres	–	Tyrosinase(Tyr)	GMCE/Fe_3O_4@SiO_2-Tyr	1.0×10^{-9}–1.0×10^{-5} M	1.0×10^{-9} M	1 month (87 %)	[121]

Table 1. (Continued)

Analyte	Porous materials		Immobilized biomolecule(s)	Electrode configuration [c]	Analytical performance		Stability	Refs.
	Type [a]	Modifier [b]			Concentration range	Detection limit		
Superoxide anions	MSLHNs	–	Superoxide dismutase (SOD)	Au/(MSLHN-chitosan)/SOD	3.11×10^{-6}–1.77×10^{-4} M	8×10^{-7} M	1 month (92%)	[129]
Sulfite	Mesop. Sb-doped SnO_2 (ATO)	–	Human sulfite oxidase (hSO)	ITO/ATO-hSO	5×10^{-7}–2×10^{-4} M	–	–	[75]
Trichloroacetic acid	Mesop. Fe_3O_4 spheres	–	Hemoglobin (Hb)	CILE/Fe_3O_4–Hb/chitosan	2.4×10^{-3}–2×10^{-2} M	3.3×10^{-5} M	1 month (91%)	[198]
Uric acid	MCM-41	–	Uricase + horseradish peroxidase (HRP)	GCE/(MCM-41 + uricase + HRP)/Nafion	2×10^{-6}–1×10^{-5} M	3.3×10^{-7} M	30 days	[137]

Abbreviations: SBA, Santa Barbara Amorphous; CMK, carbon mesostructures at KAIST; OMC, ordered mesoporous carbon; MCM, Mobil Composition of Matter; MCN, mesoporous carbon nitride material; Mg-MCM-41, Magnesium-containing mesoporous silica sieve; F127-M, F-127 block copolymer mesoporous membrane; TiO_2-NF, TiO_2 nanofibers; Fe_3O_4@SiO_2–Au@mpSiO_2, multicomponent core-shell microspheres (amino-functionalized and Au nanoparticles-modified, silica-coated Fe_3O_4 microspheres overcoated with a shell of CTAB-based mesoporous silica); F127-MST, hybrid mesoporous silica membrane; Mesop., mesoporous; FSM, Folded sheets mesoporous material; P123-M, P-123 block copolymer mesoporous silica; FDU, Fudan University (in Shanghai Materials); MSCF, mesocellular silica-carbon nanocomposite foam; IFMC, ionic liquid derived fibrillated mesoporous carbon; PMS periodic mesopourous silica; LMC, large mesoporous carbon; MSN, mesoporous silica nanoshpere; CMM, carbon mesoporous material; HAP, hydroxyapatite; OMS, ordered mesoporous silica; BGMC, bicontinuous gyroidal mesoporous carbon; MCF, mesocellular carbon foam; CNPs, mesoporous carbon nanoparticles; HMSM, hybrid mesoporous silica membrane; HMS, hexagonal mesoporous silica; BMS-CS, bimodal mesoporous silica and chitosan hybrid film; GMC-6 (SiO_2 pellets/PS), graphitized mesoporous carbon obtained from pyrolysis/carbonization of polystyrene impregnated silica pellets prepared from pressed silica particles; GMC-380, graphitized macroporous carbon (380 nm pore size); MCWC, mesoporous carbon/whisker-like carbon; OMCN, ordered mesoporous carbon nanospheres; CNTs, carbon nanotubes; MSHS, mesoporous silica hollow sphere; MSFs, mesocellular siliceous foams; Al-MSU-F, aluminosilicate, mesostructured cellular foam; KIT, Korean Institute of Technology; MCC, mesoporous carbon ceramic; MSLHNs, mesoporous silica-(L)-lysine hybrid nanodisks; [b] Abbreviations: -Pr-NH_2, aminoprolyle; NPs, nanoparticles; NPs, nanoparticles; CNT, carbon nanotube; Co(salen), cobalt(II) Schiff base; PDDA, poly(diallyl-dimethyl-ammonium chloride); MWCNTs, multi-walled carbon nanotubes; Fc-MeOH, ferrocene methanol; QDs, quantum dots. [c] Abbreviations: Acronyms used for biomolecules are found on the left column beside this one; ITO, indium-tin oxide; GCE, glassy carbon electrode; OMC, ordered mesoporous carbon; MeB, methylene blue; PVA, poly(vinyl alcohol); MCN, mesoporous carbon nitride; F127-M, F-127 block copolymer mesoporous membrane; TiO_2-NF, TiO_2 nanofibers; Fe_3O_4@SiO_2–Au@mpSiO_2, Core Au nanoparticles-modified, silica-coated Fe_3O_4 with mesoporous silica shell; MB, Meldola's Blue; BSA, bovin serum albumin; GluA, glutaraldehyde; CNT, carbon nanotube; DPGP, 1,2-dipalmitoyl-sn-glycero-3-phosphate monosodium salt; FSM, Folded sheets mesoporous material; P123-M, P-123 block copolymer mesoporous silica; imp., impregnated; PPy-GOD, electrogenerated polypyrrole in the presence of glucose oxidase; MSCF, mesocellular silica-carbon nanocomposite foam; IFMC, ionic liquid derived fibrillated mesoporous carbon; RGO-PMS reduced graphene oxide–periodic mesopourous silica; LMC, large mesoporous carbon; Co(salen), cobalt(II) Schiff base; MSN, mesoporous silica nanoshpere; PDDA, poly(diallyl-dimethyl-ammonium chloride); CMM, carbon mesoporous material; MWCNTs, multi-walled carbon nanotubes; HAP, hydroxyapatite; Pt-DENs, platinum nanoparticles in dendrimers; BGMC, bicontinuous gyroidal mesoporous carbon; Pt-cUME, platinum cavity-ultramicroelectrode; IL, ionic liquid; OMCPE, ordered mesoporous carbon paste electrode; MCF, mesocellular carbon foam; FTO, flurine-doped tin oxide; Pt@MZF, platinum electrodeposited on mesoporous zirconia thin film; CNP, carbon nanoparticle; Fc-MeOH, ferrocene methanol; HMSM, hybrid mesoporous silica membrane; HMS, hexagonal mesoporous silica; BMS-CS, bimodal mesoporous silica and chitosan hybrid film; QDs, quantum dots; {Chitosan/OMC-Hb}$_n$, multilayered films of hemoglobin-doped OMC and chitosan prepared by layer-by-layer assembly; MCNs/PDDA, mesoporous carbon nanospheres covered with PDDA; PAM-P123 polyacrylamide-P123; PLL, poly-(L)-lysine; MSHS, mesoporous silica hollow sphere; MSF, mesocellular siliceous foam; BMIM·PF6, 1-butyl-3-methylimidazolium hexafluorophosphate; SPE, screen-printed electrode; KIT, Korean Institute of Technology; MCCE, mesoporous carbon ceramic electrode; PN, Prussian Blue; HPM, hydrophobic porous membrane; CoPC, cobalt phthalocyanine; GMCE, magnetic glassy carbon electrode; GNCs, gold nanoclusters; $ABTS^{2-}$, 2,2′-azinobis-(3-ethylbenzthiazoline-6-sulfonate); CB, carbon black; MSLHNs, mesoporous silica-(L)-lysine hybrid nanodisks; ATO, antimony-doped tin oxide; CILE, carbon ionic liquid electrode.

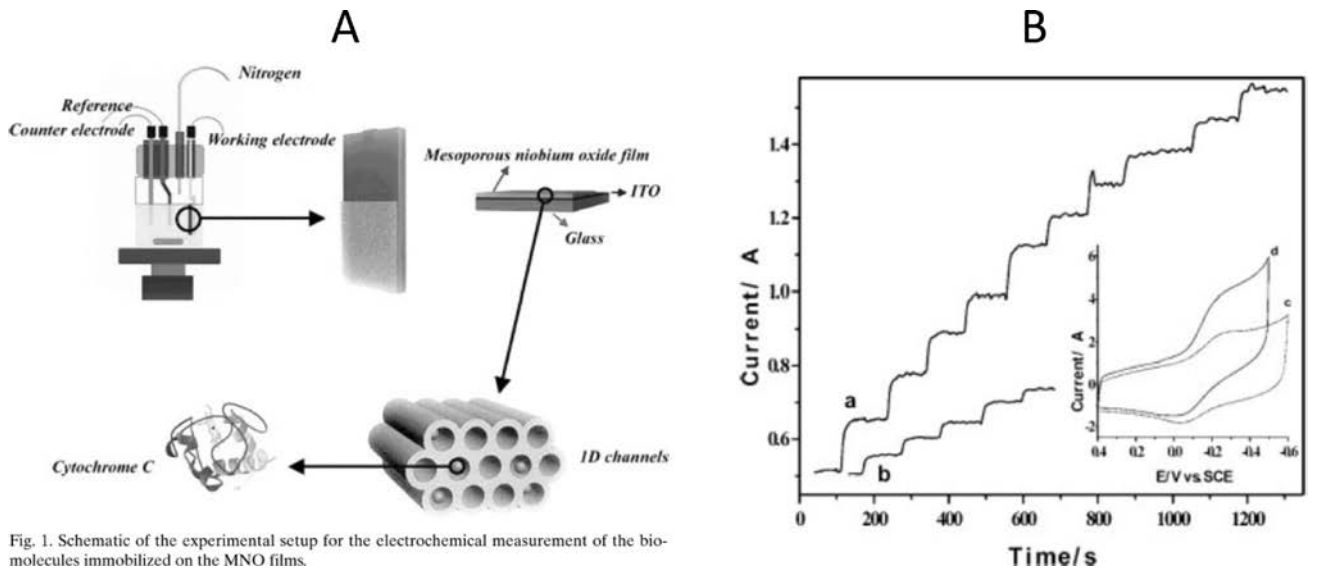

Fig. 1. Schematic of the experimental setup for the electrochemical measurement of the biomolecules immobilized on the MNO films.

Fig. 7. (A) Illustration of the experimental setup for electrochemical measurements with cytochrome c (Cyt c) immobilized in a mesoporous niobium oxide film. (B) Amperometric i-t curve for (a) Cyt c/Nb_2O_5 and (b) Nb_2O_5 electrode to successive additions of H_2O_2 in a phosphate buffer (pH 7.0; applied potential = −0.25 V). Inset: Cyclic voltammograms of Cyt c/Nb_2O_5 electrode in the absence and in the presence of H_2O_2 (Scan rate = 50 mV s^{-1}). Reprinted from [185]. Cathodic current was defined by convention positively in this work.

the modified electrode by cyclic voltammetry (Inset) and the application to the detection of H_2O_2. The cyclic voltammogram shows a pair of redox peaks in the region comprised between 0 and −0.3 V. It is slightly lower than the expected potential for Cyt c in solution, which suggests that the protein changed conformation significantly upon adsorption [226]. The addition of H_2O_2 in the solution led to the observation of an electroacatalytic peak at the characteristic potential of the direct electron transfer reaction with the protein (Figure 7B, curve d). Amperometric measurements show clear improvement for the H_2O_2 detection in the presence of Cyt c (Figure 7B, curve a) than in the absence of the protein (Figure 7B, curve b). The Cyt c protein was then immobilized in mesoporous silica thin films functionalized with aminopropyl groups and deposited on a conductive ITO electrode [105]. The pore size, 8.4 nm, and the specific surface area, 730 $m^2 g^{-1}$, were higher than for the Nb_2O_5 film described above. Despite the isolating properties of silica, well-defined redox signals were observed at potential values close to the expected ones for Cyt c in solution at an unmodified electrode. Compared to Nb_2O_5, such beneficial potential shift is probably due to the influence of amino groups covering the internal pore surfaces, in agreement with data reported for self-assembled monolayers [226]. The peak current intensities are varying linearly with the scan rate, accounting for a surface-confined electrochemical reaction. Because silica is an insulating material one can assume that the electrochemical reaction was restricted to the interface between the mesoporous silica film and the ITO electrode substrate. The bioelectrode was applied to the electrocatalytic reduction of H_2O_2, and to the electrocatalytic oxidation of ascorbic acid as well.

Stable immobilization and reversible electrochemistry of Cyt c in a mesoporous transparent ITO film was reported later on [192]. The transparency and good conductivity of this support, combined to the large surface area of the film, allowed not only the incorporation of a high amount of electroactive biomolecules but also permitted the combination of electrochemical and spectroscopic investigations. For instance, spectroelectrochemistry and resonance Raman spectroscopy revealed that there was no perturbation of the structural integrity of the redox protein in the mesoporous electrode. The formal potential was determined to be 9 mV (vs. Ag/AgCl), a value very close to the potential of Cyt c in solution (14 mV). The bioelectrode was then applied to the detection of superoxide ($O_2^{\bullet-}$) in solution upon enzymatic generation of superoxide anions in the electrochemical cell. Note that another report on superoxide has appeared [129], based on the immobilization of superoxide dismutase in a mesoporous silica – L-lysine hybrid material. Superoxide dismutase is a metalloenzyme, but not a heme protein, that has the capability for dismutation of $O_2^{\bullet-}$ to O_2 and H_2O_2 with excellent specificity [129]. Direct electron transfer reactions and excellent selectivity was observed towards $O_2^{\bullet-}$ in the presence of various interfering species, including H_2O_2 and O_2.

OMC materials were also applied to the immobilization and electrochemistry of Cyt c [170]. The electrode fabrication involved notably a Layer-by-Layer deposition of carbon nanoparticles alternately with a positively-charged polyelectrolyte. Cyt c was then adsorbed in the porous film. The electrochemical signal from the protein was increasing with the number of bilayers. The bioelectrode showed a good electrochemical activity for the re-

duction of H_2O_2 and, according to the authors, exhibited fast amperometric response, wide linear range, low detection limit and good reproducibility. Even if slightly out of the scope of the review, it is noteworthy that macroporous carbon electrodes can be also applied to the immobilization of Cyt c for the electrocatalytic detection of H_2O_2 [144].

Of related interest one can cite here the immobilization microperoxidase 11 (MP11) in mesoporous SnO_2 films [193]. MP-11 is a small size redox enzyme obtained by proteolytic digestion of Cyt c. It is an oligopeptide consisting of eleven amino acids and a covalently linked Fe^{III}–protoporphyrin IX heme [193]. The catalytic activity of the immobilized MP-11 in mesoporous SnO_2 electrodes was found to proceed via the Fenton reaction, yielding $OH^{\bullet}$ radical intermediates. A biosensor for H_2O_2 detection was demonstrated on that basis.

5.1.2 Hemoglobin and Myoglobin

Hemoglobin (Hb, 66 kDa) is nearly spherical with molecular size of $5.0 \times 5.5 \times 6.5$ nm^3 [199], i.e., bigger than Cyt c. Myoglobin (Mb, 17.6 kDa) is smaller but biologically related to hemoglobin. First developments involving Hb or Mb and mesoporous materials have been performed with hexagonal mesoporous silica displaying ca. 4 nm pore diameter [97,98]. Evidence for direct electron transfer between the redox proteins and the electrode surface, as well as illustrative applications to the detection of H_2O_2 and NO_2^-, have been provided in parallel for these two proteins. However, considering the inadequacy between the pore diameter and the protein size of hemoglobin, one can suspect that the protein was essentially adsorbed on the outer surface of the silica material, and for this reason the interest of the mesoporous structure could be limited in the case of hemoglobin.

Not only mesoporous silica [97,98,101,103,106–110,113,118,157] but also mesoporous carbon [141,147,154,155,160,180] and mesoporous polymers [203], and other metal oxides, i.e., TiO_2 [186,190], Al_2O_3 [188], ZrO_2 [194], Fe_3O_4 [198] and Nb_2O_5 [199], have been applied for the construction of hemoglobin/myoglobin biosensors. The target analyte was essentially H_2O_2 [97, 101, 103, 107–110, 118, 141, 147, 154, 155, 160, 161, 180, 188, 190, 194, 199, 203]. Few other analytes have been analyzed, such as NO_2^- [97, 188], NO [186] and tricholoroacetic acid [198].

Several authors have developed a combination of mesoporous materials, either silica [101,106,110] or carbon [160], with metal nanoparticles in order to improve the efficiency of direct electron transfer reactions with hemoglobin or myoglobin. These particles were made of Pt [160], Pd [110], gold [101] or even CdTe quantum dots [106]. Hemoglobin was used twice for the Layer-by-Layer assembly of the bioelectrode, in combination with CMK-3 [141] or carbon Al-MSU-S particles [109]. The immobilization of the protein was also made in the presence of ionic liquids, into a mesocellular silica foam [108], or in a carbon ionic liquid electrode [118]. Direct electrochemistry of hemoglobin was otherwise observed in a renewable mesoporous carbon ceramic electrode [180] and with mesoporous silica KIT-6 modified screen-printed electrodes [113].

An interesting investigation has been conducted on the optimization of the porosity of graphitized carbon electrodes, with the objective to improve the efficiency of the protein immobilization and the biosensor characteristics [154,155]; this work has been discussed in more detail in Section 3.1. Other mesoporous carbon materials have been used for the immobilization of hemoglobin, e.g., FDU-15 [160,161].

5.1.3 Horseradish Peroxidase

Horseradish peroxidase (HRP, ~44 kDa, $4.0 \times 6.7 \times 11.6$ nm^3) is bigger than the other heme proteins discussed above. The hosting material likely to accommodate HRP thus needs to provide sufficiently large pore volume. First investigations have been performed by Xu et al. using mesoporous Nb_2O_5 [73]. The direct electrochemistry of HRP was studied in a series of experiments similar as for Cyt c. The influence of both the film thickness (respectively 20 nm, 500 nm and 1 μm) and pore size (2, 6 and 10 nm) on the sensor response was studied there. Optimal responses were observed with the thickest film and for 6 nm pores. However, the effect of film thickness was not so dramatic and it is interesting to note that the materials with 2 nm pores, i.e., a size that does not allow the protein to enter into the mesopores, still displayed an important response.

A mesoporous SnO_2 film was applied for direct spectroelectrochemical investigation of immobilized cytochrome c peroxidase (CcP) and HRP [191]. The immobilized HRP was found to have less favorable interfacial electron transfer than that of CcP. A carbohydrate chain on the surface of native HRP may hinder the interfacial electron transfer through at least three ways: (1) insulating effect, (2) increasing the electron-transfer distance between the heme edge and the electrode, and (3) orientating the redox centre away from the surface. The authors have demonstrated the feasibility of using peroxidase modified mesoporous metal oxide film electrodes as H_2O_2 biosensors via both optical and electrochemical detection schemes. Employing TiO_2 electrodes, a linear increase of the absorbance measured at 418 nm is observed as a function of H_2O_2 concentration, within a range 0.04–0.8 mM, while the current response of the HRP modified electrode was linear within a range 1–20 mM.

Several works have been performed with HRP-loaded silica-based mesoporous silicas with different pore geometry and size, i.e., HMS [100], mesoporous silica hollow spheres [115], SBA-15 [122], and a hybrid mesoporous silica membrane [127]. Direct electrochemistry of HRP was investigated and the observed direct electron transfer reactions were applied to the detection of H_2O_2. Several authors have described the co-immobilization of HRP

with a second protein, i.e., tyrosinase [99] (see Section 5.3.2), glucose oxidase [114,128] (see Section 5.2.1) and uric oxidase [137] (see Section 5.2.2). Moreover, HRP is often used in electroanalysis for the indirect detection of recognition events. One can cite two examples from the literature. First, a sandwich immunoassay was built for the detection of hepatitis C Virus Non-Structural 5A [130]. A glassy carbon electrode was modified with an Au-MoO_3/chitosan nanocomposite. MCM-41 mesoporous silica was used as a nanocarrier for HRP and the polyclonal antibody as the reporter probe. Following the sandwich-type immunoreaction, HRP was captured on the surface of the electrode and could catalyze the decomposition of hydrogen peroxide. The second example proposed an amplified and selective detection of manganese peroxidase genes based on enzyme-scaffolded-gold nanoclusters and mesoporous carbon nitride [223]. Moreover, during the electrode assembly, mesoporous carbon nitride was associated to gold nanoparticles with the goal to accelerate the electron transfer events involved in the biodetection scheme.

At his point of discussion one can try to evaluate the best strategy to achieve the highest sensitivity for H_2O_2 detection. The lowest detection limits that can be found in the literature were in the range of 10^{-9} M and were achieved either with HRP [100] or hemoglobin [97,107] as the biomolecule. For these examples, the proteins were immobilized in mesoporous silica, either HMS [97,100] or SBA-15 [107], and deposited as a particulate film on glassy carbon electrode. So, in addition to enhanced stability, mesoporous silica seems to favor also the sensitivity of the biosensor, possibly because of the better stabilization of the protein in their mesopores.

5.2 Oxidases

Glucose oxidase is one of the most common enzymes used for electrochemical biosensor because of the great interest in glucose determination for monitoring diabetic people [74]. The blood-glucose concentration of people not afflicted by diabetes is usually in the 4–8 mM range. In people with diabetes the range is much wider, i.e., 2–30 mM [227]. Other biological fluids contain glucose, as tears for instance. The average concentration of glucose in tears was reported to be 0.16 mM and 0.35 mM in non-diabetic and diabetic people, respectively [228]. Concentrations up to 0.92 mM were also reported in diabetic patients [229]. A rapid look at the Table shows that most glucose biosensors are allowing its detection at concentrations lower than that usually encountered in blood. Only two biosensors are allowing the detection of glucose up to 30 mM [175,201]. However most of the biosensors display good detection limit that would make them applicable in tears glucose monitoring.

All the glucose biosensors from this review involve glucose oxidase as the enzyme. Detection can be basically made via the electrochemical determination of H_2O_2 generated by the enzymatic reaction (1st generation biosensor), or using a redox mediator (2nd generation biosensors), or by direct electron transfer from the FAD cofactor to the electrode surface (3rd generation biosensors). Figure 8A shows the possible redox reactions involving glucose oxidase. By oxidizing glucose, the FAD cofactor is reduced to $FADH_2$. In a second step $FADH_2$ is regenerated to FAD by reacting with O_2, leading to the production of H_2O_2. The use of an electrochemical mediator to regenerate FAD, instead of oxygen, is the usual strategy for disposable glucose biosensors [227]. Apart from mediated electron transfers, direct electrochemistry is often claimed in the literature, but this is still a matter of debate because of the difficulty to achieve such a direct electron transfer with the FAD cofactor deeply embedded in the center of the protein [224].

The next section will give an insight in the various works on glucose biosensors using glucose oxidase immobilized in mesoporous materials accommodated to electrodes operating either in the detection of the enzymatic reaction product, H_2O_2, or using a redox mediator to do so, and finally a discussion will be developed on the basis of the reports claiming for direct electron transfer reactions with glucose oxidase. At the end of the section, we will present other biosensors based on other oxidase enzymes or related proteins.

5.2.1 Glucose Oxidase

First Generation Glucose Biosensors

H_2O_2 is produced by glucose oxidase in the presence of glucose as a result of its oxidation. The first approach to detect glucose is thus to apply a sufficiently anodic potential to allow the oxidation of H_2O_2, or a sufficiently cathodic one to enable its reduction. Different mesoporous materials have been used to immobilized the protein, such as silica [119,133,136], carbon [143,145,151,152,182,183], MnO_2 [189] or ZrO_2 [74]. The role of the mesoporous material can be not only immobilizing the proteins but it can sometimes provide some electrocatalytic properties to detect H_2O_2 (e.g., by oxidation using mesoporous MnO_2 [189]). Pt nanoparticles have also been immobilized on mesoporous materials for improving the electrochemical detection of H_2O_2 [143,151].

An interesting comparative study has been conducted using ordered mesoporous carbon, carbon nanotubes, and glassy carbon, for the electrocatalytic oxidation of H_2O_2, suggesting that OMC offered more favorable electron-transfer kinetics than the other carbon-based electrodes. This is thought to be due to edge-plane graphite sites contributing to greatly enhance the electrochemical reactivity of H_2O_2. Similar investigations were carried out for the oxidation of NADH [145].

H_2O_2 can be reduced, either directly on the electrode surface [109,113,125, 156,157,161,162,170,173], or enzymatically using HRP [114,128]. Direct H_2O_2 reduction is catalyzed by metal or alloy nanoparticles, such as Pt [120,124,167,172], gold [136], or $NiFe_2$ [183]. The modification of mesoporous materials with these particles con-

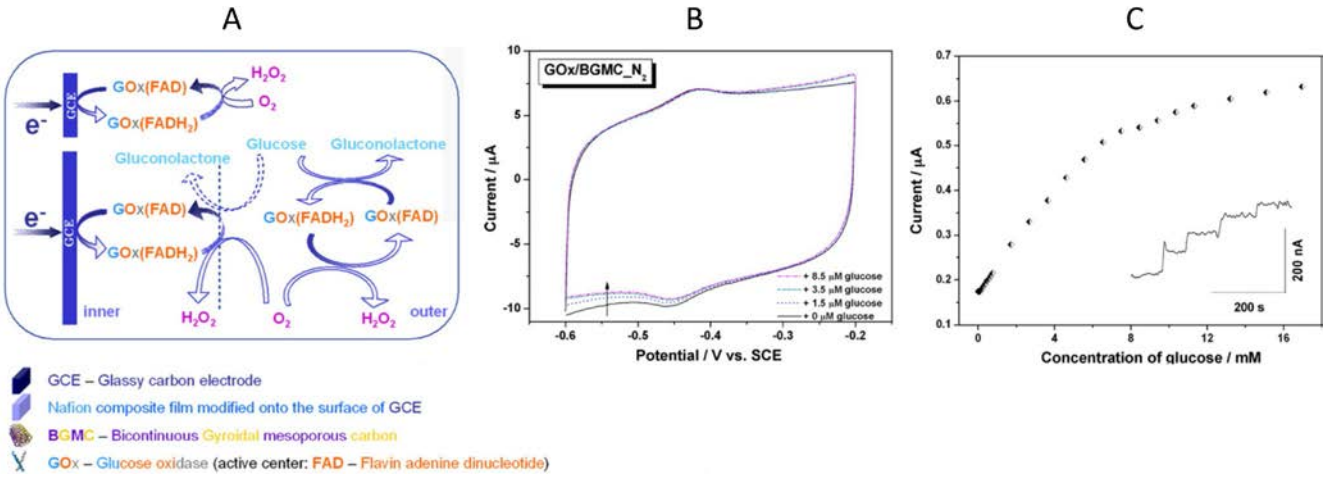

Fig. 8. (A) Schematic representation of the electron transfer and bioelectrocatalytic processes of GOx/BGMC electrode (BGMC= bicontinuous gyroidal mesoporous carbon). (B) Cyclic voltammograms of GOx/BGMC electrode recorded at a scan rate of 50 mV s^{-1} in N_2-saturated phosphate buffer (pH 7.0), respectively before and after successive additions of glucose at 30 °C. (C) Calibration curve (current versus concentration) for glucose as recorded at an applied potential of +0.6 V in air-saturated phosphate buffer (pH 7.0). Inset: Illustration of the dynamic responses of GOx/BGMC electrode to successive additions of glucose. Reprinted from [166]. Anodic current was defined by convention positively in this work.

tributes to decrease the overpotential for H_2O_2 reduction. In doing so, one can achieve detection potentials in the range from −0.4 V to −0.1 V vs. Ag/AgCl [136]. Finally, magnetic nanoparticles of Fe_3O_4 have been incorporated in a biosensor as mimetic peroxidase [168].

Horseradish peroxidase has been co-immobilized with glucose oxidase using mesoporous silica materials, either MCM-41 [128] or SBA-15 bearing gold nanoparticles (AuNPs-SBA-15) [114]. The electrochemical detection was made in the presence of catechol as redox mediator. The detection scheme was as follows: (1) oxidation of glucose to gluconolactone with H_2O_2 generation by glucose oxidase; (2) reduction of H_2O_2 and oxidation of catechol to quinone by HRP; and (3) two electron quinone reduction at the electrode surface [128]. In the absence of mediator, a direct electron transfer was investigated between HRP and AuNPs-SBA-15. This enzymatic reaction allowed the detection of glucose by applying a cathodic potential of −0.45 V vs. SCE likely to reduce H_2O_2 [114].

Mediated Electron Transfer (Second Generation Glucose Biosensors)

Only few investigations involved mediated electron transfers at mesoporous materials-modified bielectrodes bearing glucose oxidase. The example of catechol mediator in the presence of HRP has been discussed in the previous section as it was applied to the catalytic reduction of H_2O_2 and not to the wiring of FAD cofactor from glucose oxidase. Cobalt(II) Schiff base (Co(salen)) have been also incorporated in large mesoporous carbon and applied to the electrochemical detection of H_2O_2 produced by glucose oxidase [173].

Ferrocene species have been used to mediate electron transfer with glucose oxidase, either as ferrocenemethanol [104,175] or as ferrocene monocarboxylic acid [102]. The linear concentration range achieved with using a mediator is usually wider than for other detection schemes, and it can fulfil the requirement for detection of glucose in diabetic blood. The group of Willner reported the application of mesoporous carbon nanoparticles, CNPs (< 500 nm diameter of NPs, pore dimensions ~6.3 nm) to design electrically contacted enzyme electrodes for biosensing, in which the relay units, ferrocenemethanol, were loaded in the pores of CNPs, and the pores were capped with glucose oxidase proteins. [175].

Direct Electron Transfer (Third Generation Glucose Biosensors)

Several articles are claiming for direct electron transfer between oxidase proteins immobilized in a mesoporous material and an electrode surface [102,112,131,140,149–152,156,165,166,181,196,197,201,202]. In most of these papers, the electrochemistry of FAD cofactor was observed and carefully investigated. However, when applied to analytical purposes, the detection scheme involved sensing of either oxygen (consumed by the enzymatic reaction) or H_2O_2 (produced) [112,131,140,149–152,156,165,166,181,197,202], or it was performed in the presence of a mediator [102], making questionable the direct electron transfer pathway. Two research works are involving another mechanism, but the electrochemical potentials of the reactions, i.e., around 0.25–0.3 V versus SCE, should not be related to the direct electrochemistry of FAD [196,201], despite the effective electrochemical detection of glucose.

Following the previously discussed mechanism for glucose detection with glucose oxidase, involving either H_2O_2 detection or direct electrochemistry of FAD cofac-

tor (Figure 8A), the use of a bicontinuous gyroidal mesoporous carbon was claimed to favor the latter process [166]. The typical cyclic voltammogram that can be observed exhibits important capacitive currents as a result of the large electroactive surface area developed by the material, but also a noticeable pair of peaks observed at a potential close to −0.45 V vs. SCE (Figure 8B). This potential is compatible with the electrochemistry of FAD coming from glucose oxidase. The addition of glucose in the solution, in the absence of oxygen, does not allow observing a significant modification of the voltammetric signals. This experiment supports the argument that despite the effective electrochemistry of FAD cofactor on mesoporous carbon materials, its application to the electrochemical biosensing of glucose is not obvious. The authors have then applied the bioelectrode to the detection of glucose by amperometry and the current was indeed growing by increasing the concentration of glucose in solution (Figure 8C). The protein has thus maintained its enzymatic activity after immobilization on the electrode. But note that the amperometric measurement was performed at +0.6 V vs. SCE, a potential at which H_2O_2 can be detected onto the electrode surface, meaning that the biosensor was indeed likely to detect glucose but not via a direct electron transfer scheme (it was actually a 1st generation biosensor, not a 3rd generation one).

All in all, the best detection limits for glucose, using mesoporous materials-based electrochemical biosensors, have been reached with mesoporous MnO_2 [189,197], operating via the detection of H_2O_2 in either the anodic [189] or cathodic [197] mode. The concentration range achieved with these two biosensors is however not suitable for the detection of glucose in blood and should find better application in the analysis of glucose in other fluid containing lower concentrations of analyte, e.g., tears.

5.2.2 Other Oxidase-Type Enzymes

Pyranose Oxidase

Pyranose oxidase has been recently applied to the electrochemical detection of glucose. Pyranose oxidase has broader substrate specificity than glucose oxidase and an option of large scale production using recombinant E. coli, which provides it with a great potential for biofuel cell application but not necessarily for biosensing [182].

Lactate Oxidase

Lactate oxidase was applied to L-lactate determination [125,126,172]. The detection scheme was similar as for glucose oxidase. The oxidation of L-lactate by FMN cofactor in the presence of oxygen led to the production of H_2O_2 that was detected by electrochemical oxidation [125,126] or reduction [172]. The oxidation reaction was catalyzed by cobalt phthalocyanine [125] or Prussian blue [126] immobilized on the mesoporous materials, while the reduction reaction was catalyzed by Pt nanoparticles (see Figure 5 for an illustration) [172].

Cholesterol Oxidase

The detection of cholesterol involved cholesterol oxidase. Two examples are available, involving a different detection scheme. In the first one, cholesterol oxidase was immobilized in high amount on core-shell structured silica microspheres. The reaction of cholesterol with the protein in the presence of oxygen led to the production of H_2O_2 that was then detected by electrochemiluminescence in the presence of 0.67 mM luminol [132]. In the second example, cholesterol oxidase was immobilized along with cholesterol esterase on the surface of electrospun TiO_2 nanofibers (see Figure 6F for the way the electrospun fibers are obtained). Then, the electrochemical detection was performed in the presence of $Fe(CN)_6^{3-}$ as electron mediator between the enzymatic FAD cofactor of choline oxidase and the electrode surface [200].

Choline Oxidase

Choline determination was achieved through the oxidation of this substrate by choline oxidase into betaine and production of H_2O_2. The biosensor was developed by immobilization of the protein in a hybrid mesoporous membrane (see Figure 6E for illustration), giving rise to a hybrid material with 12 nm pore diameter, which was likely to detect H_2O_2 detection via its oxidation on a platinum electrode [116]. The determination range was 5.0–800 mM. The sensor was stable compared to the native enzyme sensor and 85 % of the initial response was maintained even after storage for 80 days. More recently, choline oxidase was encapsulated into a silica matrix electrodeposited onto screen-printed electrodes [230]. The deposition was performed in the presence of CTAB that can act as both protein stabilizer and template for pore generation. The sensor was applied successfully to the determination of choline in child milk.

Human Sulfite Oxidase

Human sulfate oxidase catalyzes the conversion of sulfite into sulfate. The protein is a homodimer and each monomer contains a b-type heme (Heme domain, HD) linked by a 10 amino acid flexible loop to a second domain containing a molybdenum cofactor (Moco domain, MD) and a dimerization domain [231]. The catalytic sulfite oxidation takes place at the molybdenum cofactor (Moco). To regenerate the catalytic center, two electrons are then transferred from the Moco (Mo^{IV}) via the HD to the physiological external electron acceptor cytochrome c [232]. The protein was immobilized in mesoporous ATO electrode [75]. Catalytically-active enzyme in a direct electron transfer configuration was ensured without further chemical modification of the ATO surfaces. Interestingly, the binding of hSO onto the ATO surface seems to be not only of electrostatic nature, but also originates from a strong interaction between the histidine-tag of the enzyme and the supporting material. If confirmed

with other enzymes, this property would open the way to the immobilization of other redox proteins with histidine-tag in the goal to implement new biosensing devices.

Uric Oxidase

Contrarily to the other oxidase, uricase does not have a FAD cofactor. It catalyzes the reaction of urate with oxygen to give 5-hydroxyisourate and H_2O_2. The biosensor was developed through co-immobilization of uricase and horseradish peroxidase on mesoporous silica with hexagonal symmetry (MCM-41), and applied to the determination of uric acid in serum [137]. The detection scheme involved the electrocatalytic reduction of H_2O_2 by HRP at −0.1 V vs. Ag/AgCl in the presence of catechol acting as redox mediator.

Tyrosinase and Laccase

Tyrosinase is a copper protein that catalyzes the oxidation of diphenols to o-quinones and the hydroxylation of monophenols into diphenols [171]. Figure 9A shows the principle of the experiments reported by Wang et al. [213]. The authors have immobilized tyrosinase in a graphitized mesoporous carbon. The system was then mixed with Co_3O_4 nanorods before deposition on glassy carbon electrode. The enzymatic activity in the presence of a mixture of phenols led in two steps to the production of o-quinone molecules that can then be detected electrochemically. The authors have studied the direct electron transfer between the protein and the electrode surface as illustrated in Figure 9B, but such direct electron transfer was not applied for biosensing, the detection of phenolic molecules being achieved by the electrochemical oxidation of o-quinones. A great interest of this work is the application of the biosensor to mixed phenolic samples (phenol, catechol, m-cresol, p-cresol and 4-chlorophenol) and real water samples. The analysis of tap-water and river water was successful. The electrochemical biosensor was compared to a spectrophotometric method, showing that the electrochemical approach was more rapid, sensitive, accurate and convenient. Other biosensors have been developed using tyrosinase immobilized onto mesoporous carbon [171,213], mesoporous carbon nitride [76] or mesoporous silica [99,171]. Horseradish peroxidase can also be involved in the oxidation of phenolic compounds. Dai et al. reported an original contribution showing the interest of co-immobilizing tyrosinase and HRP with mesoporous silica in order to enhance the sensitivity of the biosensor [99]. Finally, laccase was also reported for the detection of catechol [117,163]. In one example, methylene blue was immobilized in mesoporous MCM-41 in order to promote electron transfer from laccase to the electrode [117]. In a second example, copper was incorporated in mesoporous carbon and improved the electron transfer reaction at +0.45 V for the detection of catechol [163].

Comparison of the different sensors by considering the detection limit or the linear range does not allow identifying a clear trend in order to determine the best mesoporous material for this kind of biosensor. The best detection limits for catechol, between 7.8×10^{-10} M to 2.5×10^{-8} M were obtained either with MCM-41 [99,134] or mesoporous carbon materials [171,177,76,213]. More than the materials, it seems to be the combination of two enzymes (tyrosinase and HRP) that allowed to achieved the best sensitivity for catechol determination [99].

5.3 Others Enzymes

This section is presenting the biosensors prepared with other proteins than heme proteins and oxidase-type enzymes. The number of reports is much less than with the previous ones. Two main categories have been defined, NAD-dependent dehydrogenases [111,145,153,187,201], and non-redox proteins such as cholesterol esterase [200], acethylcholine esterase [135] and organophosphorus hydrolase [159,176].

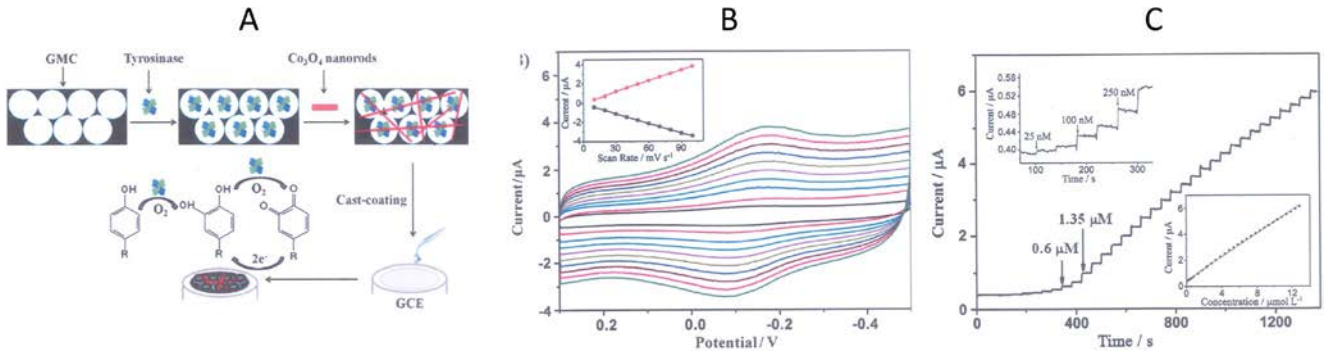

Fig. 9. (A) Schematic representation of a graphitized ordered mesoporous carbon-Co_3O_4-Tyrosinase(Tyr)-Chitosan nanocomposite prepared on glassy carbon electrode (GCE) and the corresponding biosensor mechanism. (B) Cyclic voltammograms of GMC/Co_3O_4-Tyr-Chitosan/GCE in 50 mM phosphate buffer (pH 7.0) at potential scan rates of 10, 20, 30, 40, 50, 60, 70, 80, 90, and 100 mV s^{-1}. The variation in peak currents versus scanning rates is shown in the insert. (C) Amperometric *i–t* curve for GMC/Co_3O_4-Tyr-Chitosan/GCE upon successive additions of Catechol; measurements were performed in 50 mM phosphate buffer (pH 7.0) at an applied potential of −0.1 V. Reprinted from [213]. Cathodic current was defined by convention positively in this work.

5.3.1 NAD-Dependent Dehydrogenases

The research involving dehydrogenases has been essentially conducted with alcohol dehydrogenase [145,153,187,201] and one report is available dealing with formaldehyde dehydrogenase [111]. These proteins are NAD^+/NADH-dependent. At the contrary to FAD in glucose oxidase, NAD is a labile cofactor. For biosensing applications, the enzymatic oxidation of ethanol [145,153,187,201] or formaldehyde [111], as performed in the presence of NAD^+, led to the production of NADH that could be then oxidized on the electrode surface. However, a high overpotential is observed for this electrochemical reaction on glassy carbon electrode (see curve a in Figure 4B). This overpotential was decreased by using mesoporous carbon by at least 500 mV (see curve c in Figure 4B) [145] and even more by functionalization of a mesoporous carbon electrode with Meldola's blue (Figure 4C) [153] or in the presence of quinone [111]. The detection of NADH can also be performed by electrochemiluminescence in the presence of carbon nanotubes and $Ru(bpy)_3^{2+}$; in these conditions, the biosensor response to ethanol was linear in a wide concentration range from 10^{-5} to 10^{-1} M down to a detection limit of 5×10^{-6} M [187].

The materials involved in dehydrogenase-based biosensors are mesoporous carbon [111,145,153], silica [111], titania [187], as well as a phospholipid-templated mesoporous ZnO [201]. In the latter approach, the protein was immobilized during the electrodeposition of ZnO in the presence of the phospholipid, providing an environment for protein stabilization. Of particular interest was the electrocatalytic oxidation observed at −0.1 V vs. SCE in the presence of both ZnO and 1,2-dipalmitoyl-sn-glycero-3-phosphate monosodium, a catalytic signal that was not observed in the absence of this phospholipid [201].

5.3.2 Cholesterol & Acethylcholine Esterases and Organophosphorus Hydrolase

This last section concerns enzymes that are not redox proteins. They catalyze a reaction that produces a molecule likely to be oxidized by another redox protein or directly detected at the electrode surface. Organophosphorus hydrolase was for example immobilized using a mixture of mesoporous carbon and carbon black in order to improve the sensitivity of a biosensor for *p*-nitrophenol, which is the product of the enzymatic transformation of paraoxon, a organophosphorus nerve agent [176]. The role of the conductive mesoporous material was essentially to improve the electrochemical detection of *p*-nitrophenol. Following a similar principle, the protein can be replaced in the biosensor by bacteria. A genetically engineered *Escherichia coli* strain was developed in order to express the organophosphorus hydrolase on the cell surface. Bacteria were deposited on the electrode surface, without further time-consuming enzyme-extraction and purification, providing in principle an environment favorable for the stability of the enzyme [176].

Acetylcholinesterase was encapsulated within hybrid mesoporous silica membranes and deposited on screen-printed carbon electrodes (see Fig. 6E for the electrode configuration). The membranes were then applied to the detection of both acetylcholine and organophosphorus pesticides in the presence of tetracyanoquinodimethane [135]. The principle of the experiment is the inhibition of the acetylcholinesterase activity in the presence organophosphorus and carbamate pesticides. The stability of the electrode was remarkable, with less than 10% activity loss after 60 days. This biosensor unit was able to detect dichlorvos, aldicarb and parathion [135].

The last example concerns cholesterol esterase, associated to cholesterol oxidase, immobilized on porous TiO_2 nanofibers, which were applied to cholesterol detection after esterification and oxidation by the immobilized proteins [200].

6 Conclusions and Outlook

The variety of biosensors developed with mesoporous materials is large. This can be due to the vast choice of mesoporous solids nowadays available for biomolecule immobilization, from mesoporous silica-based materials to mesoporous carbons and other non-siliceous oxides. The variety is also coming from the diversity of proteins that can be immobilized in such hosts. If the main requirement of the biosensor is on stability, silica appears to be a good choice, probably because of its biocompatibility. It could also be a suitable choice if toxicity is of concern because of direct contact with a biological fluid, e.g. in subcutaneous or tears sensors. But silica is insulating, which represents a strong limitation for protein wiring, especially if direct electron transfer reactions are required. Recent development in the functionalization of mesoporous silica based on click-chemistry could provide more opportunity in the application of mesoporous silica in biosensor development [233].

Mesoporous oxides make possible spectroelectrochemical detection. Ordered mesoporous carbon materials are attractive owing to their large conductive surface area, which can be functionalized by mediators or nanoparticles, and advantageously exploited for the detection of molecules produced by redox proteins, e.g., H_2O_2 or NADH. But the large capacitive current that results from this large surface area could be detrimental for some electroanalytical applications. Direct electron transfer reactions with redox proteins have been claimed for heme proteins, glucose oxidase and tyrosinase. While such charge transfer pathway can find a direct application in the case of heme proteins, it is not yet obvious for the other proteins, as the analytical applications involving glucose oxidase or tyrosinase were mainly based on H_2O_2 detection or mediated electrocatalysis.

The results that have been reviewed here are essentially academic. The interest of the research can sometimes

be the illustration of original ideas, at first, before reaching the fulfillment of the analytical characteristics required for real applications. The main challenge today is probably to move from this status of academic research towards applied devices taking advantage of the unique properties of mesoporous materials and providing suitable dynamic, sensitivity and stability for the target analytes.

The future in this area of research could come from continuous mesoporous carbon films that start to emerge [138,142,148,169,184], which would eventually allow a better control of the protein-material interactions. Proper engineering of the material in a way permitting better control of the immobilization of the proteins is notably necessary for tuning their conformation when attached to the electrode surface. Other materials of interest are the periodic mesoporous organosilicas that show high efficiency for enzymes immobilization [234] but remain underexploited to date in the field of biosensors. Most biosensor applications involve soluble proteins. Another direction of interest would be the immobilization of membrane proteins for biosensing and/or bioenergetic applications [174,235]. The issue here is to develop suitable hybrid materials for stabilization of the protein and promoting enzymatic activity and, possibly, efficient electron transfers. The future could be a further miniaturization and integration in lab-on-chip devices, as illustrated by the development of nanofluidic in mesoporous channels [236], nanomachine or nanomotors based on mesoporous silica particles [237,238] and nanochannel-based electrochemical assays [239].

References

[1] F. Schüth, *Chem. Mater.* **2001**, *13*, 3184.
[2] B. Lebeau, J. Patarin, C. Sanchez, *Adv. Technol. Mater. Mater. Process. J.* **2004**, *6*, 298.
[3] F. Hoffmann, M. Cornelius, J. Morell, M. Fröba, *Angew. Chem. Int. Ed.* **2006**, *45*, 3216.
[4] F. Hoffmann, M. Cornelius, J. Morell, M. Fröba, *J. Nanosci. Nanotechnol.* **2006**, *6*, 265.
[5] Y. Wan, *Chem. Rev.* **2007**, *107*, 2821.
[6] C. Sanchez, L. Rozes, F. Ribot, C. Laberty-Robert, D. Grosso, C. Sassoye, C. Boissiere, L. Nicole, *C. R. Chim.* **2010**, *13*, 3.
[7] T. Asefa, Z. Tao, *Can. J. Chem.* **2012**, *90*, 1015.
[8] L. Han, S. Che, *Chem. Soc. Rev.* **2013**, *42*, 3740.
[9] D. Zhao, S. Budhi, R. T. Koodali, *ACS Symp. Ser.* **2010**, *1045*, 97.
[10] Y. Ren, Z. Ma, P. G. Bruce, *Chem. Soc. Rev.* **2012**, *41*, 4909.
[11] H. Wang, X. Jiang, Y. Yamauchi, in *Nanoporous Materials, Synthesis and Applications* (Ed: Q. Xu), CRC Press, Boca Raton, FL, **2013**, pp. 183–200.
[12] D. Gu, F. Schüth, *Chem. Soc. Rev.* **2014**, *43*, 313.
[13] Y. Shi, Y. Wan, D. Zhao, *Chem. Soc. Rev.* **2011**, *40*, 3854.
[14] R. Lin, Y. Ding, *Materials* **2013**, *6*, 217.
[15] Y. Yamauchi, K. Kuroda, *Chem. Asian J.* **2008**, *3*, 664.
[16] S. C. Warren, U. Wiesner, *Pure Appl. Chem.* **2009**, *81*, 73.
[17] R. Ryoo, S. H. Joo, M. Kruk, M. Jaroniec, *Adv. Mater.* **2001**, *13*, 677.
[18] J. Lee, S. Han, T. Hyeon, *J. Mater. Chem.* **2004**, *14*, 478.
[19] J. Lee, J. Kim, T. Hyeon, *Adv. Mater.* **2006**, *18*, 2073.
[20] C. Liang, Z. Li, S. Dai, *Angew. Chem. Int. Ed.* **2008**, *47*, 3696.
[21] Y. Wan, Y. Shi, D. Zhao, *Chem. Mater.* **2008**, *20*, 932.
[22] Y. Xia, Z. Yang, R. Mokaya, *Nanoscale* **2010**, *2*, 639.
[23] L. Chuenchom, R. Kraehnert, B. M. Smarsly, *Soft Matter* **2012**, *8*, 10801.
[24] T.-Y. Ma, L. Liu, Z.-Y. Yuan, *Chem. Soc. Rev.* **2013**, *42*, 3977.
[25] W. Li, Q. Yue, Y. Deng, D. Zhao, *Adv. Mater.* **2013**, *25*, 5129.
[26] Y. Wan, H. Yang, D. Zhao, *ACS Symp. Ser.* **2008**, *986*, 2.
[27] I. Muylaert, A. Verberckmoes, J. De Decker, P. Van Der Voort, *Adv. Colloid Interf. Sci.* **2012**, *175*, 39.
[28] A. Walcarius, L. Mercier, *J. Mater. Chem.* **2010**, *20*, 4478.
[29] Z. Wu, D. Zhao, *Chem. Commun.* **2011**, *47*, 3332.
[30] P. K. Tripathi, L. Gan, M. Liu, N. N. Rao, *J. Nanosci. Nanotechnol.* **2014**, *14*, 1823.
[31] L. T. Gibson, *Chem. Soc. Rev.* **2014**, *43*, 5163.
[32] P. Kumar, V. V. Guliants, *Microporous Mesoporous Mater.* **2010**, *132*, 1.
[33] *Hierarchically Structured Porous Materials: From Nanoscience to Catalysis, Separation, Optics and Life Science* (Eds: K. Nakanishi, B.-L. Su, C. Sanchez, X.-Y. Yang), Wiley-VCH, Weinheim, Germany, **2011**, pp. 517–529.
[34] I. Sierra, D. Perez-Quintanilla, S. Morante, J. Ganan, *J. Chrom. A* **2014**, *1363*, 27.
[35] A. Taguchi, F. Schüth, *Microporous Mesoporous Mater.* **2005**, *77*, 1.
[36] H. Tüysüz, F. Schüth, *Adv. Catal.* **2012**, *55*, 127.
[37] C. Perego, R. Millini, *Chem. Soc. Rev.* **2013**, *42*, 3956.
[38] A. Walcarius, *Comptes Rendus Chim.* **2005**, *8*, 693.
[39] A. Walcarius, *Chem. Soc. Rev.* **2013**, *42*, 4098.
[40] B. J. Melde, B. J. Johnson, *Anal. Bioanal. Chem.* **2010**, *398*, 1565.
[41] A. Walcarius, A. Kuhn, *Trends Anal. Chem.* **2008**, *27*, 593.
[42] A. Walcarius, *Anal. Bioanal. Chem.* **2010**, *396*, 261.
[43] J. C. Ndamanisha, L. Guo, *Anal. Chim. Acta* **2012**, *747*, 19.
[44] A. Walcarius, *TrAC – Trends Anal. Chem.* **2012**, *38*, 79.
[45] T. Wagner, S. Haffer, C. Weinberger, D. Klaus, M. Tiemann, *Chem. Soc. Rev.* **2013**, *42*, 4036.
[46] A. Walcarius, *Electroanalysis* **2008**, *20*, 711.
[47] A. Walcarius, *Electroanalysis* **2015**, *27*, 1303.
[48] C. Ispas, I. Sokolov, S. Andreescu, *Anal. Bioanal. Chem.* **2009**, *393*, 543.
[49] M. Hasanzadeh, N. Shadjou, M. de la Guardia, M. Eskandani, P. Sheikhzadeh, *TrAC – Trends Anal. Chem.* **2012**, *33*, 117.
[50] M. Hasanzadeh, N. Shadjou, M. Eskandani, M. de la Guardia, *TrAC – Trends Anal. Chem.* **2012**, *40*, 106.
[51] M. Hasanzadeh, N. Shadjou, E. Omidinia, M. Eskandani, M. de la Guardia, *TrAC – Trends Anal. Chem.* **2013**, *45*, 93.
[52] Z. Dai, H. Ju, *TrAC – Trends Anal. Chem.* **2012**, *39*, 149.
[53] J.-S. Ye, X.-L. Li, F.-S. Sheu, in *Nanostructured Materials for Electrochemical Biosensors*, (Eds: Y. Umasankar, S. A. Kumar, S.-M. Chen), Nova Science Publishers, Hauppauge NY, **2009**, pp. 303–316.
[54] M. Colilla, M. Manzano, M. Vallet-Regí, *Int. J. Nanomed.* **2008**, *3*, 403.
[55] M. Manzano, M. Colilla, M. Vallet-Regí, *Expert Opin. Drug Deliv.* **2009**, *6*, 1383.
[56] S. Simovic, D. Losic, in *Nanoporous Materials: Types, Properties and Uses*, (Ed: E. S. B. Jenkins), Nova Science Publishers, Hauppauge NY, **2010**, pp. 73–161.

[57] M. Vallet-Regi, M. Colilla, B. Gonzalez, *Chem. Soc. Rev.* **2011**, *40*, 596.
[58] M. Moritz, M. Geszke-Moritz, *Mater. Sci. Eng. C* **2014**, *49*, 114.
[59] C.-H. Lee, T.-S. Lin, C.-Y. Mou, *Nano Today* **2009**, *4*, 165.
[60] M. Hartmann, D. Jung, *J. Mater. Chem.* **2010**, *20*, 844.
[61] A. Popat, S. B. Hartono, F. Stahr, J. Liu, S. Z. Qiao, G. Qing Max Lu, *Nanoscale* **2011**, *3*, 2801.
[62] Z. Zhou, M. Hartmann, *Chem. Soc. Rev.* **2013**, *42*, 3894.
[63] E. Magner, *Chem. Soc. Rev.* **2013**, *42*, 6213.
[64] N. Carlsson, H. Gustafsson, C. Thorn, L. Olsson, K. Holmberg, B. Akerman, *Adv. Colloid Interf. Sci.* **2014**, *205*, 339.
[65] J. Shi, H. Chen, Z. Hua, L. Zhang, in *Environmental Applications of Nanomaterials: Sythesis, Sorbents and Sensors*, 2nd ed. (Eds: G. E. Fryxell, G. Cao), Imperial College Press, London, UK, **2012**, pp. 473–522.
[66] N. Linares, A. M. Silvestre-Albero, E. Serrano, J. Silvestre-Albero, J. García-Martínez, *Chem. Soc. Rev.* **2014**, *43*, 7681.
[67] H. Chang, S. H. Joo, C. Pak, *J. Mater. Chem.* **2007**, *17*, 3078.
[68] Y. Ye, C. Jo, I. Jeong, J. Lee, *Nanoscale* **2013**, *5*, 4584.
[69] J. Wang, H. L. Xin, D. Wang, *Part. Part. Syst. Charact.* **2014**, *31*, 515.
[70] C. Sanchez, P. Belleville, M. Popall, L. Nicole, *Chem. Soc. Rev.* **2011**, *40*, 696.
[71] S. S. Park, M. Santha Moorthy, C.-S. Ha, *NPG Asia Mater.* **2014**, *6*, e96.
[72] D. Zhao, J. Feng, Q. Huo, N. Melosh, G. H. Fredrickson, B. F. Chmelka, G. D. Stucky, *Science* **1998**, *279*, 548.
[73] X. Xu, B. Tian, S. Zhang, J. Kong, D. Zhao, B. Liu, *Anal. Chim. Acta* **2004**, *519*, 31.
[74] Y.-S. Ko, Y.-U. Kwon, *ACS Appl. Mater. Interf.* **2013**, *5*, 3599.
[75] S. Frasca, A. Molero Milan, A. Guiet, C. Goebel, F. Pérez-Caballero, K. Stiba, S. Leimkühler, A. Fischer, U. Wollenberger, *Electrochim. Acta* **2013**, *110*, 172.
[76] Y. Zhou, L. Tang, G. Zeng, J. Chen, Y. Cai, Y. Zhang, G. Yang, Y. Liu, C. Zhang, W. Tang, *Biosens. Bioelectron.* **2014**, *61*, 519.
[77] Y. Meng, D. Gu, F. Zhang, Y. Shi, L. Cheng, D. Feng, Z. Wu, Z. Chen, Y. Wan, A. Stein, D. Zhao, *Chem. Mater.* **2006**, *18*, 4447.
[78] S. Jun, Sang Hoon Joo, R. Ryoo, M. Kruk, M. Jaroniec, Z. Liu, T. Ohsuna, O. Terasaki, *J. Am. Chem. Soc.* **2000**, *122*, 10712.
[79] D. R. Thevenot, *Pure Appl. Chem.* **1999**, *71*, 2333.
[80] O. Nadzhafova, M. Etienne, A. Walcarius, *Electrochem. Commun.* **2007**, *9*, 1189.
[81] C. Mousty, *Anal. Bioanal. Chem.* **2010**, *396*, 315.
[82] D. Shan, S. Cosnier, C. Mousty, *Anal. Chem.* **2003**, *75*, 3872.
[83] L. Gorton, A. Lindgren, T. Larsson, F. D. Munteanu, T. Ruzgas, I. Gazaryan, *Anal. Chim. Acta* **1999**, *400*, 91.
[84] U. Wollenberger, *Compr. Anal. Chem.* **2005**, *44*, 65.
[85] J. Wang, *Chem. Rev.* **2008**, *108*, 814.
[86] W.-Z. Jia, K. Wang, X.-H. Xia, *Trac – Trends Anal. Chem.* **2010**, *29*, 306.
[87] A. Badura, T. Kothe, W. Schuhmann, M. Rogner, *Energy Environ. Sci.* **2011**, *4*, 3263.
[88] C. M. Silveira, M. G. Almeida, *Anal. Bioanal. Chem.* **2013**, *405*, 3619.
[89] J. Wang, *Analyst* **2005**, *130*, 421.
[90] A. K. Sarma, P. Vatsyayan, P. Goswami, S. D. Minteer, *Biosens. Bioelectron.* **2009**, *24*, 2313.
[91] H. Li, S. Liu, Z. Dai, J. Bao, X. Yang, *Sensors* **2009**, *9*, 8547.
[92] A. A. Ansari, P. R. Solanki, A. Kaushik, B. D. Malhotra, in *Nanostructured Materials for Electrochemical Biosensors* (Eds: Y. Umasankar, S. Kumar, S.-M. Chen), Nova Science Publishers, Hauppauge, NY, **2009**, pp. 213–237.
[93] S. D. Minteer, *Top. Catal.* **2012**, *55*, 1157.
[94] A. Walcarius, S. D. Minteer, J. Wang, Y. Lin, A. Merkoçi, *J. Mater. Chem. B* **2013**, *1*, 4878.
[95] S. Prakash, T. Chakrabarty, A. K. Singh, V. K. Shahi, *Biosens. Bioelectron.* **2013**, *41*, 43.
[96] *Nanomaterials for Electrochemical Sensing and Biosensing* (Ed: M. Pumera), Taylor & Francis Group, Boca Raton FL, 2013; e-book version: Pan Stanford Publishing, **2014**.
[97] Z. Dai, S. Liu, H. Ju, H. Chen, *Biosens. Bioelectron.* **2004**, *19*, 861.
[98] Z. Dai, X. Xu, H. Ju, *Anal. Biochem.* **2004**, *332*, 23.
[99] Z. Dai, X. Xu, L. Wu, H. Ju, *Electroanalysis* **2005**, *17*, 1571.
[100] Z. Dai, H. Ju, H. Chen, *Electroanalysis* **2005**, *17*, 862.
[101] Y. Xian, Y. Xian, L. Zhou, F. Wu, Y. Ling, L. Jin, *Electrochem. Commun.* **2007**, *9*, 142.
[102] Z. H. Dai, J. Ni, X. H. Huang, G. F. Lu, J. C. Bao, *Bioelectrochem.* **2007**, *70*, 250.
[103] L. Zhang, Q. Zhang, J. Li, *Electrochem. Commun.* **2007**, *9*, 1530.
[104] Y. Bai, H. Yang, W. Yang, Y. Li, C. Sun, *Sens. Actuators B* **2007**, *124*, 179.
[105] X. Zhang, J. Wang, W. Wu, S. Qian, Y. Man, *Electrochem. Commun.* **2007**, *9*, 2098.
[106] Q. Zhang, L. Zhang, B. Liu, X. Lu, J. Li, *Biosens. Bioelectron.* **2007**, *23*, 695.
[107] Y. Liu, Q. Xu, X. Feng, J. J. Zhu, W. Hou, *Anal. Bioanal. Chem.* **2007**, *387*, 1553.
[108] J. Yu, T. Zhao, F. Zhao, B. Zeng, *Electrochim. Acta* **2008**, *53*, 5760.
[109] Z. Sun, Y. Li, T. Zhou, Y. Liu, G. Shi, L. Jin, *Talanta* **2008**, *74*, 1692.
[110] Y. Liu, J. Zhang, W. Hou, J.-J. Zhu, *Nanotechnology* **2008**, *19*, 135707.
[111] T. Shimomura, T. Itoh, T. Sumiya, F. Mizukami, M. Ono, *Sens. Actuators B* **2008**, *135*, 268.
[112] K. Wang, H. Yang, L. Zhu, J. Liao, T. Lu, W. Xing, S. Xing, Q. Lv, *J. Mol. Catal. B* **2009**, *58*, 194.
[113] Y. Teng, X. Wu, Q. Zhou, C. Chen, H. Zhao, M. Lan, *Sens. Actuators B* **2009**, *142*, 267.
[114] J. Zhang, J. Zhu, *Sci. China, Ser. B Chem.* **2009**, *52*, 815.
[115] Z. Cao, J. Zhang, J. Zeng, L. Sun, F. Xu, Z. Cao, L. Zhang, D. Yang, *Talanta* **2009**, *77*, 943.
[116] T. Shimomura, T. Itoh, T. Sumiya, F. Mizukami, M. Ono, *Talanta* **2009**, *78*, 217.
[117] X. Xu, P. Lu, Y. Zhou, Z. Zhao, M. Guo, *Mater. Sci. Eng. C* **2009**, *29*, 2160.
[118] Y. Li, X. Zeng, X. Liu, X. Liu, W. Wei, S. Luo, *Colloids Surf. B* **2010**, *79*, 241.
[119] G. Zhou, K. K. Fung, L. W. Wong, Y. Chen, R. Renneberg, S. Yang, *Talanta* **2011**, *84*, 659.
[120] X. Han, Y. Zhu, X. Yang, J. Zhang, C. Li, *J. Solid State Electrochem.* **2011**, *15*, 511.
[121] S. Wu, H. Wang, S. Tao, C. Wang, L. Zhang, Z. Liu, C. Meng, *Anal. Chim. Acta* **2011**, *686*, 81.
[122] Z. H. Fang, L. M. Lu, X. B. Zhang, H. B. Li, B. Yang, G. L. Shen, R. Q. Yu, *Electroanalysis* **2011**, *23*, 2415.
[123] R. Lei, X. Wang, S. Zhu, N. Li, *Sens. Actuators B* **2011**, *158*, 124.
[124] H. Li, J. He, Y. Zhao, D. Wu, Y. Cai, Q. Wei, M. Yang, *Electrochim. Acta* **2011**, *56*, 2960.
[125] T. Shimomura, T. Sumiya, M. Ono, T. Ito, T. A. Hanaoka, *Anal. Chim. Acta* **2012**, *714*, 114.

[126] T. Shimomura, T. Sumiya, M. Ono, T. Itoh, T. Hanaoka, *Procedia Chem.* **2012**, *6*, 46.
[127] S. Bian, K. Gao, H. Shen, X. Jiang, Y. Long, Y. Chen, *J. Mater. Chem. B* **2013**, *1*, 3267.
[128] N. Caro-Jara, R. Mundaca-Uribe, C. Zaror-Zaror, J. Carpinelli-Pavisic, M. Aranda-Bustos, C. Peña-Farfal, *Electroanalysis* **2013**, *25*, 308.
[129] M. Han, P. Guo, X. Wang, W. Tu, J. Bao, Z. Dai, *RSC Adv.* **2013**, *3*, 20456.
[130] M. Liang, L. Wang, C. Ma, M. Zhang, G. Xie, *Anal. Lett.* **2013**, *46*, 1241.
[131] J. Li, X. Qin, Z. Yang, H. Qi, Q. Xu, G. Diao, *Talanta* **2013**, *104*, 116.
[132] J. Zhang, S. Chen, X. Tan, X. Zhong, D. Yuan, Y. Cheng, *Biotechnol. Lett.* **2014**, *36*, 1835.
[133] A. Y. Khan, S. B. Noronha, R. Bandyopadhyaya, *Biochem. Eng. J.* **2014**, *91*, 1.
[134] Z. Dai, M. Q. Guo, X. J. Wang, H. F. Wang, W. Y. Chen, *J. Nanomater.* **2014**, *2014*, Article ID 458245.
[135] I. Tetsuji, T. Shimomura, A. Hayashi, A. Yamaguchi, N. Teramae, M. Ono, T. Tsunoda, F. Mizukami, G. D. Stucky, T. Hanaoka, *Analyst* **2014**, *139*, 4654.
[136] S. K. Maji, S. Sreejith, A. K. Mandal, X. Ma, Y. Zhao, *ACS Appl. Mater. Interf.* **2014**, *6*, 13648.
[137] R. Mundaca-Uribe, F. Bustos-Ramírez, C. Zaror-Zaror, M. Aranda-Bustos, J. Neira-Hinojosa, C. Peña-Farfal, *Sens. Actuators B* **2014**, *195*, 58.
[138] J. Pang, X. Li, D. Wang, Z. Wu, V. T. John, Z. Yang, Y. Lu, *Adv. Mater.* **2004**, *16*, 884.
[139] D. Lee, J. Lee, J. Kim, J. Kim, H. Bin Na, B. Kim, C. H. Shin, J. H. Kwak, A. Dohnalkova, J. W. Grate, T. Hyeon, H. S. Kim, *Adv. Mater.* **2005**, *17*, 2828.
[140] S. Wu, H. X. Ju, Y. Liu, *Adv. Funct. Mater.* **2007**, *17*, 585.
[141] J. J. Feng, J. J. Xu, H. Y. Chen, *Biosens. Bioelectron.* **2007**, *22*, 1618.
[142] S. Tanaka, Y. Katayama, M. P. Tate, H. W. Hillhouse, Y. Miyake, *J. Mater. Chem.* **2007**, *17*, 3639.
[143] J. Yu, D. Yu, T. Zhao, B. Zeng, *Talanta* **2008**, *74*, 1586.
[144] L. Zhang, *Biosens. Bioelectron.* **2008**, *23*, 1610.
[145] M. Zhou, L. Shang, B. Li, L. Huang, S. Dong, *Biosens. Bioelectron.* **2008**, *24*, 442.
[146] L. Zhu, C. Tian, D. Zhu, R. Yang, *Electroanalysis* **2008**, *20*, 1128.
[147] G. X. Ma, Y. G. Wang, C. X. Wang, T. H. Lu, Y. Y. Xia, *Electrochim. Acta* **2008**, *53*, 4748.
[148] M.-L. Lin, C.-C. Huang, M.-Y. Lo, C.-Y. Mou, *J. Phys. Chem. C* **2008**, *112*, 867.
[149] W. Sun, C. X. Guo, Z. Zhu, C. M. Li, *Electrochem. Commun.* **2009**, *11*, 2105.
[150] K. Wang, H. Yang, L. Zhu, Z. Ma, S. Xing, Q. Lv, J. Liao, C. Liu, W. Xing, *Electrochim. Acta* **2009**, *54*, 4626.
[151] C. You, X. Li, S. Zhang, J. Kong, D. Zhao, B. Liu, *Microchim. Acta* **2009**, *167*, 109.
[152] C. You, X. Xu, B. Tian, J. Kong, D. Zhao, B. Liu, *Talanta* **2009**, *78*, 705.
[153] X. Jiang, L. Zhu, D. Yang, X. Mao, Y. Wu, *Electroanalysis* **2009**, *21*, 1617.
[154] X. Lu, Y. Xiao, Z. Lei, J. Chen, *Biosens. Bioelectron.* **2009**, *25*, 244.
[155] X. Lu, Y. Xiao, Z. Lei, J. Chen, H. Zhang, Y. Ni, Q. Zhang, *J. Mater. Chem.* **2009**, *19*, 4707.
[156] J. Yu, J. Tu, F. Zhao, B. Zeng, *J. Solid State Electrochem.* **2010**, *14*, 1595.
[157] L. Zhang, Q. Zhang, J. Li, *Biosens. Bioelectron.* **2010**, *26*, 846.
[158] Z. Zhu, X. Li, Y. Zeng, W. Sun, *Biosens. Bioelectron.* **2010**, *25*, 2313.
[159] J. H. Lee, J. Y. Park, K. Min, H. J. Cha, S. S. Choi, Y. J. Yoo, *Biosens. Bioelectron.* **2010**, *25*, 1566.
[160] D. Nie, Y. Liang, T. Zhou, X. Li, G. Shi, L. Jin, *Bioelectrochemistry* **2010**, *79*, 248.
[161] S. Pei, S. Qu, Y. Zhang, *Sensors* **2010**, *10*, 1279.
[162] B. Xu, L. Peng, G. Wang, G. Cao, F. Wu, *Carbon* **2010**, *48*, 2377.
[163] X. Xu, M. Guo, P. Lu, R. Wang, *Mater. Sci. Eng. C* **2010**, *30*, 722.
[164] H. Wang, B. Qi, B. Lu, X. Bo, L. Guo, *Electrochim. Acta* **2011**, *56*, 3042.
[165] L. Wang, J. Bai, X. Bo, X. Zhang, L. Guo, *Talanta* **2011**, *83*, 1386.
[166] C. You, X. Yan, J. Kong, D. Zhao, B. Liu, *Talanta* **2011**, *83*, 1507.
[167] X. Jiang, Y. Wu, X. Mao, X. Cui, L. Zhu, *Sens. Actuators B* **2011**, *153*, 158.
[168] M. Il Kim, Y. Ye, B. Y. Won, S. Shin, J. Lee, H. G. Park, *Adv. Funct. Mater.* **2011**, *21*, 2868.
[169] D. Feng, Y. Lv, Z. Wu, Y. Dou, L. Han, Z. Sun, Y. Xia, G. Zheng, D. Zhao, *J. Am. Chem. Soc.* **2011**, *133*, 15148.
[170] Y. Wang, X. Bian, L. Liao, J. Zhu, K. Guo, J. Kong, B. Liu, *Microchim. Acta* **2012**, *178*, 277.
[171] L. Tang, Y. Zhou, G. Zeng, Z. Li, Y. Liu, Y. Zhang, G. Chen, G. Yang, X. Lei, M. Wu, *Analyst* **2013**, *138*, 3552.
[172] Y. Yu, Y. Yang, H. Gu, T. Zhou, G. Shi, *Biosens. Bioelectron.* **2013**, *41*, 511.
[173] J. Lu, J. Ju, X. Bo, H. Wang, L. Guo, *Electroanalysis* **2013**, *25*, 2531.
[174] A. De Poulpiquet, H. Marques-Knopf, V. Wernert, M. T. Giudici-Orticoni, R. Gadiou, E. Lojou, *Phys. Chem. Chem. Phys.* **2013**, *16*, 1366.
[175] A. Trifonov, K. Herkendell, R. Tel-Vered, O. Yehezkeli, M. Woerner, I. Willner, *ACS Nano* **2013**, *7*, 11358.
[176] X. Tang, T. Zhang, B. Liang, D. Han, L. Zeng, C. Zheng, T. Li, M. Wei, A. Liu, *Biosens. Bioelectron.* **2014**, *60*, 137.
[177] Z. Yaoyu, T. Lin, Z. Guangming, Z. Yi, L. Zhen, L. Yuanyuan, C. Jun, Y. Guide, Z. Lu, Z. Sheng, *Anal. Meth.* **2014**, *6*, 2371.
[178] Y. Zhou, L. Tang, X. Xie, G. Zeng, J. Wang, Y. Deng, G. Yang, C. Zhang, Y. Zhang, J. Chen, *Analyst* **2014**, *139*, 6529.
[179] Y. F. Bai, T. Bin Xu, J. H. T. Luong, H. F. Cui, *Anal. Chem.* **2014**, *86*, 4910.
[180] B. Habibi, M. Jahanbakhshi, *Microchim. Acta* **2015**, *182*, 1.
[181] B. Haghighi, B. Karimi, M. Tavahodi, H. Behzadneia, *Electroanalysis* **2014**, *26*, 2010.
[182] K. Y. Kwon, J. H. Kim, J. Youn, C. Jeon, J. Lee, T. Hyeon, H. G. Park, H. N. Chang, Y. Kwon, S. Ha, H.-T. Jung, J. Kim, *Electroanalysis* **2014**, *26*, 2075.
[183] D. Xiang, L. Yin, J. Ma, E. Guo, Q. Li, Z. Li, K. Liu, *Analyst* **2015**, *140*, 644.
[184] Z. Qiang, Y. Zhang, Y. Wang, S. M. Bhaway, K. A. Cavicchi, B. D. Vogt, *Carbon* **2015**, *82*, 51.
[185] X. Xu, B. Z. Tian, J. L. Kong, S. Zhang, B. H. Liu, D. Y. Zhao, *Adv. Mater.* **2003**, *15*, 1932.
[186] E. Topoglidis, C. J. Campbell, A. E. G. Cass, J. R. Durrant, *Electroanalysis* **2006**, *18*, 882.
[187] N. C. Han, H. Y. Sook, Y. K. Lyu, W. Y. Lee, *Electroanalysis* **2007**, *19*, 459.
[188] J. Yu, J. Ma, F. Zhao, B. Zeng, *Electrochim. Acta* **2007**, *53*, 1995.
[189] J. Yu, T. Zhao, B. Zeng, *Electrochem. Commun.* **2008**, *10*, 1318.
[190] N. Jia, Y. Wen, G. Yang, Q. Lian, C. Xu, H. Shen, *Electrochem. Commun.* **2008**, *10*, 774.

[191] Y. Astuti, E. Topoglidis, A. G. Cass, J. R. Durrant, *Anal. Chim. Acta* **2009**, *648*, 2.
[192] S. Frasca, T. von Graberg, J. J. Feng, A. Thomas, B. M. Smarsly, I. M. Weidinger, F. W. Scheller, P. Hildebrandt, U. Wollenberger, *ChemCatChem* **2010**, *2*, 839.
[193] Y. Astuti, E. Topoglidis, J. R. Durrant, *Anal. Chim. Acta* **2011**, *686*, 126.
[194] C. Liu, Y. Teng, J. Xu, Y. Yang, Z. Wu, *Int. J. Environ. Anal. Chem.* **2011**, *91*, 1367.
[195] S. Frasca, C. Richter, T. von Graberg, B. M. Smarsly, U. Wollenberger, *Eng. Life Sci.* **2011**, *11*, 554.
[196] J. Li, D. Kuang, Y. Feng, F. Zhang, M. Liu, *Microchim. Acta* **2012**, *176*, 73.
[197] P. Si, P. Chen, D.-H. Kim, *J. Mater. Chem. B* **2013**, *1*, 2696.
[198] W. Sun, Z. Sun, L. Zhang, X. Qi, G. Li, J. Wu, M. Wang, *Colloids Surf. B* **2013**, *101*, 177.
[199] W. Luo, Y. Li, J. Dong, J. Wei, J. Xu, Y. Deng, D. Zhao, *Angew. Chem. Int. Ed.* **2013**, *52*, 10505.
[200] K. Mondal, M. A. Ali, V. V. Agrawal, B. D. Malhotra, A. Sharma, *ACS Appl. Mater. Interf.* **2014**, *6*, 2516.
[201] D. Wang, Y. Tan, *Electrochim. Acta* **2014**, *116*, 495.
[202] G. Bharath, R. Madhu, S.-M. Chen, V. Veeramani, A. Balamurugan, D. Mangalaraj, C. Viswanathan, N. Ponpandian, *J. Mater. Chem. B* **2015**, *3*, 1360.
[203] J. Li, J. Tang, L. Zhou, X. Han, H. Liu, *Bioelectrochemistry* **2012**, *86*, 60.
[204] M. Etienne, A. Walcarius, in *Electrochemistry, Vol. 11, Nanosystems Electrochemistry*, The Royal Society of Chemistry, London, **2013**, pp. 124–197.
[205] J. S. Beck, J. C. Vartuli, W. J. Roth, M. E. Leonowicz, C. T. Kresge, K. D. Schmitt, C. T. W. Chu, D. H. Olson, E. W. Sheppard, *J. Am. Chem. Soc.* **1992**, *114*, 10834.
[206] G. J. de A. A. Soler-Illia, C. Sanchez, B. Lebeau, J. Patarin, *Chem. Rev.* **2002**, *102*, 4093.
[207] C. Sanchez, C. Boissière, D. Grosso, C. Laberty, L. Nicole, *Chem. Mater.* **2008**, *20*, 682.
[208] Z.-Y. Yuan, B.-L. Su, *J. Mater. Chem.* **2006**, *16*, 663.
[209] M. Tiemann, *Chem. Mater.* **2008**, *20*, 961.
[210] H. Wang, L. Zhai, Y. Li, T. Shi, *Mater. Res. Bull.* **2008**, *43*, 1607.
[211] R. Ryoo, S. H. Joo, S. Jun, *J. Phys. Chem. B* **1999**, *103*, 7743.
[212] Y. Meng, D. Gu, F. Zhang, Y. Shi, H. Yang, Z. Li, C. Yu, B. Tu, D. Zhao, *Angew. Chem. Int. Ed.* **2005**, *44*, 7053.
[213] X. Wang, X. Lu, L. Wu, J. Chen, *ChemElectroChem* **2014**, *1*, 808.
[214] Z. Zhou, M. Hartmann, *Top. Catal.* **2012**, *55*, 1081.
[215] S. Hudson, J. Cooney, E. Magner, *Angew. Chem. Int. Ed.* **2008**, *47*, 8582.
[216] J. N. Talbert, J. M. Goddard, *Colloids Surf. B.* **2012**, *93*, 8.
[217] L. Bayne, R. V. Ulijn, P. J. Halling, *Chem. Soc. Rev.* **2013**, *42*, 9000.
[218] K. Y. Kwon, J. Youn, J. H. Kim, Y. Park, C. Jeon, B. C. Kim, Y. Kwon, X. Zhao, P. Wang, B. I. Sang, J. Lee, H. G. Park, H. N. Chang, T. Hyeon, S. Ha, H.-T. Jung, J. Kim, *Biosens. Bioelectron.* **2010**, *26*, 655.
[219] C. Renault, K. D. Harris, M. J. Brett, V. Balland, B. Limoges, *Chem. Commun.* **2011**, *47*, 1863.
[220] A. Hagfeldt, M. Grätzel, *Acc. Chem. Res.* **2000**, *33*, 269.
[221] D. Grosso, F. Cagnol, G. J. de A. A. Soler-Illia, E. L. Crepaldi, H. Amenitsch, A. Brunet-Bruneau, A. Bourgeois, C. Sanchez, *Adv. Funct. Mater.* **2004**, *14*, 309.
[222] A. Walcarius, E. Sibottier, M. Etienne, J. Ghanbaja, *Nat. Mater.* **2007**, *6*, 602.
[223] Y. Zhou, L. Tang, G. Zeng, J. Chen, J. Wang, C. Fan, G. Yang, Y. Zhang, X. Xie, *Biosens. Bioelectron.* **2015**, *65*, 382.
[224] S. Borgmann, A. Schulte, S. Neugebauer, W. Schuhmann, in *Bioelectrochemistry* (Eds: R. C. Alkire, D. M. Kolb, J. Lipkowski), Wiley-VCH, Weinheim, **2011**, pp. 1–83.
[225] L. H. Guo, H. Allen, O. Hill, *Adv. Inorg. Chem.* **1991**, *36*, 341.
[226] X. Chen, R. Ferrigno, J. Yang, G. M. Whitesides, *Langmuir* **2002**, *18*, 7009.
[227] A. Heller, B. Feldman, *Chem. Rev.* **2008**, *108*, 2482.
[228] J. D. Lane, D. M. Krumholz, R. A. Sack, C. Morris, *Curr. Eye Res.* **2006**, *31*, 895.
[229] D. K. Sen, G. S. Sarin, *Br. J. Ophthalmol.* **1980**, *64*, 693.
[230] I. Mazurenko, O. Tananaiko, O. Biloivan, M. Zhybak, I. Pelyak, V. Zaitsev, M. Etienne, A. Walcarius, *Electroanalysis* **2015**, in press.
[231] C. Kisker, H. Schindelin, A. Pacheco, W. A. Wehbi, R. M. Garrett, K. V. Rajagopalan, J. H. Enemark, D. C. Rees, *Cell* **1997**, *91*, 973.
[232] A. Pacheco, J. T. Hazzard, G. Tollin, J. H. Enemark, *J. Biol. Inorg. Chem.* **1999**, *4*, 390.
[233] N. Vilà, J. Ghanbaja, E. Aubert, A. Walcarius, *Angew. Chem. Int. Ed. Eng.* **2014**, *53*, 2945.
[234] Z. Zhou, R. N. Klupp Taylor, S. Kullmann, H. Bao, M. Hartmann, *Adv. Mater.* **2011**, *23*, 2627.
[235] E. Schneider, D. S. Clark, *Biosens. Bioelectron.* **2013**, *39*, 1.
[236] M. Faustini, M. Vayer, B. Marmiroli, M. Hillmyer, H. Amenitsch, C. Sinturel, D. Grosso, *Chem. Mater.* **2010**, *22*, 5687.
[237] R. Villalonga, P. Díez, A. Sánchez, E. Aznar, R. Martínez-Máñez, J. M. Pingarrõn, *Chem. Eur. J.* **2013**, *19*, 7889.
[238] J. Simmchen, A. Baeza, D. Ruiz, M. J. Esplandiu, M. Vallet-Regí, *Small* **2012**, *8*, 2053.
[239] I. Fernández, A. Sánchez, P. Díez, P. Martínez-Ruiz, P. Di Pierro, R. Porta, R. Villalonga, J. M. Pingarrón, *Chem. Commun.* **2014**, *50*, 13356.

Received: March 16, 2015
Accepted: May 5, 2015
Published online: July 21, 2015

